分类号： __034__

密　级： __无__

单位代码：__10335__

学　号：__11324003__

浙江大学

博 士 学 位 论 文

英文论文题目： **Theoretical modelling of solitary waves in soft bars and higher harmonics in nonlinear media**

中文论文题目： 软杆中孤立波及非线性介质中高阶谐波的理论模拟

作者姓名：	王彦正
指导教师：	陈伟球　教授
合作导师：	Jan D. Achenbach　教授
专业名称：	固体力学
研究方向：	非线性波动力学
所在学院：	航空航天学院

论文提交日期__2018 年 6 月__

申请浙江大学工学博士学位论文

软杆中孤立波及非线性介质中高阶谐波的理论模拟

作者姓名： 王彦正

指导教师： 陈伟球 教授

合作导师： Jan D. Achenbach 教授

专业名称： 固体力学

所在学院： 航空航天学院

浙江大学

2018 年 6 月

Dissertation Submitted to Zhejiang University

for the Degree of Doctor of Philosophy

Theoretical modelling of solitary waves in soft bars and higher harmonics in nonlinear media

Wang Yanzheng

Directed by: Prof. Weiqiu Chen

Prof. Jan D. Achenbach

Zhejiang University

June, 2018

软杆中孤立波及非线性介质中高阶谐波的理论模拟

论文作者签名:＿＿＿＿＿＿＿

指导教师签名:＿＿＿＿＿＿＿

论文评阅人 1： 王骥 教授　 宁波大学

评阅人 2： 王毅泽 教授 北京交通大学

评阅人 3： 隐名评阅

评阅人 4： 隐名评阅

评阅人 5： 隐名评阅

答辩委员会主席： 杨卫 教授　 浙江大学

委员 1： Achenbach J.D.教授 美国西北大学

委员 2： 杨嘉实 教授 内布拉斯加林肯大学

委员 3： 杨庆大 教授　 迈阿密大学

委员 4： 王惠明 教授　 浙江大学

委员 5： 钱征华 教授　 南京航空航天大学

委员 6： 贾铮 研究员 浙江大学

答辩日期：2018 年 6 月 7 日

Theoretical modelling of solitary waves in soft bars and higher harmonics in nonlinear media

Author's signature:_____

Supervisor' s signature:_____

External Reviewers: Prof. Wang Ji   Ningbo University

Prof. Wang Yize Beijing Jiaotong University

Anonymous Reviewer

Anonymous Reviewer

Anonymous Reviewer

Examining Committee Chairperson: Prof. Yang Wei Zhejiang University

Examining Committee Members:

Prof. Achenbach J.D. Northwestern University

Prof. Yang Jiashi University of Nebraska Lincoln

Prof. Yang Qingda University of Miami

Prof. Wang Huiming Zhejiang University

Prof. Qian Zhenghua

Nanjing University of Aeronautics and Astronautics

Prof. Jia Zheng   Zhejiang University

Date of oral defence：June 7, 2018

独创性声明

本人声明所呈交的学位论文是本人在导师指导下进行的研究工作及取得的研究成果。据我所知，除了文中特别加以标注和致谢的地方外，论文中不包含其他人已经发表或撰写过的研究成果，也不包含为获得 <u>浙江大学</u> 或其他教育机构的学位或证书而使用过的材料。与我一同工作的同志对本研究所做的任何贡献均已在论文中作了明确的说明并表示谢意。

学位论文作者签名：　　　　签字日期：　　　年　　月　　日

学位论文版权使用授权书

本学位论文作者完全了解 <u>浙江大学</u> 有关保留、使用学位论文的规定，有权保留并向国家有关部门或机构送交论文的复印件和磁盘，允许论文被查阅和借阅。本人授权 <u>浙江大学</u> 可以将学位论文的全部或部分内容编入有关数据库进行检索，可以采用影印、缩印或扫描等复制手段保存、汇编学位论文。

（保密的学位论文在解密后适用本授权书）

学位论文作者签名：　　　　　　　　　导师签名：

签字日期：　　年　　月　　日　　　　签字日期：　　年　　月　　日

学位论文作者毕业后去向：

工作单位：　　　　　　　　　　　　　　　电话：

Acknowledgement

People must learn first if they want to make progress, just like the birds must flutter first if they want to fly. Most people who want to acquire knowledge have to seek helps from teachers. I sincerely thank all the teachers who gave me helps and guidance. They not only taught me professional knowledge to make me become a skilled person, but also helped me grow up with their noble personality cultivation. I'm lucky enough to meet so many excellent teachers. Specially, on the occasion of the completion of this dissertation, I would like to thank Professor Weiqiu Chen and Professor Jan D. Achenbach, both of whom gave me great guidance during my PhD study. In the past five years, they gave me so many selfless favors in the aspects of my study, work, and life. Professor Chen is knowledgeable, rigorous, modest, energetic, and passionate about scientific researches. Under the guidance of Professor Chen, I stepped into the hall of scientific research. Professor Achenbach's masterly academic style has impressed me a lot. His rigorous academic style has been kept in my mind, and his "step by step" education method has benefited me a lot. Keep their words in mind, take them as the examples, and march on the road of scientific research.

I am also grateful to the constructive suggestions from the other professors. I would like to thank Professor Hui-hui Dai at City University of Hong Kong for his guidance on Chapters 2 and 3. His final technical review of the works about solitary waves has given me the confidence. I would also like to thank Professor Jianmin Qu at Tufts University for his constructive suggestions on the work presented in Chapter 8. I am also grateful to Professor Rongqiao Xu, Professor Wang Huiming, Professor Chaofeng Lu, Professor Chunli Zhang, Professor Oluwaseyi Balogun and Professor Sridhar Krishnaswamy, who always gave me valuable advices on my every presentation during each group meeting.

I also appreciate China Scholarship Council (CSC) for the funding to support my two-years' study at Northwestern University, to give me the opportunity to work at a world-class university during my PhD study. Then I have the chance to experience the life and the culture in USA, which have broadened my horizons and enriched my life. Many thanks go to my roommates Zhongyang Li and Jun Zhu for

their helps and friendships during my living in USA. I also appreciate the other friends who I met at Northwestern University, including, but not limited to, Hao Wu, Dong Huang, Chao Yang, Chen Yang, Kesi Li, Feng Dong, Li Zhang, Ya Yang, Bin Tang, Guoqiang Liu, Zhiyuan Ma, Heming Wei, Tingting Yan, Qianqian Li, Xingyi Zhu, Yan Yu, and their families. They enriched my life, including the sports activities several times a week, which are both physically and mentally fit and healthy, and the happy festive parties. This experience will be an unforgettable memory in my life.

I would also like to thank the other group members for their warm and selfless helps, including, but not limited to, Yipin Su, Linli Zhang, Yongchao Gu, Bin Wu, Weijian Zhou, Zhi Wang, Dongying Liu, Yang Huang, Xudong Shen, Yilan Huang, Jiao Wang, Guozhan Xia, Linyuan Hu, Chengjun Wang, Xiaoyuan Wang, Shuting Lu, Renwei Mao, Yingjie Chen, Xueyan Hu, Ruoran, Chen, Jian Li and Nan Gao.

Special thanks should be given to my parents for their upbringing and unlimited love. Thank them for creating a good living environment for me, which allows me to focus on my study and researches without any interfere. Thank them for giving me a happy family, which makes me optimistic and confident. Thank them for their constant encouragements and cares, which give me an endless power. I would also thank Minqian, my soulmate, for her companionship and unconditional support and love.

Finally, I sincerely thank all the teachers and experts for their evaluations and suggestions on this dissertation.

Abstract

Theoretical modelling of solitary waves in soft bars and higher harmonics in nonlinear media

With the development of ultrasonic techniques, the influence of elastic nonlinearity on wave propagation in solids has attracted extensive attention. In this dissertation, several theoretical problems of wave propagation in materials and structures involving elastic nonlinearity are investigated. The dissertation consists of two main parts, i.e. the investigation of solitary waves propagating in soft bars under a biasing field (Part 1), and the analysis of higher harmonic generation by material nonlinearity arisen from material micro-damages (Part 2). The major achievements of this dissertation are briefly summarized as follows.

In Part 1, the tunability of solitary waves propagating in soft bars is explored. The effective material properties of soft materials can be altered significantly when subjected to biasing fields, such as electric field or pre-stretch. In this context, two cases are considered, 1) an electroelastic bar subjected to a biasing longitudinal electric displacement, and 2) a viscoelastic bar subjected to a pre-stretch. An asymptotic analysis is conducted by introducing several asymptotic expansions to simplify the rod governing equations. The boundary conditions on the lateral surface of the rod are satisfied from the asymptotic point of view. For the first case, by the reductive perturbation method, we deduce the far-field equation (i.e. the KdV equation). Then, the leading order of the electroelastic solitary wave solution is presented. Numerical examples are provided to show the influences of the biasing electric displacement and material constants on the solitary waves. It is found that the biasing electric displacement can modulate the velocity of solitary waves with a prescribed amplitude in the electroactive rod. For the second case, following the similar procedure, the KdV-Burgers equation can be formulated, which admits analytical and explicit solutions for kink and kink-like waves in pre-stretched Mooney-Rivlin elastic rods with the consideration of viscous dissipation. We find that the pre-stretch can not only make the kink waves lower and wider, but also change the wave velocity. The competition between the effects of pre-stretch and viscosity on the kink and kink-like waves is also revealed.

In Part 2, several simplified theories and simple theoretical models are proposed to work out analytical solutions to higher harmonic generations by material nonlinearity, which can be used to assess material micro-damages. As a starting point, we generally investigate harmonics of plane longitudinal and transverse waves in elastic solids with up to cubic nonlinearity in a one-dimensional setting. Some interesting and useful results for harmonic generation are uncovered. Then, we extend our work to the investigation of wave propagating on a half-space of isotropic incompressible material of cubic nonlinearity. The analytical far-field solution for the cumulative third harmonic surface wave is obtained in a relatively simple and systematic manner. The solution reveals that, in the far field, the resonant third harmonic propagates with the classic Rayleigh wave velocity, whose amplitude increases linearly with the propagation distance. The transmission of the resonant wave from a half-space of nonlinear material into a half-space of linear material is also considered. In a pipe of quadratic material nonlinearity, the analytical solution to the mixing of axisymmetric longitudinal waves and torsional waves are obtained using the shell theory. The resonant waves with difference frequencies propagate in the opposite direction of the corresponding primary wave. The nonlinear shell theory is further simplified to obtain the solution for the cumulative second longitudinal harmonics generated by self-interaction of longitudinal waves in an analytical form. From a practical point of view, some theoretical models to investigate harmonic generation from an inclusion of nonlinear material are also established. By using the continuity conditions of stress and displacement at the interface or using the reciprocity theorem of elastodynamics, the expressions of the reflection waves are obtained, whose amplitudes can provide information of the material constants of the nonlinear media. The reciprocity theorem is proven to have greater utility. As an example, the backscattering of a torsional wave from a small zone of material nonlinearity in a pipe is investigated. The analytical expression of the backscattered wave is obtained by using the reciprocity theorem, whose amplitude is determined by the nonlinearity coefficient and the size of the nonlinear region. Combining the primary wave with a higher frequency wave is proposed to increase the magnitude of the backscattered wave. Using the same method, we also investigate the intersection of two non-collinear waves at a region of quadratic material nonlinearity in an elastic layer in a three-

dimensional setting. Based on the mode expansions, the analytical solution to the amplitudes of the Lamb wave and the SH wave are obtained.

The theoretical models proposed in this dissertation and the obtained analytical solutions have the potential application in the design of novel acoustic devices and the development of nonlinear ultrasonic techniques for nondestructive evaluation.

Key words: Theoretical modelling; solitary waves; higher harmonics; asymptotic analysis; analytical solutions; soft bars; nonlinear media

摘要

随着超声波技术的不断发展，固体中非线性弹性效应对波传播的影响引起了大家广泛的关注。本文研究和发展考虑弹性非线性效应的材料和结构中波传播的理论模型，全文共分为两个部分：偏场作用下软杆中孤立波的研究和由对应微损伤的材料非线性所引起的高次谐波的研究。本文的主要内容可以概括如下。

在第一部分，我们对软杆中传播的孤立波的可调性进行了探索。在偏场（如偏置电场和预拉伸）作用下，软材料的有效材料常数会发生显著改变，由此我们研究了两种模型：第一是纵向电位移作用下的杆，第二是考虑了粘弹性效应的预拉伸杆。我们采用了渐近分析的方法，通过渐近展开，对杆的控制方程进行简化，同时杆的侧面边界条件得到渐近满足。对于第一个模型，推导了远场方程（即 KdV 方程），得到了一阶的电弹性孤立波解，并数值研究了偏置电位移和材料常数对孤立波的影响。结果表明，对于电弹性杆中给定振幅的孤立波，偏置电位移可以改变其速度。对于第二种模型，采用相似的求解方法推导得到了 KdV-Burgers 方程，从而获得了预拉伸作用下 Mooney-Rivlin 粘弹性杆中扭结波和类扭结波的显式解析解。研究发现，预拉伸不仅可以使扭结波变矮变宽，还可以改变其波速。同时，研究揭示了预拉伸和粘弹性效应对扭结波与类扭结波的影响之间的竞争机制。

在第二部分，为了获得由材料非线性引起的高次谐波的解析解，我们提出了可用于材料微损伤检测的几个相关的简化理论与简化模型。首先，一般性地研究了三次非线性弹性体中一维平面纵向与横向谐波，给出了一些有趣且实用的结果。然后，将工作拓展到各向同性不可压缩三次非线性半空间表面波的传播，以一种相对简单且规则的方法获得了累积三阶表面谐波的远场解析解，发现三次谐振波在远场处以经典的 Rayleigh 波速传播，其振幅随着传播距离的增加而线性增加。同时，研究了谐振波从非线性半空间透射到线性半空间的问题。在二次材料非线性管道中，利用壳理论获得了轴对称纵波和扭转波混频问题的解析解，具有差频的谐振波沿着与基频波相反的方向传播，通过进一步对非线性壳理论的简化，得到了纵波自相交作用产生的二阶

累积纵向谐波的解析解。从实际角度出发，还提出了一些理论模型用于研究由非线性夹杂产生的谐波，利用界面应力和位移的连续性条件或弹性动力学互易定理，可以得到反射波的表达式，其振幅包含了非线性介质的材料常数信息，并证明了互易定理的实用性。作为一个例子，研究了管道中扭转波对于材料非线性小区域的反向散射问题，利用互易定理得到了反向散射波的解析表达式，其幅度与非线性系数和非线性区域的大小相关。最后，还提出将基频波与更高频率波混合以增加反向散射波的振幅。使用相同的方法，还研究了三维弹性层中二次材料非线性区域的两条非共线入射波的相交问题，基于模态展开法，获得了 Lamb 波和 SH 波振幅的解析解。

　　本文提出的理论模型在新型声波器件的设计和非线性超声无损检测技术的开发方面具有潜在的应用价值。

关键词：理论建模；孤立波；高阶谐波；渐近分析；解析解；软杆；非线性介质

TABLE OF CONTENTS

LIST OF FIGURES

LIST OF TABLES

Chapter 1   Introduction

1.1   Background

Ultrasound is a useful and powerful tool to characterize defects or damages in materials and structures, especially their sizes, locations and properties. The linear ultrasonic technique relies on the measurement of wave velocity, attenuation and reflection and transmission coefficients. The principle of the linear ultrasonic technique is established within the frame of linear elasticity by the assumption of small deformation (linear strain-displacement relation) and linear material behavior (linear stress-strain relation).

However, modern science is undergoing profound evolution, and nonlinear science has been in a frontier field running through mathematical science, life science, space science and earth science. Recently, the researches about nonlinear ultrasound revive due to the rapid development of soft materials. The capacity of large deformation is an outstanding character of soft materials. Thus, the influence of nonlinearity on wave propagation in soft materials has to be considered.

On the other hand, the researches on nonlinear ultrasound become very active due to its potential application in the field of nondestructive field. Compared with the linear ultrasound, the nonlinear ultrasound is based on the nonlinear continuum theory by considering finite deformation (quadratic strain-displacement relation) and/or nonlinear material behavior (nonlinear stress-strain relation), which is more sensitive to microstructural damages, such as micro-cracks, plastic strains and dislocations, see Figs. 1.1 and 1.2. Figure 1.1 shows that nonlinear ultrasound is sensitive to the defects at the size from 1 nm to 1 μm, while the conventional ultrasound testing is only applicable to macroscopic defects. Figure 1.2 shows that the linear parameters almost keep unchanged, while the nonlinear ones increase quickly when the fatigue damages occur. Thus, the investigation of wave propagation, which takes geometrical and material nonlinearities into account, is of practical importance.
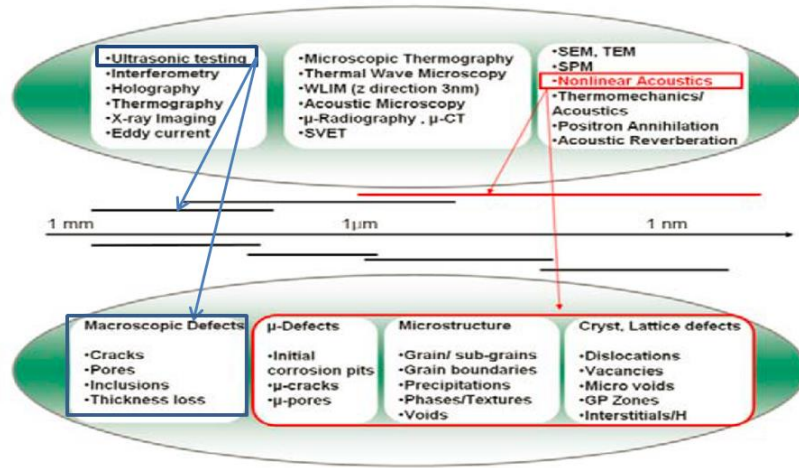
Fig. 1.1 Detectable defect size of various nondestructive and destructive methods for material characterization (Jhang, 2009)
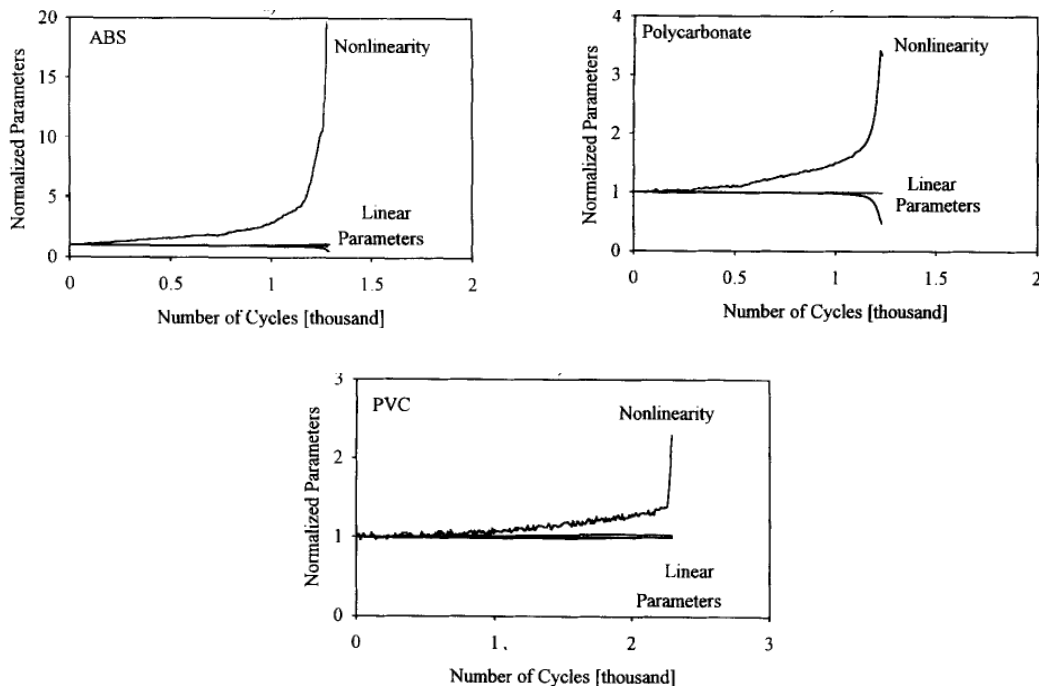
Fig. 1.2 Sensitivity of nonlinear parameters to micro-defects induced by fatigue load for three different materials (Nagy, 1998)

As a special solution to the nonlinear equations of wave motion, solitary wave is generated due to the balance between nonlinearity and dispersion or dissipation. The physical mechanism is that nonlinearity will increase the wave amplitude, while dispersion and dissipation will drop the wave amplitude. Solitary waves can propagate over a long distance without distortion. Significant progresses have been

made in the study of solitary waves related to internal water waves, nerve pulse dynamics, ion-acoustic waves in plasma, nonlinear optics, and so on.

Harmonic generation is another important solution to the nonlinear equations of wave motion. The effect of weak nonlinearity on a primary linear wave is the generation of higher harmonics which propagate at a frequency that is an integer times the frequency of the primary wave, and which may be resonant in the sense that the amplitude may increase linearly with the propagation distance.

Recently, the investigation of nonlinear elastic waves has attracted much academic attention due to a wide range of technical and industrial applications, such as geophysical exploration (Sinha and Winkler, 1999), soft tissue acoustics (Catheline et al., 2003), dynamics of elastomer (Sørensen et al., 1984), and some biomedical applications (Rudenko, 2007; Li et al., 2017). Actually, just as in fluid and gas dynamics, which have long been the kernel of the traditional nonlinear science, nonlinear effects are becoming increasingly critical in solid mechanics research (Jeffrey and Engelbrecht, 1994). Nondestructive evaluation is regarded as the most potential application of nonlinear ultrasound (Kim et al., 2006; Matlack et al., 2011). Compared with linear waves, nonlinear waves have some distinct and attracting properties. However, the analysis of nonlinear waves is more complicate than the linear one from the mathematical point of view.

Research topics about nonlinear elastic waves have been pursued for several decades. Abundant theories and experiments therefore have been proposed. However, the related techniques still have not been widely applied in engineering and industry. That's why we still need further investigations of nonlinear elastic wave propagation in terms of theory, simulation and experiment.

1.2   Wave propagation in soft materials

Soft materials such as gels, elastomers and tissues have attracted much attention due to their outstanding static and dynamic behaviors. The capability of reversible larger deformation is generally regarded as the most remarkable character of soft materials. The effective material properties of soft materials can be altered significantly when subjected to finite deformation. To describe the mechanical

behavior of soft material, general nonlinear theories of finite deformation have been developed. Two classic books written by Ogden (1997) and Holzapfel (2000) are recommended, both providing an excellent guidance to solve the problems related to soft materials subjected to finite deformation. The analysis of static and dynamic deformations can be conducted based on the approaches described therein.

As a special kind of soft solids, soft electroactive materials (such as dielectric elastomers) can change their shapes and mechanical properties under electric stimuli, which behave just like biological muscles, and hence they are often called artificial muscles. As a new kind of advanced functional materials, electroactive materials have many attractive characteristics, such as higher response speed, lower density and greater resilience (Bar-Cohen, 2002). Not surprisingly, they have triggered extensive research interests in recent years. It should be noted that the development of general nonlinear theories of electroelasticity dates back to the seminal works of Toupin (1956, 1963) and their systematic exploration and application can be found in the two monographs by Eringen and Maugin (2012) and by Maugin (2013), respectively. Recently, Dorfmann and Ogden (2005, 2010) presented a nonlinear framework for electroelasticity and investigated the superimposed linear waves in electroactive bodies under biasing fields.

In general, the theories about dynamic behavior of soft materials can be separated into "small-on-large" theory and "large-on-large" theory, which correspond to the linear and nonlinear theories of elastodynamics, respectively.

1.2.1 Constitutive relations

Many hyperelastic models have been proposed to describe finite deformation of elastic solids, which are generally expressed by the energy density function in terms of the invariants of the strain tensor and takes the geometrical nonlinearity and the material nonlinearity into account. For the large deformation of soft materials, such as rubber, whose strain may be up to more than 1000%, some empirical models are developed, whose coefficients are determined by experimental data fitting. Soft tissues are special soft materials. Some models are also set up, which is able to describe the outstanding characters of soft tissues.

The energy density can be expanded for finite deformation as

$$\rho_0 W = \frac{1}{2!} c_{ijkl} E_{ij} E_{kl} + \frac{1}{3!} c_{ijklmn} E_{ij} E_{kl} E_{mn} + \cdots \tag{1.1}$$

where c_{ijkl} and c_{ijklmn} are the second-order and third-order elastic constants, respectively, and E_{ij} are the components of the Lagrangian strain tensor. Specifically, if the terms higher than fourth-order are neglected, Eq. (1.1) can be reduced for isotropic materials to

$$\begin{aligned}
\rho_0 W &= \frac{\lambda}{2}(\mathrm{tr}\mathbf{E})^2 + \mu\,\mathrm{tr}\mathbf{E}^2 + \frac{C}{3}(\mathrm{tr}\mathbf{E})^3 + B(\mathrm{tr}\mathbf{E})\,\mathrm{tr}\mathbf{E}^2 + \frac{A}{3}\mathrm{tr}\mathbf{E}^3 + E(\mathrm{tr}\mathbf{E})\,\mathrm{tr}\mathbf{E}^3 \\
&\quad + F(\mathrm{tr}\mathbf{E})^2\,\mathrm{tr}\mathbf{E}^2 + G\left(\mathrm{tr}\mathbf{E}^2\right)^2 + H(\mathrm{tr}\mathbf{E})^4
\end{aligned} \tag{1.2}$$

where λ and μ are Lamé's constants, A, B and C are the third-order elastic constants introduced by Laudau and Lifshitz (1986), and E, F, G and H are the fourth-order elastic constants. For incompressible materials, Eq. (1.2) can be reduced to (Hamilton et al., 2004; Destrade and Ogden, 2010a)

$$\rho_0 W = \mu\,\mathrm{tr}\mathbf{E}^2 + \frac{A}{3}\mathrm{tr}\mathbf{E}^3 + G\left(\mathrm{tr}\mathbf{E}^2\right)^2 \tag{1.3}$$

The condition of incompressibility simplifies the constitutive relation greatly. Equation (1.3) can be used to investigate shear wave motions in incompressible soft materials. For rubbery materials, the constitutive relations are generally treated by statistical mechanics or continuum mechanics, wherein the material constants are usually determined by experimental data fitting. Excellent reviews on statistical mechanics models have been given by Treloar (1975) and Boyce and Arruda (2000), in which the nonlinear stress-stretch behaviors of 3-chain, 4-chain, 8-chain and full-network models were compared with each other. The continuum mechanics model is proposed based on the basic principles and in particular the principle of material frame-indifference. For an isotropic hyperelastic material, the strain energy density function can be described by three invariants. Neo-Hookean model, Mooney-Rivlin model, Yeoh model and Ogden model are all developed based on continuum mechanics for different kinds of rubbery materials under different loading conditions.

Neo-Hookean model:

$$W = C_{10}(I_1 - 3) + \frac{1}{D_1}(J-1)^2 \tag{1.4}$$

Mooney-Rivlin model:

$$W = C_{10}(I_1 - 3) + C_{01}(I_2 - 3) + \frac{1}{D_1}(J-1)^2 \tag{1.5}$$

Yeoh Model:

$$W = \sum_{i=1}^{3} C_{i0}(I_1 - 3)^i + \sum_{i=1}^{3} \frac{1}{D_i}(J-1)^{2i} \tag{1.6}$$

Ogden Model:

$$W = \sum_{i=1}^{N} \frac{2\mu_i}{\alpha_i^2}(\bar{\lambda}_1^{\alpha_i} + \bar{\lambda}_2^{\alpha_i} + \bar{\lambda}_3^{\alpha_i} - 3) + \sum_{i=1}^{N} \frac{1}{D_i}(J-1)^{2i} \tag{1.7}$$

where λ_i are the principal stretches and $\bar{\lambda}_i = J^{-1/3}\lambda_i$, $J = \lambda_1\lambda_2\lambda_3$, μ_i, α_i, D_i and C_{ij} are the material constants, I_1 and I_2 are the invariants of the strain tensor, which are given by

$$I_1 = \text{tr}\mathbf{c}, \quad I_2 = \frac{1}{2}\left[(\text{tr}\mathbf{c})^2 - \text{tr}(\mathbf{c}^2)\right] \tag{1.8}$$

where $\mathbf{c}$ is the right Cauchy-Green strain tensor. The comparison between different hyperelastic models has been made in detail by Ali et al. (2010). These models can be reduced to the ones suitable for incompressible materials by making use of the condition of incompressibility, some of which were given in Kim et al. (2012).

For many soft tissues, the strain-hardening effect should be taken into consideration. Fung model and Gent model have been proposed to capture this effect for soft tissues (Goriely, 2017). When material incompressibility is taken into consideration, the two models are mathematically expressed as

Fung model:

$$W = \frac{\mu}{2\beta}[\exp(\beta(I_1 - 3)) - 1] \tag{1.9}$$

where $\beta > 0$ is a material constant which controls the strain-hardening property.

Gent model:

$$W = -\frac{\mu}{2\beta}\log[1 - \beta(I_1 - 3)] \tag{1.10}$$

The neo-Hookean model is obtained in the limit $\beta \to 0$, either from Eq. (1.9) or Eq. (1.10). The elastic coefficients of soft tissues in these models should be determined via experimental data fitting. The assumption of incompressibility is often taken for soft materials. However, the effects of compressibility may be important in certain applications (Bischoff, 2001).

Viscoelasticity is another outstanding character of soft materials. The dissipation term has to be added into the strain density function when we consider dissipative wave motion in soft materials. In the past thirty years, Landau and Lifchitz model (Landau and Lifchitz, 1986, p. 107) has been widely used in the field of physical acoustics by adding the elastic stress tensor a "viscosity stress tensor", which is given by

$$\boldsymbol{\sigma}' = \left(\zeta - \frac{2}{3}\eta\right)\dot{E}_{ll}\mathbf{I} + 2\eta\dot{\mathbf{E}} \tag{1.11}$$

where $\eta > 0$ and $\zeta > 0$ are the shear and bulk viscosity coefficients, respectively, $\mathbf{I}$ is the unit tensor, and the superposed dot of the Lagrangian strain tensor $\mathbf{E}$ denotes the time derivative. Unfortunately, it is physically wrong for at least two reasons (Destrade et al., 2013). One reason is that the first Piola-Kirchhoff stress tensor $\boldsymbol{\sigma}$ is not symmetric while $\dot{\mathbf{E}}$ is symmetric, which will lead to inconsistence of the equation. Another reason is that $\dot{\mathbf{E}}$ is frame-invariant, while $\boldsymbol{\sigma}$ is not, so that the expression of total stress is not subjective. The corrected form of the viscous part of the first Piola-Kirchhoff stress tensor $\boldsymbol{\sigma}$ is

$$\boldsymbol{\sigma}' = \left(\zeta - \frac{2}{3}\eta \right) \mathbf{F}\mathrm{tr}(\mathbf{bd}) + 2\eta\mathbf{bdF} \tag{1.12}$$

where $\mathbf{F}$ is the deformation gradient tensor, $\mathbf{b}$ is the left Cauchy-Green strain tensor and $\mathbf{d}$ is the Eulerian stretching tensor. For incompressible materials, we have (Destrade et al., 2013; Destrade and Saccomandi, 2005)

$$\boldsymbol{\sigma}' = 2\eta\mathbf{d} \tag{1.13}$$

Soft electroactive materials are smart soft materials, which can be used as actuators, see Fig. 1.3. As the most remarkable character, the capacity of large deformation of soft electroactive materials under electric stimulus has gained an extensive academic interest. To predict the behavior of electroactive materials and to aid the design of devices, it is necessary to develop a general theory of nonlinear electroelasticity to understand the electro-mechanical coupling effects, especially the constitutive relations which describe the material properties based on experimental data fitting (Dorfmann and Ogden, 2017). Dorfmann and Ogden have conducted a series of researches on the nonlinear theory of electroelasticity (2005), the associated incremental equations (2010) and a theoretical framework of boundary value problems for electro-sensitive elastomers (2006).
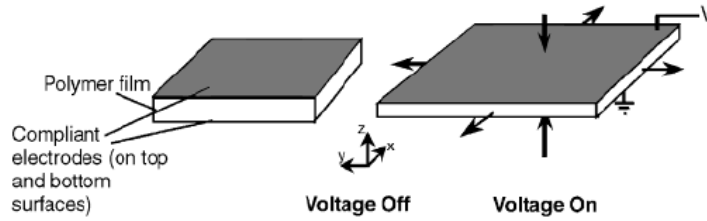
Fig. 1.3 Electroelastic actuator (Pelrine et al., 2000a)

The energy density function for electroactive materials can be separated into two parts: one part represents the contribution from pure elasticity and another part represents the electro-mechanical coupling. For example, the model considering the electro-mechanical coupling used by Dorfmann and Ogden (2010) generalizes the well-known neo-Hookean model, and it is given by

$$\Omega = \frac{1}{2}\mu(I_1 - 3) + \frac{1}{\varepsilon_0}(\alpha I_4 + \beta I_5) \tag{1.14}$$

where

$$I_4 = \mathbf{E}_l \cdot \mathbf{E}_l, \quad I_5 = \mathbf{E}_l \cdot (\mathbf{c}\mathbf{E}_l) \tag{1.15}$$

where $\mathbf{E}_l$ is the nominal electric field tensor. The following energy density function for electroactive materials is known as the generalized Mooney–Rivlin model:

$$W(\lambda_1, \lambda_2, \lambda_3, D) = U(\lambda_1, \lambda_2, \lambda_3) + V(\lambda_1, \lambda_2, \lambda_3, D) \tag{1.16}$$

where

$$U = \frac{C_1}{2}(\lambda_1^2 + \lambda_2^2 + \lambda_3^2 - 3) + \frac{C_2}{2}(\lambda_1^{-2} + \lambda_2^{-2} + \lambda_3^{-2} - 3), V = \frac{D^2}{2\varepsilon(\lambda_1, \lambda_2, \lambda_3)}\lambda_1^{-1}\lambda_2^{-1}\lambda_3 \tag{1.17}$$

The dielectric constant ε_0 in Eq. (1.14) is independent of deformation, which is appropriate for ideal dielectric materials. The nominal strain-stress and strain-electric field relation can be obtained through the differential of the energy density function. Due to the advantages of mathematical simple structure, the above energy density functions have been widely used to study the mechanical behaviors of soft solids and characterize material properties.

1.2.2 Wave propagation of small amplitude superimposed on finite pre-deformation

In some important cases, elastic wave can be viewed as an incremental motion superimposed on static finite deformation of soft materials. In general, the elastic waves propagating in pre-stretched or pre-stressed bodies are studied within the linear theory of elastodynamics when their amplitudes are small. The small-on-large motion can be accurately described by the linearized theory of the general nonlinear elasticity. The underlying pre-stretch and/or pre-stress is the most popular and effective mechanical means to modulate the wave propagation in soft materials, such as the wave velocity.

Due to the significant influence of pre-stretch on wave propagation, this research topic has attracted intensive academic interest. The history of the research on elastic waves in pre-stressed bodies dates back to Cauchy during 1822-1828 (Guz,

2002). The important breakthroughs have been made by Biot, Hayes and Rivlin, Chadwick and Jarvis, and Ogden and Sotiropoulos (Chen and Dai, 2012). Biot (1940) presented a rigorous solution to the problem of wave propagation in an elastic continuum when the influence of the initial stress is taken into account. It is shown that a uniform hydrostatic pressure does not change the laws of wave propagation. Hayes and Rivlin (1961) applied the theory of small-on-large deformations in an isotropic elastic material to study the propagation of a plane wave of small amplitude in an infinite material subjected to a static, homogenous deformation. Chadwick and Jarvis (1979) investigated the surface wave motion on a half-space subjected to pre-stress. The main results are a general uniqueness theorem and the notation of a neutral set, bounding the domain of existence of surface waves and interpretable as the totality of standing wave solutions. The reflection of homogeneous plane waves from a plane boundary in an incompressible isotropic elastic solid was investigated by Ogden and Sotiropoulos (1996) considering the influence of pre-stress and finite strain. They claimed the theoretical model can be used to characterize the material properties, the finite deformation and the associated pre-stress. The topics of elastic wave propagation in structures, like cylinders, pipes and plates, also arose extensive research interest. Belward and Wright (1987) studied small-amplitude waves propagating in a cylinder of pre-stressed Mooney material using analytical and computational techniques. Significant qualitative and quantitative differences were observed when the pre-deformation varies. Shearer et al. (2013) considered the torsional wave propagation in a pre-stressed annular cylinder of an incompressible material subjected to hydrostatic pressures acting on the inner and outer surfaces. The pressure difference creates an inhomogeneous deformation field along the radial direction, which makes the coefficients of the governing ordinary differential equation spatially varying and affects the location of the roots of the dispersion relation. The dispersion relation was then determined by using an approximate procedure (the Liouville-Green transformation). Rogerson and Fu (1995) investigated the propagation of small-amplitude travelling waves in a pre-stressed, incompressible elastic plate of finite thickness by using the asymptotic analysis; the asymptotical expansions for the wave speed as a function of wavenumber and pre-stress were obtained. Zhou et al. (2017) investigated wave propagation on a finitely pre-deformed elastic half-space

overlain by a thin coating layer (or surface film). The comprehensive reviews on small-amplitude wave propagation in pre-deformed materials were given by Guz (2002) and Akbarov (2007). Recently, the pre-stretch was also used to control the wave propagation in soft periodic structures by Huang et al. (2014) and Chen et al. (2017). Galich et al. (2017) analyzed the elastic wave propagation in highly deformable layered media and the band gap structures were calculated for the periodic laminates.

In addition to the mechanical manner like pre-stretch, the underlying electric field is another effective method to modulate the dynamic behavior of electroactive materials. The electro-elastic coupling effect has been widely used in acoustic sensors and actuators due to the rapid development of soft electroactive materials (Pelrine et al., 2000a, 2000b). The investigations related to the small-amplitude wave propagation in electroactive materials have been revived in recent years. Based on nonlinear theory of electroelasticity and the associated linear incremental equations (Dorfmann and Ogden, 2005, 2006, 2010b), the wave propagation in a soft electroactive cylinder subjected to a finite deformation in the presence of an electric biasing field was studied by Chen and Dai (2012). Su et al. (2016) extended Chen and Dai's work to the non-axisymmetric case by considering the wave propagation in an infinite soft electroactive hollow cylinder under uniform biasing fields like an axial underlying electric displacement and an axial pre-stretch. These researches uncovered the significant influence of initial deformation and electric field on wave propagation in soft electroactive materials. The Rayleigh-Lamb wave propagation in dielectric elastomer layers subjected to large deformations was investigated by Shmuel et al. (2012). The underlying deformation is induced by biasing electric field and pre-stretch, which can be used to control the phase velocities and frequencies. Shmuel and deBotton (2013) studied the axisymmetric waves in dielectric elastomer tubes under inhomogeneous biasing field produced by different voltages inserted on the outer and inner surfaces. For the same model, Wu et al. (2017) investigated the guided circumferential waves by making use of the state-space method. Galich and Rudykh (2016) analyzed the influence of external electric stimuli on the pressure and shear wave propagation in dielectric elastomers. Due to the tunability of material properties of soft electroactive materials like

dielectric elastomers, related theoretical models of periodic structures or metamaterials have been established. The thickness vibrations of a finitely deformed infinite periodic laminate composed of two layers of dielectric elastomers were studied by Shmuel and deBotton (2012), whose study indicates that the band gaps can be modulated by the electric field. Then, Shmuel (2013) extended their work to a two-dimensional system by investigating the band structure for electroelastic waves of anti-plane mode propagating in finitely strained circular fiber-reinforced composites with square lattice. Following their works, the nonlinear theory of electroelasticity and the associated incremental equations have also been applied to the investigation of wave propagation in periodic structures made of electroactive materials. Wu et al. (2018) showed that the combination of large deformation and electromechanical coupling can be a very flexible and efficient way to tune the band gaps of a phononic cylinder of soft electroactive elastomer with periodic electric boundary conditions. The concept of manipulating waves in a dielectric elastomer film by voltage was demonstrated experimentally by Ziser and Shmuel (2017). However, it should be pointed out that there is a lack of enough experimental results of wave propagation in electroactive materials at present. Also, the theoretical models have been proposed based on a series of approximations, such as the neglecting of viscoelastic effect, which should be a very important factor in the analysis of soft materials.

1.2.3　Solitary waves

The waves having finite amplitude propagating in elastic or electro-elastic materials have to be analyzed within the frame work of nonlinear theory of elastodynamics, which are often called nonlinear waves. As a special kind of nonlinear waves, solitary waves can propagate over a long distance without distortion. The solitary waves were first observed in the field of fluid mechanics in 1834 by John Scott Russell. In 1895, this fascinating phenomenon was successfully interpreted by Korteweg and de Vries who developed the well-known KdV equation. Since then, problems related to solitary wave propagation have been widely investigated. The solitary waves can cross each other without any distortion. Thus, such waves are often called solitons. Due to their remarkable characters, solitary waves are a subject of considerable interest in many fields. In the field of

superconductivity, the flux quantum in Josephus effect is actually soliton which has been used to develop the new computers with lower power and higher speed. In the field of biology, the investigation of propagation of soliton in protein may explain the mechanism of the contraction of muscle. McDonald (1974) measured the simultaneous changes in amplitude and profile of the flow and pressure waves at five sites from the ascending aorta to the saphenous artery in a dog. The features of the pulse wave such as "peaking" and "steepening" can be interpreted from the viewpoint of solitary waves, see Fig. 1.4.
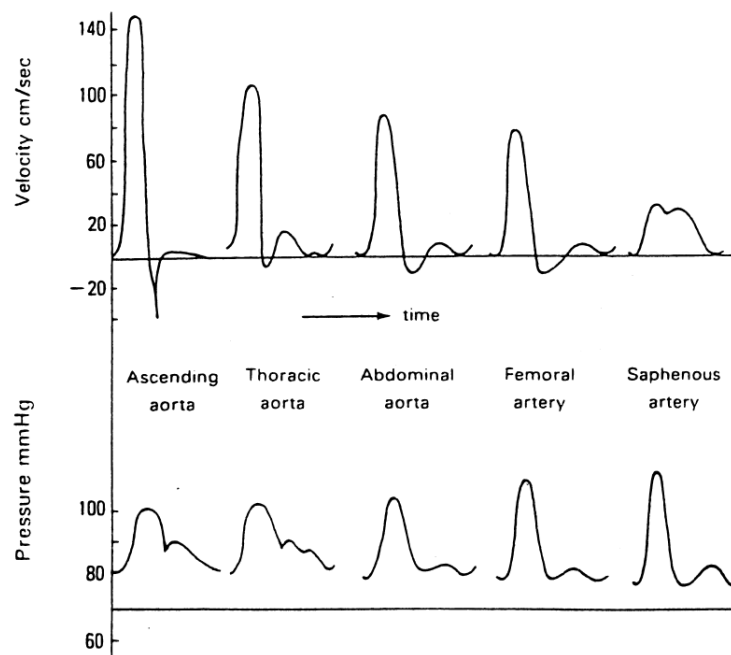
Fig. 1.4 A diagrammatical comparison of the behavior of the flow velocity and pressure pulses from the ascending aorta to the sapheneous artery (Demiray and Dost, 1998)

The pulse waves of blood pressure and flow in large arteries have widely been described as solitary waves (Choy, 2013). One of the successful application of soliton is optical soliton propagating in optical fiber. When the power increases, the nonlinearity has to be considered and the soliton forms, see Fig. 1.5. Their advantages include lower dissipation and higher bit ratio. With the development of high-resolution optical methods for wave detection, solitary waves have also been

observed experimentally in elastic solids (Samsonov and Maugin, 2001; Wu et al. 1987).
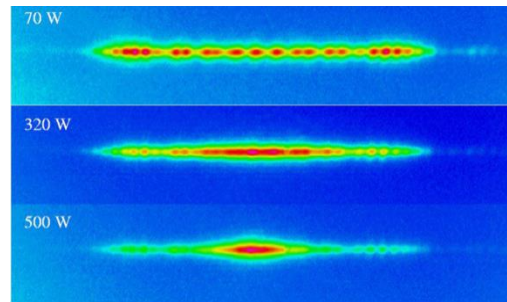
Fig. 1.5 Optical soliton (Copyright 1998 American Physical Society)

There are many excellent theoretical works on solitary waves in solids. Among them, the investigation of solitary waves in rods has gained a particular popularity due to the simple one-dimensional geometry. Nariboli (1970) studied nonlinear longitudinal dispersive waves in compressible elastic rods. Wright (1981) studied nonlinear axisymmetric waves that propagate axial-radial deformation and proved the existence of solitary waves and periodic waves in circular rods. In 1984, Soerensen et al. (1984) numerically investigated the interaction between solitary waves. Wright (1985) pointed out the existence of a large number of traveling wave solutions in rods composed of incompressible materials. In 1990, Coleman and Newman (1990) derived a one-dimensional (1D) equation from the three-dimensional (3D) theory and obtained explicit results for incompressible neo-Hookean materials. Dai and Huo (2002), without using the Navier-Bernoulli hypothesis, established asymptotically valid one-dimensional rod equations, which are consistent with the lateral boundary conditions. Besides, Yong and LeVeque (2003) investigated the longitudinal elastic strain solitary waves in a one-dimensional periodically layered medium. Maugin (2007) studied the possibilities of existence of solitary surface waves travelling over a substrate. Dai et al. (2000) studied analytically the interaction of two solitary waves in a circular cylindrical rod. By using the method of coupled series-asymptotic expansions, Dai and Peng (2011) investigated wave propagation in a pre-stretched Blatz-Ko cylinder and concluded that a variety of waves can arise, including solitary waves and kink waves. A detailed review on the study of solitary wave in solids can be referred to the paper of Maugin (2011). For nonlinear waves propagating in bodies with multi-field coupling,

Xue et al. (2011) made an important step by investigating solitary waves in a magneto-electro-elastic circular rod.

The above mentioned solitary waves are usually generated due to the balance between nonlinearity and dispersion. However, dissipation is always present in a realistic situation. There are also many works in the field of nonlinear waves in solids considering the effect of dissipation. Destrade et al. (2009) studied the nonlinear shear waves propagating in viscoelastic materials whose generation is directly linked to the nonlinear viscosity term. Hayes and Saccomandi (2000, 2004) studied the propagation of finite-amplitude shear waves in Mooney-Rivlin viscoelastic materials maintained in the static state of a pure homogenous deformation. Destrade and Saccomandi (2004) then extended to the case of inhomogeneous plane waves. They also studied the interaction of a longitudinal wave with a transverse wave in viscoelastic materials (Destrade and Saccomandi, 2005). Zabolotskaya et al. (2004) developed an evolution equation for nonlinear shear waves in soft isotropic solids with viscous dissipation. As is well–known, the combination of nonlinearity, dispersion and dissipation may lead to the generation of kink-shaped solitary waves or simply kink waves (Porubov, 2003).

For soft elastic or electroactive materials, applying a mechanical or electric biasing field can conveniently modulate their effective properties and the corresponding dynamic behaviors. However, there are few works on nonlinear waves in pre-stretched structures composed of viscoelastic materials and especially few works on solitary waves propagating in soft electroactive materials.

1.3   Nonlinear ultrasonic technique and its' application

Since the linear ultrasonic technique is insensitive to microstructural damages or material degradations, such as micro-cracks, plastic strains and dislocations, the nonlinear ultrasonic technique has been then developed, which is based on the nonlinear theory. The materials which have micro-defects or degradation behave remarkably in a nonlinear manner. The level of the damage has a strong correlation with the nonlinear material constants, i.e. higher order elastic constants. To measure the material nonlinearity, various ultrasonic methods have been proposed, including

the so-called acousto-elastic effect, which is based on the measurement of the variation of propagation velocity with the applied strain, just like the case discussed in Section 1.2.2. One problem of this technique is the difficulty in measuring the small changes in propagation time and distance accurately enough to allow the velocity to be determined (Croxford et al, 2009). The second and perhaps most widely reported method to measure the material nonlinearity is the harmonic generation technique. The drawback of the harmonic generation technique is that it is hard to separate the underlying system nonlinearity from the material nonlinearity. To avoid such interferences, the mixing wave technique has been proposed, which includes collinear and non-collinear mixing wave techniques (CMWT and NCMWT).

1.3.1 Harmonics generated by quadratic and cubic nonlinearities

(a)   (b)
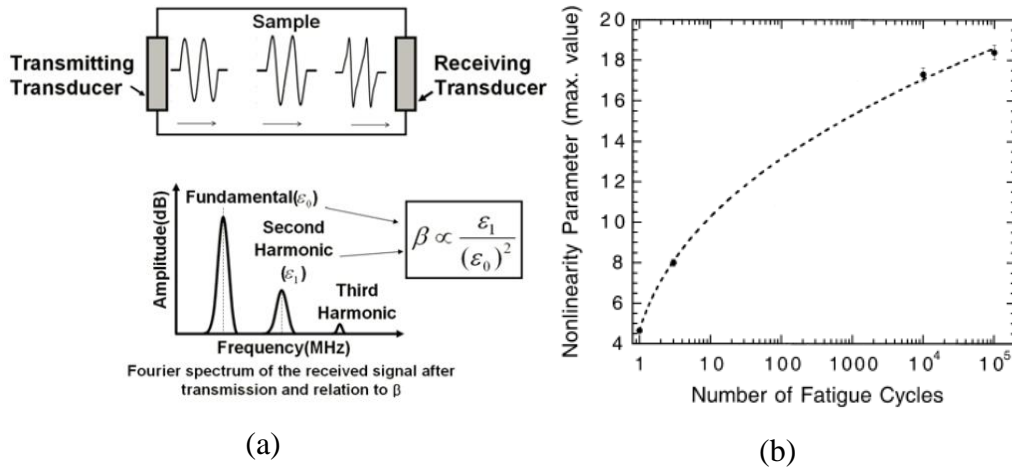
Fig. 1.6 Nonlinear ultrasonic characterization of fatigue microstructures, (a) distortion in the waveform by the elastic nonlinearity, (b) the value of measured nonlinearity parameter as a function of number of fatigue cycles for aluminum alloy 2024-T4 (Cantrell and Yost, 2001)

In recent years, utilization of harmonic generation to interrogate material nonlinearity has been widely reported. Higher harmonics are generated by the distortion of waveform of the incident wave by the nonlinear response of elastic solids, see Fig. 1.6. The resulting amplitudes of higher harmonics are related to the nonlinearity parameter, such as the expression of β.

Experimental observations and an associated theory about the generation of second harmonics due to the presence of dislocations in solids were presented by Hikata and co-authors (Hikata et al., 1965; Hikata et al., 1966; Hikata and Elbaum, 1966). A direct correlation between material nonlinearity and the level of plasticity in metal specimens was experimentally observed by Pruell et al. (2007) using higher harmonic generation by Lamb waves. Cantrell and Yost (2001) carried out experimental measurements to show a monotonic increase of nonlinear material constants with the number of fatigue cycles, see Fig. 1.6. Kim et al. (2006) developed a robust experimental method to enable a repeatable measurement of second harmonics. Frouin et al. (1999) successfully carried out a real time experiment using second harmonics to track the entire fatigue life of a dog-bone specimen. Deng et al. (2005) and Zhang et al. (2014) made experimental observations of second harmonic generation of Lamb waves in an elastic plate and in long bones. Bermes et al. (2007) developed an effective procedure to measure the nonlinearity of metallic plates using second harmonics.

Some theoretical works about the generation of second harmonics have been reported. Ten possible nonlinear elastic wave interactions described on the basis of three third-order elastic constants were presented by Korneev and Demcenko (2014). All other possible interactions out of 54 combinations were proven to be prohibited. One of the outstanding features of higher harmonics is the cumulative behavior because their amplitudes increase with the propagation distance. The self-interaction or mutual interaction of shear waves in the region of quadratic nonlinearity gives the generation of longitudinal waves, which propagate with the shear wave velocity.

Although higher harmonics in non-dispersive media have attracted wide attention, including experimental, numerical and analytical studies (Gol'dberg, 1961; Bender et al., 2013; Matlack et al. 2015), there are few investigations of higher guided harmonics in dispersive structures like pipes and rods. Due to the dispersion of guided waves, which will lead to frequency-dependent phase velocities and multi-modes, the analysis of harmonics in wave guides becomes quite complex. Recent investigations about the generation of higher guided harmonics have been made by Deng (1998, 1999), Pau and Scalea (2015) and de Lima and Hamilton (2003) by using the method of normal mode expansion. De Lima and Hamilton (2005) adopted

perturbation and modal analysis together with numerical simulation to calculate the second harmonics propagating in cylindrical rods and shells. Liu et al. (2014a, 2014b) proposed a generalized method and used a numerical approach to analyze the cumulative nature and the physical interpretation of the generation of higher harmonics in hollow circular cylinders. Liu et al. (2013a) formulated a mode selection method to consider strong higher harmonics and then simulated the interaction of torsional and longitudinal waves in nonlinear circular cylinders. Nonlinear finite element models have been adopted to analyze the cumulative second harmonics in plates and shells by Liu et al. (2013b). Chillara and Lissenden (2013) used a large radius asymptotic solution to analyze second harmonics in pipes. They concluded that only asymptotic symmetric modes can be efficiently generated from primary axisymmetric longitudinal modes.

Surface harmonic generation on a half-space has received considerable attention, but adequate theoretical results have been lacking. Early theoretical results were developed by Kalyanasundar (1981) and Kalyanasundar et al. (1982) by using the method of multiple scales. However, there are certain serious limitations to Kalyanasundar's investigations, which were pointed out by Lardner (1983). As an improvement of Kalyanasundar's analysis, Lardner gave a more complete investigation on nonlinear surface wave propagation. Tiersten and Baumhauer (1974, 1985) studied the second harmonic generation of surface waves in piezoelectric solids. Harvey et al. (1992) investigated the propagation of nonlinear surface acoustic waves in anisotropic solids, and numerical results along the particular propagation direction for magnesium oxide, copper and nickel were obtained. An experimental investigation of second harmonic propagation in metallic specimens was made by Herrmann et al. (2006). They showed a linear increase of the amplitude of a second harmonic surface wave with the increase of propagation distance. The theoretical model used in their paper is directly related to those for longitudinal waves and the nonlinearity parameter is assumed to be same as the nonlinearity parameter of a longitudinal wave. This model was also adopted by others to interpret their experimental observation (Zeitvogel et al., 2014; Walker et al., 2012), and though it is much simpler than the results mentioned above, this model lacks adequate theoretical validation.
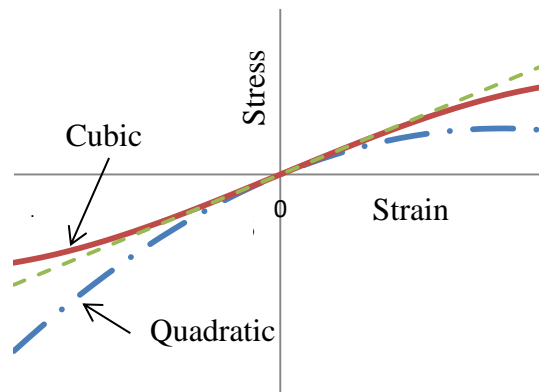
Fig. 1.7 Linear stress-strain relation and stress-strain curves for the quadratic and cubic nonlinearities

The above mentioned references show that second harmonics have been frequently employed to measure the nonlinearity of materials. The quadratic terms cause, however, non-symmetry in the stresses with respect to the origin of zero stresses.

Comparing with second harmonics, third harmonics have been less often investigated. A mathematical model was employed by Liu et al. (2013a) to predict the cumulative behavior of third harmonics. The increase of the amplitude of third harmonic with the plastic strain has been experimentally confirmed by Lissenden et al. (2014). Rénier et al. (2008) presented an experimental setup to measure the fourth-order elastic constants for shear deformation. Chillara and Lissenden (2016) proposed a new constitutive model for third harmonic generation in elastic solids. It appears that no mathematical model has yet been proposed to obtain the analytical approach to the generation of third harmonics. The main advantages of third harmonics over second harmonics are that in contrast with a quadratic nonlinearity, a cubic nonlinearity of the constitutive relation is more generally applicable, see Fig. 1.6. This figure shows that, for both quadratic and cubic nonlinear behavior, a positive strain requires a smaller stress than for the linear stress-strain relation. On the other hand, for quadratic behavior, a negative strain requires a negative stress whose absolute value is larger than for the linear stress-strain relation. This behavior which happens for some materials is referred to as the strength differential effect, see Hirth and Cohen (1970), Gil et al. (1999) and Rauch and Leslie (1972) for the

corresponding curves for tensile and compressive strain. It has been shown that dislocation dynamics can be more effectively studied by third harmonics (Hikata and Elbaum, 1966). Experimental results have confirmed the sensitivity of third harmonics to dislocation density and loop length (Hikata et al., 1966). There are also materials that show quadratic nonlinearity (Hirth and Cohen, 1970; Gil et al., 1999). The drawback of third harmonic is its smaller amplitude and higher damping.

1.3.2 Mixing wave technique

To avoid the interference from underlying system nonlinearity, the mixing wave technique has been developed. The outstanding character of this technique is that the frequency of the mixing wave is selectable, which is the sum or difference frequencies of the incident waves. Another important advantage of the mixing wave technique over the harmonic generation technique is the spatial selectivity that the nonlinear interaction is only limited to the region where the incident beams intersect (Croxford et al., 2009). For the collinear mixing wave, the position of the intersection region is figured out by making use of the wave velocity and the propagation time. The nonlinearity parameters for various elastic solids were measured by applying the CMWT by Jacob et al (2003). Experimental measurements were conducted by Liu et al. (2012) to demonstrate that the CMWT is capable of measuring the plastic strain in A1-6061 Alloys. Ju et al. (2017) measured the nonlinearity parameter by using the collinear mixing wave in concrete. The sensitivity of the wave speed and attenuation to the damage induced by alkali-silica reaction was proven to be lower than the sensitivity of nonlinearity parameter to the same damage. Tang et al. (2014) used the collinear mixing of shear and longitudinal waves to detect the localized plastic strain. When the frequencies of a pair of collinear shear and longitudinal waves satisfy the resonant condition, mixing of these two primary waves generates a resonant shear wave propagating in the opposite direction of the propagation direction of the primary shear wave. Hills et al. (2006a, 2006b) and Courtney et al. (2010) developed a special CMWT for global crack detection in structures by employing bispectral analysis. The bispectral was shown to be particularly useful in exacting the nonlinearity related to phase coupling. This method was also used by Jiao (2014) to process the nonlinear response of the samples to continuous excitation at two frequencies when they detected the fatigue

cracks by using the CMWT. All of these researches indicate that CMWT is a promising method for nondestructive assessment. Illustration of CMWT is shown in Fig. 1.8. The amplitudes of the waves with the frequencies of f_0-f_1 and f_0+f_1 are directly related to the defect properties.
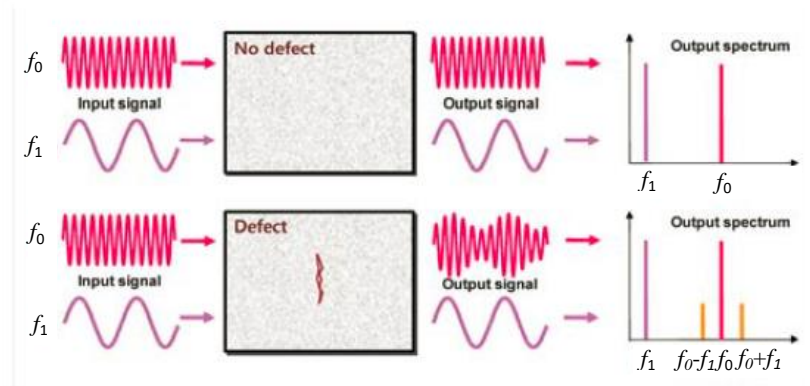
Fig. 1.8 Illustration of collinear mixing wave technique (Jhang, 2009)

Compared with CMWT, the intersection region can be determined directly through a geometrical means for NCMWT in an easier way. Illustration of NCMWT is given by Fig. 1.9. NCMWT was verified on the measurement of laboratory and field PVC test speciments by Demcenko et al. (2012). Their results confirmed that NCMWT is suitable to estimate the physical ageing state of PVC. Demcenko et al. (2014) presented an experimental non-collinear wave mixing for testing of polymers by using an immersion method. It was shown that this technique is an effective monitoring and scanning means when applied to thermoplastic ageing, epoxy curing, and nondestructive testing. Croxford et al. (2009) experimentally confirmed the sensitivity of NCMWT to plasticity and fatigue damage and the potential application to be used as a nondestructive testing technique. The deviation of the incident angle of mixing wave has an important influence on NCMWT. NCMWT was applied by Blanloeuil and Meziane (2015) for detection and characterization of closed cracks. They uncovered that the angle of incidence of the shear waves can be used to optimize the method. The relationship between the acoustic nonlinearity parameter and the incident angle was investigated by Sun et al. (2018) by making use of numerical simulation and experimental measurements for the non-collinear mixing of two shear waves. The lack of theoretical investigation for NCMWT, especially for the waves intersecting in structures, should be noted.
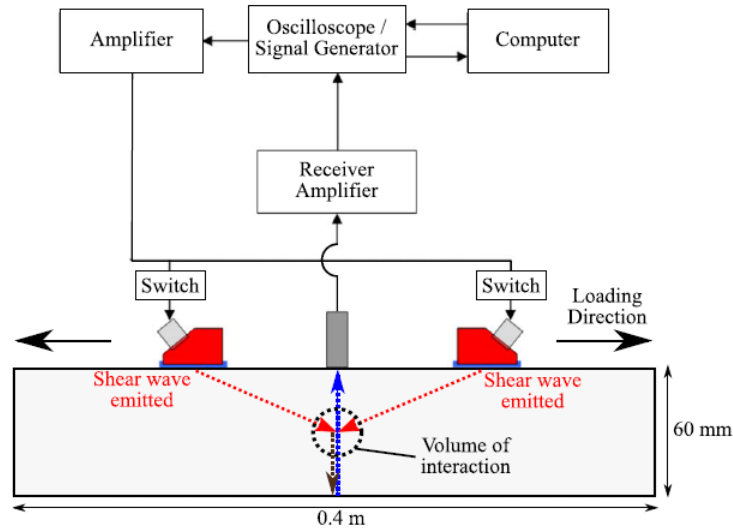
Fig. 1.9 Illustration of NCMWT (Croxford et al., 2009)

1.3.3 Scattering and reflection from a region of nonlinear material

The whole body of nonlinear material behavior is generally assumed in most published papers. From the practical point of view, the reflection, transmission and scattering of incident waves from an inclusion of nonlinear material behavior are of obvious interest. Recently, the research topics related to the interaction of elastic waves with the local region of nonlinear material behavior start to arise academic attentions. Tang et al. (2012) investigated the scattering of an incident longitudinal wave from a region of spatially-dependent quadratic nonlinearity. The scattering of elastic waves from a heterogeneous inclusion of nonlinearity contained in a linear host material was investigated by Kube (2017). For the two papers mentioned above, the geometrical nonlinearity was only assumed in the local region, which is thought to be unreasonable. For the problem of scattering from the nonlinear region, the assumption that only material nonlinearity exists in the local region without considering the geometrical nonlinearity may be more comprehensible. However, it should be noted that even very small imperfections can produce very significant excess nonlinearity which can be orders of magnitude higher than the intrinsic nonlinearity of the intact material (Nagy, 1998). So the excess material nonlinearity can be dominant over the geometrical nonlinearity and the instinct material nonlinearity and these two results will be approximately equal.

One of the most important applications of the wave reflection from nonlinear region is to measure the imperfect bounded interface. The nonlinear reflection of bulk waves from an interface between two solids of quadratic nonlinearity were reported by Zhou and Shui (1992). An experimental investigation was presented by Donskoy et al. (2001) to observe the modulation effect of highly nonlinear material behavior caused by weakly or incompletely bounded interfaces. Second harmonics were used by Richardson (1979) and Biwa et al. (2004) to analyze the contact acoustic nonlinearity of the interface between two linear elastic media. In their papers, the nonlinear stiffness property of the interface was described as a function of the nominal contact pressure. Achenbach et al. (1989) expressed the failure of an adhesive bond by a cubically nonlinear elastic model. In that case the strength of the adhesive bond can be directly measured from the reflected waves. The approach suggested by Achenbach et al. (1989) was extended by Nagy et al. (1990) to take the thickness of the adhesive bond into consideration. Zhang et al. (2016) made use of the intersection of two non-collinear shear waves at an imperfect interface to assess the bond quality. These authors claimed that their acoustic technique can avoid other forms of nonlinearity aroused by the system. For simplicity, the interfaces or adhesive bonds studied above were frequently modeled by nonlinear springs.

The investigations of scattering or reflection from local region of nonlinear material behavior, which is used to model micro-damages or material degradations, have not attracted sufficient attentions. Few theoretical and experimental results have been reported for the problem of nonlinear scattering or reflection in structures, such as plates, pipes and rods.

1.4 Objectives and outline

The objective of this dissertation is to develop several theoretical methods to investigate the nonlinear wave propagation characteristics in materials and structures with the potential application related to the design of novel acoustic devices and the development of nonlinear ultrasound techniques for nondestructive evaluation. For soft bars, the solitary waves can be generated in the limit of long wavelength if the material and geometrical nonlinearities and viscoelasticity are considered. The capacity of tunability of solitary waves in soft bars under pre-stretch or biasing

electric field is investigated. Since materials having micro-damages or material degradations behave in a nonlinear manner, the interaction of incident waves with material nonlinearity is of obvious academic interest. Our goal is to develop simplified theories and simple theoretical models based on reasonable assumptions to work out analytical solutions, which are important for the development of nonlinear ultrasound technique.

After a careful literature research, we find a number of meaningful and interesting topics have not been investigated, which motivate the present work. Specifically, they include

1. There has been no report on nonlinear solitary waves in soft electroactive materials in the presence of electric biasing field. Our goal is to find if solitary waves can be modulated by the underlying electric biasing field.

2. There are few works on nonlinear waves in pre-stretched structures composed of viscoelastic materials. Our goal is to study the influence of the pre-stretch on kink and kink-like longitudinal waves in Mooney-Rivlin viscoelastic rods.

3. No mathematical model has yet been proposed to obtain the analytical approach to the generation of third harmonics. Our goal is to present an analysis of the generation of higher harmonics based on quadratic and cubic material nonlinearity.

4. Fewer results for harmonics of surface waves on a half-space of material nonlinearity are available, especially in term of analytical solutions. One of the main purposes of the present work is to obtain an analytical solution for higher harmonic surface waves in a simple and elegant manner, which may be easily understood and applicable.

5. Rods and pipes are widely used in structures such as pipelines. However, relevant analytical solutions to nonlinear waves propagating in cylindrical wave guides are still not available. We intend to conduct an analytical investigation of higher harmonics in pipes based on shell theory with quadratic nonlinear material behavior. An analytical approach based on shell theory provides a clearer physical insight in the deformation modes. Whereas exact three-dimensional theory has to be dealt with numerically, shell theory yields relatively simple analytical solutions.

6. The reflection and scattering from local region of cubic material nonlinearity are seldom investigated. The physical mechanisms inside them are not clear. One main purpose here is to investigate the reflection and backscattering of plane elastic waves by a region of cubically nonlinear material behavior.

7. Analytical solutions to third harmonics propagating in pipes haven't been reported. We will investigate the propagation of guided waves in a pipe of cubic material nonlinearity.

8. Little attention has been paid to the investigation of scattering of incident waves from a local region of nonlinearity in structures. We intend to investigate the scattering of two orthogonal SH waves of the lowest mode from a cylindrical region of nonlinear material behavior in an elastic layer by using the reciprocity theorem of elastodynamics.

The remaining main part of this dissertation is splitted into two parts. The first part contains Chapters 2 and 3. In this part, solitary waves propagating in soft bars are investigated, which can be adjusted by pre-stretch and biasing electric field. In Chapter 2, an asymptotic analysis of solitary waves propagating in an incompressible isotropic electroactive circular rod subjected to a biasing longitudinal electric displacement is presented. In Chapter 3, we theoretically investigates kink and kink-like waves propagating in pre-stretched Mooney-Rivlin viscoelastic rods. The second part contains Chapters 4-9, which deals with higher harmonic generation by material nonlinearity. In Chapter 4, harmonics of plane longitudinal and transverse waves in nonlinear elastic solids with up to cubic nonlinearity are investigated in a one-dimensional setting. In Chapter 5, the analytical far-field solution for the cumulative third harmonic surface wave propagating on a half-space of isotropic incompressible cubically nonlinear material is obtained in a relatively simple and systematic manner. In Chapter 6, higher harmonics in pipes of quadratic nonlinear material behavior are analyzed using the shell theory. In Chapter 7, two models are proposed to obtain information on the material nonlinearity of an inclusion in a solid body. In Chapter 8, the effect of cubic material nonlinearity on the propagation in a pipe of the lowest axially symmetric torsional wave mode is investigated. Two cases, one that the material of the whole pipe is nonlinear, and the second that a small segment of the pipe is nonlinear, are

considered. In Chapter 9, the intersection of two SH waves of lowest modes with a local cylindrical region of quadratic material nonlinearity in an elastic layer is investigated.

========================

Part 1

========================

Solitary Waves Propagating

in Soft Bars

Outline

Chapter 2 Adjustable solitary wave in electroactive rods

Chapter 3 Kink and kink-like waves in pre-stretched Mooney-
Rivlin viscoelastic rods

Chapter 2 Adjustable solitary waves in electroactive rods

2.1 Introduction

As a special kind of soft solids, soft electroactive materials (such as dielectric elastomers) can change their shapes and mechanical properties under electric stimulation. Such materials behave just like biological muscles, and hence they are often called artificial muscles. As a new kind of advanced functional materials, electroactive materials have many attractive characteristics, such as higher response speed, lower density and greater resilience Cohen-Bar (2002). Not surprisingly, they have triggered wide research interests. Recently, Dorfmann and Ogden (2005, 2010b) presented a nonlinear framework for electroelasticity and investigated the linear waves in electroactive bodies under biasing fields. Shmuel et al. (2012) investigated electromechanical waves propagating in a dielectric elastomer layer with initial deformation. Chen and Dai (2012), based on the nonlinear electroelastic theory of Dorfmann and Ogden (2010), presented an exact axisymmetric wave solution for a soft electroactive cylinder with both underlying finite deformation and electric biasing field. To the best knowledge of the authors, there has been no report on nonlinear solitary waves in soft electroactive materials in the presence of electric biasing fields, and this fact motivates the present study. For nonlinear waves propagating in bodies with multi-field coupling, Xue et al. (2011) made an important step by investigating solitary waves in a magneto-electro-elastic circular rod.

Our goal is thus to study solitary waves in soft electroactive circular rods, to see if they can be modulated by the underlying electric biasing field. The asymptotically valid method is employed to study the axisymmetric solitary waves in incompressible isotropic electroactive circular rods. The similar method has been adopted in Dai and Huo (2002). We will introduce several asymptotic expansions for

the axial and radial displacements, the electric potential, and the hydrostatic pressure which is associated with the material incompressibility. The 1D equations governing the nonlinear waves in the limit of finite-small amplitude and long wavelength are derived, with the lateral boundary conditions satisfied asymptotically. To validate the adopted approach and the mathematical derivation, the reduced linear dispersion relation is compared with the one directly derived from the 3D theory (2012) in the limit of long wavelength, and perfect agreement is observed. The far-field equation, which is known as the KdV equation, is then deduced by using the reductive perturbation method. The leading order of the electroelastic solitary wave solution is finally obtained from the KdV equation. Numerical examples are given to show the effects of the biasing electric displacement and the material constants on solitary waves in electroactive rods. It is found that the velocity of solitary waves can be modulated by the biasing electric displacement while the amplitude keeps unchanged. On the other hand, by keeping the velocity unchanged, we can adjust the wavelength and amplitude of solitary waves using the electric means. Further, while it doesn't change the wave shape of the longitudinal strain or transverse displacement for a prescribed amplitude, it does have an effect on the wave shape of the longitudinal electric field. The multiple tunability of solitary waves in electroactive rods may promote certain application of solitary waves in solids.

2.2 Nonlinear framework of electroelasticity

We consider a slender circular rod of diameter $2a$ with its end surfaces coated with soft electrodes. The axis of the rod coincides with the Z-axis, see Fig. 2.1.

To study the axisymmetric motion of the rod, which is made of a homogeneous, incompressible, isotropic, electroactive material, we shall first review here the nonlinear framework for electroelasticity formulated by Dorfmann and Ogden (2005, 2010). Suppose that the undeformed body occupies a region Γ_0 with the boundary $\partial\Gamma_0$ and the outward normal $\mathbf{N}$. This is taken to be the reference configuration.

Let χ describe the motion of a material point at $\mathbf{X}$, the position vector in the reference configuration, which moves to $\mathbf{x}$ at time T according to $\mathbf{x} = \chi(\mathbf{X}, T)$. The body then has the current configuration Γ with a boundary $\partial\Gamma$ and the outward normal $\mathbf{n}$. We define the deformation gradient tensor as $\mathbf{F} = \operatorname{Grad}\chi$, and $\mathbf{c} = \mathbf{F}^{\mathrm{T}}\mathbf{F}$ is the right Cauchy-Green tensor. For incompressible materials, we have the incompressibility constraint $J \equiv \det \mathbf{F} = 1$.
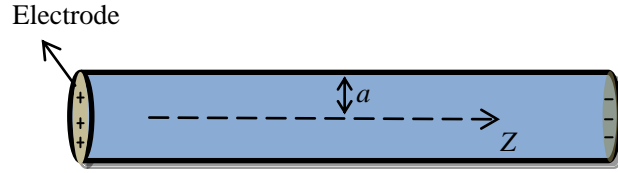
Fig. 2.1. An electroactive rod subjected to a biasing electric field applied through the end electrodes

The equations of motion can be written as

$$\operatorname{Div}\mathbf{\Sigma} = \rho \frac{\partial^2 \mathbf{x}}{\partial T^2} \tag{2.1a}$$

where the nominal stress tensor $\mathbf{\Sigma}$ can be calculated by

$$\begin{aligned}
\mathbf{\Sigma} &= 2\Omega_1 \mathbf{F}^{\mathrm{T}} + 2\Omega_2 (I_1 \mathbf{F}^{\mathrm{T}} - \mathbf{c} \cdot \mathbf{F}^{\mathrm{T}}) - P\mathbf{F}^{-1} + 2\Omega_5 \mathbf{D}_l \otimes \mathbf{F}\mathbf{D}_l \\
&\quad + 2\Omega_6 [\mathbf{D}_l \otimes (\mathbf{F} \cdot \mathbf{c}\mathbf{D}_l) + \mathbf{c}\mathbf{D}_l \otimes \mathbf{F}\mathbf{D}_l]
\end{aligned} \tag{2.1b}$$

where $\mathbf{D}_l$ is the Lagrangian counterpart of the electric displacement, P is a Lagrangian multiplier associated with the incompressibility constraint, $\Omega = \Omega(\mathbf{F}, \mathbf{D}_l)$ is the energy density per unit volume in Γ_0, and $\Omega_m = \partial\Omega / \partial I_m$ $(m = 1, 2, 4, 5, 6)$, with I_m being the scalar invariants defined by

$$I_1 = \operatorname{tr}\mathbf{c}, \ I_2 = \frac{1}{2}[(\operatorname{tr}\mathbf{c})^2 - \operatorname{tr}(\mathbf{c}^2)], \ I_4 = \mathbf{D}_l \cdot \mathbf{D}_l, \ I_5 = \mathbf{D}_l \cdot (\mathbf{c}\mathbf{D}_l), \ I_6 = \mathbf{D}_l \cdot (\mathbf{c}^2 \mathbf{D}_l)$$

$$\tag{2.1c}$$

Under the quasi-electrostatic approximation, the equations governing the electric field read

$$\mathrm{Curl}\mathbf{E}_l = 0 \tag{2.2a}$$

$$\mathrm{Div}\mathbf{D}_l = 0 \tag{2.2b}$$

where Curl and Div are the curl and divergence operators in Γ_0 and $\mathbf{E}_l$ is the Lagrangian counterpart of the electric field, which can be expressed in terms of $\mathbf{D}_l$ for soft electroactive materials as (Dorfmann and Ogden, 2010)

$$\mathbf{E}_l = 2(\Omega_4\mathbf{I} + \Omega_5\mathbf{c})\mathbf{D}_l \tag{2.3}$$

where $\mathbf{I}$ is the unit vector.

The mechanical boundary condition is

$$\mathbf{\Sigma}^{\mathrm{T}}\mathbf{N} = \mathbf{t}_A \tag{2.4a}$$

where $\mathbf{t}_A$ is defined by $\mathbf{t}_A\,\mathrm{d}A = \mathbf{t}_a\,\mathrm{d}a$, with $\mathbf{t}_a$ being the applied mechanical traction per unit area in Γ, and $\mathrm{d}A$ and $\mathrm{d}a$ the differential areas in Γ_0 and Γ, respectively. The electric boundary condition is

$$\mathbf{D}_l \cdot \mathbf{N} = q_0 \tag{2.4b}$$

where q_0 is the surface charge density in Γ_0. The above nonlinear framework for electroelasticity is suitable for describing the dynamic behavior of incompressible isotropic dielectric elastomers (Dorfmann and Ogden, 2005, 2010).

In this Chapter, we consider the case that the lateral surface is free from both mechanical tractions and surface charges, i.e. $\mathbf{t}_A = \mathbf{0}$ and $q_0 = 0$. It is noted that the influence of the electric field exterior to the rod is neglected for simplicity. Such simplification has also been adopted in earlier works (Zhang et al., 2012; Ericksen, 2007; Suo et al., 2008) on account of the fact that the permittivity of eletroactive materials is usually much larger than that of vacuum.

2.3 Model equations

To study the axisymmetric motion of the circular rod, we shall adopt cylindrical coordinate systems (R, Θ, Z) and (r, θ, z), which correspond to the reference and current configurations, respectively. The Z-axis is already shown in Fig. 2.1. The two systems completely coincide with each other, but the same material point will mostly have different positions in them.

We assume that there exists an initial biasing electric displacement along the Z-axis

$$\mathbf{D}_l^0 = \left(0, \ 0, \ D\right)^{\mathrm{T}} \tag{2.5a}$$

Making use of Eqs. (2.3) and (2.5a), we can get the corresponding electric field

$$\mathbf{E}_l^0 = \left(0, \ 0, \ E\right)^{\mathrm{T}} \tag{2.5b}$$

where $E = 2(\Omega_4 + \Omega_5)D$, which is obtained under the assumption that no mechanical deformation (i.e. $\mathbf{F} = \mathbf{I}$) is induced along with the biasing electric displacement. This further gives a result of the corresponding Lagrangian multiplier, i.e. $p_0 = 2\Omega_1 + 4\Omega_2$ which is obtained from the traction-free boundary conditions. It should be pointed out that, Ω_m are all assumed to be constant for simplicity (especially, $\Omega_6 = 0$) in the following analysis. This assumption is valid at least for some simple material models, such as the Mooney-Rivlin material model (and the neo-Hookean model as its special case), which will be considered in the numerical part. For more complex models which contain higher-order elastic constants (Hamilton et al., 2004), the analysis is essentially the same, though the mathematical derivation may become more tedious.

The axisymmetric motion and the electric field of the rod are described by

$$z(R,Z,T) = Z + W(R,Z,T), \ r(R,Z,T) = R + U(R,Z,T), \ \theta = \Theta \tag{2.6a}$$

$$P = p_0 + p \tag{2.6b}$$

$$\mathbf{E}_l = \left(\Delta E_{(R)}, \ 0, \ E + \Delta E_{(Z)} \right)^{\mathrm{T}} \tag{2.6c}$$

where, as a convention, the subscripts inside the brackets denote components; otherwise, they signify differentiations with respect to the corresponding coordinate variables.

The deformation gradient tensor and the right Cauchy-Green tensor are then given by

$$\mathbf{F} = \begin{bmatrix} 1+U_R & 0 & U_Z \\ 0 & 1+U/R & 0 \\ W_R & 0 & 1+W_Z \end{bmatrix} \tag{2.7a}$$

$$\mathbf{c} = \begin{bmatrix} (1+U_R)^2 + W_R^2 & 0 & (1+U_R)U_Z + (1+W_Z)W_R \\ 0 & (1+U/R)^2 & 0 \\ (1+U_R)U_Z + (1+W_Z)W_R & 0 & U_Z^2 + (1+W_Z)^2 \end{bmatrix} \tag{2.7b}$$

While, the incompressibility constraint $J = 1$ can be written approximately as

$$W_Z + U_R + \frac{U}{R} + U_R W_Z - U_Z W_R + \frac{UW_Z}{R} + \frac{UU_R}{R} = 0 \tag{2.8}$$

It should be noted that, for a weakly nonlinear analysis, we have neglected in Eq. (2.8) the terms which are higher than the second order, which will also be followed in the derivation below.

To satisfy Eq. (2.2a), we introduce the electric potential ϕ such that

$$\Delta E_{(R)} = -\phi_R, \ \Delta E_{(Z)} = -\phi_Z \tag{2.9}$$

In view of Eqs. (2.3), (2.6c), (2.8) and (2.9), we can get the following approximate expressions of the nonzero components of $\mathbf{D}_l$:

$$\begin{aligned} D_{l(R)} = {} & -\eta_3 D U_Z - \eta_3 D W_R - \eta_2 \phi_R + \eta_1 U_Z \phi_Z + \eta_1 W_R \phi_Z - 2\eta_1 W_Z \phi_R \\ & - 2\eta_3^2 D \frac{U W_R}{R} - 2\eta_3^2 D \frac{U U_Z}{R} - 2\eta_2 \eta_3 \frac{U \phi_R}{R} \end{aligned} \tag{2.10a}$$

$$\begin{aligned} D_{l(Z)} = {} & D + 2\eta_3 D U_R - \eta_2 \phi_Z + 2\eta_3 D \frac{U}{R} + \eta_1 U_Z \phi_R + \eta_1 W_R \phi_R - 2\eta_1 U_R \phi_Z \\ & + 4\eta_3^2 D \frac{U U_R}{R} - 2\eta_2 \eta_3 \frac{U \phi_Z}{R} + 4\eta_3^2 D \frac{U^2}{R^2} + 2\eta_3 D (U_R W_Z - U_Z W_R \\ & + \frac{U W_Z}{R} + \frac{U U_R}{R}) \end{aligned} \tag{2.10b}$$

where $\eta_1 = \Omega_5 / 2(\Omega_4 + \Omega_5)^2$, $\eta_2 = 1/2(\Omega_4 + \Omega_5)$, and $\eta_3 = \Omega_5 / (\Omega_4 + \Omega_5)$. The

relations $E\eta_1 = \eta_3 D$ and $E\eta_2 = D$ have been noticed above. In view of Eqs.

(2.1b), (2.7) and (2.10), we can also get the approximate expressions of the nonzero

components of Σ , which are all listed in Appendix 2A.

Eqs. (2.1a) and (2.2b) can be written in the following form

$$-\rho W_{TT} + (\Sigma_{(Rz)})_R + (\Sigma_{(Zz)})_Z + \frac{\Sigma_{(Rz)}}{R} = 0 \tag{2.11a}$$

$$-\rho U_{TT} + (\Sigma_{(Rr)})_R + (\Sigma_{(Zr)})_Z + \frac{1}{R}(\Sigma_{(Rr)} - \Sigma_{(\Theta\theta)}) = 0 \tag{2.11b}$$

$$(D_{l(R)})_R + (D_{l(Z)})_Z + \frac{D_{l(R)}}{R} = 0 \tag{2.11c}$$

Taking Eqs. (2.10a), (2.10b) and (2A.1)-(2A.5) into the above equations, we get

$$-\rho W_{TT} + (2\Omega_2 + 6\eta_3\Omega_5 D^2)U_{RZ} + (2\Omega_1 + 2\Omega_2 - 2\eta_3\Omega_5 D^2)W_{RR} - \eta_3 D\phi_{RR} - p_z$$

$$+ (p_0 + 2D^2\Omega_5)W_{ZZ} - 2\eta_3 D\phi_{ZZ} + (2\Omega_1 + 2\Omega_2 - 2\eta_3\Omega_5 D^2)\frac{W_R}{R} - \eta_3 D\frac{\phi_R}{R}$$

$$+ (2\Omega_2 + 6\eta_3 D^2\Omega_5)\frac{U_Z}{R} + p_R U_Z - p_Z U_R - (2\Omega_2 + 4\eta_3^2 D^2\Omega_5)U_{RR}U_Z$$

$$+ (2\Omega_2 + 12\eta_3^2 D^2\Omega_5)U_R U_{RZ} + (2\Omega_2 + 14\eta_3\Omega_5 D^2)U_{RZ}W_Z - 4\eta_3^2 D^2\Omega_5 U_{RR}W_R$$

$$- 4(\Omega_2 + 3\eta_3\Omega_5 D^2)U_Z W_{RZ} - (2\Omega_2 + 10\eta_3\Omega_5 D^2)U_{ZZ}W_R - 4\eta_3^2 D^2\Omega_5 U_R W_{RR}$$

$$+ (4\Omega_2 + 16\eta_3\Omega_5 D^2)U_R W_{ZZ} - 2\eta_3\Omega_5 D^2 W_{RR}W_Z - 6\eta_3\Omega_5 D^2 W_R W_{RZ} - 2\eta_3 D W_{RZ}\phi_R$$

$$- (2\eta_3^2 D + \eta_3 D)W_Z\phi_{RR} + (4\eta_3^2 D - \eta_3 D)W_R\phi_{RZ} + 2\eta_3^2 D W_{RR}\phi_Z - 2\eta_3 D W_Z\phi_{ZZ}$$

$$- 2\eta_3 D W_{ZZ}\phi_Z - 6\eta_3^2 D U_{RZ}\phi_Z + 4\eta_3^2 D U_Z\phi_{RZ} - 4\eta_1 D\Omega_5 U_{RR}\phi_R - 4\eta_1 D\Omega_5 U_R\phi_{RR}$$

$$- 8\eta_3^2 D U_R\phi_{ZZ} + 2\eta_3^2 D U_{ZZ}\phi_R + 2\Omega_5\eta_2^2\phi_{RR}\phi_Z + 2\Omega_5\eta_2^2\phi_R\phi_{RZ} + 4\eta_2^2\Omega_5\phi_Z\phi_{ZZ}$$

$$+ (20\eta_3^2\Omega_5 D^2 + 8\Omega_5\eta_3 D^2 - 2\Omega_2)\frac{U_R U_Z}{R} + (2\Omega_2 + 14\eta_3 D^2\Omega_5)\frac{U_Z W_Z}{R}$$

$$+ (4\Omega_2 + 16\eta_3 D^2\Omega_5)\frac{U W_{ZZ}}{R} - 2\eta_3\Omega_5 D^2\frac{W_R W_Z}{R} + (4\Omega_2 - 12\eta_3^2 D^2\Omega_5)\frac{U_R W_R}{R}$$

$$+ (4\Omega_2 - 8\eta_3^2 D^2\Omega_5)\frac{U W_{RR}}{R} + (24\eta_3^2 D^2\Omega_5 + 8\Omega_5\eta_3 D^2)\frac{U U_{RZ}}{R} - 8\eta_3^2 D\frac{U\phi_{ZZ}}{R}$$

$$+ (4\Omega_2 + 48\eta_3^2 D^2\Omega_5)\frac{U U_Z}{R^2} - \frac{p_Z U}{R} - (2\eta_3^2 D + \eta_3 D)\frac{W_Z\phi_R}{R} - 6\eta_3^2 D\frac{U_R\phi_R}{R}$$

$$- 4\eta_3^2 D\frac{U\phi_{RR}}{R} - 6\eta_3^2 D\frac{U_Z\phi_Z}{R} + 2\eta_3^2 D\frac{W_R\phi_Z}{R} + 2\Omega_5\eta_2^2\frac{\phi_R\phi_Z}{R} = 0$$

$$\tag{2.12a}$$

$$-\rho U_{TT} - p_R + p_0 U_{RR} - p_0 \frac{U}{R^2} + p_0 \frac{U_R}{R} + (2\Omega_1 + 2\Omega_2 - 2\eta_3 \Omega_5 D^2 + 2\Omega_5 D^2) U_{ZZ}$$

$$+ (2\Omega_2 - 2\eta_3 \Omega_5 D^2) W_{RZ} - \eta_3 D\phi_{RZ} - p_R W_Z + p_Z W_R - 4(\eta_3 \Omega_5 D^2 + \Omega_2) U_{RZ} W_R$$

$$+ (4\eta_3^2 \Omega_5 D^2 - 2\eta_3 \Omega_5 D^2 - 2\Omega_2) U_Z W_{RR} + (2\Omega_2 - 2\eta_3 \Omega_5 D^2 - 4\eta_3^2 \Omega_5 D^2) U_R W_{RZ}$$

$$+ 4\Omega_2 U_{RR} W_Z + 2\Omega_2 W_Z W_{RZ} - 2\Omega_2 W_R W_{ZZ} + 4\Omega_5 \eta_3^2 D^2 W_R W_{RR} + 2\Omega_5 \eta_3 D^2 U_{RZ} U_Z$$

$$+ \eta_3 \Omega_5 D^2 (6 - 4\eta_3) U_R U_{ZZ} - 2\eta_3 D U_{RZ}\phi_R + (2\eta_3^2 D - \eta_3 D) U_Z \phi_{RR} - 2\eta_3^2 D U_R \phi_{RZ}$$

$$- \eta_3 D U_R \phi_{RZ} + (2\eta_3^2 D - 2\eta_3 D)(U_{ZZ}\phi_Z + U_Z \phi_{ZZ}) + 2\eta_3^2 D W_{RR}\phi_R + 2\eta_3^2 D W_R \phi_{RR}$$

$$+ 2\eta_3^2 D W_{RZ}\phi_Z + 2\eta_3^2 D W_R \phi_{ZZ} - 4\eta_1 D\Omega_5 W_{ZZ}\phi_R - 4\eta_1 D\Omega_5 W_Z \phi_{RZ} + 2\eta_2^2 \Omega_5 \phi_{RZ}\phi_Z$$

$$+ 2\eta_2^2 \Omega_5 \phi_R \phi_{ZZ} + 4\Omega_5 \eta_2^2 \phi_R \phi_{RR} + 4\Omega_2 \frac{U_R W_Z}{R} - (4\eta_3^2 \Omega_5 D^2 + 2\eta_3 \Omega_5 D^2 + 2\Omega_2) \frac{U_Z W_R}{R}$$

$$+ (2\Omega_5 \eta_3^2 D^2 - 2\Omega_2) \frac{W_R^2}{R} + (6\eta_3 \Omega_5 D^2 - 6\Omega_5 \eta_3^2 D^2 + 2\Omega_2) \frac{U_Z^2}{R} - 8\eta_3^2 D^2 \Omega_5 \frac{UW_{RZ}}{R}$$

$$- (2\eta_3^2 D + \eta_3 D) \frac{U_Z \phi_R}{R} + 2\eta_3^2 D \frac{W_R \phi_R}{R} + 2\Omega_5 \eta_2^2 \frac{\phi_R^2}{R} + 2\Omega_2 \frac{U_R^2}{R} - 2\Omega_2 \frac{U^2}{R^3} - \frac{p_R U}{R}$$

$$- 4\Omega_2 \frac{UW_Z}{R^2} + 4\Omega_2 \frac{UU_{RR}}{R} + [4\Omega_2 + 8\eta_3 D^2 \Omega_5 (1 - \eta_3)]\frac{UU_{ZZ}}{R} - 4\eta_3^2 D \frac{U\phi_{RZ}}{R} = 0$$

$$(2.12b)$$

$$(2\eta_1 E - \eta_3 D) U_{RZ} - \eta_3 D W_{RR} - \eta_2 (\phi_{RR} + \phi_{ZZ}) + \frac{1}{R}(\eta_3 D U_Z - \eta_3 D W_R - \eta_2 \phi_R)$$

$$+ \eta_1(-U_{RZ}\phi_Z + 2U_Z \phi_{RZ} + W_{RR}\phi_Z + 2W_R \phi_{RZ} + U_{ZZ}\phi_R - W_{RZ}\phi_R - 2W_Z \phi_{RR} - 2U_R \phi_{ZZ})$$

$$+ (\eta_1 - 2\eta_2 \eta_3) \frac{U_Z \phi_Z}{R} + \eta_1 \frac{W_R \phi_Z}{R} - 2\eta_3^2 D \frac{U_R W_R}{R} - 2\eta_3^2 D \frac{UW_{RR}}{R} + 2\eta_3^2 D \frac{U_Z U_R}{R}$$

$$+ 2\eta_3^2 D \frac{UU_{RZ}}{R} - 2\eta_1 \frac{W_Z \phi_R}{R} - 2\eta_2 \eta_3 \frac{U\phi_{ZZ}}{R} - 2\eta_2 \eta_3 \frac{U_R \phi_R}{R} - 2\eta_2 \eta_3 \frac{U\phi_{RR}}{R} + 8\eta_3^2 D \frac{UU_Z}{R^2}$$

$$+ 2\eta_3 D(U_{RZ} W_Z + U_R W_{ZZ} - U_{ZZ} W_R - U_Z W_{RZ} + \frac{U_Z W_Z}{R} + \frac{UW_{ZZ}}{R} + \frac{U_Z U_R}{R} + \frac{UU_{RZ}}{R}) = 0$$

$$(2.12c)$$

Since the lateral surface is free from mechanical tractions and surface charges, we have

$$\Sigma_{(Rr)} = 0, \ \Sigma_{(Rz)} = 0, \ D_{l(R)} = 0 \ \text{ at } \ R = a \tag{2.13}$$

Making use of Eqs. (B1), (B2) and (2.10a), we get the following approximate boundary conditions at $R = a$:

$$\Sigma_{(Rr)} = -p - 2\Omega_1 W_Z + p_0 U_R - 2\Omega_1 \frac{U}{R} - pW_Z - \frac{pU}{R} - p_0 \frac{UW_Z}{R} + 2\Omega_2 \frac{U^2}{R^2}$$

$$+ 4\Omega_2 \frac{UU_R}{R} + (4\eta_3^2 \Omega_5 D^2 - 2\eta_3 \Omega_5 D^2 - 2\Omega_2) U_Z W_R + 4\Omega_2 U_R W_Z \qquad (2.14a)$$

$$+ 2\Omega_2 W_Z^2 + 2\Omega_5 \eta_3^2 D^2 W_R^2 + (2\Omega_5 \eta_3^2 D^2 - 2\eta_3 \Omega_5 D^2) U_Z^2$$

$$+ (2\eta_3^2 D - \eta_3 D) U_Z \phi_R + 2\eta_3^2 D W_R \phi_R + 2\Omega_5 \eta_2^2 \phi_R^2 = 0,$$

$$\Sigma_{(Rz)} = (2\Omega_1 + 2\Omega_2 - 2\eta_3 \Omega_5 D^2)(U_Z + W_R) - \eta_3 D \phi_R - (2\Omega_2 + 4\eta_3^2 D^2 \Omega_5) U_R U_Z$$

$$- 4\eta_1 D\Omega_5 U_R \phi_R - 4\eta_3^2 D^2 \Omega_5 U_R W_R - (2\Omega_2 + 2\eta_3 \Omega_5 D^2) U_Z W_Z + 2\eta_3^2 D U_Z \phi_Z$$

$$- (\eta_3 D + 2\eta_3^2 D) W_Z \phi_R - 2\eta_3 \Omega_5 D^2 W_R W_Z + 2\eta_3^2 D W_R \phi_Z + 2\Omega_5 \eta_2^2 \phi_R \phi_Z + pU_Z$$

$$+ (4\Omega_2 - 8\eta_3^2 D^2 \Omega_5) \frac{UW_R}{R} - 4\eta_3^2 D \frac{U\phi_R}{R} + (p_0 - 8\eta_3^2 D^2 \Omega_5) \frac{UU_Z}{R} = 0,$$

$$(2.14b)$$

$$D_{l(R)} = -\eta_3 D(U_Z + W_R) - \eta_2 \phi_R + \eta_1 U_Z \phi_Z + \eta_1 W_R \phi_Z - 2\eta_1 W_Z \phi_R$$

$$- 2\eta_3^2 D \frac{UW_R}{R} - 2\eta_1 \frac{U\phi_R}{R} - 2\eta_3^2 D \frac{UU_Z}{R} = 0, \qquad (2.14c)$$

The governing equations (2.8) and (2.12a)-(2.12c) and the boundary conditions (2.14a)-(2.14c) derived above will be used to approximately describe the nonlinear dynamics of electroactive rods.

For convenience, we introduce the following transformations:

$$W = W(Z, S, T), U = RV(Z, S, T), p = p(Z, S, T), \phi = \phi(Z, S, T) \qquad (2.15)$$

where $S = R^2$. Making use of the above transformations, we can obtain the governing equations and boundary conditions in an alternative and useful form, see Appendix 2B. The importance of the above transformations is that the factor $1/R$ is eliminated from the governing differential system, as can be seen from Eqs. (2B.1)-(2B.7). Also, the square root $\sqrt{S} \equiv R$ does not appear in the resulting system, which implies that for axisymmetric deformations or motions $S = R^2$ is a more natural radial variable for the new unknown functions in Eq. (2.15).

For waves with finite-small amplitude and long wavelength, it is convenient to introduce the following scales to non-dimensionalize the above-mentioned equations

$$W = hw, Z = lx, S = l^2 s, T = \frac{l}{c}t, V = \frac{h}{l}v, p = \mu \frac{h}{l}\bar{p}, \phi = h\sqrt{\frac{\mu}{\varepsilon_0}}\Phi \qquad (2.16a)$$

where h is a characteristic axial displacement, l is a characteristic wavelength, c is a characteristic velocity, μ is the shear modulus of the material, and ε_0 is the permittivity of vacuum. We also transform Ω_m into the following dimensionless constants

$$\bar{\Omega}_1 = \mu^{-1}\Omega_1, \quad \bar{\Omega}_2 = \mu^{-1}\Omega_2, \quad \bar{\Omega}_4 = \varepsilon_0\Omega_4, \quad \bar{\Omega}_5 = \varepsilon_0\Omega_5 \qquad (2.16b)$$

In view of Eqs. (2.16a) and (2.16b), from Eqs. (2B.1)-(2B.4), we obtain

$$2v + w_x + 2sv_s + \varepsilon(2vw_x + 2sv_sw_x - 2sv_xw_s + v^2 + 2svv_s) = 0 \qquad (2.17a)$$

$$
\begin{aligned}
&-\frac{\rho c^2}{\mu}w_{tt} - \bar{p}_x + 4(\bar{\Omega}_2 + 3\eta_3\eta_5^2\bar{\Omega}_5)(v_x + sv_{sx}) + 8(\bar{\Omega}_1 + \bar{\Omega}_2 - \eta_3\eta_5^2\bar{\Omega}_5)(w_s + sw_{ss}) \\
&\quad - 4\eta_3\eta_5\Phi_s - 2\eta_3\eta_5\Phi_{xx} + (2\bar{\Omega}_1 + 4\bar{\Omega}_2 + 2\eta_5^2\bar{\Omega}_5)w_{xx} - 4\eta_3\eta_5 s\Phi_{ss} \\
&\quad + \varepsilon[2s\bar{p}_s v_x - 2\bar{p}_x v - 2\bar{p}_x sv_s + (40\eta_3^2\eta_5^2\bar{\Omega}_5 + 16\bar{\Omega}_5\eta_5^2\eta_3 - 12\bar{\Omega}_2)sv_s v_x \\
&\quad - 8(\bar{\Omega}_2 + 2\eta_3^2\eta_5^2\bar{\Omega}_5)s^2 v_{ss}v_x + 4(\bar{\Omega}_2 + 26\eta_3^2\eta_5^2\bar{\Omega}_5 + 4\bar{\Omega}_5\eta_5^2\eta_3)vv_x \\
&\quad + 4(\bar{\Omega}_2 + 22\eta_3^2\eta_5^2\bar{\Omega}_5)svv_{sx} + 8(\bar{\Omega}_2 + 6\eta_3^2\eta_5^2\bar{\Omega}_5)s^2 v_s v_{sx} - 32\eta_3^2\eta_5^2\bar{\Omega}_5 s^2 v_{ss}w_s \\
&\quad - 8(\bar{\Omega}_2 + 3\eta_3\eta_5^2\bar{\Omega}_5)sv_x w_{sx} - 4(\bar{\Omega}_2 + 5\eta_3\eta_5^2\bar{\Omega}_5)sv_{xx}w_s - 16\eta_3^2\eta_5 v\Phi_{xx} \\
&\quad + 4(\bar{\Omega}_2 + 7\eta_3\eta_5^2\bar{\Omega}_5)(v_x w_x + sv_{sx}w_x) + 16(\bar{\Omega}_2 - 7\eta_3^2\eta_5^2\bar{\Omega}_5)sv_s w_s \\
&\quad + 16(\bar{\Omega}_2 - 3\eta_3^2\eta_5^2\bar{\Omega}_5)(vw_s + svw_{ss}) + 8(\bar{\Omega}_2 + 4\eta_3\eta_5^2\bar{\Omega}_5)vw_{xx} \\
&\quad - 8\eta_3\eta_5^2\bar{\Omega}_5(w_s w_x + sw_{ss}w_x) - (4\eta_3\eta_5 + 8\eta_3^2\eta_5)(w_x\Phi_s + sw_x\Phi_{ss}) \\
&\quad - 32\eta_3^2\eta_5^2\bar{\Omega}_5 s^2 v_s w_{ss} - 8\eta_3\eta_5 sw_{sx}\Phi_s - 12\eta_3^2\eta_5(v_x\Phi_x + sv_{sx}\Phi_x) \\
&\quad - 24\eta_3\eta_5^2\bar{\Omega}_5 sw_s w_{xx} + 8\eta_3^2\eta_5 v_x\Phi_{sx} - 16\eta_3^2\eta_5 sv_s\Phi_{xx} + 4\eta_3^2\eta_5 sv_{xx}\Phi_s \\
&\quad - 56\eta_3^2\eta_5 sv_s\Phi_s - 16\eta_3^2\eta_5 s^2 v_{ss}\Phi_s - 24\eta_3^2\eta_5 v\Phi_s - 2\eta_3\eta_5 w_x\Phi_{xx} \\
&\quad + 8(\bar{\Omega}_2 + 4\eta_3\eta_5^2\bar{\Omega}_5)sv_s w_{xx} - 24\eta_3^2\eta_5 sv\Phi_{ss} - 16\eta_3^2\eta_5 s^2 v_s\Phi_{ss} \\
&\quad + 8\eta_3^2\eta_5(w_s\Phi_x + sw_{ss}\Phi_x) - 2\eta_3\eta_5 w_{xx}\Phi_x + 2\eta_4^2\bar{\Omega}_5(\Phi_s\Phi_x + s\Phi_{ss}\Phi_x) \\
&\quad + 4(4\eta_3^2 - \eta_3)\eta_5 sw_s\Phi_{sx} + 2\eta_4^2\bar{\Omega}_5 s\Phi_s\Phi_{sx} + \eta_4^2\bar{\Omega}_5\Phi_x\Phi_{xx}] = 0
\end{aligned}
\qquad (2.17b)
$$

$$
\begin{aligned}
&-\frac{\rho c^2}{\mu}v_{tt} - 2\bar{p}_s + 8(\bar{\Omega}_1 + 2\bar{\Omega}_2)(2v_s + sv_{ss}) + 4(\bar{\Omega}_2 - \eta_3\eta_5^2\bar{\Omega}_5)w_{sx} \\
&\quad + 2(\bar{\Omega}_1 + \bar{\Omega}_2 - \eta_3\eta_5^2\bar{\Omega}_5 + \eta_5^2\bar{\Omega}_5)v_{xx} - 2\eta_3\eta_5\bar{\Omega}_5\Phi_{sx} \\
&\quad + \varepsilon[-2\bar{p}_s w_x + 2\bar{p}_x w_s - 2\bar{p}_s v - 16(\eta_3\eta_5^2\bar{\Omega}_5 + \bar{\Omega}_2)v_x w_s \\
&\quad - 16(\eta_3\eta_5^2\bar{\Omega}_5 + \bar{\Omega}_2)sv_{xx}w_s + 32\bar{\Omega}_2 v_s w_x + 4\bar{\Omega}_2 w_x w_{sx}
\end{aligned}
$$

$$-4\bar{\Omega}_2 w_s w_{xx} + 4(4\eta_3^2\eta_5^2\bar{\Omega}_5 - 2\eta_3\eta_5^2\bar{\Omega}_5 - 2\bar{\Omega}_2)sw_{ss}v_x$$
$$+(4\bar{\Omega}_2 - 4\eta_3\eta_5^2\bar{\Omega}_5 - 24\eta_3^2\eta_5^2\bar{\Omega}_5)vw_{sx} + 16\bar{\Omega}_2 svv_{ss}$$
$$+(24\eta_3^2\eta_5^2\bar{\Omega}_5 - 8\bar{\Omega}_2)w_s^2 + 4\eta_3\eta_5^2\bar{\Omega}_5(3-2\eta_3)sv_s v_{xx}$$
$$+8(\bar{\Omega}_2 - \eta_3\eta_5^2\bar{\Omega}_5 - 2\eta_3^2\eta_5^2\bar{\Omega}_5)sv_s w_{sx} - 8\eta_3\eta_5 v_x\Phi_s$$
$$+16\bar{\Omega}_2 sv_{ss}w_x + 32\eta_3^2\eta_5^2\bar{\Omega}_5 sw_{ss}w_s + 4\eta_3\eta_5^2\bar{\Omega}_5 sv_{sx}v_x$$
$$+(8\eta_3\eta_5^2\bar{\Omega}_5 - 6\eta_3^2\eta_5^2\bar{\Omega}_5 + 2\bar{\Omega}_2)v_x^2 + 32\bar{\Omega}_2 vv_s + 8\bar{\Omega}_2 sv_s^2$$
$$+(4\bar{\Omega}_2 + 14\eta_3\eta_5^2\bar{\Omega}_5 - 12\eta_3^2\eta_5^2\bar{\Omega}_5)vv_{xx} - 8\eta_3\eta_5 sv_{sx}\Phi_s \tag{2.17c}$$
$$+(2\eta_3^2\eta_5 - 2\eta_3\eta_5)(v_{xx}\Phi_x + v_x\Phi_{xx}) - 4\eta_3\eta_5(1+2\eta_3)sv_s\Phi_{sx}$$
$$-(2\eta_3\eta_5 + 12\eta_3^2\eta_5)v\Phi_{sx} + 4(2\eta_3^2\eta_5 - \eta_3\eta_5)sv_x\Phi_{ss}$$
$$+\eta_3^2\eta_5(24w_s\Phi_s + 16sw_{ss}\Phi_s + 16sw_s\Phi_{ss} + 4w_{sx}\Phi_x$$
$$+4w_s\Phi_{xx} - 4\eta_3^2\eta_5 w_{xx}\Phi_s - 4\eta_3^2\eta_5 w_x\Phi_{sx})$$
$$+\eta_4^2\bar{\Omega}_5(\Phi_{sx}\Phi_x + \Phi_s\Phi_{xx} + 6\Phi_s^2 + 8s\Phi_s\Phi_{ss})] = 0$$

$$-\eta_3\eta_5(-2v_x - 2sv_{sx} + 4w_s + 4sw_{ss}) - \frac{1}{2}\eta_4(4\Phi_s + 4s\Phi_{ss} + \Phi_{xx})$$
$$+\varepsilon[\eta_4\eta_3(-v_x\Phi_x + 2sv_x\Phi_{sx} - sv_{sx}\Phi_x + sv_{xx}\Phi_s - 2sv_s\Phi_{xx} + 2w_s\Phi_x$$
$$+2sw_{ss}\Phi_x + 4sw_s\Phi_{sx} - 2sw_{sx}\Phi_s - 4w_x\Phi_s - 4sw_x\Phi_{ss} - 2v\Phi_{xx}$$
$$-4v\Phi_s - 4sv_s\Phi_s - 4sv\Phi_{ss}) + \eta_3^2\eta_5(-8vw_s - 8sv_s w_s - 8svw_{ss} + 12vv_x \tag{2.17d}$$
$$+4sv_x v_s + 4svv_{sx}) + 2\eta_3\eta_5(2v_x w_x + 2sv_{sx}w_x + 2vw_{xx} + 2sv_s w_{xx}$$
$$-2sv_{xx}w_s - 2sv_x w_{sx} + 2vv_x + 2sv_s v_x + 2svv_{sx})] = 0$$

where $\eta_4 = 1/(\bar{\Omega}_4 + \bar{\Omega}_5)$, $\eta_5 = D/\sqrt{\mu\varepsilon_0}$, and $\varepsilon = h/l$, which is a small parameter

for finite-small waves. Making use of Eqs. (2.16a) and (2.16b), we can rewrite the

boundary conditions in Eqs. (2B.5)-(2B.7) as follows

$$-\bar{p} - 2\bar{\Omega}_1 w_x + 4\bar{\Omega}_2 v + 4(\bar{\Omega}_1 + 2\bar{\Omega}_2)sv_s$$
$$+\varepsilon[-\bar{p}w_x - \bar{p}v - 2\bar{\Omega}_1 vw_x + 6\bar{\Omega}_2 v^2 + 8\bar{\Omega}_2 svv_s + 8\bar{\Omega}_2 sv_s w_x + 2\bar{\Omega}_2 w_x^2$$
$$+2(4\eta_3^2\eta_5^2\bar{\Omega}_5 - 2\eta_3\eta_5^2\bar{\Omega}_5 - 2\bar{\Omega}_2)sv_x w_s + 2\eta_5^2\bar{\Omega}_5(\eta_3^2 - \eta_3)sv_x^2$$
$$+8\eta_3^2\eta_5^2\bar{\Omega}_5 sw_s^2 + 2(2\eta_3^2 - \eta_3)\eta_5 sv_x\Phi_s + 8\eta_3^2\eta_5 sw_s\Phi_s + 2\bar{\Omega}_5\eta_4^2 s\Phi_s^2] = 0$$

$$\tag{2.18a}$$

$$(2\bar{\Omega}_1 + 2\bar{\Omega}_2 - 2\eta_3\eta_5^2\bar{\Omega}_5)(v_x + 2w_s) - 2\eta_3\eta_5\Phi_s + \varepsilon[\bar{p}v_x + 2(\bar{\Omega}_1 + \bar{\Omega}_2 - 6\eta_3^2\eta_5^2\bar{\Omega}_5)vv_x$$
$$-4(\bar{\Omega}_2 + 2\eta_3^2\eta_5^2\bar{\Omega}_5)sv_s v_x + 8(\bar{\Omega}_2 - 3\eta_3^2\eta_5^2\bar{\Omega}_5)vw_s - (2\bar{\Omega}_2 + 2\eta_3\eta_5^2\bar{\Omega}_5)v_x w_x$$
$$-16\eta_3^2\eta_5^2\bar{\Omega}_5 sv_s w_s - 4\eta_3\eta_5^2\bar{\Omega}_5 w_s w_x - 2\eta_3\eta_5 w_x\Phi_s + 4\eta_3^2\eta_5 w_s\Phi_x - 4\eta_3^2\eta_5 w_x\Phi_s$$
$$+2\eta_3^2\eta_5 v_x\Phi_x - 12\eta_3^2\eta_5 v\Phi_s - 8\eta_3^2\eta_5 sv_s\Phi_s + \eta_4^2\bar{\Omega}_5\Phi_s\Phi_x] = 0$$

$$\tag{2.18b}$$

$$-\eta_3\eta_5(v_x + 2w_s) - \eta_4\Phi_s + \varepsilon[\bar{\Omega}_5\eta_4^2(\frac{1}{2}v_x\Phi_x + w_s\Phi_x) - 4\eta_3^2\eta_5 vw_s$$

$$-2\eta_3^2\eta_5 vv_x - 2\eta_4^2\bar{\Omega}_5 v\Phi_s - 2\eta_4^2\bar{\Omega}_5 w_x\Phi_s] = 0 \tag{2.18c}$$

at $s = \delta$, where $\delta = a^2/l^2$ is small for long waves in slender rods. Hence, Eqs. (2.17a)-(2.17d) and (2.18a)-(2.18c) govern the problem under study, which depends on three variables (x, s, t) and involves two small parameters (ε, δ).

In order to further simplify the problem, we expand asymptotically, for slender rods, w, v, $\bar{p}$ and Φ in the neighborhood of $s = 0$ in the following way:

$$w = w_0(x,t) + sw_1(x,t) + s^2 w_2(x,t) + \cdots \tag{2.19a}$$

$$v = v_0(x,t) + sv_1(x,t) + s^2 v_2(x,t) + \cdots \tag{2.19b}$$

$$\bar{p} = \bar{p}_0(x,t) + s\bar{p}_1(x,t) + s^2\bar{p}_2(x,t) + \cdots \tag{2.19c}$$

$$\Phi = \Phi_0(x,t) + s\Phi_1(x,t) + s^2\Phi_2(x,t) + \cdots \tag{2.19d}$$

Inserting Eqs. (2.19a)-(2.19d) into Eqs. (2.17a)-(2.17d) and (2.18a)-(2.18c), we can get the 1D governing equations describing the weakly nonlinear long waves propagating in electroactive rods, which will be given in Section 5. In the following section, however, we will first perform the linear analysis for the sake of verification.

2.4　Linear dispersion relations

The linear part of Eqs. (2.17a)-(2.17d) corresponds to the dimensionless governing equations which describe the linear waves in soft incompressible electroactive rods and are given as follows:

$$2v + w_x + 2sv_s = 0 \tag{2.20a}$$

$$-\frac{\rho c^2}{\mu}w_{tt} + 4(\bar{\Omega}_2 + 3\eta_3\eta_5^2\bar{\Omega}_5)(v_x + sv_{xx}) + 8(\bar{\Omega}_1 + \bar{\Omega}_2 - \eta_3\eta_5^2\bar{\Omega}_5)(w_s + sw_{ss})$$

$$+ (2\bar{\Omega}_1 + 4\bar{\Omega}_2 + 2\eta_5^2\bar{\Omega}_5)w_{xx} - 4\eta_3\eta_5\Phi_s - 4\eta_3\eta_5 s\Phi_{ss} - \bar{p}_x - 2\eta_3\eta_5\Phi_{xx} = 0 \tag{2.20b}$$

$$-\frac{\rho c^2}{\mu}v_{tt} - 2\bar{p}_s + 8(\bar{\Omega}_1 + 2\bar{\Omega}_2)(2v_s + sv_{ss}) + 4(\bar{\Omega}_2 - \eta_3\eta_5^2\bar{\Omega}_5)w_{sx}$$

$$+ 2(\bar{\Omega}_1 + \bar{\Omega}_2 - \eta_3\eta_5^2\bar{\Omega}_5 + \eta_5^2\bar{\Omega}_5)v_{xx} - 2\eta_3\eta_5\bar{\Omega}_5\Phi_{sx} = 0 \qquad (2.20c)$$

$$\eta_3\eta_5(2v_x + 2sv_{sx} - 4w_s - 4sw_{ss}) - \frac{1}{2}\eta_4(4\Phi_s + 4s\Phi_{ss} + \Phi_{xx}) = 0 \qquad (2.20d)$$

The corresponding linearized boundary conditions from Eqs. (2.18a)-(2.18c) are

$$-\bar{p} - 2\bar{\Omega}_1 w_x + 4\bar{\Omega}_2 v + 4(\bar{\Omega}_1 + 2\bar{\Omega}_2)sv_s = 0, \qquad (2.21a)$$

$$(2\bar{\Omega}_1 + 2\bar{\Omega}_2 - 2\eta_3\eta_5^2\bar{\Omega}_5)(v_x + 2w_s) - 2\eta_3\eta_5\Phi_s = 0, \qquad (2.21b)$$

$$-\eta_3\eta_5(v_x + 2w_s) - \eta_4\Phi_s = 0, \qquad (2.21c)$$

at $s = \delta$.

Substituting the expansions in Eqs. (2.19a)-(2.19d) into Eqs. (2.20a)-(2.20d) and (2.21a)-(2.21c) and setting the coefficients of each power of s to be zero, we get the 1D governing equations as

$$2v_0 + w_{0x} = 0 \qquad (2.22a)$$

$$4v_1 + w_{1x} = 0 \qquad (2.22b)$$

$$6v_2 + w_{2x} = 0 \qquad (2.22c)$$

$$-\frac{\rho c^2}{\mu}w_{0tt} - \bar{p}_{0x} + 4(\bar{\Omega}_2 + 3\eta_3\eta_5^2\bar{\Omega}_5)v_{0x} + 8(\bar{\Omega}_1 + \bar{\Omega}_2 - \eta_3\eta_5^2\bar{\Omega}_5)w_1$$

$$+ (2\bar{\Omega}_1 + 4\bar{\Omega}_2 + 2\eta_5^2\bar{\Omega}_5)w_{0xx} - 4\eta_3\eta_5\Phi_1 - 2\eta_3\eta_5\Phi_{0xx} = 0 \qquad (2.22d)$$

$$-\frac{\rho c^2}{\mu}w_{1tt} - \bar{p}_{1x} + 8(\bar{\Omega}_2 + 3\eta_3\eta_5^2\bar{\Omega}_5)v_{1x} + 32(\bar{\Omega}_1 + \bar{\Omega}_2 - \eta_3\eta_5^2\bar{\Omega}_5)w_2$$

$$+ (2\bar{\Omega}_1 + 4\bar{\Omega}_2 + 2\eta_5^2\bar{\Omega}_5)w_{1xx} - 16\eta_3\eta_5\Phi_2 - 2\eta_3\eta_5\Phi_{1xx} = 0 \qquad (2.22e)$$

$$-\frac{\rho c^2}{\mu}w_{2tt} - \bar{p}_{2x} + 12(\bar{\Omega}_2 + 3\eta_3\eta_5^2\bar{\Omega}_5)v_{2x} + 72(\bar{\Omega}_1 + \bar{\Omega}_2 - \eta_3\eta_5^2\bar{\Omega}_5)w_3$$

$$+ (2\bar{\Omega}_1 + 4\bar{\Omega}_2 + 2\eta_5^2\bar{\Omega}_5)w_{2xx} - 36\eta_3\eta_5\Phi_3 - 2\eta_3\eta_5\Phi_{2xx} = 0 \qquad (2.22f)$$

$$-\frac{\rho c^2}{\mu}v_{0tt} - 2\bar{p}_1 + 16(\bar{\Omega}_1 + 2\bar{\Omega}_2)v_1 + 4(\bar{\Omega}_2 - \eta_3\eta_5^2\bar{\Omega}_5)w_{1x}$$

$$+ 2(\bar{\Omega}_1 + \bar{\Omega}_2 - \eta_3\eta_5^2\bar{\Omega}_5 + \eta_5^2\bar{\Omega}_5)v_{0xx} - 2\eta_3\eta_5\bar{\Omega}_5\Phi_{1x} = 0 \qquad (2.22g)$$

$$-\frac{\rho c^2}{\mu} v_{1tt} - 4\bar{p}_2 + 48(\bar{\Omega}_1 + 2\bar{\Omega}_2)v_2 + 8(\bar{\Omega}_2 - \eta_3\eta_5^2\bar{\Omega}_5)w_{2x} \tag{2.22h}$$
$$+ 2(\bar{\Omega}_1 + \bar{\Omega}_2 - \eta_3\eta_5^2\bar{\Omega}_5 + \eta_5^2\bar{\Omega}_5)v_{1xx} - 4\eta_3\eta_5\bar{\Omega}_5\Phi_{2x} = 0$$

$$-\eta_3\eta_5(-2v_{0x} + 4w_1) - \frac{1}{2}\eta_4(4\Phi_1 + \Phi_{0xx}) = 0 \tag{2.22i}$$

$$-\eta_3\eta_5(-4v_{1x} + 16w_2) - \frac{1}{2}\eta_4(16\Phi_2 + \Phi_{1xx}) = 0 \tag{2.22g}$$

$$-\eta_3\eta_5(-6v_{2x} + 36w_3) - \frac{1}{2}\eta_4(36\Phi_3 + \Phi_{2xx}) = 0 \tag{2.22k}$$

The corresponding boundary conditions are obtained similarly

$$-\bar{p}_0 - 2\bar{\Omega}_1 w_{0x} + 4\bar{\Omega}_2 v_0 + \delta[-\bar{p}_1 - 2\bar{\Omega}_1 w_{1x} + 4(\bar{\Omega}_1 + 3\bar{\Omega}_2)v_1]$$
$$+ \delta^2[-\bar{p}_2 - 2\bar{\Omega}_1 w_{2x} + 4(2\bar{\Omega}_1 + 5\bar{\Omega}_2)v_2] \tag{2.22l}$$
$$+ O(\delta^3) = 0$$

$$(2\bar{\Omega}_1 + 2\bar{\Omega}_2 - 2\eta_3\eta_5^2\bar{\Omega}_5)(v_{0x} + 2w_1) - 2\eta_3\eta_5\Phi_1$$
$$+ \delta[(2\bar{\Omega}_1 + 2\bar{\Omega}_2 - 2\eta_3\eta_5^2\bar{\Omega}_5)(v_{1x} + 4w_2) - 4\eta_3\eta_5\Phi_2]$$
$$+ \delta^2[(2\bar{\Omega}_1 + 2\bar{\Omega}_2 - 2\eta_3\eta_5^2\bar{\Omega}_5)(v_{2x} + 6w_3) - 6\eta_3\eta_5\Phi_3] \tag{2.22m}$$
$$+ O(\delta^3) = 0$$

$$-\eta_3\eta_5(v_{0x} + 2w_1) - \eta_4\Phi_1 + \delta[-\eta_3\eta_5(v_{1x} + 4w_2) - 2\eta_4\Phi_2]$$
$$+ \delta^2[-\eta_3\eta_5(v_{2x} + 6w_3) - 3\eta_4\Phi_3] \tag{2.22n}$$
$$+ O(\delta^3) = 0$$

There are totally fourteen differential equations in Eqs. (2.22a)-(2.22n), giving a mathematically closed system about the fourteen unknown functions w_m, v_n, $\bar{p}_n$ and Φ_m ($m = 0, 1, 2, 3$ and $n = 0, 1, 2$).

To derive the dispersion relations, we assume

$$w_m = A_m e^{i(kx-\omega t)}, \ v_n = B_n e^{i(kx-\omega t)}, \ \bar{p}_n = C_n e^{i(kx-\omega t)}, \ \Phi_m = \Psi_m e^{i(kx-\omega t)} \tag{2.23}$$

Inserting Eq. (2.23) into Eqs. (2.22a)-(2.22n), we get

$$\mathbf{SX} = 0 \tag{2.24}$$

where $\mathbf{X} = \left(A_0, A_1, A_2, A_3, B_0, B_1, B_2, C_0, C_1, C_2, \Psi_0, \Psi_1, \Psi_2, \Psi_3\right)^T$, and

$$\mathbf{S} = \begin{bmatrix} \mathbf{S}_{11} & \mathbf{S}_{12} \\ \mathbf{S}_{21} & \mathbf{S}_{22} \end{bmatrix}$$

is the coefficient matrix with the four submatrices given by

$$\mathbf{S}_{11} = \begin{bmatrix} k\,\mathrm{i} & 0 & 0 & 0 & 2 & 0 & 0 \\ 0 & k\,\mathrm{i} & 0 & 0 & 0 & 4 & 0 \\ 0 & 0 & k\,\mathrm{i} & 0 & 0 & 0 & 6 \\ \Gamma_1 & 8\Gamma_4 & 0 & 0 & 4\Gamma_3 k\,\mathrm{i} & 0 & 0 \\ 0 & \Gamma_1 & 32\Gamma_4 & 0 & 0 & 8\Gamma_3 k\,\mathrm{i} & 0 \\ 0 & 0 & \Gamma_1 & 72\Gamma_4 & 0 & 0 & 12\Gamma_3 k\,\mathrm{i} \\ 0 & 4\Gamma_5 k\,\mathrm{i} & 0 & 0 & \Gamma_2 & 16(\Omega_1+2\Omega_2) & 0 \end{bmatrix}$$

$$\mathbf{S}_{12} = \begin{bmatrix} 0 & 0 & 0 & 0 & 0 & 0 & 0 \\ 0 & 0 & 0 & 0 & 0 & 0 & 0 \\ 0 & 0 & 0 & 0 & 0 & 0 & 0 \\ -k\,\mathrm{i} & 0 & 0 & 2\eta_3\eta_5 k^2 & -4\eta_3\eta_5 & 0 & 0 \\ 0 & -k\,\mathrm{i} & 0 & 0 & 2\eta_3\eta_5 k^2 & -16\eta_3\eta_5 & 0 \\ 0 & 0 & -k\,\mathrm{i} & 0 & 0 & 2\eta_3\eta_5 k^2 & -36\eta_3\eta_5 \\ 0 & -2 & 0 & 0 & -2\eta_3\eta_5\bar{\Omega}_5 k\,\mathrm{i} & 0 & 0 \end{bmatrix}$$

$$\mathbf{S}_{21} = \begin{bmatrix} 0 & 0 & 8\Gamma_5 k\,\mathrm{i} & 0 & 0 & \Gamma_2 & 48(\bar{\Omega}_1+2\bar{\Omega}_2) \\ 0 & -4\eta_3\eta_5 & 0 & 0 & 2\eta_3\eta_5 k\,\mathrm{i} & 0 & 0 \\ 0 & 0 & -16\eta_3\eta_5 & 0 & 0 & 4\eta_3\eta_5 k\,\mathrm{i} & 0 \\ 0 & 0 & 0 & -36\eta_3\eta_5 & 0 & 0 & 6\eta_3\eta_5 k\,\mathrm{i} \\ -2\bar{\Omega}_1 k\,\mathrm{i} & -2\bar{\Omega}_1 k\delta\,\mathrm{i} & -2\bar{\Omega}_1 k\delta^2\,\mathrm{i} & 0 & 4\bar{\Omega}_2 & 4(\bar{\Omega}_1+3\bar{\Omega}_2)\delta & 4(2\bar{\Omega}_1+5\bar{\Omega}_2)\delta^2 \\ 0 & 4\Gamma_4 & 8\Gamma_4\delta & 12\Gamma_4\delta^2 & 2\Gamma_4 k\,\mathrm{i} & 2\delta\Gamma_4 k\,\mathrm{i} & 2\delta^2\Gamma_4 k\,\mathrm{i} \\ 0 & -2\eta_3\eta_5 & -4\eta_3\eta_5\delta & -6\eta_3\eta_5\delta^2 & -\eta_3\eta_5\delta k\,\mathrm{i} & -\eta_3\eta_5\delta k\,\mathrm{i} & -\eta_3\eta_5\delta^2 k\,\mathrm{i} \end{bmatrix}$$

$$\mathbf{S}_{22} = \begin{bmatrix} 0 & 0 & -4 & 0 & 0 & -4\eta_3\eta_5\bar{\Omega}_5 k\,\mathrm{i} & 0 \\ 0 & 0 & 0 & \frac{1}{2}\eta_4 k^2 & -2\eta_4 & 0 & 0 \\ 0 & 0 & 0 & 0 & \frac{1}{2}\eta_4 k^2 & -8\eta_4 & 0 \\ 0 & 0 & 0 & 0 & 0 & \frac{1}{2}\eta_4 k^2 & -18\eta_4 \\ -1 & -\delta & -\delta^2 & 0 & 0 & 0 & 0 \\ 0 & 0 & 0 & 0 & -2\eta_3\eta_5 & -4\delta\eta_3\eta_5 & -6\delta^2\eta_3\eta_5 \\ 0 & 0 & 0 & 0 & -\eta_4 & -2\eta_4\delta & -3\eta_4\delta^2 \end{bmatrix}$$

where

$$\Gamma_1 = \frac{\rho c^2}{\mu}\omega^2 - (2\bar{\Omega}_1 + 4\bar{\Omega}_2 + 2\eta_5^2\bar{\Omega}_5)k^2,$$

$$\Gamma_2 = \frac{\rho c^2}{\mu}\omega^2 - 2(\bar{\Omega}_1 + \bar{\Omega}_2 - \eta_3\eta_5^2\bar{\Omega}_5 + \eta_5^2\bar{\Omega}_5)k^2 \,,$$

$$\Gamma_3 = \bar{\Omega}_2 + 3\eta_3\eta_5^2\bar{\Omega}_5 \,, \quad \Gamma_4 = \bar{\Omega}_1 + \bar{\Omega}_2 - \eta_3\eta_5^2\bar{\Omega}_5 \,, \quad \Gamma_5 = (\bar{\Omega}_2 - \eta_3\eta_5^2\bar{\Omega}_5) \,.$$

For nontrivial solutions, the determinant of the matrix of coefficients must be zero, i.e.

$$\det \mathbf{S} = 0 \tag{2.25}$$

which is the dispersion equation. In the numerical part of this paper, we will compare the results from Eq. (2.25) with the one derived directly from the 3D linear theory so as to validate the above method and derivation.

2.5 The far-field equation

Because Eqs. (2.17a)-(2.17d) and (2.18a)-(2.18c) are complex two-dimensional (2D) nonlinear partial differential equations, it is very difficult to get an analytical wave solution directly. We will thus focus on the far-field equation, which balances the nonlinearity and dispersion. To do so, we shall first simplify Eqs. (2.17a)-(2.17d) and (2.18a)-(2.18c) to the 1D form as in the linear analysis in Section 4. Substituting Eq. (2.19a)-(2.19d) into Eqs. (2.17a)-(2.17d) and (2.18a)-(2.18c) and setting the coefficients of each power of s to be zero, we obtain

$$2v_0 + w_{0x} + \varepsilon(2v_0 w_{0x} + v_0^2) = 0 \tag{2.26a}$$

$$4v_1 + w_{1x} + \varepsilon(4v_1 w_{0x} + 2v_0 w_{1x} - 2v_{0x}w_1 + 4v_0 v_1) = 0 \tag{2.26b}$$

$$
\begin{aligned}
&-\frac{\rho c^2}{\mu}w_{0tt} + 4(\bar{\Omega}_2 + 3\eta_3\eta_5^2\bar{\Omega}_5)v_{0x} + 8(\bar{\Omega}_1 + \bar{\Omega}_2 - \eta_3\eta_5^2\bar{\Omega}_5)w_1 - 4\eta_3\eta_5\Phi_1 - 2\eta_3\eta_5\Phi_{0xx} \\
&+ (2\bar{\Omega}_1 + 4\bar{\Omega}_2 + 2\eta_5^2\bar{\Omega}_5)w_{0xx} - \bar{p}_{0x} + \varepsilon[-2\bar{p}_{0x}v_0 + 4(\bar{\Omega}_2 + 7\eta_3\eta_5^2\bar{\Omega}_5)v_{0x}w_{0x} \\
&+ (4\bar{\Omega}_2 + 104\eta_3^2\eta_5^2\bar{\Omega}_5 + 16\bar{\Omega}_5\eta_5^2\eta_3)v_0 v_{0x} + (16\bar{\Omega}_2 - 48\eta_3^2\eta_5^2\bar{\Omega}_5)v_0 w_1 - 8\eta_3\eta_5^2\bar{\Omega}_5 w_1 w_{0x} \\
&+ 8(\bar{\Omega}_2 + 4\eta_3\eta_5^2\bar{\Omega}_5)v_0 w_{0xx} - 4\eta_3\eta_5(1 + 2\eta_3)w_{0x}\Phi_1 - 24\eta_3^2\eta_5 v_0\Phi_1 - 16\eta_3^2\eta_5 v_0\Phi_{0xx} \\
&- 12\eta_3^2\eta_5 v_{0x}\Phi_{0x} + 8\eta_3^2\eta_5 w_1\Phi_{0x} - 2\eta_3\eta_5 w_{0x}\Phi_{0xx} - 2\eta_3\eta_5 w_{0xx}\Phi_{0x} \\
&+ 2\eta_4^2\bar{\Omega}_5\Phi_1\Phi_{0x} + \eta_4^2\bar{\Omega}_5\Phi_{0x}\Phi_{0xx}] = 0
\end{aligned}
$$

$$\tag{2.26c}$$

$$-\frac{\rho c^2}{\mu}w_{1tt}+8(\bar{\Omega}_2+3\eta_3\eta_5^2\bar{\Omega}_5)v_{1x}+32(\bar{\Omega}_1+\bar{\Omega}_2-\eta_3\eta_5^2\bar{\Omega}_5)w_2-16\eta_3\eta_5\Phi_2$$

$$-2\eta_3\eta_5\Phi_{1xx}+(2\bar{\Omega}_1+4\bar{\Omega}_2+2\eta_5^2\bar{\Omega}_5)w_{1xx}-\bar{p}_{1x}+\varepsilon[2\bar{p}_1v_{0x}-2(\bar{p}_{1x}v_0+2\bar{p}_{0x}v_1)$$

$$-32\eta_3\eta_5^2\bar{\Omega}_5w_2w_{0x}-32\eta_3\eta_5^2\bar{\Omega}_5w_1w_{1x}+(144\eta_3^2\eta_5^2\bar{\Omega}_5+32\bar{\Omega}_5\eta_3\eta_5^2-8\bar{\Omega}_2)v_1v_{0x}$$

$$-4(\bar{\Omega}_2-5\eta_3\eta_5^2\bar{\Omega}_5)v_{0xx}w_1+(8\bar{\Omega}_2+176\eta_3^2\eta_5^2\bar{\Omega}_5+32\bar{\Omega}_5\eta_3\eta_5^2)v_0v_{1x}$$

$$-4(\bar{\Omega}_2-3\eta_3\eta_5^2\bar{\Omega}_5)v_{0x}w_{1x}-24\eta_3^2\eta_5v_{1x}\Phi_{0x}+8(\bar{\Omega}_2+7\eta_3\eta_5^2\bar{\Omega}_5)v_{1x}w_{0x}$$

$$+32(\bar{\Omega}_2-5\eta_3^2\eta_5^2\bar{\Omega}_5)v_1w_1+64(\bar{\Omega}_2-3\eta_3^2\eta_5^2\bar{\Omega}_5)v_0w_2+16(\bar{\Omega}_2+4\eta_3\eta_5^2\bar{\Omega}_5)v_1w_{0xx}$$

$$+8(\bar{\Omega}_2+4\eta_3\eta_5^2\bar{\Omega}_5)v_0w_{1xx}-(8\eta_3^2\eta_5+12\eta_3\eta_5)w_{1x}\Phi_1-16(\eta_3\eta_5+2\eta_3^2\eta_5)w_{0x}\Phi_2$$

$$+4\eta_3^2\eta_5v_{0xx}\Phi_1+4(3\eta_3^2\eta_5-4\eta_3^2\eta_5)v_{0x}\Phi_{1x}-80\eta_3^2\eta_5v_1\Phi_1-96\eta_3^2\eta_5v_0\Phi_2$$

$$-32\eta_3^2\eta_5v_1\Phi_{0xx}-16\eta_3^2\eta_5v_0\Phi_{1xx}+32\eta_3^2\eta_5w_2\Phi_{0x}+(24\eta_3^2\eta_5-4\eta_3\eta_5)w_1\Phi_{1x}$$

$$-2\eta_3\eta_5(w_{1x}\Phi_{0xx}+w_{0x}\Phi_{1xx})-2\eta_3\eta_5w_{1xx}\Phi_{0x}-2\eta_3\eta_5w_{0xx}\Phi_{1x}$$

$$+4\eta_4^2\bar{\Omega}_5(2\Phi_2\Phi_{0x}+\Phi_1\Phi_{1x})+\eta_4^2\bar{\Omega}_5(\Phi_{1x}\Phi_{0xx}+\Phi_{0x}\Phi_{1xx})]=0$$

(2.26d)

$$-\frac{\rho c^2}{\mu}v_{0tt}-2\bar{p}_1+16(\bar{\Omega}_1+2\bar{\Omega}_2)v_1+4(\bar{\Omega}_2-\eta_3\eta_5^2\bar{\Omega}_5)w_{1x}-2\eta_3\eta_5\bar{\Omega}_5\Phi_{1x}$$

$$+2(\bar{\Omega}_1+\bar{\Omega}_2-\eta_3\eta_5^2\bar{\Omega}_5+\eta_5^2\bar{\Omega}_5)v_{0xx}+\varepsilon[-2\bar{p}_1w_{0x}+2\bar{p}_{0x}w_1-2\bar{p}_1v_0+32\bar{\Omega}_2v_1w_{0x}$$

$$-16(\eta_3\eta_5^2\bar{\Omega}_5+\bar{\Omega}_2)v_{0x}w_1+4(\bar{\Omega}_2-\eta_3\eta_5^2\bar{\Omega}_5-6\eta_3^2\eta_5^2\bar{\Omega}_5)v_0w_{1x}+4\bar{\Omega}_2w_{0x}w_{1x}$$

$$-4\bar{\Omega}_2w_1w_{0xx}+(24\eta_3^2\eta_5^2\bar{\Omega}_5-8\bar{\Omega}_2)w_1^2+(8\eta_3\eta_5^2\bar{\Omega}_5-6\eta_3^2\eta_5^2\bar{\Omega}_5+2\bar{\Omega}_2)v_{0x}^2+32\bar{\Omega}_2v_0v_1$$

$$+(4\bar{\Omega}_2+14\eta_3\eta_5^2\bar{\Omega}_5-12\eta_3^2\eta_5^2\bar{\Omega}_5)v_0v_{0xx}-8\eta_3\eta_5v_{0x}\Phi_1-(2\eta_3\eta_5+12\eta_3^2\eta_5)v_0\Phi_{1x}$$

$$+(2\eta_3^2\eta_5-2\eta_3\eta_5)(v_{0xx}\Phi_{0x}+v_{0x}\Phi_{0xx})+\eta_3^2\eta_5(24w_1\Phi_1+4w_{1x}\Phi_{0x}+4w_1\Phi_{0xx})$$

$$-4\eta_3^2\eta_5w_{0xx}\Phi_1-4\eta_3^2\eta_5w_{0x}\Phi_{1x}+\eta_4^2\bar{\Omega}_5(\Phi_{1x}\Phi_{0x}+\Phi_1\Phi_{0xx}+6\Phi_1^2)]=0$$

(2.26e)

$$-\eta_3\eta_5(-2v_{0x}+4w_1)-\frac{1}{2}\eta_4(4\Phi_1+\Phi_{0xx})+\varepsilon[\eta_4\eta_3(-v_{0x}\Phi_{0x}$$

$$+2w_1\Phi_{0x}-4w_{0x}\Phi_1-2v_0\Phi_{0xx}-4v_0\Phi_1)+\eta_3^2\eta_5(-8v_0w_1+12v_0v_{0x})$$

$$+2\eta_3\eta_5(2v_{0x}w_{0x}+2v_0w_{0xx}+2v_0v_{0x})]=0$$

(2.26f)

$$-\eta_3\eta_5(-4v_{1x}+16w_2)-\frac{1}{2}\eta_4(16\Phi_2+\Phi_{1xx})+\varepsilon[\eta_4\eta_3(v_{0x}\Phi_{1x}+v_{0xx}\Phi_1+8w_2\Phi_{0x}$$

$$+6w_1\Phi_{1x}-6w_{1x}\Phi_1-16w_{0x}\Phi_2-4v_1\Phi_{0xx}-2v_{1x}\Phi_{0x}-2v_0\Phi_{1xx}-8v_1\Phi_1-16v_0\Phi_2)$$

$$+\eta_3^2\eta_5(-16v_1w_1-32v_0w_2+16v_0v_{1x}+16v_{0x}v_1)+2\eta_3\eta_5(4v_{1x}w_{0x}+4v_1w_{0xx}+2v_0w_{1xx}$$

$$-2v_{0xx}w_1+4v_1v_{0x}+4v_0v_{1x})]=0$$

(2.26g)

The corresponding boundary conditions are given by

$$-\bar{p}_0 - 2\bar{\Omega}_1 w_{0x} + 4\bar{\Omega}_2 v_0 + \varepsilon[-\bar{p}_0 w_{0x} - \bar{p}_0 v_0 - 2\bar{\Omega}_1 v_0 w_{0x} + 6\bar{\Omega}_2 v_0^2$$
$$+ 2\bar{\Omega}_2 w_{0x}^2] + \delta[-\bar{p}_1 - 2\bar{\Omega}_1 w_{1x} + 4(\bar{\Omega}_1 + 3\bar{\Omega}_2)v_1] + O(\varepsilon\delta, \varepsilon^2) = 0 \tag{2.26h}$$

$$(2\bar{\Omega}_1 + 2\bar{\Omega}_2 - 2\eta_3\eta_5^2\bar{\Omega}_5)(v_{0x} + 2w_1) - 2\eta_3\eta_5\Phi_1 + \varepsilon[\bar{p}_0 v_{0x}$$
$$+ 2(\bar{\Omega}_1 + \bar{\Omega}_2 - 6\eta_3^2\eta_5^2\bar{\Omega}_5)v_0 v_{0x} + 8(\bar{\Omega}_2 - 3\eta_3^2\eta_5^2\bar{\Omega}_5)v_0 w_1$$
$$- (2\bar{\Omega}_2 + 2\eta_3\eta_5^2\bar{\Omega}_5)v_{0x}w_{0x} - 4\eta_3\eta_5^2\bar{\Omega}_5 w_1 w_{0x} - (2\eta_3\eta_5 + 4\eta_3^2\eta_5)w_{0x}\Phi_1 \tag{2.26i}$$
$$+ 2\eta_3^2\eta_5 v_{0x}\Phi_{0x} - 12\eta_3^2\eta_5 v_0\Phi_1 + 4\eta_3^2\eta_5 w_1\Phi_{0x} + \eta_4^2\bar{\Omega}_5\Phi_1\Phi_{0x}]$$
$$+ \delta[(2\bar{\Omega}_1 + 2\bar{\Omega}_2 - 2\eta_3\eta_5^2\bar{\Omega}_5)(v_{1x} + 4w_2) - 4\eta_3\eta_5\Phi_2] + O(\delta\varepsilon, \varepsilon^2) = 0$$

$$-\eta_3\eta_5(v_{0x} + 2w_1) - \eta_4\Phi_1 + \varepsilon[\bar{\Omega}_5\eta_4^2(\frac{1}{2}v_{0x}\Phi_{0x} + w_1\Phi_{0x}) - 4\eta_3^2\eta_5 v_0 w_1 - 2\eta_3^2\eta_5 v_0 v_{0x}$$
$$- 2\eta_4\eta_3 v_0\Phi_1 - 2\eta_4^2\bar{\Omega}_5 w_{0x}\Phi_1] + \delta[-\eta_3\eta_5(v_{1x} + 4w_2) - 2\eta_4\Phi_2] + O(\delta\varepsilon, \varepsilon^2) = 0$$

$$\tag{2.26j}$$

The above ten equations give the nonlinear 1D governing equations, in which the terms $O(\delta\varepsilon, \varepsilon^2)$ will be neglected.

To derive the asymptotically valid far-field equation, we adopt here the reductive perturbation method (Jeffrey and Kawahara, 1982) and introduce the following transformations (Dai and Huo, 2002)

$$\xi = x - t, \ \tau = \varepsilon t \tag{2.27a}$$

It is assumed that w_i, v_j, $\bar{p}_j$ and Φ_i ($i = 0, 1, 2$ and $j = 0, 1$) in Eq. (2.26) have the following perturbation expansions

$$w_i = w_{i0} + \varepsilon w_{i1} + \cdots, \ v_j = v_{j0} + \varepsilon v_{j1} + \cdots,$$
$$\bar{p}_j = \bar{p}_{j0} + \varepsilon\bar{p}_{j1} + \cdots, \ \Phi_i = \Phi_{i0} + \varepsilon\Phi_{i1} + \cdots \tag{2.27b}$$

Substituting Eqs. (2.27a) and (2.27b) into Eqs. (2.26a)-(2.26j), we obtain at $O(\varepsilon^0)$

$$\mathbf{MH}_0 = \mathbf{0} \tag{2.28}$$

where $\mathbf{H}_0 = \left(w_{00\xi}, w_{10}, w_{20}, v_{00}, v_{10}, \bar{p}_{00}, \bar{p}_{10}, \Phi_{00\xi}, \Phi_{10}, \Phi_{20}\right)^{\mathrm{T}}$, and

$$\mathbf{M} = \begin{bmatrix} \mathbf{M}_{11} & \mathbf{M}_{12} \\ \mathbf{M}_{21} & \mathbf{M}_{22} \end{bmatrix}$$

$$\mathbf{M}_{11} = \begin{bmatrix} 1 & 0 & 0 & 2 & 0 \\ 0 & \dfrac{\partial}{\partial \xi} & 0 & 0 & 4 \\ d_1 \dfrac{\partial}{\partial \xi} & 8d_4 & 0 & 4d_3 \dfrac{\partial}{\partial \xi} & 0 \\ 0 & d_1 \dfrac{\partial^2}{\partial \xi^2} & 32d_4 & 0 & 8d_3 \dfrac{\partial}{\partial \xi} \\ 0 & 4d_6 \dfrac{\partial}{\partial \xi} & 0 & d_2 \dfrac{\partial^2}{\partial \xi^2} & 16d_5 \end{bmatrix}$$

$$\mathbf{M}_{12} = \begin{bmatrix} 0 & 0 & 0 & 0 & 0 \\ 0 & 0 & 0 & 0 & 0 \\ -\dfrac{\partial}{\partial \xi} & 0 & -2\eta_3 \eta_5 \dfrac{\partial}{\partial \xi} & -4\eta_3 \eta_5 & 0 \\ 0 & -\dfrac{\partial}{\partial \xi} & 0 & -2\eta_3 \eta_5 \dfrac{\partial^2}{\partial \xi^2} & -16\eta_3 \eta_5 \\ 0 & -2 & 0 & -2\eta_3 \eta_5 \bar{\Omega}_5 \dfrac{\partial}{\partial \xi} & 0 \end{bmatrix}$$

$$\mathbf{M}_{21} = \begin{bmatrix} 0 & -4\eta_3 \eta_5 & 0 & 2\eta_3 \eta_5 \dfrac{\partial}{\partial \xi} & 0 \\ 0 & 0 & -16\eta_3 \eta_5 & 0 & 4\eta_3 \eta_5 \dfrac{\partial}{\partial \xi} \\ -2\bar{\Omega}_1 & 0 & 0 & 4\bar{\Omega}_2 & 0 \\ 0 & 4d_4 & 0 & 2d_4 \dfrac{\partial}{\partial \xi} & 0 \\ 0 & -2\eta_3 \eta_5 & 0 & -\eta_3 \eta_5 \dfrac{\partial}{\partial \xi} & 0 \end{bmatrix}$$

$$\mathbf{M}_{22} = \begin{bmatrix} 0 & 0 & -\dfrac{1}{2}\eta_4 \dfrac{\partial}{\partial \xi} & -2\eta_4 & 0 \\ 0 & 0 & 0 & -\dfrac{1}{2}\eta_4 \dfrac{\partial^2}{\partial \xi^2} & -8\eta_4 \\ -1 & 0 & 0 & 0 & 0 \\ 0 & 0 & 0 & -2\eta_3 \eta_5 & 0 \\ 0 & 0 & 0 & -\eta_4 & 0 \end{bmatrix}$$

where

$$d_1 = 2\bar{\Omega}_1 + 4\bar{\Omega}_2 + 2\eta_5^2\bar{\Omega}_5 - \rho c^2 / \mu, \quad d_2 = 2(\bar{\Omega}_1 + \bar{\Omega}_2 - \eta_3\eta_5^2\bar{\Omega}_5 + \eta_5^2\bar{\Omega}_5) - \rho c^2 / \mu,$$

$$d_3 = \bar{\Omega}_2 + 3\eta_3\eta_5^2\bar{\Omega}_5, \quad d_4 = \bar{\Omega}_1 + \bar{\Omega}_2 - \eta_3\eta_5^2\bar{\Omega}_5, \quad d_5 = \bar{\Omega}_1 + 2\bar{\Omega}_2, \quad d_6 = \bar{\Omega}_2 - \eta_3\eta_5^2\bar{\Omega}_5$$

In order to find the nontrivial solutions, we let

$$\det \mathbf{M} = 0 \tag{2.29}$$

which leads to

$$\frac{\rho c^2}{\mu} = 2(3\bar{\Omega}_1 + 3\bar{\Omega}_2 + \eta_5^2\bar{\Omega}_5) \tag{2.30}$$

It is noted that the above result is identical to the one obtained by Dai and Huo (2002) for neo-Hookean elastic materials, for which $\bar{\Omega}_1 = 1/2$, $\bar{\Omega}_2 = 0$, $\bar{\Omega}_5 = 0$.

From Eq. (2.28), we have

$$v_{00} = -\frac{1}{2}w_{00\xi}, v_{10} = -\frac{1}{16}w_{00\xi\xi\xi}, w_{10} = \frac{1}{4}w_{00\xi\xi}, w_{20} = (\frac{3}{64} + \frac{1}{32}\frac{\eta_3\eta_5^2\bar{\Omega}_5}{\bar{\Omega}_1 + \bar{\Omega}_2})w_{00\xi\xi\xi\xi},$$

$$\bar{p}_{00} = -2(\bar{\Omega}_1 + \bar{\Omega}_2)w_{00\xi}, \bar{p}_{10} = \frac{1}{2}(\bar{\Omega}_1 + \bar{\Omega}_2)w_{00\xi\xi\xi}, \Phi_{00\xi} = -4\bar{\Omega}_5\eta_5 w_{00\xi},$$

$$\Phi_{10} = 0, \Phi_{20} = -\frac{\bar{\Omega}_5\eta_5}{16}(2 + \frac{\eta_3\eta_5^2\bar{\Omega}_5}{\bar{\Omega}_1 + \bar{\Omega}_2})w_{00\xi\xi\xi\xi}$$

$$\tag{2.31}$$

The left eigenvector $\mathbf{L}_e$ of the matrix $\mathbf{M}$ is given by

$$\mathbf{L}_e = \left(2(\bar{\Omega}_1 + \bar{\Omega}_2)\frac{\partial}{\partial\xi}, 0, 1, 0, 0, -4\eta_5\bar{\Omega}_5, 0, -\frac{\partial}{\partial\xi}, -2, 8\eta_5\bar{\Omega}_5 \right) \tag{2.32}$$

At $O(\varepsilon)$, we can get another ten equations. Inserting Eq. (2.31) into these equations, we obtain

$$\mathbf{MH}_1 + \mathbf{Q}_1 w_{00\xi\tau} + \mathbf{Q}_2 w_{00\xi}^2 + \mathbf{Q}_3 w_{00\xi}w_{00\xi\xi\xi} + \mathbf{Q}_4 w_{00\xi\xi}^2 + \mathbf{Q}_5 w_{00\xi\xi\xi} = 0 \tag{2.33}$$

where $\mathbf{H}_1 = \left(w_{01\xi}, w_{11}, w_{21}, v_{01}, v_{11}, \bar{p}_{01}, \bar{p}_{11}, \Phi_{01\xi}, \Phi_{11}, \Phi_{21} \right)^{\mathrm{T}}$, and

$$\mathbf{Q}_1 = \left(0, 0, 4d_7, d_7\frac{\partial^2}{\partial\xi^2}, -2d_7\frac{\partial}{\partial\xi}, 0, 0, 0, 0, 0 \right)^{\mathrm{T}},$$

$$\mathbf{Q}_2 = \left(-\frac{3}{4}, 0, -d_8\frac{\partial}{\partial\xi}, 0, 0, (-2\eta_3^2\eta_5 - \frac{3}{2}\eta_3\eta_5)\frac{\partial}{\partial\xi}, 0, 2\bar{\Omega}_1 + \frac{9}{2}\bar{\Omega}_2, \frac{3}{4}(\bar{\Omega}_1 + \bar{\Omega}_2)\frac{\partial}{\partial\xi}, 0 \right)^{\mathrm{T}},$$

$$\mathbf{Q}_3 = \left(0, -\frac{3}{8}, 0, \beta_1\frac{\partial}{\partial\xi}, -\frac{1}{2}\bar{\Omega}_1, 0, (\frac{1}{4}\eta_3^2 - \frac{3}{4}\eta_3)\frac{\partial}{\partial\xi}, 0, 0, 0 \right)^{\mathrm{T}},$$

$$\mathbf{Q}_4 = \left(0, \frac{1}{4}, 0, -\beta_2 \frac{\partial}{\partial \xi}, -\bar{\Omega}_1, 0, (-\frac{1}{4}\eta_3^2 \eta_5 + \frac{1}{2}\eta_3) \frac{\partial}{\partial \xi}, 0, 0, 0\right)^{\mathrm{T}},$$

$$\mathbf{Q}_5 = \left(0, 0, 0, 0, 0, 0, 0, -\frac{5}{4}\frac{\delta}{\varepsilon}(\bar{\Omega}_1 + \bar{\Omega}_2), \beta_3 \frac{\delta}{\varepsilon} \frac{\partial}{\partial \xi}, \frac{1}{8}\frac{\delta}{\varepsilon}\eta_3 \eta_5 \frac{\partial}{\partial \xi}\right)^{\mathrm{T}},$$

where

$$\beta_1 = \frac{1}{2}\bar{\Omega}_1 - \frac{9}{4}\bar{\Omega}_2 - 4\eta_3^2 \eta_5^2 \bar{\Omega}_5 - \frac{\bar{\Omega}_2}{\bar{\Omega}_1 + \bar{\Omega}_2}\eta_3 \eta_5^2 \bar{\Omega}_5,$$

$$\beta_2 = \frac{3}{4}\bar{\Omega}_1 - \frac{1}{4}\bar{\Omega}_2 + \frac{1}{2}\eta_3^2 \eta_5^2 \bar{\Omega}_5 - \eta_3 \eta_5^2 \bar{\Omega}_5 - \frac{1}{2}\frac{\bar{\Omega}_2}{\bar{\Omega}_1 + \bar{\Omega}_2}\eta_3 \eta_5^2 \bar{\Omega}_5,$$

$$\beta_3 = \frac{1}{4}(\bar{\Omega}_1 + \bar{\Omega}_2 + 2\eta_3 \eta_5^2 \bar{\Omega}_5), \quad d_7 = 3\bar{\Omega}_1 + 3\bar{\Omega}_2 + \eta_5^2 \bar{\Omega}_5,$$

$$d_8 = \bar{\Omega}_1 + \frac{9}{2}\bar{\Omega}_2 + 8\eta_3^2 \eta_5^2 \bar{\Omega}_5 + 6\eta_3 \eta_5^2 \bar{\Omega}_5.$$

To suppress the secular terms, which might arise from Eq. (2.33), we multiply the left-hand side of it by the left eigenvector $\mathbf{L}_e$, and arrive at

$$w_{00\xi\tau} + \Lambda_1 w_{00\xi} w_{00\xi\xi} + \Lambda_2 w_{00\xi\xi\xi\xi} = 0 \qquad (2.34a)$$

where

$$\Lambda_1 = \frac{-3(\bar{\Omega}_1 + 2\bar{\Omega}_2)}{3\bar{\Omega}_1 + 3\bar{\Omega}_2 + \eta_5^2 \bar{\Omega}_5}, \quad \Lambda_2 = \frac{3(\bar{\Omega}_1 + \bar{\Omega}_2)}{16(3\bar{\Omega}_1 + 3\bar{\Omega}_2 + \eta_5^2 \bar{\Omega}_5)}\frac{\delta}{\varepsilon} \qquad (2.34b)$$

Eq. (2.34a) is of the type of the well-known Korteweg-de Vries (KdV) equation, which is the asymptotically valid far-field equation for $w_{00\xi}$ for nonlinear waves in electroactive circular rods. Eq. (2.34a), which incorporates both nonlinearity and dispersion, admits a single-soliton solution, namely solitary wave. Λ_1 and Λ_2 are the coefficients of the nonlinear term and the linear dispersive term, respectively, and they can get modulated by changing the biasing electric displacement. If we neglect the nonlinear term, we can get the linearized KdV equation, namely

$$w_{00\xi\tau} + \Lambda_2 w_{00\xi\xi\xi\xi} = 0 \qquad (2.35a)$$

From Eq. (2.35a), we can get the asymptotically valid dispersion relation as

$$\omega = k - \varepsilon\Lambda_2 k^3 \qquad (2.35b)$$

This equation will be compared numerically with Eq. (2.25) and the one derived directly from the 3D linear theory in the next section.

The solitary wave solution to the KdV equation (2.34a) is known to be

$$w_{00\xi} = -H\operatorname{sech}^2\left[\sqrt{H/2}\left(\lambda_1\xi - H\lambda_2\tau - y_0\right)\right] \tag{2.36a}$$

where $H > 0$ is the wave amplitude, which is a given parameter in the nonlinear analysis, y_0 is a phase constant, which will be made zero without loss of generality in the numerical part, and

$$\lambda_1 = \sqrt{\frac{8(\bar{\Omega}_1 + 2\bar{\Omega}_2)}{3(\bar{\Omega}_1 + \bar{\Omega}_2)}\frac{\varepsilon}{\delta}}, \quad \lambda_2 = \frac{\bar{\Omega}_1 + 2\bar{\Omega}_2}{3\bar{\Omega}_1 + 3\bar{\Omega}_2 + \eta_5^2\bar{\Omega}_5}\lambda_1 \tag{2.36b}$$

Inserting Eq. (2.36a) into Eq. (2.31), we can obtain the expressions of $\Phi_{00\xi}$ and v_{00} as follows

$$\Phi_{00\xi} = 4\bar{\Omega}_5\eta_5 H\operatorname{sech}^2\left[\sqrt{H/2}\left(\lambda_1\xi - H\lambda_2\tau - y_0\right)\right] \tag{2.36c}$$

$$v_{00} = \frac{1}{2}H\operatorname{sech}^2\left[\sqrt{H/2}\left(\lambda_1\xi - H\lambda_2\tau - y_0\right)\right] \tag{2.36d}$$

From Eq. (2.36d), we recognize that the solitary wave is an expansion wave (i.e. the cross-section of the rod expanses while the solitary wave propagates). Due to electroelastic coupling, we can also get the electric field corresponding to the solitary wave, as given in Eq. (2.36c). Clearly, the amplitude of the electric field depends on the biasing electric displacement.

We then can get the leading order of the solitary wave solution from Eqs. (2.36a, c, d) as

$$w_x = -H\operatorname{sech}^2\left\{\sqrt{H/2}\left[\lambda_1 x - (\lambda_1 + H\lambda_2\varepsilon)t - y_0\right]\right\} \tag{2.37a}$$

$$\Phi_x = 4\bar{\Omega}_5\eta_5 H\operatorname{sech}^2\left\{\sqrt{H/2}\left[\lambda_1 x - (\lambda_1 + H\lambda_2\varepsilon)t - y_0\right]\right\} \tag{2.37b}$$

$$v = \frac{1}{2}H\operatorname{sech}^2\left\{\sqrt{H/2}\left[\lambda_1 x - (\lambda_1 + H\lambda_2\varepsilon)t - y_0\right]\right\} \tag{2.37c}$$

Thus, after a tedious derivation, we get a simple solitary wave solution as specified in Eqs. (2.37a)-(2.37c). It is interesting that the biasing electric displacement only affects the wave velocity but doesn't change the wave shape of

the longitudinal strain or the transverse displacement when the amplitude is specified. From Eq. (2.37c), we find that the transverse displacement has its amplitude proportional to the longitudinal strain, and its propagation velocity equal to the wave velocity in the rod. This particular character is often used to measure the longitudinal wave velocity (Samsonov, 2001). As expected, the longitudinal electric field also has the same wave velocity, and this property may be used to measure the velocity of solitary waves in electroactive rods through the electric means. More detailed discussions based on numerical calculations will be given in the following section.

2.6   Numerical investigation and discussions

2.6.1   The linear case

To verify the present approach and the mathematical derivation, we compare the linear dispersion relations in Eqs. (2.25) and (2.35b) with the one derived directly from the 3D linear theory as given by Chen and Dai (2012). For convenience, we will adopt the same dimensionless quantities as the ones in the paper of Chen and Dai, and they are related to those in the present paper by

$$\omega = \delta^{-1/2}\sqrt{\frac{\mu}{\rho c^2}}\bar{\omega}, \ k = \delta^{-1/2}\bar{k} \tag{2.38}$$

where $\bar{\omega}$ and $\bar{k}$ are the dimensionless wave frequency and wave number defined in the paper (Chen and Dai, 2012). Then, Eq. (2.35b) can be expressed by $\bar{k}$ and $\bar{\omega}$ as

$$\bar{\omega} = \sqrt{2(3\bar{\Omega}_1 + 3\bar{\Omega}_2 + \eta_5^2\bar{\Omega}_5)}\bar{k} - \frac{3\sqrt{2}(\bar{\Omega}_1 + \bar{\Omega}_2)}{16\sqrt{3\bar{\Omega}_1 + 3\bar{\Omega}_2 + \eta_5^2\bar{\Omega}_5}}\bar{k}^3 \tag{2.39}$$

We adopt the following energy function, which is a modification of the classical neo-Hookean elastic model (Dorfmann and Ogden, 2010),

$$\Omega = \frac{1}{2}\mu(I_1 - 3) + \frac{1}{\varepsilon_0}(\gamma_1 I_4 + \gamma_2 I_5) \tag{2.40a}$$

where μ is the shear modulus of the material, and γ_1 and γ_2 are two dimensionless electroelastic coupling parameters. Thus, we can obtain the following parameters

$$\bar{\Omega}_1 = \frac{1}{2}, \ \bar{\Omega}_2 = 0, \ \bar{\Omega}_4 = \gamma_1, \ \bar{\Omega}_5 = \gamma_2 \tag{2.40b}$$

The components of the coefficient matrix in Eq. (2.25) in terms of $\bar{k}$ and $\bar{\omega}$ for the above modified neo-Hookean materials are given in Appendix 4C.

Table 2.1 Comparison of three dispersion relations under two different biasing electric fields

$\bar{k}$	$\eta_5 = 0.5$			$\eta_5 = 1.0$		
	Eq. (2.25)	Eq. (2.39)	Chen & Dai	Eq. (2.25)	Eq. (2.39)	Chen & Dai
0.01	0.01936	0.01936	0.01936	0.02449	0.02449	0.02449
0.03	0.05809	0.05809	0.05809	0.07348	0.07348	0.07348
0.05	0.09681	0.09681	0.09681	0.12246	0.12246	0.12246
0.10	0.19355	0.19355	0.19355	0.24487	0.24487	0.24487
0.20	0.38652	0.38652	0.38652	0.48928	0.48929	0.48928
0.30	0.57833	0.57833	0.57833	0.73274	0.73278	0.73276
0.40	0.76838	0.76840	0.76840	0.97473	0.97490	0.97482
0.50	0.95609	0.95614	0.95613	1.21469	1.21518	1.21495

It should be noted that Eq. (2.25) admits both the numerical solution and the asymptotic solution (Dai and Huo, 2002). In this Section, however, we will only discuss the numerical solution. We set $\gamma_1 = 0.5$ and $\gamma_2 = 1.5$ in the numerical calculation, and the results are given in Table 2.1. It is shown that both linear dispersion relations (2.25) and (2.39) agree well with the 3D one in the reference (Chen and Dai, 2012) for long wavelengths, which validates, at least in part, our

approach, derivation and computation. It also should be emphasized that both δ and γ_1 have no influence on the results in the limit of small wave number, as is seen from Eq. (2.39).

2.6.2 The nonlinear case

In this part, we will discuss how the parameters affect the behavior of the nonlinear solitary waves. We will adopt the following energy function derived on the base of the incompressible elastic Mooney-Rivlin material model:

$$\Omega = \frac{1}{2}\mu(\frac{1}{2}+\beta)(I_1-3) + \frac{1}{2}\mu(\frac{1}{2}-\beta)(I_2-3) + \frac{1}{\varepsilon_0}(\gamma_1 I_4 + \gamma_2 I_5) \qquad (2.41)$$

where μ is the shear modulus of the material, $-1/2 < \beta \leq 1/2$ is the material constant, and γ_1 and γ_2 are two dimensionless electroelastic coupling parameters. The following dimensionless quantities are then obtained:

$$\bar\Omega_1 = \frac{1}{4} + \frac{\beta}{2}, \ \bar\Omega_2 = \frac{1}{4} - \frac{\beta}{2}, \ \bar\Omega_4 = \gamma_1, \ \bar\Omega_5 = \gamma_2 \qquad (2.42)$$

It is noticed that Eq. (2.41) will be degenerated to Eq. (2.40a) when $\beta = 1/2$, which represents a simpler situation, but solitary wave solutions are still obtainable, as may be seen from Eq. (2.36b).

Since the dimensionless variable t in Eqs. (2.37a)-(2.37c) is related to the underlying electric displacement, it is inconvenient to show clearly the influence of the underlying electric displacement on the solitary wave. Thus, we adopt the following new dimensionless expressions of the solitary wave

$$w_x = -H\mathrm{sech}^2\left[\sqrt{H/2}\lambda_1\left(x - c_p t_0\right)\right] \qquad (2.43a)$$

$$\Phi_x = 4\bar\Omega_5\eta_5 H\mathrm{sech}^2\left[\sqrt{H/2}\lambda_1\left(x - c_p t_0\right)\right] \qquad (2.43b)$$

$$v = \frac{1}{2}H\mathrm{sech}^2\left[\sqrt{H/2}\lambda_1\left(x - c_p t_0\right)\right] \qquad (2.43c)$$

where $t_0 = c_T T/l$ is the dimensionless time, with $c_T = \sqrt{\mu/\rho}$ being the shear wave velocity, and the solitary wave velocity can be given by

$$c_p = \sqrt{3 + 2\gamma_2 \eta_5^2} + 2H\varepsilon \frac{\overline{\Omega}_1 + 2\overline{\Omega}_2}{\sqrt{3 + 2\gamma_2 \eta_5^2}} \tag{2.44}$$

which indicates that the biasing electric field can modulate the solitary wave velocity. Similar observation is also reported in the published paper (Pouget, 1986) that the applied electric field can change the velocity of solitary waves in elastic ferroelectrics.
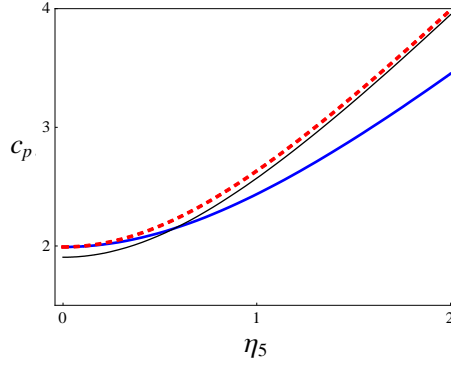
Fig. 2.2. Variations of wave velocity with the biasing electric displacement: thick solid line - ($\beta = 0$, $\gamma_2 = 1$), dotted line - ($\beta = 0$, $\gamma_2 = 1.5$), thin solid line -

$$(\beta = 1/2, \quad \gamma_2 = 1.5)$$

Fig. 2.2 displays the wave velocity as functions of the underlying biasing electric displacement, under different combinations of the two parameters β and γ_2 for $\varepsilon = \delta$=0.3 and $H = 1$. It is shown that the wave velocity increases monotonically with the increasing of the biasing electric displacement when the product $H \cdot \varepsilon$ is small enough, which can be readily seen from Eq. (2.44). Comparing the curves with each other or referring to Eq. (2.44), we find that only the elastic constant (β) and the electroelastic coupling parameter (γ_2) have influences on the wave velocity. An interesting phenomenon is that solitary waves propagating in rods of different materials, when subjected to some particular biasing electric displacements, may have the same velocity, see the cross of the thick and thin solid lines in Fig. 2.2. Moreover, for a large underlying electric displacement, the material constant β almost has no influence on the wave velocity. It also

should be mentioned that the electroelastic coupling parameters (γ_2) will not affect the velocity of the solitary wave if the biasing electric displacement is absent (i.e. $\eta_5 = 0$), as can be seen from Fig. 2.2.

Fig. 2.3 and Fig. 2.4 show the longitudinal strains of solitary waves with different amplitudes and/or subjected to different biasing electric displacements. The other parameters are fixed as $\beta = 0$, $\delta = 0.3$, $\gamma_2 = 1$ and $\varepsilon = 0.3$. Comparing the two solitary waves in the absence of biasing electric displacement (i.e. $\eta_5 = 0$) in Fig. 2.3, we find that higher and narrower waves travel faster (see Fig. 2.3b), which is the particular character of elastic solitary waves in pure elastic rods. This result also can be directly seen from Eq. (2.36a) by setting $\eta_5 = 0$. It is known that the biasing electric displacement can change the effective material properties for linear waves in electroactive materials (Dorfmann and Ogden, 2010; Chen and Dai, 2012). For the nonlinear solitary waves in electroactive rods, comparing the two waves with the same amplitude ($H = 1.5$) but subjected to different biasing electric displacements ($\eta_5 = 0$ and $\eta_5 = 1$), we find that the biasing electric displacement can change the wave velocity. However, it doesn't affect the wave shape, as shown in Fig. 2.3. An important conclusion from Fig. 2.3 is that solitary waves with the same shape may travel at different speeds in a rod when it is exposed to different biasing electric displacements.

(a)   (b)
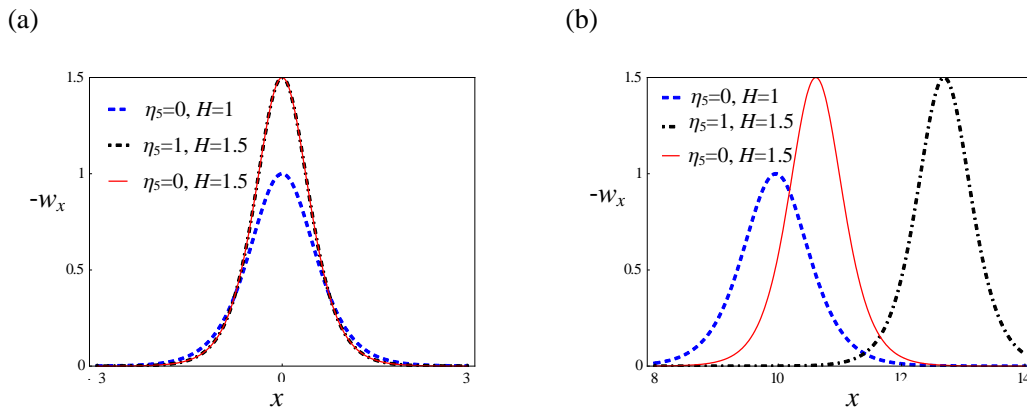
Fig. 2.3. Comparison of longitudinal strains of solitary waves with different

amplitudes subjected to different biasing electric displacements at (a) $t_0 = 0$ and (b)

$$t_0 = 5$$

It is noted that the solitary waves given by Eq. (2.37) or (2.43) are amplitude-dominant. The KdV equation (2.34a) admits another form of solution (Liu and Liu, 2000):

$$w_{00\xi} = \frac{3\mathcal{V}}{\Lambda_1} \sec h^2 \sqrt{\frac{\mathcal{V}}{4\Lambda_2}} \left(\xi - \mathcal{V}\tau - y_0 \right) \qquad (2.45)$$

which is velocity-dominant, where $\mathcal{V} > 0$ is a constant velocity. By expressing the solitary waves in this form, we can see that their wavelengths and wave amplitudes can also be modulated by the biasing electric displacement. In fact, Fig. 2.3 already indicates that if we keep the wave velocity unchanged, different biasing electric displacements will give rise to different wavelengths and wave amplitudes. This fact is now more clearly shown in Fig. 2.4.
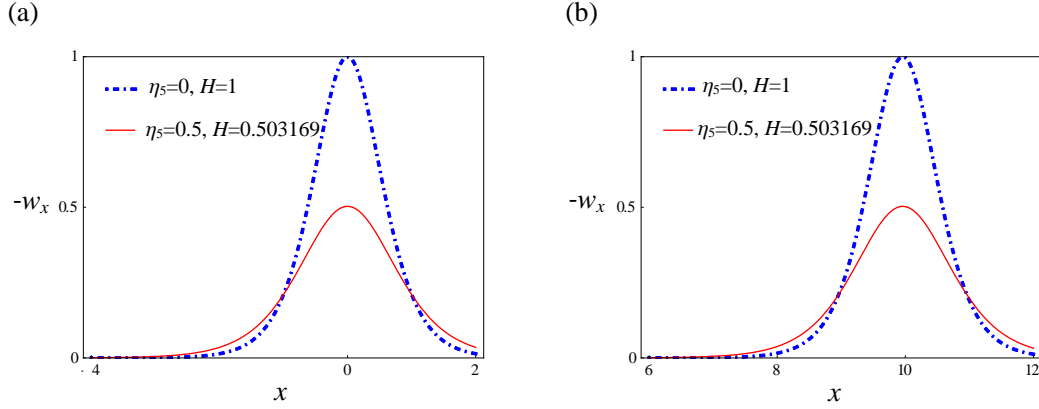
Fig. 2.4. Two different longitudinal strains of solitary waves travelling at the same velocity subjected to different biasing electric displacements at (a) $t_0 = 0$ and (b)

$$t_0 = 5$$

For an electroactive rod, there exists an electric field corresponding to the solitary wave due to the electroelastic coupling. Fig. 2.5 displays the longitudinal electric fields (at $t_0 = 0$ and $t_0 = 5$) of solitary waves in the rod subjected to different biasing electric displacements ($\eta_5 = 0.5$, 1.0, 1.5) for $\beta = 0$, $\gamma_2 = 1$,

$\varepsilon = \delta = 0.3$ and $H = 1$. It is seen that the biasing electric displacement has a significant effect on the shapes of the electric field associated with the solitary wave. A particular point should be noticed that the longitudinal electric field of the solitary wave is different from the longitudinal strain of solitary wave. For the longitudinal electric field of the solitary wave, a larger biasing electric displacement will generate a larger amplitude, while the corresponding wavelength keep unchanged, as is clearly seen from Fig. 2.5. This is different from that shown in Fig. 2.3. To the authors' knowledge, there are few studies on solitary waves propagating in solids with multi-field coupling. The above result indicates that it is important to study other physical fields of solitary waves (e.g. the electric field considered in this work) as well, in addition to the elastic field, which may exhibit a different characteristic that may be utilized in practical applications.

(a)   (b)
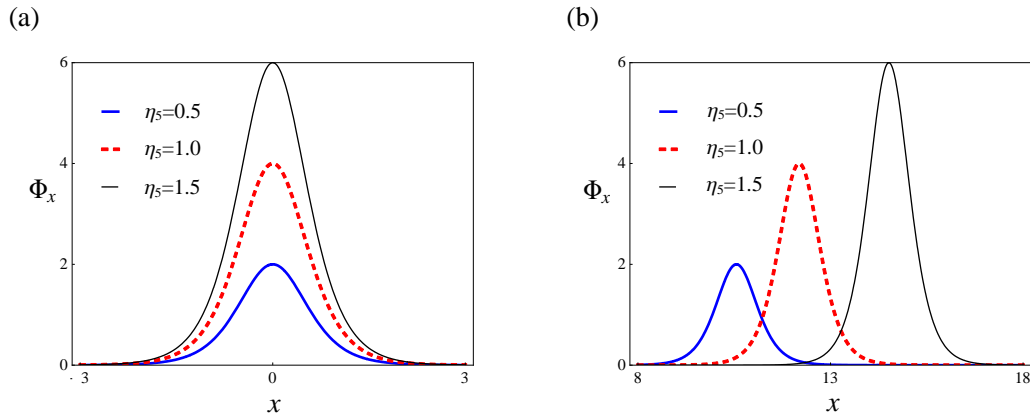
Fig. 2.5. Longitudinal electric fields of solitary waves with different biasing electric displacements at (a) $t_0 = 0$ and (b) $t_0 = 5$

2.7 Conclusions

A simplified nonlinear dynamic model of electroactive rods was explored here to obtain the analytical and explicit wave solutions. We established the asymptotically valid 1D governing equations on the basis of the 3D nonlinear theory of electroelasticity. As a degenerate case, the linear dispersion relation obtained in this Chapter numerically agrees well with the one directly derived from the 3D

linear theory in the limit of long wavelength. Following the procedure of the reductive perturbation method, we got the KdV equation in which the effect of the biasing electric field is involved. The leading order of the electroelastic solitary wave solution was then presented for soft electroactive rods.

The analytical results show that the material constants and the biasing longitudinal electric displacement both have influences on the solitary waves in soft electroactive rods. We mainly paid our attention to the effect of the biasing electric displacement, which can modulate the velocity or wavelength/amplitude of solitary waves. For the longitudinal strain and transverse displacement, if we keep their amplitudes unchanged, the biasing electric displacement will not change their wave shapes. While for the longitudinal electric field, the biasing electric field can change its wave shapes. The unique feature of solitary waves in electroactive rods is that they can be modulated by the biasing electric displacement, which may promote the applications of solitary waves in solids. For example, one may generate solitary waves experimentally under different biasing electric displacements so as to determine the electroelastic coupling coefficients.

We also would like to point out that the conclusions made above have been obtained only theoretically, and they should be carefully examined by comparison with experiments in a future study.

Appendix 2A Approximate expressions of the nonzero components of the nominal stress tensor

$$
\begin{aligned}
\Sigma_{(Rr)} = & -p - 2\Omega_1 W_Z + p_0 U_R - 2\Omega_1 \frac{U}{R} - pW_Z - \frac{pU}{R} - p_0 \frac{UW_Z}{R} + 2\Omega_2 \frac{U^2}{R^2} + 4\Omega_2 \frac{UU_R}{R} \\
& + (4\eta_3^2 \Omega_5 D^2 - 2\eta_3 \Omega_5 D^2 - 2\Omega_2) U_Z W_R + 4\Omega_2 U_R W_Z + 2\Omega_2 W_Z^2 + 2\Omega_5 \eta_3^2 D^2 W_R^2 \\
& + (2\Omega_5 \eta_3^2 D^2 - 2\eta_3 \Omega_5 D^2) U_Z^2 + (2\eta_3^2 D - \eta_3 D) U_Z \phi_R + 2\eta_3^2 D W_R \phi_R + 2\Omega_5 \eta_2^2 \phi_R^2
\end{aligned}
$$

$$(2A.1)$$

$$\Sigma_{(Rz)} = (2\Omega_1 + 2\Omega_2 - 2\eta_3\Omega_5 D^2)(U_Z + W_R) - \eta_3 D\phi_R + pU_Z - (2\Omega_2 + 4\eta_3^2 D^2\Omega_5)U_R U_Z$$
$$- (2\Omega_2 + 2\eta_3\Omega_5 D^2)U_Z W_Z - 4\eta_3^2 D^2\Omega_5 U_R W_R - 2\eta_3\Omega_5 D^2 W_R W_Z - 4\eta_1 D\Omega_5 U_R \phi_R$$
$$- (2\eta_3 + 1)\eta_3 D W_Z \phi_R + 2\eta_3^2 D U_Z \phi_Z + 2\eta_3^2 D W_R \phi_Z + 2\Omega_5 \eta_2^2 \phi_R \phi_Z - 4\eta_3^2 D\frac{U\phi_R}{R}$$
$$+ (p_0 - 8\eta_3^2 D^2\Omega_5)\frac{UU_Z}{R} + (4\Omega_2 - 8\eta_3^2 D^2\Omega_5)\frac{UW_R}{R}$$

$$(2A.2)$$

$$\Sigma_{(\Theta\theta)} = -p - 2\Omega_1(U_R + W_Z) + p_0\frac{U}{R} - pU_R + p_0 U_Z W_R - pW_Z - p_0 U_R W_Z + 2\Omega_2 U_R^2$$
$$+ 2\Omega_2 U_Z^2 + 2\Omega_2 W_R^2 + 2\Omega_2 W_Z^2 + 4\Omega_2\frac{UW_Z}{R} + 4\Omega_2\frac{UU_R}{R}$$

$$(2A.3)$$

$$\Sigma_{(Zr)} = (2\Omega_1 + 2\Omega_2 - 2\eta_3\Omega_5 D^2)W_R + (2\Omega_1 + 2\Omega_2 - 2\eta_3\Omega_5 D^2 + 2\Omega_5 D^2)U_Z - \eta_3 D\phi_R$$
$$- (2\Omega_2 + 2\eta_3\Omega_5 D^2 + 4\eta_3^2 D^2\Omega_5)U_R W_R + (6 - 4\eta_3)\eta_3\Omega_5 D^2 U_R U_Z - 2\Omega_2 W_R W_Z$$
$$- (\eta_3 D_Z + 2\eta_3^2 D)U_R \phi_R + (2\eta_3^2 D - 2\eta_3 D)U_Z \phi_Z + 2\eta_3^2 D W_R \phi_Z - 4\eta_1 D\Omega_5 W_Z \phi_R$$
$$+ pW_R + 2\eta_2^2\Omega_5 \phi_R \phi_Z + [8\eta_3 D^2\Omega_5(1 - \eta_3) + 4\Omega_2]\frac{UU_Z}{R} + (p_0 - 8\eta_3^2 D^2\Omega_5)\frac{UW_R}{R}$$
$$- 4\eta_3^2 D\frac{U\phi_R}{R}$$

$$(2A.4)$$

$$\Sigma_{(Zz)} = 2D^2\Omega_5 - p + (8\eta_3\Omega_5 D^2 - 2\Omega_1)U_R + (p_0 + 2D^2\Omega_5)W_Z + (8\eta_3 D^2\Omega_5 - 2\Omega_1)\frac{U}{R}$$
$$- 2\eta_3 D\phi_Z + (2\Omega_2 + 8\eta_3^2 D^2\Omega_5)U_R^2 - (2\Omega_2 + 10\eta_3\Omega_5 D^2)U_Z W_R - 8\eta_3^2 D U_R \phi_Z$$
$$- pU_R + (4\Omega_2 + 16\eta_3\Omega_5 D^2)U_R W_Z - 2\eta_3\Omega_5 D^2 W_R^2 + 2\eta_3^2 D U_Z \phi_R - 2\eta_3 D W_Z \phi_Z$$
$$+ (2\eta_3^2 D - \eta_3 D)W_R \phi_R + 2\eta_2^2\Omega_5 \phi_Z^2 - \frac{pU}{R} - 8\eta_3^2 D\frac{U\phi_Z}{R} + (2\Omega_2 + 24\eta_3^2 D^2\Omega_5)\frac{U^2}{R^2}$$
$$+ (4\Omega_2 + 16\eta_3 D^2\Omega_5)\frac{UW_Z}{R} + (32\eta_3^2\Omega_5 D^2 + 8\Omega_5\eta_3 D^2 - p_0)\frac{UU_R}{R}$$

$$(2A.5)$$

Appendix 2B. Governing equations and boundary conditions in terms of S and V

The governing equations are:

$$2V + W_Z + 2SV_S + 2VW_Z + 2SV_S W_Z - 2SV_Z W_S + V^2 + 2SVV_S = 0 \qquad (2B.1)$$

$$-\rho W_{TT} + 4(\Omega_2 + 3\eta_3\Omega_5 D^2)(V_Z + SV_{SZ}) + 8(\Omega_1 + \Omega_2 - \eta_3\Omega_5 D^2)(W_S + SW_{SS})$$

$$+ (p_0 + 2D^2\Omega_5)W_{ZZ} - 4\eta_3 D\phi_S - 4\eta_3 DS\phi_{SS} - p_Z - 2\eta_3 D\phi_{ZZ} + 2Sp_S V_Z - 2p_Z V$$

$$- 2p_Z SV_S + (40\eta_3^2 D^2\Omega_5 + 16\Omega_5 D^2\eta_3 - 12\Omega_2)SV_S V_Z - 8(\Omega_2 + 2\eta_3^2 D^2\Omega_5)S^2 V_{SS} V_Z$$

$$+ 4(\Omega_2 + 26\eta_3^2 D^2\Omega_5 + 4\Omega_5 D^2\eta_3)VV_Z + 4(\Omega_2 + 10\eta_3^2 D^2\Omega_5 + 4\Omega_5 D^2\eta_3)SVV_{SZ}$$

$$+ 8(\Omega_2 + 6\eta_3^2 D^2\Omega_5)S^2 V_S V_{SZ} + 4(\Omega_2 + 7\eta_3\Omega_5 D^2)V_Z W_Z + 4(\Omega_2 + 7\eta_3\Omega_5 D^2)SV_{SZ}W_Z$$

$$- 8(\Omega_2 + 3\eta_3\Omega_5 D^2)SV_Z W_{SZ} - 4(\Omega_2 + 5\eta_3\Omega_5 D^2)SV_{ZZ}W_S + 16(\Omega_2 - 3\eta_3^2 D^2\Omega_5)VW_S$$

$$+ (16\Omega_2 - 112\eta_3^2 D^2\Omega_5)SV_S W_S + (16\Omega_2 - 48\eta_3^2 D^2\Omega_5)SVW_{SS} - 32\eta_3^2 D^2\Omega_5 S^2 V_{SS}W_S$$

$$+ 8(\Omega_2 + 4\eta_3 D^2\Omega_5)(VW_{ZZ} + SV_S W_{ZZ}) - 32\eta_3^2 D^2\Omega_5 S^2 V_S W_{SS} - 24\eta_3\Omega_5 D^2 SW_S W_{SZ}$$

$$- 8\eta_3\Omega_5 D^2(W_S W_Z + SW_{SS}W_Z) - 8\eta_3 DSW_{SZ}\phi_S - (4\eta_3 D + 8\eta_3^2 D)(W_Z\phi_S + SW_Z\phi_{SS})$$

$$- 12\eta_3^2 D(V_Z\phi_Z + SV_{SZ}\phi_Z) + 8\eta_3^2 DSV_Z\phi_{SZ} + 4\eta_3^2 DSV_{ZZ}\phi_S - 56\eta_3^2 DSV_S\phi_S - 16\eta_3^2 DV\phi_{ZZ}$$

$$- 32\eta_1 D\Omega_5 S^2 V_{SS}\phi_S - 24\eta_3^2 DV\phi_S - 24\eta_3^2 D_Z SV\phi_{SS} - 32\eta_1 D\Omega_5 S^2 V_S\phi_{SS} - 16\eta_3^2 DSV_S\phi_{ZZ}$$

$$+ 8\eta_3^2 D(W_S\phi_Z + SW_{SS}\phi_Z) + 4(4\eta_3^2 D - \eta_3 D)SW_S\phi_{SZ} - 2\eta_3 DW_Z\phi_{ZZ} - 2\eta_3 DW_{ZZ}\phi_Z$$

$$+ 8\Omega_5\eta_2^2(\phi_S\phi_Z + S\phi_{SS}\phi_Z) + 8\Omega_5\eta_2^2 S\phi_S\phi_{SZ} + 4\eta_2^2\Omega_5\phi_Z\phi_{ZZ} = 0$$

$$(2B.2)$$

$$-\rho V_{TT} - 2p_S + 8p_0 V_S + 4(\Omega_2 - \eta_3\Omega_5 D^2)W_{SZ} + 2(\Omega_1 + \Omega_2 - \eta_3\Omega_5 D^2 + \Omega_5 D^2)V_{ZZ}$$

$$+ 4p_0 SV_{SS} - 2\eta_3 D\phi_{SZ} - 2p_S W_Z + 2p_Z W_S - 2p_S V + 32\Omega_2 V_S W_Z + 16\Omega_2 SV_{SS}W_Z$$

$$- 16(\eta_3\Omega_5 D^2 + \Omega_2)V_Z W_S - 16(\eta_3\Omega_5 D^2 + \Omega_2)SV_{SZ}W_S + 4\Omega_2 W_Z W_{SZ} - 4\Omega_2 W_S W_{ZZ}$$

$$+ 4(\Omega_2 - \eta_3\Omega_5 D^2 - 6\eta_3^2 D^2\Omega_5)VW_{SZ} + 8(\Omega_2 - \eta_3\Omega_5 D^2 - 2\eta_3^2\Omega_5 D^2)SV_S W_{SZ}$$

$$+ 32\Omega_5\eta_3^2 D^2 SW_{SS}W_S + 4(4\eta_3^2\Omega_5 D^2 - 2\eta_3\Omega_5 D^2 - 2\Omega_2)SW_{SS}V_Z + 4\Omega_5\eta_3 D^2 SV_{SZ}V_Z$$

$$+ (24\Omega_5\eta_3^2 D^2 - 8\Omega_2)W_S^2 + \eta_3\Omega_5 D^2(12 - 8\eta_3)SV_S V_{ZZ} + 32\Omega_2 VV_S + 8\Omega_2 SV_S^2$$

$$+ 16\Omega_2 SVV_{SS} + (8\eta_3\Omega_5 D^2 - 6\Omega_5\eta_3^2 D^2 + 2\Omega_2)V_Z^2 - 8\eta_3 DV_Z\phi_S - 8\eta_3 DSV_{SZ}\phi_S$$

$$+ (4\Omega_2 + 14\eta_3\Omega_5 D^2 - 12\eta_3^2\Omega_5 D^2)VV_{ZZ} + 4(2\eta_3^2 D - \eta_3 D)SV_Z\phi_{SS} + 24\eta_3^2 DW_S\phi_S$$

$$- (2\eta_3 D + 12\eta_3^2 D)V\phi_{SZ} - (8\eta_3^2 D + 4\eta_3 D)SV_S\phi_{SZ} - 8\eta_1 D\Omega_5 W_{ZZ}\phi_S - 8\eta_1 D\Omega_5 W_Z\phi_{SZ}$$

$$+ (2\eta_3^2 D - 2\eta_3 D)(V_{ZZ}\phi_Z + V_Z\phi_{ZZ}) + 16\eta_3^2 DSW_{SS}\phi_S + 16\eta_3^2 DSW_S\phi_{SS} + 4\eta_3^2 DW_{SZ}\phi_Z$$

$$+ 4\eta_3^2 DW_S\phi_{ZZ} + 4\eta_2^2\Omega_5\phi_{SZ}\phi_Z + 4\eta_2^2\Omega_5\phi_S\phi_{ZZ} + 8\Omega_5\eta_2^2(3\phi_S^2 + 4S\phi_S\phi_{SS}) = 0$$

$$(2B.3)$$

$$-\eta_3 D(-2V_Z - 2SV_{SZ} + 4W_S + 4SW_{SS}) - \eta_2(4\phi_S + 4S\phi_{SS} + \phi_{ZZ}) + \eta_1(-2V_Z\phi_Z - 2SV_{SZ}\phi_Z$$

$$+ 4SV_Z\phi_{SZ} + 2SV_{ZZ}\phi_S + 4W_S\phi_Z + 4SW_{SS}\phi_Z + 8SW_S\phi_{SZ} - 4SW_{SZ}\phi_S - 8W_Z\phi_S - 8SW_Z\phi_{SS}$$

$$- 4SV_S\phi_{ZZ} - 4V\phi_{ZZ} - 8V\phi_S - 8SV_S\phi_S - 8SV\phi_{SS}) + \eta_3^2(-8DVW_S - 8DSV_S W_S - 8DSVW_{SS}$$

$$+ (4 + 8\eta_3^2)DVV_Z + 4DSV_Z V_S + 4DSVV_{SZ}) + 2\eta_3 D(2V_Z W_Z + 2SV_{SZ}W_Z + 2VW_{ZZ}$$

$$+ 2SV_S W_{ZZ} - 2SV_{ZZ}W_S - 2SV_Z W_{SZ} + 2VV_Z + 2SV_S V_Z + 2SVV_{SZ}) = 0$$

$$(2C.4)$$

The boundary conditions are:

$$-p - 2\Omega_1 W_Z + 4\Omega_2 V + 2p_0 SV_S - pW_Z - pV - 2\Omega_1 VW_Z + 6\Omega_2 V^2 + 8\Omega_2 SVV_S + 2\Omega_2 W_Z^2$$
$$+ 2(4\eta_3^2 \Omega_5 D^2 - 2\eta_3 \Omega_5 D^2 - 2\Omega_2) SV_Z W_S + 8\Omega_2 SV_S W_Z + 2\Omega_5 D^2 (\eta_3^2 - \eta_3) SV_Z^2$$
$$+ 8\Omega_5 \eta_3^2 D^2 SW_S^2 + 2(2\eta_3^2 D - \eta_3 D) SV_Z \phi_S + 8\eta_3^2 DSW_S \phi_S + 8\Omega_5 \eta_2^2 S\phi_S^2 = 0,$$

$$(2C.5)$$

$$(2\Omega_1 + 2\Omega_2 - 2\eta_3 \Omega_5 D^2)(V_Z + 2W_S) - 2\eta_3 D\phi_S + pV_Z + (2\Omega_1 + 2\Omega_2 - 12\eta_3^2 D^2 \Omega_5)VV_Z$$
$$- (4\Omega_2 + 8\eta_3^2 D^2 \Omega_5) SV_S V_Z + (8\Omega_2 - 24\eta_3^2 D^2 \Omega_5)VW_S - 16\eta_3^2 D^2 \Omega_5 SV_S W_S - 8\eta_3^2 DSV_S \phi_S$$
$$- (2\Omega_2 + 2\eta_3 \Omega_5 D^2)V_Z W_Z - 4\eta_3 \Omega_5 D^2 W_S W_Z - 12\eta_3^2 DV \phi_S - (2\eta_3 D + 4\eta_3^2 D)W_Z \phi_S$$
$$+ 2\eta_3^2 DV_Z \phi_Z + 4\eta_3^2 DW_S \phi_Z + 4\Omega_5 \eta_2^2 \phi_S \phi_Z = 0,$$

$$(2C.6)$$

$$-\eta_3 D(V_Z + 2W_S) - 2\eta_2 \phi_S + \eta_1 (V_Z \phi_Z + 2W_S \phi_Z - 4V\phi_S - 4W_Z \phi_S) - 4\eta_3^2 DVW_S$$
$$- 2\eta_3^2 DVV_Z = 0,$$

$$(2C.7)$$

at $S = a^2$.

Appendix 2C. Dimensionless coefficient matrix in Eq. (2.25)

The components of the coefficient matrix in Eq. (2.25) in terms of $\bar{k}$ and $\bar{\omega}$

for the modified neo-Hookean materials are given by

$$\mathbf{S}_{11} = \begin{bmatrix} \delta^{-1/2}\bar{k}\,\mathrm{i} & 0 & 0 & 0 & 2 & 0 & 0 \\ 0 & \delta^{-1/2}\bar{k}\,\mathrm{i} & 0 & 0 & 0 & 4 & 0 \\ 0 & 0 & \delta^{-1/2}\bar{k}\,\mathrm{i} & 0 & 0 & 0 & 6 \\ \alpha_1 & \alpha_2 & 0 & 0 & 12\eta_3\eta_5^2\gamma_2\delta^{-1/2}\bar{k}\,\mathrm{i} & 0 & 0 \\ 0 & \alpha_1 & 4\alpha_2 & 0 & 0 & 24\eta_3\eta_5^2\gamma_2\delta^{-1/2}\bar{k}\,\mathrm{i} & 0 \\ 0 & 0 & \alpha_1 & 9\alpha_2 & 0 & 0 & 36\eta_3\eta_5^2\gamma_2\delta^{-1/2}\bar{k}\,\mathrm{i} \\ 0 & 0 & 0 & 0 & \alpha_3 & 8 & 0 \end{bmatrix}$$

$$\mathbf{S}_{12} = \begin{bmatrix} 0 & 0 & 0 & 0 & 0 & 0 & 0 \\ 0 & 0 & 0 & 0 & 0 & 0 & 0 \\ 0 & 0 & 0 & 0 & 0 & 0 & 0 \\ -\delta^{-1/2}\bar{k}\,\mathrm{i} & 0 & 0 & 2\eta_3\eta_5\delta^{-1}\bar{k}^2 & -4\eta_3\eta_5 & 0 & 0 \\ 0 & -\delta^{-1/2}\bar{k}\,\mathrm{i} & 0 & 0 & 2\eta_3\eta_5\delta^{-1}\bar{k}^2 & -16\eta_3\eta_5 & 0 \\ 0 & 0 & -\delta^{-1/2}\bar{k}\,\mathrm{i} & 0 & 0 & 2\eta_3\eta_5\delta^{-1}\bar{k}^2 & -36\eta_3\eta_5 \\ 0 & -2 & 0 & 0 & -2\eta_3\eta_5\gamma_2\delta^{-1/2}\bar{k}\,\mathrm{i} & 0 & 0 \end{bmatrix}$$

$$\mathbf{S}_{21} = \begin{bmatrix} 0 & 0 & -8\eta_3\eta_5^{\,2}\gamma_2\delta^{-1/2}\bar{k}\,\mathrm{i} & 0 & 0 & \alpha_3 & 24 \\ 0 & -4\eta_3\eta_5 & 0 & 0 & 2\eta_3\eta_5\delta^{-1/2}\bar{k}\,\mathrm{i} & 0 & 0 \\ 0 & 0 & -16\eta_3\eta_5 & 0 & 0 & 4\eta_3\eta_5\delta^{-1/2}\bar{k}\,\mathrm{i} & 0 \\ 0 & 0 & 0 & -36\eta_3\eta_5 & 0 & 0 & 6\eta_3\eta_5\delta^{-1/2}\bar{k}\,\mathrm{i} \\ -\delta^{-1/2}\bar{k}\,\mathrm{i} & -\delta^{1/2}\bar{k}\,\mathrm{i} & -\delta^{3/2}\bar{k}\,\mathrm{i} & 0 & 0 & 2\delta & 4\delta^2 \\ 0 & \dfrac{1}{2}\delta^2 & \delta\alpha_2 & \dfrac{2}{3}\delta^2\alpha_2 & \dfrac{1}{4}\alpha_2\delta^{-1/2}\bar{k}\,\mathrm{i} & \dfrac{1}{4}\alpha_2\delta^{1/2}\bar{k}\,\mathrm{i} & \dfrac{1}{4}\alpha_2\delta^{3/2}\bar{k}\,\mathrm{i} \\ 0 & -2\eta_3\eta_5 & -4\eta_3\eta_5\delta & -6\eta_3\eta_5\delta^2 & -\eta_3\eta_5\delta^{-1/2}\bar{k}\,\mathrm{i} & -\eta_3\eta_5\delta^{1/2}\bar{k}\,\mathrm{i} & -\eta_3\eta_5\delta^{3/2}\bar{k}\,\mathrm{i} \end{bmatrix}$$

$$\mathbf{S}_{22} = \begin{bmatrix} 0 & 0 & -4 & 0 & 0 & -4\eta_3\eta_5\gamma_2\delta^{-1/2}\bar{k}\,\mathrm{i} & 0 \\ 0 & 0 & 0 & \dfrac{1}{2}\eta_4\delta^{-1}\bar{k}^{\,2} & -2\eta_4 & 0 & 0 \\ 0 & 0 & 0 & 0 & \dfrac{1}{2}\eta_4\delta^{-1}\bar{k}^{\,2} & -8\eta_4 & 0 \\ 0 & 0 & 0 & 0 & 0 & \dfrac{1}{2}\eta_4\delta^{-1}\bar{k}^{\,2} & -18\eta_4 \\ -1 & -\delta & -\delta^2 & 0 & 0 & 0 & 0 \\ 0 & 0 & 0 & 0 & -2\eta_3\eta_5 & -4\delta\eta_3\eta_5 & -6\delta^2\eta_3\eta_5 \\ 0 & 0 & 0 & 0 & -\eta_4 & -2\eta_4\delta & -3\eta_4\delta^2 \end{bmatrix}$$

where

$$\alpha_1 = [\bar{\omega}^2 - (1 + 2\eta_5^{\,2}\gamma_2)\bar{k}^{\,2}]\delta^{-1}, \quad \alpha_2 = 4 - 8\eta_3\eta_5^{\,2}\gamma_2,$$

$$\alpha_3 = [\bar{\omega}^2 - (1 - 2\eta_3\eta_5^{\,2}\gamma_2 + 2\eta_5^{\,2}\gamma_2)\bar{k}^{\,2}]\delta^{-1}.$$

Chapter 3 Kink and kink-like waves in pre-stretched Mooney-Rivlin viscoelastic rods

3.1 Introduction

Solitary waves are generally produced due to the balance between nonlinearity and dispersion. However, dissipation is always present in a realistic situation, especially for soft materials. There are so many works in the field of nonlinear waves in solids considering the effect of dissipation. Destrade et al. (2009) studied the nonlinear shear waves propagating in viscoelastic materials whose generation is directly linked to the nonlinear viscosity term. Hayes and Saccomandi (2000, 2004) studied the propagation of finite amplitude shear waves in Mooney-Rivlin viscoelastic materials maintained in the static state of a pure homogenous deformation. Destrade and Saccomandi (2004) then extended to the case of inhomogeneous plane waves. They also studied the interaction of a longitudinal wave with a transverse wave in viscoelastic materials (Destrade and Saccomandi, 2005). It should be noted that the nonlinear elastic and dissipative behavior of rocks has been recently observed in many experiments (Rasolofasan et al., 1997). As is well–known, the combination of nonlinearity, dispersion and dissipation may lead to the generation of kink-shaped solitary waves or simply kink waves (Porubov, 2003). However, to the authors' knowledge, there are few works on nonlinear waves in pre-stretched structures composed of viscoelastic materials, which motivates the present work. Pre-stretch is also regarded as an efficient mean to modulate elastic waves in soft materials.

The present chapter focuses on the investigation of kink and kink-like longitudinal waves in pre-stretched Mooney-Rivlin viscoelastic rods. The Cauchy stress is split into an elastic part, which is derived from the classical Mooney-Rivlin elastic material, and a dissipative part, which is identical to the one in fluid. In the

limit of finite-small amplitude and long wavelength, we simplify the three-dimensional (3D) nonlinear governing equations to one-dimensional (1D) ones by making use of the asymptotic expansions of variables as in Dai and Huo (2002). Then, using the reductive perturbation method gives rise to the far-field equation (the KdV-Burgers equation). Finally, two kinds of explicit wave solutions are presented, namely the kink and kink-like waves, which correspond to the saddle-node heteroclinic orbit and the saddle-focus heteroclinic orbit of the equation, respectively. Examples are given to show the influences of pre-stretch and viscosity on the wave shape and wave velocity. The potential application of such waves is to measure the viscosity coefficient of the material. The competition between the effects of pre-stretch and viscosity on kink and kink-like waves is also uncovered.

3.2 Preliminaries

3.2.1 Basic formulations

Let a material point, in an undeformed body which occupies a region Γ_0 with the outward normal $\mathbf{N}$ in the reference configuration, be identified by its position vector $\mathbf{X}$. After a time T, the material point is at the position vector $\mathbf{x}$, which occupies a region Γ with the outward normal $\mathbf{n}$ in the current configuration. Thus, the motion of the body can be described by

$$\mathbf{x} = \chi(\mathbf{X}) \tag{3.1}$$

For an incompressible Mooney-Rivlin material with energy density function Ω, the (elastic) Cauchy stress tensor can be described by the constitutive relations (Chen and Dai, 2012)

$$\boldsymbol{\tau}^E = 2\Omega_1 \mathbf{b} + 2\Omega_2 (I_1 \mathbf{b} - \mathbf{b}^2) - P\mathbf{I} \tag{3.2}$$

where $\Omega_m = \partial\Omega / \partial I_m$ (m=1, 2), $\mathbf{I}$ is the unit tensor, $\mathbf{b} = \mathbf{F}\mathbf{F}^{\mathrm{T}}$ is the left Cauchy-Green strain tensor with $\mathbf{F} = \partial\mathbf{x} / \partial\mathbf{X}$ being the deformation gradient tensor,

P is the undetermined pressure related to the constraint of incompressibility $\det\mathbf{F} = 1$, and I_m are the scalar invariants:

$$I_1 = \mathrm{tr}\mathbf{b}, \; I_2 = \frac{1}{2}[(\mathrm{tr}\mathbf{b})^2 - \mathrm{tr}(\mathbf{b}^2)] \tag{3.3}$$

where "tr" is the trace operator.

To describe the effects of dissipation, we adopt the following viscous stress tensor for the incompressible viscoelastic materials (Destrade et al., 2009; Destrade and Saccomandi, 2004)

$$\boldsymbol{\tau}^D = 2\eta\mathbf{D} \tag{3.4}$$

where $\mathbf{D} = 1/2(\mathbf{L} + \mathbf{L}^T)$ is the rate of deformation tensor with $\mathbf{L} = (\partial\mathbf{F}/\partial T)\mathbf{F}^{-1}$, η is the viscosity coefficient which should be positive, and T is the time. A detailed discussion of proper formation of the viscous stress tensor can be found in (Destrade et al., 2013). Through simple combination, the nonlinear constitutive equation of a viscoelastic material may be expressed by

$$\boldsymbol{\tau} = -P\mathbf{I} + 2(\Omega_1 + \Omega_2 I_1)\mathbf{b} - 2\Omega_2\mathbf{b}^2 + 2\eta\mathbf{D} \tag{3.5}$$

where $\Omega_1 = 1/2\mu(1/2 + \beta) > 0$ and $\Omega_2 = 1/2\mu(1/2 - \beta) \geq 0$, with μ being the shear modulus and β a material constant.

The equations of motion, in the absence of body forces in Γ_0, are given by

$$\mathrm{Div}\boldsymbol{\Sigma} = \rho\frac{\partial^2\mathbf{x}}{\partial T^2} \tag{3.6}$$

where $\boldsymbol{\Sigma} = \mathbf{F}^{-1}\boldsymbol{\tau}$ is the nominal stress tensor and "Div" is the divergence operator.

The boundary conditions in Γ_0 are given by

$$\boldsymbol{\Sigma}^T\mathbf{N} = \mathbf{t}_A \tag{3.7}$$

where $\mathbf{t}_A$ is defined by $\mathbf{t}_A\mathrm{dA} = \mathbf{t}_a\mathrm{da}$. Here dA and da are the unit areas in Γ_0 and Γ, respectively, and $\mathbf{t}_a$ is the applied mechanical traction vector per unit area in

Γ .

3.2.2 Longitudinal waves with small but finite amplitude

To study the axisymmetric wave motion in a circular rod, we prefer adopting cylinder coordinates, with (R, Θ, Z) and (r, θ, z) corresponding to the reference and current configurations, respectively. Considering the axisymmetric motion superposed on a finite static axisymmetric deformation:

$$r = \lambda_1 R + U(R,Z,T), \ \theta = \Theta, \ z = \lambda_2 Z + W(R,Z,T), \ P = p_0 + p(R,Z,T) \quad (3.8)$$

where λ_1 and λ_2 are the pre-stretches, U and W are the displacements along the r and z directions, respectively, p_0 is the pressure in the deformed state, and p is the incremental pressure. From Eq. (3.8), we obtain

$$\mathbf{F} = \begin{pmatrix} U_R + \lambda_1 & 0 & U_Z \\ 0 & \dfrac{U}{R} + \lambda_1 & 0 \\ W_R & 0 & W_Z + \lambda_2 \end{pmatrix} \quad (3.9)$$

Furthermore, we can arrive

$$\det \mathbf{F} = \left(\dfrac{U}{R} + \lambda_1 \right) \left(-U_Z W_R + (U_R + \lambda_1)(W_Z + \lambda_2) \right) \quad (3.10)$$

and

$$\mathbf{L} = \begin{bmatrix} \lambda_1 \lambda_2 U_{RT} & 0 & \lambda_1^2 U_{ZT} \\ 0 & \lambda_1 \lambda_2 \dfrac{U_T}{R} & 0 \\ \lambda_1 \lambda_2 W_{RT} & 0 & \lambda_1^2 W_{ZT} \end{bmatrix} \quad (3.11)$$

To obtain Eq. (3.11), we have made use of the constraint of incompressibility $\det \mathbf{F} = 1$ and neglected the terms which are higher than the first order. As a convention, here and hereafter, the subscript letter denotes partial differentiation, while the subscript letter inside the brackets denotes coordinate direction.

With Eqs. (3.9) and (3.11) substituted into Eq. (3.5), we get the expressions of the Cauchy stress tensor including the effect of viscosity. The nominal stress tensor

can be derived as well. It is noted that for the finite but small disturbance, it is reasonable to neglect the higher order terms. Furthermore, for weakly viscoelastic materials, it is reasonable to assume that the viscous stresses are much smaller than the elastic stresses (Hamilton and Morfey, 1999). Similar assumption was adopted by Zabolotskaya et al. (2004) and Catheline et al. (2003) Thus, for the elastic stresses, we neglect the terms which are higher than the second order, while for the viscous stresses, we only retain the first order terms. With the approximate expressions for nominal stresses thus obtained (see Appendix 3A), the equations of motion (3.6) can be rewritten as

$$
\begin{aligned}
&-\rho W_{TT} + 2\lambda_1\lambda_2\Omega_2 U_{RZ} - \lambda_1^2 p_Z + 2\lambda_1\lambda_2\Omega_2 \frac{U_Z}{R} + (2\lambda_1^2\Omega_2 + 2\Omega_1)W_{RR} \\
&+ (2\Omega_1 + 4\lambda_1^2\Omega_2)W_{ZZ} + (2\lambda_1^2\Omega_2 + 2\Omega_1)\frac{W_R}{R} + \eta[(\lambda_1 U_{RZT} + \lambda_2 W_{RRT}) \\
&+ 2\lambda_1^4 W_{ZZT} + \frac{1}{R}(\lambda_1 U_{ZT} + \lambda_2 W_{RT})] + \lambda_1 p_R U_Z + 2\lambda_1\Omega_2 U_{RZ}W_Z \\
&- 4\lambda_1\Omega_2 U_Z W_{RZ} - 2\lambda_2\Omega_2 U_{RR}U_Z + 2\lambda_2\Omega_2 U_R U_{RZ} - \lambda_1 p_Z U_R \\
&- 2\lambda_1\Omega_2 U_{ZZ}W_R + 4\lambda_1\Omega_2 U_R W_{ZZ} - \lambda_1 \frac{p_Z U}{R} + 4\lambda_2\Omega_2 \frac{UU_Z}{R^2} \\
&+ 2\lambda_1\Omega_2 \frac{U_Z W_Z}{R} + 4\lambda_1\Omega_2 \frac{UW_{ZZ}}{R} - 2\lambda_2\Omega_2 \frac{U_R U_Z}{R} + 4\lambda_1\Omega_2 \frac{U_R W_R}{R} \\
&+ 4\lambda_1\Omega_2 \frac{UW_{RR}}{R} = 0
\end{aligned}
\tag{3.12}
$$

$$
\begin{aligned}
&-\rho U_{TT} + 2\lambda_1\lambda_2\Omega_2 W_{RZ} - \lambda_1\lambda_2 p_R + (-2\Omega_1 - 2\lambda_2^2\Omega_2 - 2\lambda_1^2\Omega_2)\frac{U}{R^2} \\
&+ (2\Omega_1 + 2\lambda_1^2\Omega_2 + 2\lambda_2^2\Omega_2)\frac{U_R}{R} + (2\Omega_1 + 2\lambda_1^2\Omega_2 + 2\lambda_2^2\Omega_2)U_{RR} \\
&+ (2\Omega_1 + 2\lambda_1^2\Omega_2)U_{ZZ} + \eta(2\lambda_2 U_{RRT} + \lambda_1^4 U_{ZZT} + \lambda_1 W_{RZT} - 2\lambda_2 \frac{U_T}{R^2} \\
&+ 2\lambda_2 \frac{U_{RT}}{R}) + 2\lambda_1\Omega_2 W_Z W_{RZ} - 2\lambda_1\Omega_2 W_R W_{ZZ} - 4\lambda_2\Omega_2 U_{RZ}W_R \\
&- 2\lambda_2\Omega_2 U_Z W_{RR} + 4\lambda_2\Omega_2 U_{RR}W_Z + 2\lambda_2\Omega_2 U_R W_{RZ} - \lambda_1 p_R W_Z \\
&+ \lambda_1 p_Z W_R - \lambda_2 \frac{p_R U}{R} + 4\lambda_1\Omega_2 \frac{UU_{RR}}{R} + 4\lambda_1\Omega_2 \frac{UU_{ZZ}}{R} \\
&- 2\lambda_2\Omega_2 \frac{U_Z W_R}{R} + 4\lambda_2\Omega_2 \frac{U_R W_Z}{R} - 4\lambda_2\Omega_2 \frac{UW_Z}{R^2} - 2\lambda_1\Omega_2 \frac{U^2}{R^3} \\
&+ 2\lambda_1\Omega_2 \frac{U_R^2}{R} + 2\lambda_1\Omega_2 \frac{U_Z^2}{R} - 2\lambda_1\Omega_2 \frac{W_R^2}{R} = 0
\end{aligned}
\tag{3.13}
$$

We assume that the lateral surface is free from tractions. From Eq. (3.7), we get the boundary conditions as

$$\Sigma_{(Rr)} = 0, \ \Sigma_{(Rz)} = 0, \ \text{at } R = a \tag{3.14}$$

which reduce to

$$
\begin{aligned}
&(4\lambda_1\lambda_2\Omega_2 - \lambda_1 p_0)W_Z + (2\Omega_1 + 2\lambda_1^2\Omega_2 + 2\lambda_2^2\Omega_2)U_R - \lambda_1\lambda_2 p \\
&+ (4\lambda_1^2\Omega_2 - \lambda_2 p_0)\frac{U}{R} + 2\lambda_1\Omega_2 W_Z^2 - 2\lambda_2\Omega_2 U_Z W_R + 4\lambda_2\Omega_2 U_R W_Z \\
&- \lambda_1 p W_Z - p_0\frac{UW_Z}{R} - \lambda_2\frac{pU}{R} + 2\lambda_1\Omega_2\frac{U^2}{R^2} + 4\lambda_1\Omega_2\frac{UU_R}{R} \\
&+ 2\eta\lambda_2 U_{RT} = 0
\end{aligned}
\tag{3.15}
$$

$$
\begin{aligned}
&(\lambda_1 p_0 - 2\lambda_1\lambda_2\Omega_2)U_Z + (2\lambda_1^2\Omega_2 + 2\Omega_1)W_R + p_0\frac{UU_Z}{R} + \lambda_1 p U_Z \\
&+ 4\lambda_1\Omega_2\frac{UW_R}{R} - 2\lambda_1\Omega_2 U_Z W_Z - 2\lambda_2\Omega_2 U_R U_Z + \eta(\lambda_1 U_{ZT} + \lambda_2 W_{RT}) = 0
\end{aligned}
\tag{3.16}
$$

at $R = a$, where $p_0 = 2\lambda_1^2\Omega_1 + 2\lambda_1^4\Omega_2 + 2\lambda_2\Omega_2$ which can be obtained from the boundary condition $\Sigma_{(Rr)} = 0$ of the rod in the deformed state.

From Eq. (3.10), the constraint of material incompressibility can be reduced to

$$\lambda_1\lambda_2 U_R + \lambda_1^2 W_Z + \lambda_1\lambda_2\frac{U}{R} - \lambda_1 U_Z W_R + \lambda_1 U_R W_Z + \lambda_1\frac{UW_Z}{R} + \lambda_2\frac{UU_R}{R} = 0 \tag{3.17}$$

where the terms which are higher than the second order have been omitted, and the following relation has been noticed

$$\lambda_1^2\lambda_2 = 1 \tag{3.18}$$

Eqs. (3.12), (3.13) and (3.15)-(3.17) can be used to completely describe the nonlinear dynamics of viscoelastic rods in the limit of finite but small amplitude.

For such axisymmetric problems, $S = R^2$ will be a more natural radial variable than R (Dai and Huo, 2002). Also, the transformation $U = RV(Z, S, T)$ is introduced. These two changes of variables are now used to simplify the governing equations (3.12), (3.13) and (3.15)-(3.17). For convenience, we will further adopt the following scales to non-dimensionalize the governing equations

$$W = hw, Z = lx, S = l^2 s, T = \frac{l}{c}t, V = \frac{h}{l}v, p = \mu \frac{h}{l}\bar{p}, \tag{3.19}$$

where μ is the shear modulus of the material, h is a characteristic axial displacement, and l is a characteristic wavelength, c is a characteristic speed to be determined later (see Eq. (3.41)). For long waves with finite but small amplitudes, $\varepsilon = h/l$ is a small dimensionless parameter. The following dimensionless material constants will also be needed:

$$\bar{\Omega}_1 = \mu^{-1}\Omega_1, \bar{\Omega}_2 = \mu^{-1}\Omega_2, \bar{\eta} = \mu^{-1}\frac{c}{h}\eta, \bar{p}_0 = 2\lambda_1^2\bar{\Omega}_1 + 2\lambda_1^4\bar{\Omega}_2 + 2\lambda_2\bar{\Omega}_2 \tag{3.20}$$

Thus, in view of Eqs. (3.19) and (3.20), we get the dimensionless governing equations as follows:

$$
\begin{aligned}
&2v + 2sv_s + \lambda_1^3 w_x + \varepsilon(2\lambda_1^2 vw_x - 2\lambda_1^2 sv_x w_s + 2\lambda_1^2 sv_s w_x + \lambda_1\lambda_2 v^2 \\
&+ 2\lambda_1\lambda_2 svv_s) = 0
\end{aligned}
\tag{3.21}
$$

$$
\begin{aligned}
&-\frac{\rho c^2}{\mu} w_{tt} + 4\lambda_1\lambda_2\bar{\Omega}_2 v_x + 4s\lambda_1\lambda_2\bar{\Omega}_2 v_{sx} - \lambda_1^2\bar{p}_x \\
&+ 8(\lambda_1^2\bar{\Omega}_2 + \bar{\Omega}_1)w_s + 8s(\lambda_1^2\bar{\Omega}_2 + \bar{\Omega}_1)w_{ss} + (2\bar{\Omega}_1 + 4\lambda_1^2\bar{\Omega}_2)w_{xx} \\
&+ \varepsilon[\bar{\eta}(2\lambda_1 v_{xt} + 2\lambda_1 sv_{sxt} + 4\lambda_2 w_{st} + 4\lambda_2 sw_{sst} + 2\lambda_1^4 w_{xxt}) \\
&+ 2\lambda_1 s\bar{p}_s v_x + 4\lambda_1\bar{\Omega}_2 v_x w_x + 4s\lambda_1\bar{\Omega}_2 v_{sx} w_x - 8\lambda_1\bar{\Omega}_2 sv_x w_{sx} \\
&- 4\lambda_1\bar{\Omega}_2 sv_{xx} w_s + 8\lambda_1\bar{\Omega}_2 vw_{xx} + 8\lambda_1\bar{\Omega}_2 sv_s w_{xx} + 16\lambda_1\bar{\Omega}_2 vw_s \\
&+ 16\lambda_1\bar{\Omega}_2 sv_s w_s + 16\lambda_1\bar{\Omega}_2 svw_{ss} - 12\lambda_2\bar{\Omega}_2 sv_s v_x - 8\lambda_2\bar{\Omega}_2 s^2 v_{ss} v_x \\
&+ 4\lambda_2\bar{\Omega}_2 vv_x + 4\lambda_2\bar{\Omega}_2 svv_{sx} + 8\lambda_2\bar{\Omega}_2 s^2 v_s v_{sx} - 2\lambda_1\bar{p}_x v - 2\lambda_1 s\bar{p}_x v_s] = 0
\end{aligned}
\tag{3.22}
$$

$$
\begin{aligned}
&-\frac{\rho c^2}{\mu} v_{tt} + 4\lambda_1\lambda_2\bar{\Omega}_2 w_{sx} - 2\lambda_1\lambda_2\bar{p}_s + 16(\bar{\Omega}_1 + \lambda_1^2\bar{\Omega}_2 + \lambda_2^2\bar{\Omega}_2)v_s \\
&\quad + 2(\bar{\Omega}_1 + \lambda_1^2\bar{\Omega}_2)v_{xx} + 8(\bar{\Omega}_1 + \lambda_1^2\bar{\Omega}_2 + \lambda_2^2\bar{\Omega}_2)sv_{ss} \\
&\quad + \varepsilon[\bar{\eta}(16\lambda_2 v_{st} + 8\lambda_2 sv_{sst} + \lambda_1^4 v_{xxt} + 2\lambda_1 w_{sxt}) \\
&\quad + 4\lambda_1\bar{\Omega}_2 w_x w_{sx} - 4\lambda_1\bar{\Omega}_2 w_s w_{xx} - 8\lambda_1\bar{\Omega}_2 w_s^2 \\
&\quad - 16\lambda_2\bar{\Omega}_2 v_x w_s - 16\lambda_2\bar{\Omega}_2 sv_{sx} w_s - 8\lambda_2\bar{\Omega}_2 sv_x w_{ss} \\
&\quad + 32\lambda_2\bar{\Omega}_2 v_s w_x + 16\lambda_2\bar{\Omega}_2 sv_{ss} w_x + 4\lambda_2\bar{\Omega}_2 vw_{sx} + 8\lambda_2\bar{\Omega}_2 sv_s w_{sx} \\
&\quad - 2\lambda_1\bar{p}_s w_x + 2\lambda_1\bar{p}_x w_s - 2\lambda_2\bar{p}_s v + 32\lambda_1\bar{\Omega}_2 vv_s + 16\lambda_1\bar{\Omega}_2 svv_{ss} \\
&\quad + 4\lambda_1\bar{\Omega}_2 vv_{xx} + 8\lambda_1\bar{\Omega}_2 sv_s^2 + 2\lambda_1\bar{\Omega}_2 v_x^2] = 0
\end{aligned}
\tag{3.23}
$$

The corresponding boundary conditions are

$$
\begin{aligned}
& 2(\lambda_1\lambda_2\bar{\Omega}_2 - \lambda_1^3\bar{\Omega}_1 - \lambda_1^5\bar{\Omega}_2)w_x + 4\lambda_1^2\bar{\Omega}_2 v \\
& + 4(\bar{\Omega}_1 + \lambda_1^2\bar{\Omega}_2 + \lambda_2^2\bar{\Omega}_2)sv_s - \lambda_1\lambda_2\bar{p} \\
& + \varepsilon[2\lambda_2\bar{\eta}(v_t + 2sv_{st}) + 2\lambda_1\bar{\Omega}_2 w_x w_s - 4\lambda_2\bar{\Omega}_2 sv_x w_s \\
& + 2(\lambda_2\bar{\Omega}_2 - \lambda_1^2\bar{\Omega}_1 - \lambda_1^4\bar{\Omega}_2)vw_x + 8\lambda_2\bar{\Omega}_2 sv_s w_x - \lambda_1\bar{p}w_x \\
& - \lambda_2\bar{p}v + 6\lambda_1\bar{\Omega}_2 v^2 + 8\lambda_1\bar{\Omega}_2 svv_s] = 0
\end{aligned}
\tag{3.24}
$$

$$
\begin{aligned}
& 2(\lambda_1^5\bar{\Omega}_2 + \lambda_1^3\bar{\Omega}_1)v_x + 4(\lambda_1^2\bar{\Omega}_2 + \bar{\Omega}_1)w_s \\
& + \varepsilon[\bar{\eta}(\lambda_1 v_{xt} + 2\lambda_2 w_{st}) + 2(\lambda_1^4\bar{\Omega}_2 + \lambda_1^2\bar{\Omega}_1)vv_x \\
& + \lambda_1\bar{p}v_x + 8\lambda_1\bar{\Omega}_2 vw_s - 2\lambda_1\bar{\Omega}_2 v_x w_s - 4\lambda_2\bar{\Omega}_2 sv_s v_x] = 0
\end{aligned}
\tag{3.25}
$$

at $s = \delta$, where $\delta = a^2/l^2$ is also a small parameter for long waves. As can be seen, the variable R doesn't appear explicitly in the resulting system of governing equations, and s seems to be a more natural radial variable as compared with R in the original system.

Eqs. (3.21)-(3.25) are complex two-dimensional (2D) nonlinear partial differential equations, which are still too difficult to get an analytical solution. For a slender rod, to further simplify the equations, we adopt the asymptotical method introduced by Dai and Huo (2002) to tackle such a complicated system. First, the unknowns (w, v and $\bar{p}$) can be expanded in the neighborhood of $s = 0$ as follows:

$$
w = w_0(x,t) + sw_1(x,t) + s^2 w_2(x,t) + \cdots
\tag{3.26}
$$

$$
v = v_0(x,t) + sv_1(x,t) + s^2 v_2(x,t) + \cdots
\tag{3.27}
$$

$$
\bar{p} = \bar{p}_0(x,t) + s\bar{p}_1(x,t) + s^2\bar{p}_2(x,t) + \cdots
\tag{3.28}
$$

Substituting Eqs. (3.26)-(3.28) into Eqs. (3.21)-(3.25) and setting the coefficient of each power of s to be zero, we can transform the 2D problem to the 1D problem involving only two variables (x and t). The governing equations are

$$
2v_0 + \lambda_1^3 w_{0x} + \varepsilon(2\lambda_1^2 v_0 w_{0x} + \lambda_1\lambda_2 v_0^2) = 0
\tag{3.29}
$$

$$
2v_1 + 2v_1 + \lambda_1^3 w_{1x} + \varepsilon(4\lambda_1^2 v_1 w_{0x} + 2\lambda_1^2 v_0 w_{1x} - 2\lambda_1^2 v_{0x} w_1 + 4\lambda_1\lambda_2 v_0 v_1) = 0
\tag{3.30}
$$

$$-\frac{\rho c^2}{\mu}w_{0tt}+4\lambda_1\lambda_2\bar{\Omega}_2 v_{0x}-\lambda_1^2\bar{p}_{0x}+4(2\lambda_1^2\bar{\Omega}_2+2\bar{\Omega}_1)w_1$$
$$+(2\bar{\Omega}_1+4\lambda_1^2\bar{\Omega}_2)w_{0xx}+\varepsilon[\bar{\eta}(2\lambda_1 v_{0xt}+4\lambda_2 w_{1t}+2\lambda_1^4 w_{0xxt})$$
$$+4\lambda_1\bar{\Omega}_2 v_{0x}w_{0x}+8\lambda_1\bar{\Omega}_2 v_0 w_{0xx}+16\lambda_1\bar{\Omega}_2 v_0 w_1 \tag{3.31}$$
$$+4\lambda_2\bar{\Omega}_2 v_0 v_{0x}-2\lambda_1\bar{p}_{0x}v_0]=0$$

$$-\frac{\rho c^2}{\mu}w_{1tt}+4\lambda_1\lambda_2\bar{\Omega}_2 v_{1x}+4\lambda_1\lambda_2\bar{\Omega}_2 v_{1x}-\lambda_1^2\bar{p}_{1x}$$
$$+16(2\lambda_1^2\bar{\Omega}_2+2\bar{\Omega}_1)w_2+(2\bar{\Omega}_1+4\lambda_1^2\bar{\Omega}_2)w_{1xx}$$
$$+\varepsilon[\bar{\eta}(4\lambda_1 v_{1xt}+16\lambda_2 w_{2t}+2\lambda_1^4 w_{1xxt})+8\lambda_1\bar{\Omega}_2 v_{1x}w_{0x} \tag{3.32}$$
$$-4\lambda_1\bar{\Omega}_2 v_{0x}w_{1x}-4\lambda_1\bar{\Omega}_2 v_{0xx}w_1+16\lambda_1\bar{\Omega}_2 v_1 w_{0xx}+8\lambda_1\bar{\Omega}_2 v_0 w_{1xx}$$
$$+32\lambda_1\bar{\Omega}_2 v_1 w_1+64\lambda_1\bar{\Omega}_2 v_0 w_2-8\lambda_2\bar{\Omega}_2 v_1 v_{0x}+8\lambda_2\bar{\Omega}_2 v_0 v_{1x}$$
$$+2\lambda_1\bar{p}_1 v_{0x}-2\lambda_1\bar{p}_{1x}v_0-4\lambda_1\bar{p}_{0x}v_1]=0$$

$$-\frac{\rho c^2}{\mu}v_{0tt}+4\lambda_1\lambda_2\bar{\Omega}_2 w_{1x}+8(2\bar{\Omega}_1+2\lambda_1^2\bar{\Omega}_2+2\lambda_2^2\bar{\Omega}_2)v_1$$
$$-2\lambda_1\lambda_2\bar{p}_1+(2\bar{\Omega}_1+2\lambda_1^2\bar{\Omega}_2)v_{0xx}+\varepsilon[\bar{\eta}(16\lambda_2 v_{1t}+\lambda_1^4 v_{0xxt}+2\lambda_1 w_{1xt})$$
$$+4\lambda_1\bar{\Omega}_2 w_{0x}w_{1x}-4\lambda_1\bar{\Omega}_2 w_1 w_{0xx}-8\lambda_1\bar{\Omega}_2 w_1^2-16\lambda_2\bar{\Omega}_2 v_{0x}w_1 \tag{3.33}$$
$$+32\lambda_2\bar{\Omega}_2 v_1 w_{0x}+4\lambda_2\bar{\Omega}_2 v_0 w_{1x}-2\lambda_1\bar{p}_1 w_{0x}+2\lambda_1\bar{p}_{0x}w_1-2\lambda_2\bar{p}_1 v_0$$
$$+32\lambda_2\bar{\Omega}_2 v_0 v_1+4\lambda_1\bar{\Omega}_2 v_0 v_{0xx}+2\lambda_1\bar{\Omega}_2 v_{0x}^2]=0$$

The corresponding boundary conditions are

$$(2\lambda_1\lambda_2\bar{\Omega}_2-2\lambda_1^3\bar{\Omega}_1-2\lambda_1^5\bar{\Omega}_2)w_{0x}-\lambda_1\lambda_2\bar{p}_0+4\lambda_1^2\bar{\Omega}_2 v_0+\varepsilon\{2\lambda_2\bar{\eta}v_{0t}$$
$$+(2\lambda_2\bar{\Omega}_2-2\lambda_1^2\bar{\Omega}_1-2\lambda_1^4\bar{\Omega}_2)v_0 w_{0x}+2\lambda_1\bar{\Omega}_2 w_{0x}^2-\lambda_1\bar{p}_0 w_{0x}-\lambda_2\bar{p}_0 v_0$$
$$+6\lambda_1\bar{\Omega}_2 v_0^2+\frac{\delta}{\varepsilon}[(2\lambda_1\lambda_2\bar{\Omega}_2-2\lambda_1^3\bar{\Omega}_1-2\lambda_1^5\bar{\Omega}_2)w_{1x}-\lambda_1\lambda_2\bar{p}_1 \tag{3.34}$$
$$+2(2\bar{\Omega}_1+4\lambda_1^2\bar{\Omega}_2+2\lambda_2^2\bar{\Omega}_2)v_1]\}=0$$

$$(2\lambda_1^5\bar{\Omega}_2+2\lambda_1^3\bar{\Omega}_1)v_{0x}+2(2\lambda_1^2\bar{\Omega}_2+2\bar{\Omega}_1)w_1+\varepsilon\{\bar{\eta}(\lambda_1 v_{0xt}+2\lambda_2 w_{1t})$$
$$+\lambda_1\bar{p}_0 v_{0x}+8\lambda_1\bar{\Omega}_2 v_0 w_1-2\lambda_1\bar{\Omega}_2 v_{0x}w_{0x}+(2\lambda_1^4\bar{\Omega}_2+2\lambda_1^2\bar{\Omega}_1)v_0 v_{0x} \tag{3.35}$$
$$+\frac{\delta}{\varepsilon}[(2\lambda_1^5\bar{\Omega}_2+2\lambda_1^3\bar{\Omega}_1)v_{1x}+4(2\lambda_1^2\bar{\Omega}_2+2\bar{\Omega}_1)w_2]\}=0$$

where $\delta/\varepsilon=O(1)$ is assumed. The above seven equations give a set of 1D nonlinear equations for seven unknowns w_i, v_j and p_j ($i=0,1,2$ and $j=0,1$), in which we have neglected $O(\delta\varepsilon,\varepsilon^2)$ terms.

3.3 The far-field equation

3.3.1 Derivation of the KdV-Burgers equation

To derive the far-field equation, we follow the procedure of the reductive perturbation method and introduce the following transformation (Jeffery and Kawahara, 1982):

$$\xi = x - t, \ \tau = \varepsilon t \tag{3.36}$$

and w_i, v_j and p_j $(i = 0, 1, 2 \text{ and } j = 0, 1)$ have the following perturbation expansions

$$
\begin{aligned}
w_i &= w_{i0} + \varepsilon w_{i1} + \cdots, \\
v_j &= v_{j0} + \varepsilon v_{j1} + \cdots, \\
\bar{p}_j &= \bar{p}_{j0} + \varepsilon \bar{p}_{j1} + \cdots
\end{aligned}
\tag{3.37}
$$

Inserting Eqs. (3.36) and (3.37) into Eqs. (3.29)-(3.35), we obtain at $O(\varepsilon^0)$

$$\mathbf{M}_0 \mathbf{H}_0 = \mathbf{0} \tag{3.38}$$

where $\mathbf{H}_0 = \left(w_{00\xi}, w_{10}, w_{20}, v_{00}, v_{10}, \bar{p}_{00}, \bar{p}_{10} \right)^{\mathrm{T}}$, and

$$
\mathbf{M}_0 = \begin{pmatrix}
\lambda_1^3 & 0 & 0 & 2 & 0 & 0 & 0 \\[2mm]
0 & \lambda_1^3 \dfrac{\partial}{\partial \xi} & 0 & 0 & 4 & 0 & 0 \\[2mm]
d_2 \dfrac{\partial}{\partial \xi} & 8d_1 & 0 & 4\lambda_1\lambda_2\bar{\Omega}_2 \dfrac{\partial}{\partial \xi} & 0 & -\lambda_1^2 \dfrac{\partial}{\partial \xi} & 0 \\[2mm]
0 & d_2 \dfrac{\partial^2}{\partial \xi^2} & 32d_1 & 0 & 8\lambda_1\lambda_2\bar{\Omega}_2 \dfrac{\partial}{\partial \xi} & 0 & -\lambda_1^2 \dfrac{\partial}{\partial \xi} \\[2mm]
0 & 4\lambda_1\lambda_2\bar{\Omega}_2 \dfrac{\partial}{\partial \xi} & 0 & d_5 \dfrac{\partial^2}{\partial \xi^2} & 16d_3 & 0 & -2\lambda_1\lambda_2 \\[2mm]
2d_4 & 0 & 0 & 4\lambda_1^2\bar{\Omega}_2 & 0 & -\lambda_1\lambda_2 & 0 \\[2mm]
0 & 4d_1 & 0 & 2\lambda_1^3 d_1 \dfrac{\partial}{\partial \xi} & 0 & 0 & 0
\end{pmatrix}
$$

where

$$
\begin{aligned}
& d_1 = \lambda_1^2 \bar{\Omega}_2 + \bar{\Omega}_1, d_2 = -\rho c^2 / \mu + 2\bar{\Omega}_1 + 4\lambda_1^2 \bar{\Omega}_2, d_3 = \bar{\Omega}_1 + \lambda_1^2 \bar{\Omega}_2 + \lambda_2^2 \bar{\Omega}_2, \\
& d_4 = \lambda_1\lambda_2\bar{\Omega}_2 - \lambda_1^3 d_1, d_5 = -\rho c^2 / \mu + 2d_1
\end{aligned}
\tag{3.39}
$$

In order to obtain the nontrivial solutions, we set

$$\det\mathbf{M}_0 = 0 \tag{3.40}$$

which gives

$$\frac{\rho c^2}{\mu} = 4\lambda_1^6 \bar{\Omega}_1 + 2\bar{\Omega}_1 + 6\lambda_1^8 \bar{\Omega}_2 \tag{3.41}$$

It determines the characteristic speed c, which depends on the pre-stretch λ_1. This result coincides with the one obtained in (Dai and Huo, 2002) if we set $\lambda_1 = \lambda_2 = 1$.

Substituting Eq. (3.41) into Eq. (3.38), we obtain

$$
\begin{aligned}
&v_{00} = -\frac{\lambda_1^3}{2} w_{00\xi}, \bar{p}_{00} = (2\bar{\Omega}_2 - 2\lambda_1^4 \bar{\Omega}_1 - 4\lambda_1^6 \bar{\Omega}_2) w_{00\xi}, w_{10} = \frac{\lambda_1^6}{4} w_{00\xi\xi}, \\
&v_{10} = -\frac{\lambda_1^9}{16} w_{00\xi\xi\xi}, \bar{p}_{10} = (\frac{1}{2}\lambda_1^{10}\bar{\Omega}_1 + \lambda_1^{12}\bar{\Omega}_2 - \frac{1}{2}\lambda_1^6 \bar{\Omega}_2) w_{00\xi\xi\xi}, \\
&w_{20} = \frac{3}{64}\lambda_1^{12} + \frac{\lambda_1^8(\lambda_1^6 - 1)\bar{\Omega}_2}{32(\lambda_1^2\bar{\Omega}_2 + \bar{\Omega}_1)}
\end{aligned} \tag{3.42}
$$

The left eigenvector $\mathbf{L}_e$ of the coefficient matrix $\mathbf{M}_0$ is

$$\mathbf{L}_e = \begin{pmatrix} d_6 & 0 & 1 & 0 & 0 & -\lambda_1^3 \dfrac{\partial}{\partial\xi} & -2 \end{pmatrix} \tag{3.43}$$

where $d_6 = (4\lambda_1^5\bar{\Omega}_2 + 2\lambda_1^3\bar{\Omega}_1 - 2\lambda_1^{-1}\bar{\Omega}_2)\partial/\partial\xi$.

Similar to Eq. (3.38), another seven equations at $O(\varepsilon^1)$ can be easily obtained. Making use of Eq. (3.42), we can simplify these equations to

$$
\begin{aligned}
&\mathbf{M}_0\mathbf{H}_1 + \mathbf{Q}_1 w_{00\xi\tau} + \mathbf{Q}_2 w_{00\xi}^2 + \mathbf{Q}_3 w_{00\xi}w_{00\xi\xi\xi} + \mathbf{Q}_4 w_{00\xi\xi}^2 + \mathbf{Q}_5 w_{00\xi\xi} + \mathbf{Q}_6 w_{00\xi\xi\xi} \\
&+ \mathbf{Q}_7 w_{00\xi\xi\xi\xi} + \mathbf{Q}_8 w_{00\xi\xi\xi\xi\xi} = 0
\end{aligned} \tag{3.44}
$$

where $\mathbf{Q}_1 \sim \mathbf{Q}_8$ are coefficients (in vector form) given in Appendix 3B. In order to suppress the secular term, we multiply the left-hand side of Eq. (3.44) with the left eigenvector $\mathbf{L}_e$ to get the following nonlinear evaluation equation

$$w_{00\xi\tau} + C_1 w_{00\xi}w_{00\xi\xi} - C_2 w_{00\xi\xi\xi} + C_3 w_{00\xi\xi\xi\xi} = 0 \tag{3.45}$$

where

$$C_1 = \frac{-3(2\lambda_1^{10}\overline{\Omega}_2 + \lambda_1^8\overline{\Omega}_1)}{2\lambda_1^6\overline{\Omega}_1 + \overline{\Omega}_1 + 3\lambda_1^8\overline{\Omega}_2}, C_2 = \frac{3\sqrt{2}\lambda_1^4\overline{\eta}_0}{4\sqrt{2\lambda_1^6\overline{\Omega}_1 + \overline{\Omega}_1 + 3\lambda_1^8\overline{\Omega}_2}},$$

$$C_3 = \frac{(4\lambda_1^{14}\overline{\Omega}_2 + 3\lambda_1^{12}\overline{\Omega}_1 - \lambda_1^8\overline{\Omega}_2)}{16(2\lambda_1^6\overline{\Omega}_1 + \overline{\Omega}_1 + 3\lambda_1^8\overline{\Omega}_2)}\frac{\delta}{\varepsilon}$$

where $\overline{\eta}_0 = \mu^{-1}c_T\eta/h$ is also a dimensionless viscosity coefficient, which is independent of the pre-stretch, and $c_T = \sqrt{\mu/\rho}$ is the shear wave velocity.

Eq. (3.45) is the KdV-Burgers type equation with the nonlinear coefficient C_1, the dissipative coefficient C_2, and the dispersive coefficient C_3. In this chapter, we only consider the case of $\lambda_1 \geq 1$ (i.e. the rod is subjected to a pre-stretch, not pre-compression). Thus, we have $C_3 > 0$. Due to the balance of nonlinearity, dissipation and dispersion, there exists a steady kink (or kink-like) wave propagating in the rod. If the dissipation is neglected, we can reduce the KdV-Burgers equation into the KdV equation. Furthermore, when $\lambda_1 = 1$, the KdV equation thus obtained is identical to the one in Chapter 2 if the electroelastic coupling is neglected there.

3.3.2 Travelling wave solutions

Eq. (3.45) is not a standard KdV-Burgers equation. We take the following transformation

$$w_{00\xi} = \frac{\Lambda}{C_1} \tag{3.46}$$

Inserting Eq. (3.46) into Eq. (3.45), we obtain

$$\Lambda_\tau + \Lambda\Lambda_\xi - C_2\Lambda_{\xi\xi} + C_3\Lambda_{\xi\xi\xi} = 0 \tag{3.47}$$

Eq. (3.47) admits both travelling wave solutions corresponding to saddle-node and saddle-focus heteroclinic orbits, respectively (Liu and Liu, 1992). In order to obtain the travelling wave solution, we assume

$$\Lambda = \Lambda(\zeta), \ \zeta = \xi - \nu\tau \tag{3.48}$$

Substituting Eq. (3.48) into Eq. (3.47) and integrating once with respect to ζ both sides of the equation, we can get

$$-\nu\Lambda + \frac{1}{2}\Lambda^2 - C_2\Lambda_\zeta + C_3\Lambda_{\zeta\zeta} = A \tag{3.49}$$

where A is an integral constant, which depends on the initial conditions. When the variable ζ approaches infinity, Λ, Λ_ζ and $\Lambda_{\zeta\zeta}$ should gradually become zero. Thus, it's reasonable to set $A = 0$.

The solution corresponding to the saddle-node heteroclinic orbit for the KdV-Burgers equation was first obtained in Jeffrey and Xu (1989) through a nonlinear transformation method. Alternatively, the solution may be obtained through the expansion of tangential function (Johnson, 1970), as follows

$$\Lambda = \frac{6}{25}\frac{C_2^2}{C_3}[1 - \tanh\frac{C_2}{10C_3}\zeta + \frac{1}{2}\text{sech}^2\frac{C_2}{10C_3}\zeta] \tag{3.50}$$

where $\nu = 6C_2^2 / 25C_3$ has been determined in the process of derivation.

For the saddle-focus heteroclinic orbit, the analytical solution can be obtained by following Liu and Liu (1992) for $C_3 > 0$ as

$$\Lambda = \begin{cases} 2\nu + \nu e^{\frac{C_2}{2C_3}\zeta}\cos\sqrt{\frac{\nu}{C_3} - \frac{C_2^2}{4C_3^2}}\zeta, & (-\infty, 0] \\ 3\nu\,\text{sech}^2\sqrt{\frac{\nu}{4C_3}}\zeta, & [0, +\infty) \end{cases} \tag{3.51}$$

where ν will be a given parameter. This wave can be divided into two parts: the right part is a solitary wave in which the dissipative term is neglected, and the left is a damped oscillation due to dissipation.

Inserting Eqs. (3.50) and (3.51) into Eq. (3.46), we can get the expression of $w_{00\xi}$, which in turn gives rise to the following leading order of the travelling wave solutions:

$$w_x = \frac{6}{25}\frac{C_2^2}{C_1 C_3}\left[1 - \tanh\frac{C_2}{10C_3}\left(x - (1+\varepsilon\frac{6C_2^2}{25C_3})t\right) + \frac{1}{2}\operatorname{sech}^2\frac{C_2}{10C_3}\left(x - (1+\varepsilon\frac{6C_2^2}{25C_3})t\right)\right] \quad (3.52)$$

and

$$w_x = \begin{cases} \dfrac{1}{C_1}\left(2\nu + \nu e^{\frac{C_2}{2C_3}(x-(1+\varepsilon\nu)t)}\cos\sqrt{\dfrac{\nu}{C_3} - \dfrac{C_2^2}{4C_3^2}}\left(x - (1+\varepsilon\nu)t\right)\right), & (-\infty, 0] \\[4mm] \dfrac{3\nu}{C_1}\operatorname{sech}^2\sqrt{\dfrac{\nu}{4C_3}}\left(x - (1+\varepsilon\nu)t\right), & [0, +\infty) \end{cases} \quad (3.53)$$

Eqs. (3.52) and (3.53) are the kink and kink-like waves, respectively. It should be pointed out that the kink-like wave in Eq. (3.53), which corresponds to the saddle-focus heteroclinic orbit, is often overlooked in literatures. However, such a wave profile is exactly the same as what has been observed in fluid (Liu and Liu, 1992; Johnson, 1970). Thus, it should be important both in practice and in science and technology. The kink wave in Eq. (3.52) corresponds to the saddle-node heteroclinic orbit. As expected, the kink (kink-like) waves can be modulated by the pre-stretch λ_1. Substituting Eqs. (3.52) and (3.53) into Eq. (3.42), we can get the expressions of other physical quantities, including the expression of v_{00}, which is very important to the experiment (Samsonov, 2001). In the next part, we will discuss the influence of pre-stretch and viscosity on the wave shape and wave velocity.

3.4 Numerical results and discussions

In this part, we shall discuss through numerical examples but based on the analytical solutions obtained in the last section how the pre-stretch and viscosity affect the wave shape and wave velocity. In the calculation, we take $\beta = 1/6$ and $\varepsilon = \delta = 0.3$ for example. It is noted that the Mooney-Rivlin model can be degenerated into the neo-Hookean model when $\beta = 1/2$. In this case, the kink wave solutions are still available, which can be proven from Eq. (3.45).

For the discussion about the influence of pre-stretch on the wave velocity, it becomes inappropriate to use the dimensionless variable t since it depends on the

pre-stretch, see Eq. (3.19). Thus, we employ the following new dimensionless time variable:

$$t_0 = \frac{c_T T}{l} \tag{3.54}$$

where $c_T = \sqrt{\mu / \rho}$ is defined below Eq. (3.45).

Then, Eqs. (3.52) and (3.53) can be rewritten as

$$w_x = \frac{6}{25} \frac{C_2^2}{C_1 C_3} \left[1 - \tanh \frac{x - c_{p1} t_0}{l_w} + \frac{1}{2} \operatorname{sech}^2 \frac{x - c_{p1} t_0}{l_w} \right] \tag{3.55}$$

where

$$l_w = \frac{10 C_3}{C_2}, \tag{3.56}$$

$$c_{p1} = (1 + \varepsilon \frac{6 C_2^2}{25 C_3}) \sqrt{4 \lambda_1^6 \overline{\Omega}_1 + 2 \overline{\Omega}_1 + 6 \lambda_1^8 \overline{\Omega}_2} \tag{3.57}$$

$$H = \frac{12}{25} \frac{C_2^2}{C_1 C_3} \tag{3.58}$$

are the wavelength, wave velocity, and wave amplitude, respectively, and

$$w_x = \begin{cases} \dfrac{1}{C_1} \left(2\nu + \nu e^{\frac{C_2}{2 C_3} \left(x - c_{p2} t_0 \right)} \cos \sqrt{\dfrac{\nu}{C_3} - \dfrac{C_2^2}{4 C_3^2}} \left(x - c_{p2} t_0 \right) \right), & (-\infty, 0] \\[4mm] \dfrac{3\nu}{C_1} \operatorname{sech}^2 \sqrt{\dfrac{\nu}{4 C_3}} \left(x - c_{p2} t_0 \right), & [0, +\infty) \end{cases} \tag{3.59}$$

where $c_{p2} = (1 + \varepsilon \nu) \sqrt{4 \lambda_1^6 \overline{\Omega}_1 + 2 \overline{\Omega}_1 + 6 \lambda_1^8 \overline{\Omega}_2}$ is also the wave velocity.

Fig. 3.1 depicts three different kink waves underlying different pre-stretches at $t_0 = 0$. It should be noted that these wave solutions have a saddle-node herteroclinic orbit, and result from the balance of dissipation, dispersion, and nonlinearity (see Eq. (3.55)). If the dissipation is ignored, the dissipative coefficient C_2 would be zero, so the kink waves would not be generated. It is seen that the pre-stretch makes the wave lower and wider. Therefore, the pre-stretch has a repressive function on the wave.
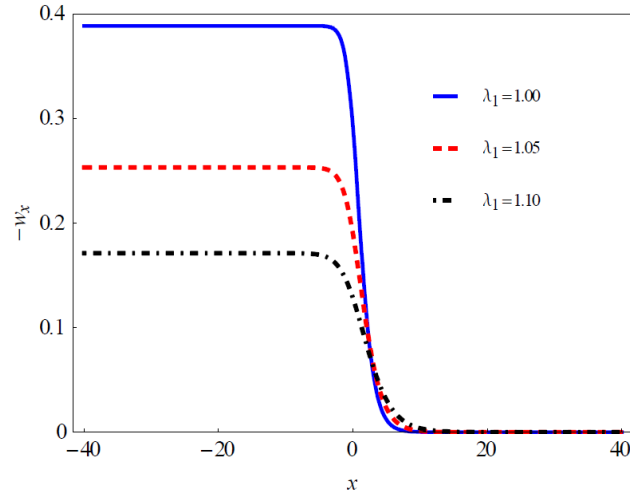
Fig. 3.1 Axial strain of kink waves underlying different pre-stretches with $\bar{\eta}_0 = 0.3$

at $t_0 = 0$
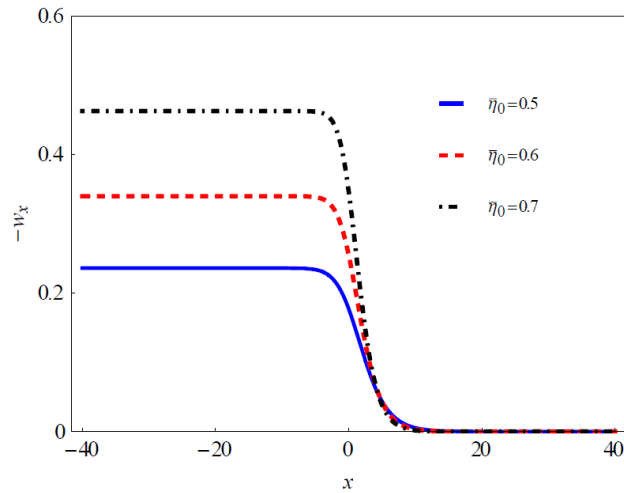
Fig. 3.2 Axial strains of kink waves with different viscosity coefficients and

$\lambda_1 = 1.2$ at $t_0 = 0$

Fig. 3.2 depicts three different kink waves propagating in the rod with different viscosity coefficients at $t_0 = 0$. Comparing these waves with each other, we find that the kink wave with a larger viscosity will have a higher amplitude and narrower wavelength. If the viscosity is small enough (for example, $\bar{\eta}_0 = 0.5$ as in Fig. 3.2), the wave will gradually become flatted. From Figs. 3.1 and 3.2, we recognize that the pre-stretch and viscosity of the material have absolutely opposite influence on

such kind of kink waves. So it is not surprising that waves propagating in the rod with two different viscosity coefficients may have very similar wave shapes if the underlying pre-stretches are appropriately applied, see Fig. 3.3.
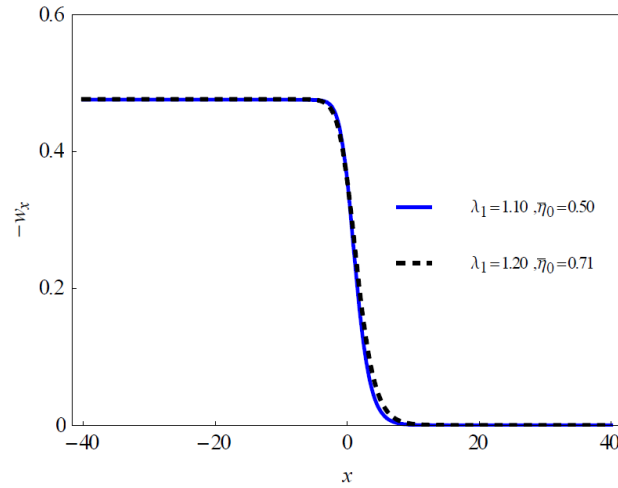
Fig. 3.3 Two similar axial strains of kink waves at $t_0 = 0$
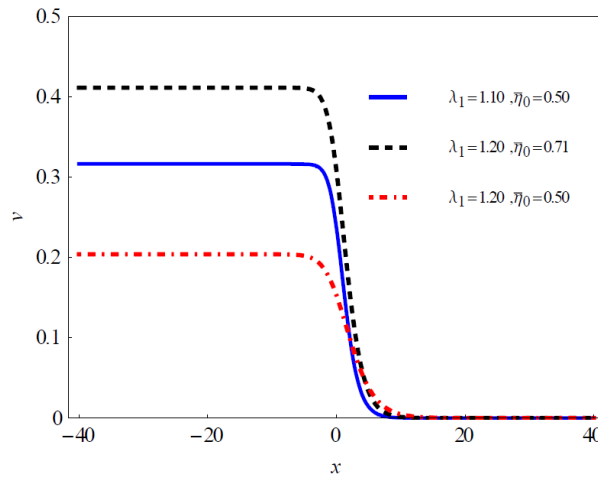
Fig. 3.4 Radial displacements of kink waves at $t_0 = 0$

From Eq. $(3.42)_1$, we find that the radial displacement is proportional to the longitudinal strain with the same wave velocity. This enables us to determine the nonlinear wave characteristics in rods through measuring the radial displacement which is experimentally more feasible (Samsonov, 2001). Fig. 3.4 shows three different radial displacements of kink waves propagating in the viscoelastic rod. As expected, we find that the influences of the pre-stretch and viscosity on the wave

shape are the same as on the axial strain. It is noticed that the radial displacements for $\lambda_1 = 1.1$, $\bar{\eta}_0 = 0.5$ and $\lambda_1 = 1.2$, $\bar{\eta}_0 = 0.71$ are with different shapes, unlike the situation for the axial strains in Fig. 3.3. This is simply due to the fact that the proportional factor in Eq. $(3.42)_1$ depends on the pre-stretch.

All the results show that for kink waves, the viscosity coefficient of the material has a dominant effect on the wave shape. Thus, we may use this property to measure the viscosity coefficient of the material. For example, we can use the measured wave amplitude to calculate the viscosity coefficient by

$$\bar{\eta}_0 = \frac{5}{6} \lambda_1^2 \sqrt{\frac{\lambda_1(2\lambda_1^2\bar{\Omega}_2 + \bar{\Omega}_1)(4\lambda_1^6\bar{\Omega}_2 + 3\lambda_1^4\bar{\Omega}_1 - \bar{\Omega}_2)}{2\lambda_1^6\bar{\Omega}_1 + \bar{\Omega}_1 + 3\lambda_1^8\bar{\Omega}_2}} \frac{\delta}{\varepsilon} \sqrt{H_v} \qquad (3.60)$$

where H_v is the wave amplitude of the radial displacement.
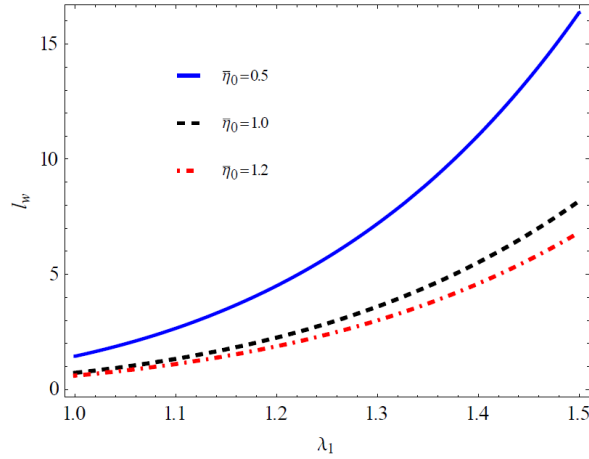
Fig. 3.5 Variation of wavelength with the pre-stretch

Figs. 3.5-3.7 show the variations of wavelength, wave velocity and wave amplitude with the pre-stretch. From Fig. 3.5, we find that, with the increase of viscosity, the wavelength becomes smaller and with the increase of pre-stretch, the wavelength becomes larger, which may be explained intuitively that the dispersion is strengthened due to the decrease of the radius of the rod when it is stretched. It is interesting that the influence of the viscosity on the wavelength becomes significant when the pre-stretch is large enough. Furthermore, the influence of viscosity on the wave velocity become smaller as the pre-stretch increases, see Fig. 3.6. When the

viscosity is large enough (for example, $\bar{\eta}_0 = 2.0$), the variation of wave velocity becomes no longer monotonous. Thus, there should be a range where the wave velocity will decrease with the increase of pre-stretch. This is somehow against the intuition. On the other hand, just as expected, the influence of viscosity on the wave amplitude will gradually become small with the increase of pre-stretch. When the pre-stretch is big enough, the wave amplitude will approach to zero, see Fig. 3.7.
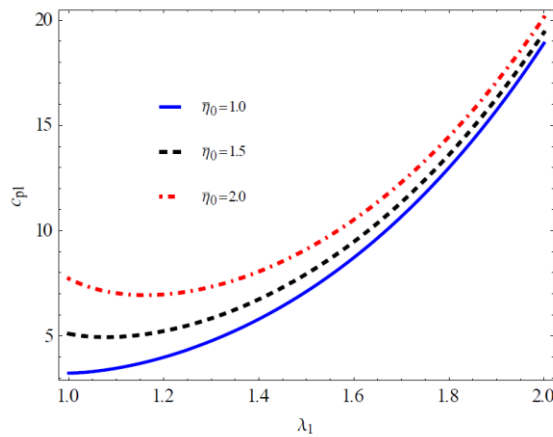
Fig. 3.6 Variation of wave velocity with the pre-stretch
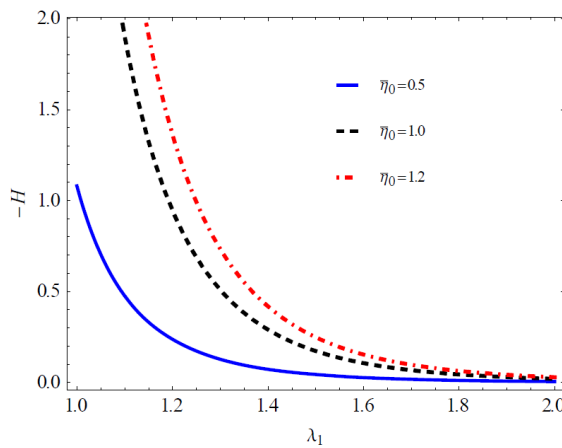
Fig. 3.7 Variation of wave amplitude with the pre-stretch

Fig. 3.8 depicts the kink-like waves, which correspond to the saddle-focus heteroclinic orbit of the KdV-Burgers equation. The other parameters are fixed as $\bar{\eta}_0 = 1$ and $\nu = 20$. At the right-most part of the wave, it behaves like a solitary wave for which the dissipation can be neglected. When the wave amplitude arrives at the maximum point, the field is controlled by damped oscillation due to

dissipation, and the amplitude will gradually become smaller and smaller. Finally, the axial strain will approach a constant. This kind of waves actually reflects the cascading down process of energy, which is an important property of turbulence (Liu and Liu, 1992). By comparing Figs. 3.8(a), 3.8(b) and 3.8(c) with each other, the influence of pre-stretch on such kind of waves can be uncovered. Just like the kink waves, the wave amplitude of kink-like waves will become lower and the wavelength will become wider with the increase of pre-stretch. Furthermore, we also find that the left part of the wave in Fig. 3.8(a) decays more rapidly than the corresponding ones in Fig. 3.8(b) and Fig. 3.8(c). Therefore, we can get the conclusion that the pre-stretch can weaken the effect of viscosity on of the kink-like waves.
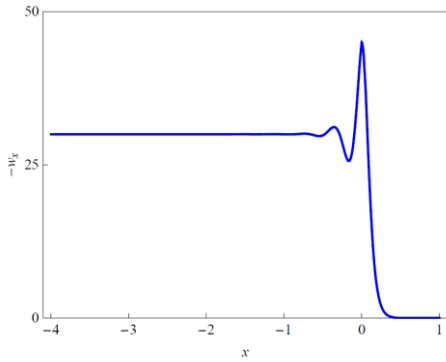
(a) $\lambda_1 = 1$
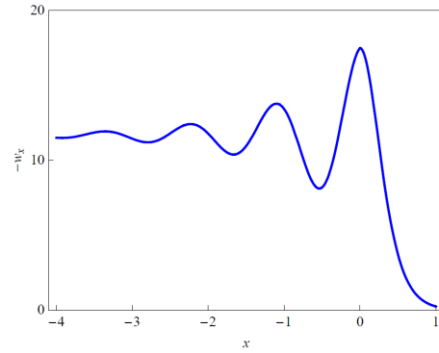
(b) $\lambda_1 = 1.4$
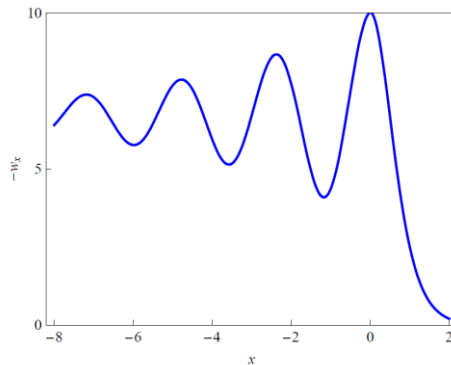
(c) $\lambda_1 = 1.8$

Fig. 3.8. Kink-like waves with a saddle-focus heteroclinic orbit at $t_0 = 0$

3.5   Concluding remarks

We studied the propagation of kink and kink-like waves in pre-stretched Mooney-Rivlin elastic rods with the consideration of viscous dissipation. The Cauchy stress tensor consists of an elastic part and a dissipative part. Several asymptotic expansions were introduced to simplify the 3D governing equations for a rod to the 1D ones. The boundary conditions on the lateral surface of the rod were satisfied asymptotically. Using the reductive perturbation method, we obtained the KdV-Burgers equation, which admits analytical and explicit wave solutions.

Two kinds of travelling wave solutions for the KdV-Burgers equation are given in the present chapter. They correspond to the saddle-node heteroclinic orbit and saddle-focus heteroclinic orbit of travelling wave solutions, respectively. For the discussions, we mainly paid our attention to the influences of pre-stretch and viscosity on the wave shape and wave velocity. We found that the pre-stretch will make the kink waves lower and wider. Moreover, the pre-stretch can also be used to modulate the wave velocity. Furthermore, a larger viscosity coefficient will lead to a higher and narrower wave. Thus, we may use kink waves to measure the viscosity coefficient of the material.

Last but not least, we uncover the competition between the influences of pre-stretch and viscosity on kink (kink-like) waves. For example, for the wave with a saddle-node heteroclinic orbit, as the pre-stretch increases, the effect of viscosity on the wavelength will become more remarkable; while its effect on the wave amplitude and wave velocity becomes smaller with the increase of pre-stretch. Furthermore, if the viscosity coefficient is large enough, the variation of wave velocity will no longer monotonously vary with the pre-stretch. For the wave with a saddle-focus heteroclinic orbit, we uncover that the pre-stretch can weaken the effect of viscosity, which will decrease the wave amplitude.

Appendix 3A. Approximate expressions of the nonzero components of the nominal stress tensor

$$
\begin{aligned}
\Sigma_{(Rr)} &= (4\lambda_1\lambda_2\Omega_2 - \lambda_1 p_0)W_Z - \lambda_1\lambda_2 p + (4\lambda_1^2\Omega_2 - \lambda_2 p_0)\frac{U}{R} \\
&\quad + 2\lambda_1\Omega_2 W_Z^2 + (2\Omega_1 + 2\lambda_1^2\Omega_2 + 2\lambda_2^2\Omega_2)U_R - 2\lambda_2\Omega_2 U_Z W_R \\
&\quad + 4\lambda_2\Omega_2 U_R W_Z - \lambda_1 pW_Z - p_0\frac{UW_Z}{R} - \lambda_2\frac{pU}{R} + 2\lambda_1\Omega_2\frac{U^2}{R^2} \\
&\quad + 4\lambda_1\Omega_2\frac{UU_R}{R} + 2\eta\lambda_2 U_{RT}
\end{aligned}
\tag{3A.1}
$$

$$
\begin{aligned}
\Sigma_{(Rz)} &= (\lambda_1 p_0 - 2\lambda_1\lambda_2\Omega_2)U_Z + (2\lambda_1^2\Omega_2 + 2\Omega_1)W_R + p_0\frac{UU_Z}{R} + \lambda_1 pU_Z \\
&\quad + 4\lambda_1\Omega_2\frac{UW_R}{R} - 2\lambda_1\Omega_2 U_Z W_Z - 2\lambda_2\Omega_2 U_R U_Z + \eta(\lambda_1 U_{ZT} + \lambda_2 W_{RT})
\end{aligned}
\tag{3A.2}
$$

$$
\begin{aligned}
\Sigma_{(\Theta\theta)} &= (4\lambda_1^2\Omega_2 - \lambda_2 p_0)U_R - \lambda_1\lambda_2 p + (2\Omega_1 + 2\lambda_1^2\Omega_2 + 2\lambda_2^2\Omega_2)\frac{U}{R} \\
&\quad + p_0 U_Z W_R + (4\lambda_1\lambda_2\Omega_2 - \lambda_1 p_0)W_Z - p_0 U_R W_Z + 2\lambda_1\Omega_2 U_R^2 \\
&\quad + 2\lambda_1\Omega_2 U_Z^2 + 2\lambda_1\Omega_2 W_R^2 - \lambda_2 pU_R - \lambda_1 pW_Z + 2\lambda_1\Omega_2 W_Z^2 \\
&\quad + 4\lambda_2\Omega_2\frac{UW_Z}{R} + 4\lambda_1\Omega_2\frac{UU_R}{R} + 2\eta\lambda_2\frac{U_T}{R}
\end{aligned}
\tag{3A.3}
$$

$$
\begin{aligned}
\Sigma_{(Zr)} &= (\lambda_1 p_0 - 2\lambda_1\lambda_2\Omega_2)W_R + (2\Omega_1 + 2\lambda_1^2\Omega_2)U_Z + \lambda_1 pW_R \\
&\quad + 4\lambda_1\Omega_2\frac{UU_Z}{R} + p_0\frac{UW_R}{R} - 2\lambda_1\Omega_2 W_R W_Z - 2\lambda_2\Omega_2 U_R W_R \\
&\quad + \eta(\lambda_1^4 U_{ZT} + \lambda_1 W_{RT})
\end{aligned}
\tag{3A.4}
$$

$$
\begin{aligned}
\Sigma_{(Zz)} &= -p_0\lambda_1^2 + 2\lambda_2\Omega_1 + 4\lambda_1^2\lambda_2\Omega_2 - \lambda_1^2 p + (4\lambda_1\lambda_2\Omega_2 - \lambda_1 p_0)\frac{U}{R} \\
&\quad - p_0\frac{UU_R}{R} + (4\lambda_1\lambda_2\Omega_2 - \lambda_1 p_0)U_R + (2\Omega_1 + 4\lambda_1^2\Omega_2)W_Z \\
&\quad + 4\lambda_1\Omega_2 U_R W_Z + 2\lambda_2\Omega_2 U_R^2 - 2\lambda_1\Omega_2 U_Z W_R - \lambda_1 pU_R \\
&\quad + 4\lambda_1\Omega_2\frac{UW_Z}{R} + 2\lambda_2\Omega_2\frac{U^2}{R^2} - \lambda_1\frac{pU}{R} + 2\eta\lambda_1^4 W_{ZT}
\end{aligned}
\tag{3A.5}
$$

Appendix 3B. The coefficients of Eq. (3.44)

These are given in vector form as follows:

$$\mathbf{Q}_1 = \begin{pmatrix} 0 & 0 & 4\beta_2 & \lambda_1^6\beta_2\dfrac{\partial}{\partial\xi} & -2\lambda_1^3\beta_2\dfrac{\partial}{\partial\xi} & 0 & 0 \end{pmatrix}^{\mathrm{T}} \tag{3B.1}$$

$$\mathbf{Q}_2 = \begin{pmatrix} -\dfrac{3}{4}\lambda_1^5 & 0 & \beta_1 & 0 & 0 & \beta_8 & \beta_9 \end{pmatrix}^{\mathrm{T}} \tag{3B.2}$$

$$\mathbf{Q}_3 = \begin{pmatrix} 0 & -\dfrac{3}{8}\lambda_1^{11} & 0 & \beta_3 & -\dfrac{1}{2}\lambda_1^{11}\bar{\Omega}_1 & 0 & 0 \end{pmatrix}^{\mathrm{T}} \tag{3B.3}$$

$$\mathbf{Q}_4 = \begin{pmatrix} 0 & \dfrac{1}{4}\lambda_1^{11} & 0 & \beta_4 & \beta_5 & 0 & 0 \end{pmatrix}^{\mathrm{T}} \tag{3B.4}$$

$$\mathbf{Q}_5 = \begin{pmatrix} 0 & 0 & -2\lambda_1^4\bar{\eta}\dfrac{\partial}{\partial\xi} & 0 & 0 & \lambda_1\bar{\eta} & 0 \end{pmatrix}^{\mathrm{T}} \tag{3B.5}$$

$$\mathbf{Q}_6 = \begin{pmatrix} 0 & 0 & 0 & 0 & 0 & \beta_6 & \beta_7 \end{pmatrix}^{\mathrm{T}} \tag{3B.6}$$

$$\mathbf{Q}_7 = \begin{pmatrix} 0 & 0 & 0 & 0 & \bar{\eta}\lambda_1^7 & 0 & 0 \end{pmatrix}^{\mathrm{T}} \tag{3B.7}$$

$$\mathbf{Q}_8 = \begin{pmatrix} 0 & 0 & 0 & \beta_{10} & 0 & 0 & 0 \end{pmatrix}^{\mathrm{T}}, \tag{3B.8}$$

where,

$$\beta_1 = -(\frac{3}{2}\lambda_1^4\bar{\Omega}_2 + \lambda_1^8\bar{\Omega}_1 + 3\lambda_1^{10}\bar{\Omega}_2)\frac{\partial}{\partial\xi}, \beta_2 = 2\lambda_1^6\bar{\Omega}_1 + \bar{\Omega}_1 + 3\lambda_1^8\bar{\Omega}_2,$$

$$\beta_3 = (\frac{1}{2}\lambda_1^{14}\bar{\Omega}_1 - \frac{7}{4}\lambda_1^{10}\bar{\Omega}_2 - \frac{1}{2}\lambda_1^{16}\bar{\Omega}_2 - \frac{\lambda_1^{12}(\lambda_1^6-1)\bar{\Omega}_2^2}{(\lambda_1^2\bar{\Omega}_2 + \bar{\Omega}_1)})\frac{\partial}{\partial\xi},$$

$$\beta_4 = \frac{5}{4}\lambda_1^{10}\bar{\Omega}_2 - \lambda_1^{16}\bar{\Omega}_2 - \frac{3}{4}\lambda_1^{14}\bar{\Omega}_1 + \frac{\lambda_1^{12}(\lambda_1^6-1)\bar{\Omega}_2^2}{2(\lambda_1^2\bar{\Omega}_2 + \bar{\Omega}_1)}\frac{\partial}{\partial\xi},$$

$$\beta_5 = 2\lambda_1^{10}\bar{\Omega}_2 - \frac{5}{2}\lambda_1^{13}\bar{\Omega}_2 - \lambda_1^{11}\bar{\Omega}_1 + \frac{1}{2}\lambda_1^7\bar{\Omega}_2,$$

$$\beta_6 = \frac{\delta}{\varepsilon}(\frac{3}{4}\lambda_1^5\bar{\Omega}_2 - \frac{5}{4}\lambda_1^9\bar{\Omega}_1 - 2\lambda_1^{11}\bar{\Omega}_2), \beta_7 = \frac{1}{4}\frac{\delta}{\varepsilon}(2\lambda_1^{14}\bar{\Omega}_2 + \lambda_1^{12}\bar{\Omega}_1 - \lambda_1^8\bar{\Omega}_2)\frac{\partial}{\partial\xi},$$

$$\beta_8 = 2\lambda_1^5\bar{\Omega}_1 + \frac{9}{2}\lambda_1^7\bar{\Omega}_2, \beta_9 = \frac{3}{4}(\lambda_1^{10}\bar{\Omega}_2 + \lambda_1^8\bar{\Omega}_1)\frac{\partial}{\partial\xi}, \beta_{10} = -\bar{\eta}(\lambda_1^{10} + \frac{\lambda_1^6(\lambda_1^6-1)\bar{\Omega}_2}{2(\lambda_1^2\bar{\Omega}_2 + \bar{\Omega}_1)}).$$

Part 2

Harmonic Generation in Nonlinear Media

Outline

Chapter 4 Interesting effects in harmonic generation by plane elastic waves

4.1 Introduction

Due to elastic nonlinearity, higher harmonics can be generated by self-interaction or mutual-interaction of primary waves, and some interesting results can be concluded. One of the outstanding features of higher harmonics is the cumulative behavior because their amplitudes increase with the propagation distance. The self-interaction or mutual interaction of shear waves in the region of quadratic nonlinearity gives the generation of longitudinal waves, which propagate with the shear wave velocity. It is shown by Tang et al. (2012) that incident waves can be scattered by a region of material nonlinearity, which can produce higher order backscattered waves.

In this chapter, an analysis of the generation of higher harmonics based on quadratic and cubic material nonlinearity is presented first. The cubic nonlinearity is defined by fourth order elastic constants, which are stated in (Hamilton et al., 2004). A second order perturbation method has been adopted to obtain the harmonics for the cubically nonlinear one-dimensional problem. For the primary transverse waves, a longitudinal second harmonics and transverse first and third harmonics are obtained from the first and second order perturbations, respectively. The amplitudes of the transverse first and third harmonics increase linearly with the propagation distance. It is of interest that the amplitudes of these harmonics are determined by the squares of third order elastic constants. Thus, comparing with second harmonics, the first and third harmonics are more sensitive to the third order constants. The fourth order elastic constants also contribute to the generation of first and third harmonics. For the primary longitudinal waves, the cumulative longitudinal second harmonics are obtained from the first order perturbation. For the second order perturbation, the longitudinal first and third harmonics, whose amplitudes increase quadratically with the propagation distance, are obtained. This effect in the generation is of considerable interest.

In the next part of the chapter, we investigate the second harmonic generation by an interface between materials of linear and nonlinear material behaviors. Some works have been reported on the nonlinear reflection of bulk waves from an interface between two solids (Zhou and Shui, 1992; Deng, 1999), and the nonlinear reflection from a free boundary (Bender, 2003). As a problem of practical interest, we consider a case where the interface connects a half space of quadratical material nonlinearity with a half space of linear material behavior. The linear material properties are same across the whole space. The present model can be used to investigate a structure where there exists a large region of microstructural damages. We show that, in addition to the generation of a second harmonic, two compensatory waves with double the frequencies of the incident wave will be generated when the incident wave passes through the interface. One of the two compensatory waves is back-propagating wave. Such a wave can be used for nondestructive evaluation of the nonlinearity in the adjoining region. Finally, for the purpose of amplitude amplification of the compensatory waves, we consider the mixing of two incident waves.

4.2 Governing Equations

In this section, the governing equations of plane harmonic waves propagating in nonlinear elastic solids are presented. It is well-known that nonlinearities due to material behavior and due to large deformation both give rise to the generation of higher harmonics by primary waves. When micro damage has developed, the additional material nonlinearity may be much higher than the nonlinearity of the basic material (Nagy, 1998; Zhang et al., 2016). For small-amplitude disturbances, the geometrical nonlinearity is then negligible and only the material nonlinearity is considered to give rise to higher harmonics. In this chapter, the one-dimensional propagation of waves in a material with up to cubic material nonlinearity is investigated. Relative to a rectangular coordinate system $\{x, \text{y}\}$ the displacements in these two directions are labeled u and v. The longitudinal and transverse waves propagating in the x-direction are, respectively, represented by

$$u = u(x,t), \; v = v(x,t) \tag{4.1}$$

Expressions for the nonlinear stresses are given in the Appendix 4A.

$$\tau_{xy} = \mu\frac{\partial v}{\partial x} + \left(\frac{A}{2} + B\right)\frac{\partial u}{\partial x}\frac{\partial v}{\partial x} + \left(\frac{3}{2}E + F + 2G\right)\left(\frac{\partial u}{\partial x}\right)^2\frac{\partial v}{\partial x} + G\left(\frac{\partial v}{\partial x}\right)^3 \tag{4.2}$$

and

$$\begin{aligned}
\tau_{xx} &= (\lambda + 2\mu)\frac{\partial u}{\partial x} + (A + 3B + C)\left(\frac{\partial u}{\partial x}\right)^2 + \left(\frac{A}{4} + \frac{B}{2}\right)\left(\frac{\partial v}{\partial x}\right)^2 \\
&+ (4F + 4H + 4E + 4G)\left(\frac{\partial u}{\partial x}\right)^3 + \left(\frac{3}{2}E + F + 2G\right)\frac{\partial u}{\partial x}\left(\frac{\partial v}{\partial x}\right)^2
\end{aligned} \tag{4.3}$$

where λ and μ are Lamé constants, A, B, and C are third order elastic constants, and E, F, G and H are fourth order elastic constants (Lissenden et al., 2014). It can be easily checked from Eqs. (4.2) and (4.3) that the nonlinear parts of the stresses are totally determined by higher order elastic constants, which are independent of finite deformation. For the problem at hand, the equations of motion are

$$\frac{\partial \tau_{xx}}{\partial x} = \rho\frac{\partial^2 u}{\partial t^2} \tag{4.4}$$

$$\frac{\partial \tau_{xy}}{\partial x} = \rho\frac{\partial^2 v}{\partial t^2} \tag{4.5}$$

Substituting Eqs. (4.2) and (4.3) into Eqs. (4.4) and (4.5), respectively, we obtain

$$\rho\frac{\partial^2 u}{\partial t^2} - (\lambda + 2\mu)\frac{\partial^2 u}{\partial x^2} = F_L \tag{4.6}$$

$$\rho\frac{\partial^2 v}{\partial t^2} - \mu\frac{\partial^2 v}{\partial x^2} = F_T \tag{4.7}$$

where F_L and F_T can be considered as body forces given by

$$\begin{aligned}
F_L &= 2(A + 3B + C)\frac{\partial u}{\partial x}\frac{\partial^2 u}{\partial x^2} + 3(4F + 4H + 4E + 4G)\left(\frac{\partial u}{\partial x}\right)^2\frac{\partial^2 u}{\partial x^2} \\
&+ 2\left(\frac{A}{4} + \frac{B}{2}\right)\frac{\partial v}{\partial x}\frac{\partial^2 v}{\partial x^2} + \left(\frac{3}{2}E + F + 2G\right)\left(\frac{\partial^2 u}{\partial x^2}\left(\frac{\partial v}{\partial x}\right)^2 + 2\frac{\partial u}{\partial x}\frac{\partial v}{\partial x}\frac{\partial^2 v}{\partial x^2}\right)
\end{aligned} \tag{4.8}$$

$$F_T = \left(\frac{A}{2} + B\right)\left(\frac{\partial^2 u}{\partial x^2}\frac{\partial v}{\partial x} + \frac{\partial u}{\partial x}\frac{\partial^2 v}{\partial x^2}\right)$$
$$+ \left(\frac{3}{2}E + F + 2G\right)\left(\left(\frac{\partial u}{\partial x}\right)^2\frac{\partial^2 v}{\partial x^2} + 2\frac{\partial u}{\partial x}\frac{\partial^2 u}{\partial x^2}\frac{\partial v}{\partial x}\right) + 3G\left(\frac{\partial v}{\partial x}\right)^2\frac{\partial^2 v}{\partial x^2} \tag{4.9}$$

If the terms of cubic nonlinearity are neglected, Eqs. (4.6) and (4.7) can be reduced to the equations governing primary waves and second harmonics (Chen et al., 2014). However, cubic nonlinearity gives rise to higher order harmonics that are of interest. In addition, some materials only show material behavior of cubic nonlinearity, when the quadratic material nonlinearity is negligible (Liu et al., 2013; Chillara and Lissenden, 2016).

The perturbation method can be used to obtain solutions of the nonlinear equations (4.6) and (4.7).

$$u = u^{(0)} + u^{(1)} + u^{(2)} + \cdots \tag{4.10}$$

$$v = v^{(0)} + v^{(1)} + v^{(2)} + \cdots \tag{4.11}$$

Here, it is assumed that

$$u^{(0)}, v^{(0)} \propto O(\varepsilon^0)$$
$$u^{(1)}, v^{(1)}, u^{(0)}v^{(0)}, \left(u^{(0)}\right)^2, \left(v^{(0)}\right)^2 \propto O(\varepsilon^1) \tag{4.12}$$
$$u^{(2)}, v^{(2)}, \left(u^{(0)}\right)^3, \left(v^{(0)}\right)^3, u^{(1)}v^{(0)}, u^{(1)}u^{(0)}, v^{(1)}v^{(0)}, v^{(1)}u^{(0)} \propto O(\varepsilon^2)$$

where ε is a small quantity. Substituting Eqs. (4.10) and (4.11) into Eqs. (4.6) and (4.7), we can split the nonlinear governing equations into three sets of linear equations at three different orders of ε.

At ε^0, we have equations for the zero order displacements.

$$\rho\frac{\partial^2 u^{(0)}}{\partial t^2} - (\lambda + 2\mu)\frac{\partial^2 u^{(0)}}{\partial x^2} = 0 \tag{4.13}$$

$$\rho\frac{\partial^2 v^{(0)}}{\partial t^2} - \mu\frac{\partial^2 v^{(0)}}{\partial x^2} = 0 \tag{4.14}$$

At ε^1, we have equations for the first order displacements.

$$\rho\frac{\partial^2 u^{(1)}}{\partial t^2} - (\lambda + 2\mu)\frac{\partial^2 u^{(1)}}{\partial x^2} = F_L^{(1)} \tag{4.15}$$

$$\rho\frac{\partial^2 v^{(1)}}{\partial t^2} - \mu\frac{\partial^2 v^{(1)}}{\partial x^2} = F_T^{(1)} \tag{4.16}$$

where

$$F_L^{(1)} = 2(A+3B+C)\frac{\partial u^{(0)}}{\partial x}\frac{\partial^2 u^{(0)}}{\partial x^2} + 2\left(\frac{A}{4}+\frac{B}{2}\right)\frac{\partial v^{(0)}}{\partial x}\frac{\partial^2 v^{(0)}}{\partial x^2} \tag{4.17}$$

$$F_T^{(1)} = \left(\frac{A}{2}+B\right)\left(\frac{\partial^2 u^{(0)}}{\partial x^2}\frac{\partial v^{(0)}}{\partial x}+\frac{\partial u^{(0)}}{\partial x}\frac{\partial^2 v^{(0)}}{\partial x^2}\right) \tag{4.18}$$

At ε^2, we have equations for the second order displacements.

$$\rho\frac{\partial^2 u^{(2)}}{\partial t^2} - (\lambda + 2\mu)\frac{\partial^2 u^{(2)}}{\partial x^2} = F_L^{(2)} \tag{4.19}$$

$$\rho\frac{\partial^2 v^{(2)}}{\partial t^2} - \mu\frac{\partial^2 v^{(2)}}{\partial x^2} = F_T^{(2)} \tag{4.20}$$

where

$$\begin{aligned}
F_L^{(2)} = \ &2(A+3B+C)\left(\frac{\partial u^{(1)}}{\partial x}\frac{\partial^2 u^{(0)}}{\partial x^2}+\frac{\partial u^{(0)}}{\partial x}\frac{\partial^2 u^{(1)}}{\partial x^2}\right) \\
&+2\left(\frac{A}{4}+\frac{B}{2}\right)\left(\frac{\partial v^{(1)}}{\partial x}\frac{\partial^2 v^{(0)}}{\partial x^2}+\frac{\partial v^{(0)}}{\partial x}\frac{\partial^2 v^{(1)}}{\partial x^2}\right) \\
&+\left(\frac{3}{2}E+F+2G\right)\left(\frac{\partial^2 u^{(0)}}{\partial x^2}\left(\frac{\partial v^{(0)}}{\partial x}\right)^2+2\frac{\partial u^{(0)}}{\partial x}\frac{\partial v^{(0)}}{\partial x}\frac{\partial^2 v^{(0)}}{\partial x^2}\right) \\
&+3(4F+4H+4E+4G)\left(\frac{\partial u^{(0)}}{\partial x}\right)^2\frac{\partial^2 u^{(0)}}{\partial x^2}
\end{aligned} \tag{4.21}$$

$$F_T^{(2)} = \left(\frac{A}{2}+B\right)\left(\frac{\partial^2 u^{(1)}}{\partial x^2}\frac{\partial v^{(0)}}{\partial x}+\frac{\partial^2 u^{(0)}}{\partial x^2}\frac{\partial v^{(1)}}{\partial x}+\frac{\partial u^{(1)}}{\partial x}\frac{\partial^2 v^{(0)}}{\partial x^2}+\frac{\partial u^{(0)}}{\partial x}\frac{\partial^2 v^{(1)}}{\partial x^2}\right)$$

$$+\left(\frac{3}{2}E+F+2G\right)\left(\left(\frac{\partial u^{(0)}}{\partial x}\right)^2\frac{\partial^2 v^{(0)}}{\partial x^2}+2\frac{\partial u^{(0)}}{\partial x}\frac{\partial^2 u^{(0)}}{\partial x^2}\frac{\partial v^{(0)}}{\partial x}\right) \qquad (4.22)$$

$$+3G\left(\frac{\partial v^{(0)}}{\partial x}\right)^2\frac{\partial^2 v^{(0)}}{\partial x^2}$$

Equations (4.15), (4.16), (4.19) and (4.20) are inhomogeneous equations governing forced wave motions. Starting with the primary waves as the driving waves, higher order equations can be solved one step at the time to obtain higher harmonics. In this chapter, we consider the harmonics of primary transverse and longitudinal waves.

4.3 Primary transverse wave

For Eqs. (4.13) and (4.14), we consider a harmonic solution of the following form in an unbounded solid

$$u^{(0)} = 0, \ v^{(0)} = V\cos[\omega(t-\frac{x}{c_T})] \qquad (4.23)$$

where V is the amplitude of the transverse wave and $c_T = \sqrt{\mu/\rho}$ is the shear wave velocity. Equation (4.23) shows that initially there is only a primary transverse wave propagating in the solid. Substituting Eq. (4.23) into Eqs. (4.17) and (4.18), we obtain

$$F_L^{(1)} = -\left(\frac{A}{2}+B\right)\frac{\omega^3}{2c_T^3}V^2\sin[2\omega(t-\frac{x}{c_T})] \qquad (4.24)$$

$$F_T^{(1)} = 0 \qquad (4.25)$$

By substituting Eqs. (4.24) and (4.25) into Eqs. (4.15) and (4.16), we can obtain the solutions to the first order governing equations as

$$u^{(1)} = -\left(\frac{A}{2}+B\right)\frac{1}{\lambda+\mu}\frac{\omega}{8c_T}V^2\sin[2\omega(t-\frac{x}{c_T})], \ v^{(1)} = 0 \qquad (4.26)$$

Equation (4.26) shows that the primary transverse wave generates a second longitudinal harmonic, which propagates with the velocity of shear waves, because the driving body force contains the transverse wave term from the primary transverse wave, see Eq. (4.24).

Substituting Eqs. (4.23) and (4.26) into Eqs. (4.21) and (4.22) results in

$$F_L^{(2)} = 0 \tag{4.27}$$

$$
\begin{aligned}
F_T^{(2)} = & \left[\frac{1}{4}\left(\frac{A}{2}+B \right)^2 \frac{1}{(\lambda+\mu)} - \frac{3}{2}G \right] \frac{\omega^4}{c_T^4} V^3 \cos[\omega(t-\frac{x}{c_T})] \\
& + \left[\frac{3}{2}G - \frac{1}{2}\left(\frac{A}{2}+B \right)^2 \frac{1}{(\lambda+\mu)} \right] \frac{\omega^4}{c_T^4} V^3 \cos[3\omega(t-\frac{x}{c_T})]
\end{aligned}
\tag{4.28}
$$

Substituting Eqs. (4.27) and (4.28) into Eqs. (4.19) and (4.20), we obtain the solutions to the governing equations at second order as

$$u^{(2)} = 0 \tag{4.29}$$

$$
\begin{aligned}
v^{(2)} = & -\frac{1}{2}\left[\frac{1}{4}\left(\frac{A}{2}+B \right)^2 \frac{1}{\mu(\lambda+\mu)} - \frac{3G}{2\mu} \right] \frac{\omega^3}{c_T^3} V^3 x \sin\omega\left(t-\frac{x}{c_T} \right) \\
& -\frac{1}{6}\left[\frac{3G}{2\mu} - \frac{1}{2}\left(\frac{A}{2}+B \right)^2 \frac{1}{\mu(\lambda+\mu)} \right] \frac{\omega^3}{c_T^3} V^3 x \sin 3\omega\left(t-\frac{x}{c_T} \right)
\end{aligned}
\tag{4.30}
$$

From Eqs. (4.29) and (4.30), it is noted that the cubic nonlinearity gives only transverse harmonics for the primary transverse waves. The amplitudes of the harmonics generated by cubic nonlinearity are determined by both the third and fourth order elastic constants. Furthermore, the amplitudes of the first and third harmonics are dependent on the square of the third order elastic constants (*A* and *B*), which implies that first and third harmonics are more sensitive than second harmonics to microstructural changes. The fourth order elastic constants can make a significant contribution to the transverse harmonics only if their magnitudes are comparable to the square of the third order elastic constants. Equation (4.30) also shows that the amplitudes of the first and third transverse harmonics will increase linearly with the propagation distance, which is an advantage over the second transverse harmonics, see Eq. (4.26). It should be noted that the contribution to the

third harmonics from the mutual-interaction between the primary transverse wave and second longitudinal wave was not included in references (Rénier et al., 2008; Hamilton et al., 2004).

4.4 Primary longitudinal wave

In this section, we consider a longitudinal wave as the primary wave. The following solutions to Eqs. (4.13) and (4.14) are considered

$$u^{(0)} = U\cos[\omega(t-\frac{x}{c_L})], \ v^{(0)} = 0 \tag{4.31}$$

where U is the amplitude of longitudinal wave and $c_L = \sqrt{(\lambda+2\mu)/\rho}$ is the longitudinal wave velocity. By substituting Eq. (4.31) into Eqs. (4.17) and (4.18), we have

$$F_L^{(1)} = -\left(A+3B+C\right)U^2\frac{\omega^3}{c_L^3}\sin[2\omega(t-\frac{x}{c_L})] \tag{4.32}$$

$$F_T^{(1)} = 0 \tag{4.33}$$

By virtue of Eqs. (4.32) and (4.33), Eqs. (4.15) and (4.16) then give the following second harmonic

$$u^{(1)} = U^{(1)}x\cos[2\omega(t-\frac{x}{c_L})], \ \ v^{(1)} = 0 \tag{4.34}$$

where

$$U^{(1)} = \frac{A+3B+C}{4(\lambda+2\mu)}\frac{\omega^2}{c_L^2}U^2 \tag{4.35}$$

Substitution of Eqs. (4.31) and (4.34) into Eqs. (4.21) and (4.22) yields

$$
\begin{aligned}
F_L^{(2)} = {}&(\lambda+2\mu)\beta_1\frac{\omega^4}{c_L^4}U^3\cos[\omega(t-\frac{x}{c_L})] + (\lambda+2\mu)\beta_2\frac{\omega^4}{c_L^4}U^3\cos[3\omega(t-\frac{x}{c_L})] \\
&+ (\lambda+2\mu)\beta_3\frac{\omega^5}{c_L^5}U^3 x\left(\sin[\omega(t-\frac{x}{c_L})] - 3\sin[3\omega(t-\frac{x}{c_L})]\right)
\end{aligned} \tag{4.36}
$$

where

$$\beta_1 = \frac{3(A+3B+C)^2}{4(\lambda+2\mu)^2} - \frac{3(F+H+E+G)}{\lambda+2\mu},$$

$$\beta_2 = \frac{3(F+H+E+G)}{(\lambda+2\mu)} - \frac{5(A+3B+C)^2}{4(\lambda+2\mu)^2}, \quad \beta_3 = \frac{(A+3B+C)^2}{2(\lambda+2\mu)^2}$$

(4.37)

$$F_T^{(2)} = 0 \tag{4.38}$$

Equation (4.36) is the expression of the driving term in Eq. (4.19), which can be regarded as the summation of four different body forces. The higher harmonics have been calculated below separately for each body force.

For the body force 1, we have

$$F_L^{(2)} = (\lambda+2\mu)\beta_3 \frac{\omega^5}{c_L^5} U^3 x \sin[\omega(t-\frac{x}{c_L})] \tag{4.39}$$

In view of Eq. (4.39), the solution to Eq. (4.19) is considered to have the following form

$$u^{(2)} = U_1^{(2)} x^2 \cos[\omega(t-\frac{x}{c_L})] + U_2^{(2)} x \sin[\omega(t-\frac{x}{c_L})] \tag{4.40}$$

Substituting Eqs. (4.39) and (4.40) into Eq. (4.19), we obtain

$$-4(\lambda+2\mu)U_1^{(2)} x \frac{\omega}{c_L} \sin[\omega(t-\frac{x}{c_L})]$$

$$+2(\lambda+2\mu)\left(U_2^{(2)} \frac{\omega}{c_L} - U_1^{(2)} \right) \cos \omega[\omega(t-\frac{x}{c_L})]$$

$$= (\lambda+2\mu)\beta_3 \frac{\omega^5}{c_L^5} U^3 x \sin[\omega(t-\frac{x}{c_L})]$$

(4.41)

Equation (4.40) has to be satisfied for the sine and the cosine terms separately. Thus, we have

$$-4(\lambda+2\mu)U_1^{(2)} \frac{\omega}{c_L} = (\lambda+2\mu)\beta_3 \frac{\omega^5}{c_L^5} U^3 \tag{4.42}$$

$$U_2^{(2)} \frac{\omega}{c_L} - U_1^{(2)} = 0 \tag{4.43}$$

Through Eqs. (4.42) and (4.43), the amplitudes of the first harmonics in Eq. (4.40) can be obtained as

$$U_1^{(2)} = -\frac{\beta_3}{4} \frac{\omega^4}{c_L^4} U^3, \quad U_2^{(2)} = -\frac{\beta_3}{4} \frac{\omega^3}{c_L^3} U^3 \tag{4.44}$$

In view of Eq. (4.44), Eq. (4.39) can be rewritten as

$$u^{(2)} = -\frac{\beta_3}{4} \frac{\omega^4}{c_L^4} U^3 x^2 \cos[\omega(t - \frac{x}{c_L})] - \frac{\beta_3}{4} \frac{\omega^3}{c_L^3} U^3 x \sin[\omega(t - \frac{x}{c_L})] \tag{4.45}$$

For the body force 2, we have

$$F_L^{(2)} = -3(\lambda + 2\mu)\beta_3 \frac{\omega^5}{c_L^5} U^3 x \sin[3\omega(t - \frac{x}{c_L})] \tag{4.46}$$

Substituting Eq. (4.46) into Eq. (4.19), the expressions of third harmonics can be obtained following the same procedure as for the calculation of Eqs. (4.40) and (4.41).

$$u^{(2)} = \frac{\beta_3}{4} \frac{\omega^4}{c_L^4} U^3 x^2 \cos[3\omega(t - \frac{x}{c_L})] + \frac{\beta_3}{12} \frac{\omega^3}{c_L^3} U^3 x \sin[3\omega(t - \frac{x}{c_L})] \tag{4.47}$$

For the body force 3, we have

$$F_L^{(2)} = (\lambda + 2\mu)\beta_1 \frac{\omega^4}{c_L^4} U^3 \cos[\omega(t - \frac{x}{c_L})] \tag{4.48}$$

The generated harmonic has the following form

$$u^{(2)} = \frac{\beta_1}{2} \frac{\omega^3}{c_L^3} U^3 x \sin[\omega(t - \frac{x}{c_L})] \tag{4.49}$$

For the body force 4, we have

$$F_L^{(2)} = (\lambda + 2\mu)\beta_2 \frac{\omega^4}{c_L^4} U^3 \cos[3\omega(t - \frac{x}{c_L})] \tag{4.50}$$

The solution to Eq. (4.19) is obtained as

$$u^{(2)} = \frac{\beta_2}{6} \frac{\omega^3}{c_L^3} U^3 x \sin[3\omega(t - \frac{x}{c_L})] \tag{4.51}$$

Summation of Eqs. (4.45), (4.47), (4.49) and (4.51) yields the total solution as

$$u^{(2)} = \frac{\beta_3}{4} \frac{\omega^4}{c_L^4} U^3 x^2 \left[\cos[3\omega(t - \frac{x}{c_L})] - \cos[\omega(t - \frac{x}{c_L})] \right]$$
$$+ \left(\frac{\beta_1}{2} - \frac{\beta_3}{4} \right) \frac{\omega^3}{c_L^3} U^3 x \sin[\omega(t - \frac{x}{c_L})] + \left(\frac{\beta_3}{12} + \frac{\beta_2}{6} \right) \frac{\omega^3}{c_L^3} U^3 x \sin[3\omega(t - \frac{x}{c_L})]$$

$$\tag{4.52}$$

where β_1, β_2 and β_3 are coefficients expressed in terms of elastic constants, which are defined by Eq. (4.37). For the primary longitudinal wave, the cubic nonlinearity gives two first and two third longitudinal harmonics. We obtain two quadratically cumulative harmonics in addition to the linearly cumulative harmonics. When the propagation distance is large enough, the waves whose amplitudes increase quadratically with the propagation distance will be dominant. It should be pointed out that the amplitudes of the dominant waves are independent of the fourth order elastic constant (i.e. E, F, G and H), see the expression of β_3 in Eq. (4.37). Making a comparison between Eq. (4.30) and Eq. (4.52), it can be concluded that the transverse primary waves are more suitable than the longitudinal primary waves to detect the fourth order elastic constants. To the knowledge of authors, not much research has been devoted to harmonics whose amplitudes increase quadratically with the propagation distance, which can amplify the amplitudes of the first and third harmonics quickly. Another advantage over second harmonics is that they are more sensitive to the changes of third order elastic constants.

4.5   Reflection of second harmonics from an interface

Of practical interest for applications to quantitative non-destructive evaluation is the case that the region defined by $x \geq 0$ displays nonlinear material behavior due to damage of the material. For some cases such a damaged region may not be directly accessible, and ultrasonic waves for detection of the nonlinear behavior

have to propagate through the undamaged material and cross the interface between linear and nonlinear material behavior. The geometry is shown in Fig. 4.1. In this section, it is shown that the interface at $x=0$ gives rise to a returning wave motion which contains important information on the nonlinearity of the adjoining material.
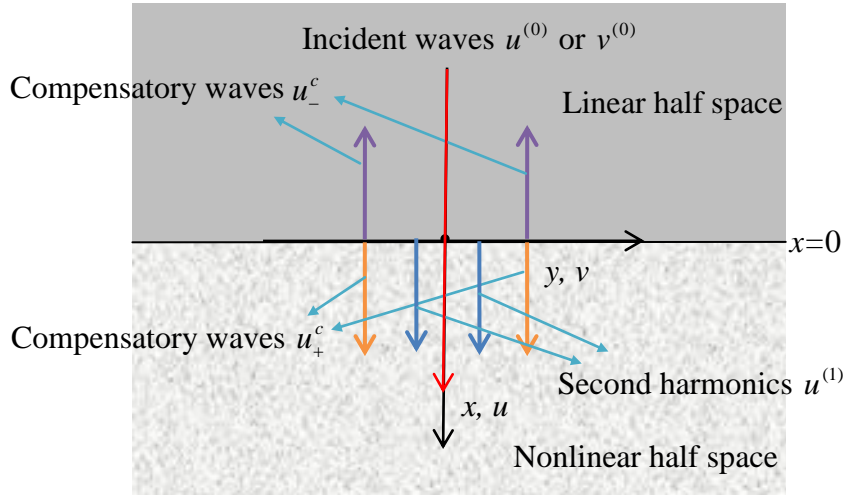
Fig. 4.1 Wave propagation in a linearly elastic half space and a nonlinearly elastic half space with the same linear material properties

4.5.1 Incident longitudinal wave

Since the materials on both sides of the interface $x=0$ display the same linear behavior, an incident longitudinal wave of the form given by Eq. (4.31) passes through the interface without interference. However, as soon as it enters the damaged region $x \geq 0$, a second harmonic is generated, which is given by Eq. (4.34) as

$$u^{(1)} = U^{(1)}x\cos[2\omega(t-\frac{x}{c_L})] \tag{4.53}$$

where

$$U^{(1)} = \frac{A+3B+C}{4(\lambda+2\mu)}\frac{\omega^2}{c_L^2}U^2 \tag{4.54}$$

This displacement vanishes at $x=0^+$, but $\tau_{xx}^{(1)}$ has the following value at $x=0^+$

$$\tau_{xx}^{(1)} = (\lambda + 2\mu)U^{(1)}\cos(2\omega t) - \frac{1}{2}(A + 3B + C)\frac{\omega^2}{c_L^2}U^2\cos(2\omega t) \qquad (4.55)$$

The static stress term is not considered here. The following identity has been used

$$1 - 2\sin^2\theta = \cos 2\theta \qquad (4.56)$$

For stress equilibration at $x = 0$, this stress generates two compensatory second harmonics which propagate in opposite directions from $x = 0^+$ and $x = 0^-$ as

$$u_+^c = U_+^c \sin[2\omega(t - \frac{x}{c_L})] \qquad (4.57)$$

$$u_-^c = U_-^c \sin[2\omega(t + \frac{x}{c_L})] \qquad (4.58)$$

Equality of displacement at $x = 0^+$ and $x = 0^-$ yields

$$U_+^c = U_-^c \qquad (4.59)$$

Dynamic equilibrium of stress at $x = 0^+$ and $x = 0^-$ requires

$$\begin{aligned} U^{(1)}\cos(2\omega t) - \frac{1}{2}\frac{\omega^2}{c_L^2}\frac{A+3B+C}{\lambda+2\mu}U^2\cos(2\omega t) - U_+^c\frac{2\omega}{c_L}\cos(2\omega t) \\ = U_-^c\frac{2\omega}{c_L}\cos(2\omega t) \end{aligned} \qquad (4.60)$$

It should be noted that the stresses higher than second order are omitted. Equations (4.54), (4.58) and (4.59) yield

$$U_+^c = U_-^c = -\frac{A+3B+C}{16(\lambda+2\mu)}\frac{\omega}{c_L}U^2 \qquad (4.61)$$

4.5.2 Incident transverse wave

As an incident transverse wave of the type given by Eq. (4.23) crosses the interface, it generates a second longitudinal harmonic of the form given by Eq. (4.26) as

$$u_+^{(1)} = -\frac{1}{8}\left(\frac{A}{2}+B\right)\frac{1}{\lambda+\mu}\frac{\omega}{c_T}V^2\sin[2\omega(t-\frac{x}{c_T})] \tag{4.62}$$

The displacement and the stress do not vanish at $x = 0$, and $\tau_{xx}^{(1)}$ has the following value at $x = 0^+$

$$\tau_{xx}^{(1)} = \frac{1}{4}\left(\frac{A}{2}+B\right)\left(\frac{\lambda+2\mu}{\lambda+\mu}-1\right)\frac{\omega^2}{c_T^2}V^2\cos(2\omega t) \tag{4.63}$$

To equate the displacements and stresses at $x = 0^\pm$, two compensatory waves are generated propagating in opposite directions

$$u_+^c = V_+^c\sin[2\omega(t-\frac{x}{c_L})] \tag{4.64}$$

$$u_-^c = V_-^c\sin[2\omega(t+\frac{x}{c_L})] \tag{4.65}$$

Equality of displacements at $x = 0^\pm$ yields

$$-\frac{1}{8}\left(\frac{A}{2}+B\right)\frac{1}{\lambda+\mu}\frac{\omega}{c_T}V^2\sin(2\omega t)+V_+^c\sin(2\omega t)=V_-^c\sin(2\omega t) \tag{4.66}$$

Dynamic equilibrium of stress at the interface yields

$$\begin{aligned}&\frac{1}{4}\left(\frac{A}{2}+B\right)\left(\frac{1}{\lambda+\mu}-\frac{1}{\lambda+2\mu}\right)\frac{\omega^2}{c_T^2}V^2\cos(2\omega t)-V_+^c\frac{2\omega}{c_L}\cos(2\omega t)\\&=V_-^c\frac{2\omega}{c_L}\cos(2\omega t)\end{aligned} \tag{4.67}$$

Equations (4.64) and (4.65) can be solved for V_-^c and V_+^c as

$$V_-^c = \frac{1}{16}\left(\frac{A}{2}+B\right)\frac{1}{\lambda+\mu}\frac{\omega}{c_T}\left(\frac{\mu}{\lambda+2\mu}\frac{c_L}{c_T}-1\right)V^2 \tag{4.68}$$

$$V_+^c = \frac{1}{16}\left(\frac{A}{2}+B\right)\frac{1}{\lambda+\mu}\frac{\omega}{c_T}\left(\frac{\mu}{\lambda+2\mu}\frac{c_L}{c_T}+1\right)V^2 \tag{4.69}$$

4.5.3   Incidence of two longitudinal waves

To increase the amplitude of the back-propagating compensatory wave, the incidence of two waves is considered. The combination of two longitudinal waves is considered as an example. The total displacement of the primary waves can be written as

$$u^{(0)} = U_1 \cos[\omega_1(t - \frac{x}{c_L})] + U_2 \cos[\omega_2(t - \frac{x}{c_L})] \qquad (4.70)$$

Substituting Eq. (4.70) into Eq. (4.17) yields the expression for the related body force as

$$F_L^{(1)} = -2(A + 3B + C) \begin{bmatrix} \dfrac{\omega_1^3}{2c_L^3} U_1^2 \sin[2\omega_1(t - \dfrac{x}{c_L})] + \dfrac{\omega_2^3}{2c_L^3} U_2^2 \sin[2\omega_2(t - \dfrac{x}{c_L}) \\[2mm] + \left(\dfrac{\omega_1^2 \omega_2}{2c_L^3} + \dfrac{\omega_1 \omega_2^2}{2c_L^3} \right) U_1 U_2 \sin[(\omega_1 + \omega_2)(t - \dfrac{x}{c_L})] \\[2mm] - \left(\dfrac{\omega_1^2 \omega_2}{2c_L^3} - \dfrac{\omega_1 \omega_2^2}{2c_L^3} \right) U_1 U_2 \sin[(\omega_1 - \omega_2)(t - \dfrac{x}{c_L})] \end{bmatrix} \qquad (4.71)$$

We select the following body force from Eq. (4.71) for further consideration

$$F_L^{(1)} = (A + 3B + C) \left(\frac{\omega_1^2 \omega_2}{c_L^3} - \frac{\omega_1 \omega_2^2}{c_L^3} \right) U_1 U_2 \sin[(\omega_1 - \omega_2)(t - \frac{x}{c_L})] \qquad (4.72)$$

Equation (4.72) generates a resonant wave in the form

$$u^{(1)} = -\frac{1}{2} \frac{A + 3B + C}{\lambda + 2\mu} \frac{\omega_1 \omega_2}{c_L^2} U_1 U_2 x \cos[(\omega_1 - \omega_2)(t - \frac{x}{c_L})] \qquad (4.73)$$

The displacement vanishes, but the stress has a value at $x = 0$. Therefore, two compensatory waves are introduced

$$u_+^c = U_+^c \sin[(\omega_1 - \omega_2)(t - \frac{x}{c_L})] \qquad (4.74)$$

$$u_-^c = U_-^c \sin[(\omega_1 - \omega_2)(t + \frac{x}{c_L})] \qquad (4.75)$$

The equality of displacement at the interface $x = 0$ yields

$$U_+^c = U_-^c \tag{4.76}$$

Continuity of stress at the interface $x = 0$ gives

$$\frac{1}{2}\frac{(A+3B+C)}{\lambda+2\mu}\frac{\omega_1\omega_2}{c_L^2}U_1U_2\cos(\omega_1-\omega_2)t - U_+^c\frac{\omega_1-\omega_2}{c_L}\cos(\omega_1-\omega_2)t$$
$$= U_-^c\frac{\omega_1-\omega_2}{c_L}\cos(\omega_1-\omega_2)t \tag{4.77}$$

It follows from Eqs. (4.76) and (4.77) that

$$U_+^c = U_-^c = \frac{1}{4}\frac{(A+3B+C)}{\lambda+2\mu}\frac{\omega_1\omega_2}{c_L(\omega_1-\omega_2)}U_1U_2 \tag{4.78}$$

If we consider

$$\omega_1 = 3\omega_2, \quad \omega_1 - \omega_2 = 2\omega \tag{4.79}$$

$$U_1 = U_2 = U \tag{4.80}$$

Equation (4.78) then becomes

$$U_+^c = U_-^c = \frac{3}{8}\frac{(A+3B+C)}{\lambda+2\mu}\frac{\omega}{c_L}U^2 \tag{4.81}$$

Comparing the expressions for the compensatory waves, the ratio of the amplitudes given by Eqs. (4.61) and (4.81) for the two cases is obtained as

$$\left|\frac{(U_-^c)_2}{(U_-^c)_1}\right| = \left|\frac{(U_+^c)_2}{(U_+^c)_1}\right| = 6 \tag{4.82}$$

It is noted that the amplitude of the compensatory wave has been increased six times, while its frequency remains unchanged, i.e., 2ω. Compensatory waves can be generated through any other body force given in Eq. (4.71). Since the procedure is much similar to the one shown above, specific expressions are not presented here.

In summary, the interface between regions of linear and nonlinear material

properties generates two additional compensatory waves. The analysis of this section can be used to measure the third order elastic constants of the nonlinear region near the interface. The compensatory wave u_-^c provides a simple method to the evaluation of nonlinear region by using higher harmonics.

4.6 Conclusions

In this chapter, we have investigated the generation by primary waves of higher harmonics due to quadratic and cubic material nonlinearity, related to third and fourth order elastic constants, respectively, in the stress-strain relation, as well as the effects of wave incidence on an interface between regions on linear and nonlinear material behaviors. Due to the quadratic nonlinearity a transverse wave generates a second longitudinal harmonic, which, however, propagates with the velocity of transverse waves, as well as resonant transverse first and third harmonics due to the cubic and quadratic nonlinearities. A longitudinal wave generates a resonant longitudinal second harmonic as well as first and third harmonics whose amplitudes increase linearly and quadratically with the distance propagated.

We have also considered the case that a region has quadratic nonlinear material behavior only on one side of an interface, while it has the same linear terms in the stress-strain relation on both sides. This case is relevant to a region, a part of which has suffered from the microstructural damages. The second harmonic in the nonlinear part generates two compensatory waves at the nonlinear interface. These waves have twice the frequency of the incident wave, and their amplitudes correlate with the nonlinear material behavior. Even though a back-propagated compensatory wave in a linear material is not resonant when compared with the higher harmonics propagating in nonlinear materials, such waves can still be used for a test technique to obtain material properties using an appropriate measurement method. To increase the amplitudes of the back-propagating compensatory waves, the single incident wave is replaced by two incident waves of different frequencies. The method of this chapter should be useful to measure the higher order elastic constants.

Appendix 4A: Cubic nonlinear constitutive relation for small deformation

The expansion of the energy density up to fourth order was presented in (Hamilton et al., 2004) as:

$$
\begin{aligned}
\rho_0 W = {} & \frac{\lambda}{2}\left(\mathrm{tr}\mathbf{E}\right)^2 + \mu\,\mathrm{tr}\mathbf{E}^2 + \frac{C}{3}\left(\mathrm{tr}\mathbf{E}\right)^3 + B\left(\mathrm{tr}\mathbf{E}\right)\mathrm{tr}\mathbf{E}^2 + \frac{A}{3}\,\mathrm{tr}\mathbf{E}^3 + E\left(\mathrm{tr}\mathbf{E}\right)\mathrm{tr}\mathbf{E}^3 \\
& + F\left(\mathrm{tr}\mathbf{E}\right)^2\mathrm{tr}\mathbf{E}^2 + G\left(\mathrm{tr}\mathbf{E}^2\right)^2 + H\left(\mathrm{tr}\mathbf{E}\right)^4
\end{aligned}
\tag{4A.1}
$$

where λ and μ are Lamé coefficients, $A,\ B,$ and C are third order elastic coefficients, $E,\ F,\ G$ and H are fourth order elastic coefficients, $\mathbf{E}$ is the Langrange strain tensor, the component of which for small deformation can be given by

$$
E_{ij} = \frac{1}{2}\left(\frac{\partial U_i}{\partial a_j} + \frac{\partial U_j}{\partial a_i}\right)
\tag{4A.2}
$$

where U_i and a_j define components of displacement and a rectilinear coordinate, respectively. Thus, the Cauchy stress tensor, which is the same as the first Piola-Kirchhoff stress tensor, can be given by

$$
\begin{aligned}
\boldsymbol{\tau} = {} & \lambda(\mathrm{tr}\mathbf{E})\mathbf{I} + 2\mu\mathbf{E}^{\mathrm{T}} + C(\mathrm{tr}\mathbf{E})^2\mathbf{I} + B(\mathrm{tr}\mathbf{E}^2)\mathbf{I} + 2B(\mathrm{tr}\mathbf{E})\mathbf{E}^{\mathrm{T}} + A(\mathbf{E}^2)^{\mathrm{T}} \\
& + E(\mathrm{tr}\mathbf{E}^3)\mathbf{I} + 3E(\mathrm{tr}\mathbf{E})(\mathbf{E}^2)^{\mathrm{T}} + 2F(\mathrm{tr}\mathbf{E})^2\mathbf{E}^{\mathrm{T}} + 2F(\mathrm{tr}\mathbf{E}^2)(\mathrm{tr}\mathbf{E})\mathbf{I} \\
& + 4G(\mathrm{tr}\mathbf{E}^2)\mathbf{E}^{\mathrm{T}} + 4H(\mathrm{tr}\mathbf{E})^3\mathbf{I}
\end{aligned}
\tag{4A.3}
$$

Substituting the expression for the strain into the above equation, we obtain the relation of stress and displacement. The stress has the following form

$$
\begin{aligned}
\tau_{ij} = {} & \lambda \frac{\partial U_l}{\partial a_l} \delta_{ij} + \mu \left(\frac{\partial U_j}{\partial a_i} + \frac{\partial U_i}{\partial a_j} \right) \\
& + \frac{A}{4} \left(\frac{\partial U_i}{\partial a_l} \frac{\partial U_j}{\partial a_l} + \frac{\partial U_i}{\partial a_l} \frac{\partial U_l}{\partial a_j} + \frac{\partial U_j}{\partial a_l} \frac{\partial U_l}{\partial a_i} + \frac{\partial U_l}{\partial a_i} \frac{\partial U_l}{\partial a_j} \right) + C \frac{\partial U_m}{\partial a_m} \frac{\partial U_l}{\partial a_l} \delta_{ij} \\
& + \frac{B}{2} \left(\frac{\partial U_l}{\partial a_k} \frac{\partial U_k}{\partial a_l} + \frac{\partial U_l}{\partial a_k} \frac{\partial U_l}{\partial a_k} \right) \delta_{ij} + B \left(\frac{\partial U_l}{\partial a_l} \frac{\partial U_i}{\partial a_j} + \frac{\partial U_l}{\partial a_l} \frac{\partial U_j}{\partial a_i} \right) \\
& + \frac{1}{8} E \left(\frac{\partial U_m}{\partial a_k} \frac{\partial U_l}{\partial a_m} + \frac{\partial U_l}{\partial a_m} \frac{\partial U_k}{\partial a_m} + \frac{\partial U_m}{\partial a_k} \frac{\partial U_m}{\partial a_l} + \frac{\partial U_m}{\partial a_l} \frac{\partial U_k}{\partial a_m} \right) \left(\frac{\partial U_k}{\partial a_l} + \frac{\partial U_l}{\partial a_k} \right) \delta_{ij} \\
& + \frac{3}{4} E \left(\frac{\partial U_i}{\partial a_l} \frac{\partial U_l}{\partial a_j} + \frac{\partial U_l}{\partial a_i} \frac{\partial U_l}{\partial a_j} + \frac{\partial U_i}{\partial a_l} \frac{\partial U_j}{\partial a_l} + \frac{\partial U_l}{\partial a_i} \frac{\partial U_j}{\partial a_l} \right) \frac{\partial U_m}{\partial a_m} \\
& + F \frac{\partial U_m}{\partial a_m} \frac{\partial U_n}{\partial a_n} \left(\frac{\partial U_i}{\partial a_j} + \frac{\partial U_j}{\partial a_i} \right) + F \left(\frac{\partial U_m}{\partial a_k} \frac{\partial U_k}{\partial a_m} + \frac{\partial U_m}{\partial a_k} \frac{\partial U_m}{\partial a_k} \right) \frac{\partial U_l}{\partial a_l} \delta_{ij} \\
& + G \left(\frac{\partial U_m}{\partial a_k} \frac{\partial U_k}{\partial a_m} + \frac{\partial U_m}{\partial a_k} \frac{\partial U_m}{\partial a_k} \right) \left(\frac{\partial U_i}{\partial a_j} + \frac{\partial U_j}{\partial a_i} \right) + 4H \frac{\partial U_m}{\partial a_m} \frac{\partial U_n}{\partial a_n} \frac{\partial U_k}{\partial a_k} \delta_{ij}
\end{aligned}
$$

$$(4A.4)$$

Here, a repeated index defines a summation. As a choice, we decompose the expression of stress into the linear and nonlinear parts, which can be written in the following vector form.

$$
\boldsymbol{\tau} = \boldsymbol{\tau}^1 + \boldsymbol{\tau}^2 + \boldsymbol{\tau}^3 \tag{4A.5}
$$

where

$$
\boldsymbol{\tau}^1 = \lambda \left(\nabla \cdot \mathbf{U} \right) \mathbf{I} + \mu (\nabla \mathbf{U} + (\nabla \mathbf{U})^{\mathrm{T}}) \tag{4A.6}
$$

$$
\begin{aligned}
\boldsymbol{\tau}^2 = {} & \frac{A}{4} (\nabla \mathbf{U} \cdot [\nabla \mathbf{U}]^{\mathrm{T}} + \nabla \mathbf{U} \cdot \nabla \mathbf{U} + [\nabla \mathbf{U}]^{\mathrm{T}} \cdot [\nabla \mathbf{U}]^{\mathrm{T}} + [\nabla \mathbf{U}]^{\mathrm{T}} \cdot \nabla \mathbf{U}) \\
& + \frac{B}{2} \left(\nabla \mathbf{U} : \nabla \mathbf{U} + \nabla \mathbf{U} : [\nabla \mathbf{U}]^{\mathrm{T}} \right) \mathbf{I} + B \left(\nabla \cdot \mathbf{U} \right) (\nabla \mathbf{U} + [\nabla \mathbf{U}]^{\mathrm{T}}) \\
& + C (\nabla \cdot \mathbf{U})^2 \mathbf{I}
\end{aligned} \tag{4A.7}
$$

$$\boldsymbol{\tau}^3 = \frac{1}{8} E \begin{pmatrix} \nabla\mathbf{U}\cdot\nabla\mathbf{U} + \nabla\mathbf{U}\cdot(\nabla\mathbf{U})^T \\ +(\nabla\mathbf{U})^T\cdot(\nabla\mathbf{U}) + (\nabla\mathbf{U}\cdot\nabla\mathbf{U})^T \end{pmatrix} : \left(\nabla\mathbf{U}+(\nabla\mathbf{U})^T\right)\mathbf{I}$$

$$+ \frac{3}{4} E \left(\nabla\mathbf{U}\cdot\nabla\mathbf{U} + (\nabla\mathbf{U})^T\cdot(\nabla\mathbf{U}) + \nabla\mathbf{U}\cdot(\nabla\mathbf{U})^T + (\nabla\mathbf{U}\cdot\nabla\mathbf{U})^T\right)\nabla\cdot\mathbf{U} \quad (4A.8)$$

$$+ F\left(\nabla\cdot\mathbf{U}\right)^2\left(\nabla\mathbf{U}+(\nabla\mathbf{U})^T\right) + F\left(\nabla\mathbf{U}:\nabla\mathbf{U} + \nabla\mathbf{U}:(\nabla\mathbf{U})^T\right)(\nabla\cdot\mathbf{U})\mathbf{I}$$

$$+ G\left(\nabla\mathbf{U}:\nabla\mathbf{U} + \nabla\mathbf{U}:(\nabla\mathbf{U})^T\right)\left(\nabla\mathbf{U}+(\nabla\mathbf{U})^T\right) + 4H\left(\nabla\cdot\mathbf{U}\right)^3\mathbf{I}$$

Chapter 5 Far-field resonant third harmonic surface wave on a half-space of incompressible material of cubic nonlinearity

5.1 Introduction

In the present chapter, we consider the waves propagating in a material which displays incompressibility and cubic nonlinearity. As pointed out by Destrade and Ogden (2010), incompressibility applies for some soft materials (such as a biomaterial), but also to some hard materials like fully saturated soils in undrained condition. We consider cubic nonlinearity because quadratic material nonlinearity cannot produce second harmonics, as mentioned by Fu and Devenish (1996). It was pointed out by Zabolotskaya et al. (2007) that, on a half-space of incompressible material, second surface wave harmonics can only be generated by geometric nonlinearity. Another reason for cubic nonlinearity is that the stress-strain relation is symmetric with respect to the unloaded case.

There is limited information on higher harmonic surface wave generation due to material nonlinearity on a half-space of incompressible material. The main purpose of the present work is to obtain an analytical solution for higher harmonic surface waves on a half-space of incompressible material of cubic nonlinearity, in a simple and elegant manner, which may be easily understood and applicable.

Using the perturbation method, a set of zero-order homogeneous differential equations and a set of first-order inhomogeneous differential equations are obtained, which can be uncoupled, based on the assumption that the amplitudes of the primary waves are much larger than the amplitudes of the generated harmonics. After solving the differential equations at different orders step by step, a simple analytical solution for the resonant third harmonic surface wave is obtained in the far field, whose structure except for the frequency of 3ω and the dependence of the amplitude on a multiplication factor x is exactly the same as the structure of the

primary surface wave of frequency ω. It is shown that the velocity of the resonant third harmonic wave is the classic Rayleigh wave velocity, and the amplitude depends on the nonlinear material constant (i.e. the fourth order elastic constant G) and increases linearly with the propagation distance.

As an application, we consider the transmission of the third harmonic surface wave through an interface between quarter-spaces of nonlinear and linear material. The interface is located at $x = L$, where L is assumed to be large. The harmonic surface wave which is transmitted into the linear material is obtained using the continuity conditions of stress and displacement at the interface.

5.2 Constitutive relations for nonlinear material behavior

The expansion of the energy density up to fourth order has been presented in the Appendix in Chapter 4, which is given by

$$
\begin{aligned}
\rho_0 W = {} &\frac{\lambda}{2}\left(\mathrm{tr}\mathbf{E}\right)^2 + \mu\,\mathrm{tr}\mathbf{E}^2 + \frac{C}{3}\left(\mathrm{tr}\mathbf{E}\right)^3 + B\left(\mathrm{tr}\mathbf{E}\right)\mathrm{tr}\mathbf{E}^2 + \frac{A}{3}\,\mathrm{tr}\mathbf{E}^3 + E\left(\mathrm{tr}\mathbf{E}\right)\mathrm{tr}\mathbf{E}^3 \\
&+ F\left(\mathrm{tr}\mathbf{E}\right)^2 \mathrm{tr}\mathbf{E}^2 + G\left(\mathrm{tr}\mathbf{E}^2\right)^2 + H\left(\mathrm{tr}\mathbf{E}\right)^4,
\end{aligned}
\tag{5.1}
$$

where λ and μ are the Lamé elastic constants, A, B, and C are third order elastic constants, E, F, G and H are fourth order elastic constants ,and the Langrangian strain tensor is given by

$$
\mathbf{E} = \frac{1}{2}\left(\mathbf{F}^{\mathrm{T}}\mathbf{F} - \mathbf{1}\right)
\tag{5.2}
$$

where $\mathbf{F}$ is the deformation gradient. For small strains the components of the strain tensor simplify to

$$
E_{ij} = \frac{1}{2}\left(\frac{\partial u_i}{\partial x_j} + \frac{\partial u_j}{\partial x_i} + \frac{\partial u_k}{\partial x_i}\frac{\partial u_k}{\partial x_j}\right) \approx \frac{1}{2}\left(\frac{\partial u_i}{\partial x_j} + \frac{\partial u_j}{\partial x_i}\right)
\tag{5.3}
$$

In Eq. (5.3) u_i and x_j define the components of the displacement and a Cartesian coordinate system, respectively.

In the present chapter we consider small deformations. Since the geometrical

nonlinearity is negligible for small deformation, the micro-damage correlates only with the higher order elastic constants of the material nonlinearity. This correlation can be determined by investigating the higher harmonics generated by material nonlinearity.

The propagation of surface waves on a half-space of an isotropic incompressible material was considered by Destrade (2001), Destrade et al. (2002), Ogden and Vinh (2004) and Zabolotskaya et al. (2007). For an incompressible material, the following condition has to be satisfied.

$$\mathrm{tr}\mathbf{E} = \frac{\partial u_i}{\partial x_i} = 0 \tag{5.4}$$

Substituting Eq. (5.4) into Eq. (5.1) yields

$$\rho_0 W = \mu \mathrm{tr}\mathbf{E}^2 + \frac{A}{3}\mathrm{tr}\mathbf{E}^3 + G\left(\mathrm{tr}\mathbf{E}^2\right)^2 \tag{5.5}$$

Equation (5.5), which is the energy density expanded to fourth order for isotropic incompressible materials, was also employed by Destrade and Ogden (2010) and Hamilton et al. (2004). The expression for the stress tensor can be represented by

$$\boldsymbol{\tau} = \rho_0 \mathbf{F} \cdot \frac{\partial W}{\partial \mathbf{E}} \cdot \mathbf{F}^T - p\mathbf{I} \tag{5.6}$$

where p is the pressure, which is introduced to accommodate the internal constraint of incompressibility (Destrade and Ogden, 2010). It should be noted that the incompressibility condition is not only justified for certain kinds of soft materials (such as biomaterials) but also for some hard materials (like fully saturated soils in undrained condition) (Destrade and Ogden, 2010).

Substitution of Eq. (5.5) into Eq. (5.6) gives the stress-strain relation as

$$\boldsymbol{\tau} = -p\mathbf{I} + 2\mu\mathbf{E}^{\mathrm{T}} + A(\mathbf{E}^2)^{\mathrm{T}} + 4G(\mathrm{tr}\mathbf{E}^2)\mathbf{E}^{\mathrm{T}} \tag{5.7}$$

Hence the stress components are defined by

$$\tau_{ij} = -p\delta_{ij} + \mu\left(\frac{\partial u_j}{\partial x_i} + \frac{\partial u_i}{\partial x_j}\right) + \frac{A}{4}\left(\frac{\partial u_i}{\partial x_l}\frac{\partial u_j}{\partial x_l} + \frac{\partial u_i}{\partial x_l}\frac{\partial u_l}{\partial x_j} + \frac{\partial u_j}{\partial x_l}\frac{\partial u_l}{\partial x_i} + \frac{\partial u_l}{\partial x_i}\frac{\partial u_l}{\partial x_j}\right)$$
$$+ G(\frac{\partial u_m}{\partial x_k}\frac{\partial u_k}{\partial x_m} + \frac{\partial u_m}{\partial x_k}\frac{\partial u_m}{\partial x_k})(\frac{\partial u_i}{\partial x_j} + \frac{\partial u_j}{\partial x_i})$$
$$(5.8)$$

As usual repeated subscripts denote a summation.

5.3   Equations of motion of a surface wave
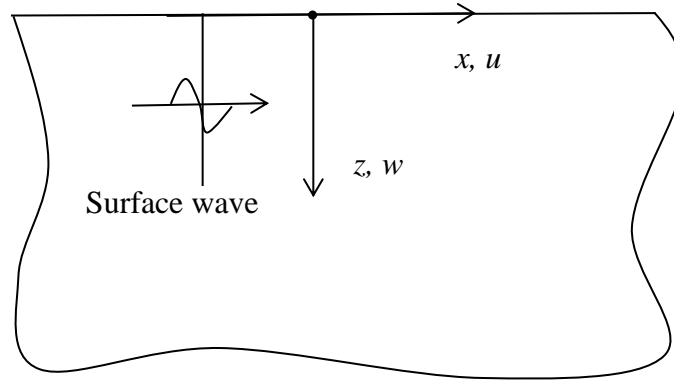
Fig. 5.1 Surface wave on a half-space

Surface waves, whose amplitudes decay exponentially with distance from the surface, are confined to a region near the surface. We investigate surface waves in a two-dimensional plane strain setting of plane waves propagating in the *x*-direction, see Fig. 5.1. The displacement components are

$$u = u(x, z, t), \quad w = w(x, z, t) \tag{5.9}$$

The incompressibility condition, Eq. (5.4), can be written as

$$\frac{\partial u}{\partial x} + \frac{\partial w}{\partial z} = 0 \tag{5.10}$$

It has been noted that quadratic material nonlinearity (third order elastic constants) does not generate a second harmonic of surface wave propagation in an incompressible material (Fu and Devenish, 1996; Zabolotskaya et al., 2007). This has also been shown analytically in unpublished related work by the authors. In the present chapter, we consider cubic material nonlinearity, which produces first and

third harmonics. Second harmonics generated by quadratic nonlinearity have received much more attention than third harmonics caused by cubic nonlinearity. However, cubic nonlinearity of the constitutive relations is required for materials with symmetric tension-compression behavior, see Fig. 1.7.

For cubic material nonlinearity (fourth order elastic constant), the use of Eqs. (5.9) and (5.10) in Eq. (5.8) yields

$$\tau_{xx} = -p + 2\mu\frac{\partial u}{\partial x} + \tau_{xx}^{NL}; \quad \tau_{zz} = -p + 2\mu\frac{\partial w}{\partial z} + \tau_{zz}^{NL};$$

$$\tau_{xz} = \mu\left(\frac{\partial u}{\partial z} + \frac{\partial w}{\partial x}\right) + \tau_{xz}^{NL} \tag{5.11}$$

where the nonlinear parts are given by

$$\tau_{xx}^{NL} = 2G\left[\left(\frac{\partial u}{\partial z} + \frac{\partial w}{\partial x}\right)^2 - 4\frac{\partial u}{\partial x}\frac{\partial w}{\partial z}\right]\frac{\partial u}{\partial x}; \quad \tau_{zz}^{NL} = -\tau_{xx}^{NL};$$

$$\tau_{xz}^{NL} = G\left[\left(\frac{\partial u}{\partial z} + \frac{\partial w}{\partial x}\right)^2 - 4\frac{\partial u}{\partial x}\frac{\partial w}{\partial z}\right]\left(\frac{\partial u}{\partial z} + \frac{\partial w}{\partial x}\right) \tag{5.12}$$

It is noted that only one nonlinear material constant, G, appears in Eqs. (5.12).

5.4 Surface wave propagation

The stress equations of motion for plane strain are given by

$$\frac{\partial \tau_{xx}}{\partial x} + \frac{\partial \tau_{xz}}{\partial z} = \rho\frac{\partial^2 u}{\partial t^2}; \quad \frac{\partial \tau_{xz}}{\partial x} + \frac{\partial \tau_{zz}}{\partial z} = \rho\frac{\partial^2 w}{\partial t^2} \tag{5.13}$$

Substitution of Eq. (5.11) into Eq. (5.13) yields

$$-\frac{\partial p}{\partial x} + \mu\nabla u - \rho\frac{\partial^2 u}{\partial t^2} = F_u; \quad -\frac{\partial p}{\partial z} + \mu\nabla w - \rho\frac{\partial^2 w}{\partial t^2} = F_w \tag{5.14}$$

where Laplace's operator is defined by $\nabla = \partial^2/\partial x^2 + \partial^2/\partial z^2$, and the right-hand side nonlinear terms are defined by

$$F_u(u,w) = -\frac{\partial \tau_{xx}^{NL}}{\partial x} - \frac{\partial \tau_{xz}^{NL}}{\partial z}, \quad F_w(u,w) = -\frac{\partial \tau_{xz}^{NL}}{\partial x} + \frac{\partial \tau_{xx}^{NL}}{\partial z} \tag{5.15}$$

The surface ($z = 0$) is free of tractions, hence the boundary conditions can be written as

$$z = 0: \quad \tau_{zz} = -p + 2\mu\frac{\partial w}{\partial z} + \tau_{zz}^{NL} = 0,$$
$$\tau_{xz} = \mu\left(\frac{\partial u}{\partial z} + \frac{\partial w}{\partial x}\right) + \tau_{xz}^{NL} = 0 \tag{5.16}$$

Since the nonlinear terms appearing in the governing equations are assumed to be small, the material nonlinearity can be treated as a weak perturbation. The perturbation method is therefore adopted to solve the boundary-value problem for nonlinear material behavior, and the pressure and the displacement components are expanded as

$$p = p^{(0)} + p^{(1)} + \cdots;$$
$$u = u^{(0)} + u^{(1)} + \cdots;$$
$$w = w^{(0)} + w^{(1)} + \cdots \tag{5.17}$$

where $\left|\bullet\right|^{(1)}$ is sufficiently smaller than $\left|\bullet\right|^{(0)}$. Substituting Eq. (5.17) into the governing equations, Eqs. (5.10) and (5.14), and the boundary condition, Eq. (5.16), yields the zero-order governing equations as:

$$\frac{\partial u^{(0)}}{\partial x} + \frac{\partial w^{(0)}}{\partial z} = 0 \tag{5.18}$$

$$-\frac{\partial p^{(0)}}{\partial x} + \mu\nabla u^{(0)} - \rho\frac{\partial^2 u^{(0)}}{\partial t^2} = 0 \tag{5.19}$$

$$-\frac{\partial p^{(0)}}{\partial z} + \mu\nabla w^{(0)} - \rho\frac{\partial^2 w^{(0)}}{\partial t^2} = 0, \tag{5.20}$$

and the zero-order boundary condition as:

$$z = 0: \quad \tau_{zz} = -p^{(0)} + 2\mu\frac{\partial w^{(0)}}{\partial z} = 0 \tag{5.21}$$

$$\tau_{xz} = \mu\left(\frac{\partial w^{(0)}}{\partial x} + \frac{\partial u^{(0)}}{\partial z}\right) = 0 \tag{5.22}$$

The first-order governing equations are obtained as:

$$\frac{\partial u^{(1)}}{\partial x} + \frac{\partial w^{(1)}}{\partial z} = 0 \tag{5.23}$$

$$-\frac{\partial p^{(1)}}{\partial x} + \mu\nabla u^{(1)} - \rho\frac{\partial^2 u^{(1)}}{\partial t^2} = F_u^{(1)} \tag{5.24}$$

$$-\frac{\partial p^{(1)}}{\partial z} + \mu\nabla w^{(1)} - \rho\frac{\partial^2 w^{(1)}}{\partial t^2} = F_w^{(1)} \tag{5.25}$$

where $F_u^{(1)} = F_u(u^{(0)}, w^{(0)})$ and $F_w^{(1)} = F_u(u^{(0)}, w^{(0)})$. The first-order boundary conditions are

$$z = 0: \quad \tau_{zz}^{(1)} = -p^{(1)} + 2\mu\frac{\partial w^{(1)}}{\partial z} - 8G\frac{\partial u^{(0)}}{\partial x}\left(\frac{\partial w^{(0)}}{\partial z}\right)^2 = 0 \tag{5.26}$$

$$\tau_{xz}^{(1)} = \mu\left(\frac{\partial u^{(1)}}{\partial z} + \frac{\partial w^{(1)}}{\partial x}\right) = 0 \tag{5.27}$$

It should be noted that Eqs. (5.26) and (5.27) have been simplified by the use of Eq. (5.22).

We first solve the zero-order equations which govern linear surface wave propagation. Taking the derivative with respect to x of Eq. (5.19) and the derivative with respect to z of Eq. (5.20), and summing the resulting two equations yields the following uncoupled equation for $p^{(0)}$.

$$\frac{\partial^2 p^{(0)}}{\partial x^2} + \frac{\partial^2 p^{(0)}}{\partial z^2} = 0, \tag{5.28}$$

where the incompressibility condition, Eq. (5.18), has been used.

The displacement and pressure variables for the linear surface wave propagation are taken as

$$p^{(0)} = \mu P^{(0)}(z)\cos(kx - \omega t); \quad u^{(0)} = U^{(0)}(z)\sin(kx - \omega t);$$
$$w^{(0)} = W^{(0)}(z)\cos(kx - \omega t) \tag{5.29}$$

Substituting Eq. (5.29$_1$) into Eq. (5.28) yields

$$\frac{d^2 P^{(0)}}{dz^2} - k^2 P^{(0)} = 0 \tag{5.30}$$

The solution to Eq. (5.30) is

$$P^{(0)} = \overline{A} e^{-kz} \tag{5.31}$$

where $\overline{A}$ is a constant. Substituting Eqs. (5.29) and (5.31) into Eqs. (5.19) and (5.20), we obtain

$$U^{(0)}(z) = \overline{B} e^{-bz} - \frac{1}{k\zeta} \overline{A} e^{-kz} \tag{5.32}$$

and

$$W^{(0)}(z) = \overline{C} e^{-bz} - \frac{1}{k\zeta} \overline{A} e^{-kz}, \tag{5.33}$$

where $\overline{B}$ and $\overline{C}$ are unknown constants, and

$$b = k\left(1 - \zeta\right)^{1/2}, \quad c = \frac{\omega}{k}, \quad c_T^2 = \frac{\mu}{\rho}, \quad \zeta = c^2 / c_T^2 \tag{5.34}$$

Substituting Eqs. (5.29$_2$) and (5.29$_3$) together with Eqs. (5.32) and (5.33) into the incompressibility condition, Eq. (5.18), yields

$$\overline{B} = \frac{b}{k} \overline{C} \tag{5.35}$$

By virtue of Eqs. (5.29), (5.31)-(5.33) and (5.35), the boundary conditions, given by Eqs. (5.21) and (5.22), can be written as

$$\left(1 - \frac{2}{\zeta}\right)\overline{A} + 2k\left(1 - \zeta\right)^{1/2} \overline{C} = 0 \tag{5.36}$$

$$\frac{2}{\zeta}\overline{A} - k(2-\zeta)\overline{C} = 0 \tag{5.37}$$

The secular equation is obtained by setting the determinant of the coefficient matrix of Eqs. (5.36) and (5.37) equal to zero, which yields

$$(2-\zeta)^2 - 4(1-\zeta)^{1/2} = 0 \tag{5.38}$$

Equation (5.38) was obtained by Rayleigh by considering the limit of incompressibility ($\lambda \to \infty$) of the classic equation for the velocity of surface waves for an isotropic linear elastic material. Using Eqs. (5.35)-(5.37), the zero-order pressure and displacement solutions (the primary wave) can be represented by

$$p^{(0)} = \mu \overline{A} e^{-kz} \cos(kx - \omega t) \tag{5.39}$$

$$u^{(0)} = \frac{1}{k}\left(\eta_1 e^{-bz} - \frac{1}{\zeta}e^{-kz}\right)\overline{A}\sin(kx - \omega t) \tag{5.40}$$

$$w^{(0)} = \frac{1}{k}\left(\frac{k}{b}\eta_1 e^{-bz} - \frac{1}{\zeta}e^{-kz}\right)\overline{A}\cos(kx - \omega t) \tag{5.41}$$

where

$$\eta_1 = \frac{2-\zeta}{2\zeta} = \frac{b}{k}\frac{2}{\zeta(2-\zeta)} \tag{5.42}$$

By virtue of Eqs. (5.12), (5.15), (5.40) and (5.41), the nonlinear terms in Eqs. (5.24) and (5.25) can be represented by

$$
\begin{aligned}
F_u^{(1)} &= \left[6k\eta_2 e^{-3bz} + 4k\left(\eta_4 e^{-(2b+k)z} + \eta_5 e^{-(b+2k)z}\right)\right]G\overline{A}^3 \sin 3(kx - \omega t) \\
&\quad + 2k\left[\eta_7 e^{-3bz} - \eta_8 e^{-(2b+k)z} + \eta_9 e^{-(b+2k)z} - \frac{16}{\zeta^3}e^{-3kz}\right]G\overline{A}^3 \sin(kx - \omega t)
\end{aligned}
\tag{5.43}
$$

$$
\begin{aligned}
F_w^{(1)} &= \left[-6k\eta_3 e^{-3bz} + 4k\left(\eta_6 e^{-(2b+k)z} - \eta_5 e^{-(2k+b)z}\right)\right]G\overline{A}^3 \cos 3(kx - \omega t) \\
&\quad + 2k\left\{\eta_{10} e^{-3bz} + \eta_{11} e^{-(2b+k)z} + \eta_{12} e^{-(2k+b)z} + \frac{16}{\zeta^3}e^{-3kz}\right\}G\overline{A}^3 \cos(kx - \omega t)
\end{aligned}
\tag{5.44}
$$

where

$$\eta_2 = \left(\eta_1 - \frac{1}{\zeta}\frac{b}{k}\right)\left(\eta_1^2 - \frac{1}{\zeta^2}\right), \quad \eta_3 = \left(\frac{b}{k}\eta_1 - \frac{1}{\zeta}\right)\left(\eta_1^2 - \frac{1}{\zeta^2}\right) \qquad (5.45)$$

Since the dimensionless coefficients $\eta_4 - \eta_{12}$ will not be used in the sequel, their expressions are omitted here. Only the terms containing e^{-3bz}, which in combination with the trigonometric functions generate the resonant harmonic wave with frequency 3ω, are retained in Eqs. (5.43) and (5.44). Resonant waves increase in amplitude when they propagate and they become dominant at a sufficiently long distance. Since they have a different frequency from the primary wave, the resonant waves can be effectively isolated. It should be pointed out that the term containing e^{-3kz}, can be left out because it does not generate of a resonant wave in combination with a trigonometric function of frequency ω.

Thus, the following nonlinear terms are taken into account

$$F_u^{(1)}(u^{(0)}, w^{(0)}) = 6k\eta_2 G\bar{A}^3 e^{-3bz} \sin 3(kx - \omega t) \qquad (5.46)$$

$$F_w^{(1)}(u^{(0)}, w^{(0)}) = -6k\eta_3 G\bar{A}^3 e^{-3bz} \cos 3(kx - \omega t) \qquad (5.47)$$

By differentiating Eqs. (5.24) and (5.25) with respect to x and z, respectively, we obtain

$$\begin{aligned} -\frac{\partial^2 p^{(1)}}{\partial x^2} + \mu\nabla\frac{\partial}{\partial x}u^{(1)} - \rho\frac{\partial}{\partial x}\frac{\partial^2 u^{(1)}}{\partial t^2} &= \frac{\partial}{\partial x}F_u^{(1)}, \\ -\frac{\partial^2 p^{(1)}}{\partial z^2} + \mu\nabla\frac{\partial}{\partial z}w^{(1)} - \rho\frac{\partial}{\partial z}\frac{\partial^2 w^{(1)}}{\partial t^2} &= \frac{\partial}{\partial z}F_w^{(1)} \end{aligned} \qquad (5.48)$$

In view of Eqs. (5.23), (5.46) and (5.47), the summation of the above two equations yields

$$\frac{\partial^2 p^{(1)}}{\partial x^2} + \frac{\partial^2 p^{(1)}}{\partial z^2} = -18k^2\left(\eta_2 + \frac{b}{k}\eta_3\right)G\bar{A}^3 e^{-3bz}\cos 3(kx - \omega t) \qquad (5.49)$$

The full solution to the inhomogeneous differential equation Eq. (5.49) is in the form of

$$p^{(1)} = p_g^{(1)} + p_s^{(1)} \tag{5.50}$$

where $p_g^{(1)}$ represents a solution of the homogenous equation and $p_s^{(1)}$ represents the solution of the inhomogeneous equation. The special solution $p_s^{(1)}$ of Eq. (5.49) is obtained as

$$p_s^{(1)} = \frac{2}{\zeta}\left(\eta_2 + \frac{b}{k}\eta_3\right)G\bar{A}^3 e^{-3bz}\cos 3\left(kx - \omega t\right) \tag{5.51}$$

For the homogenous version of Eq. (5.49), we consider a solution of the following form

$$p_g^{(1)} = \mu P_g^{(1)}(x)e^{-3kz}\sin 3\left(kx - \omega t\right) \tag{5.52}$$

where $P_g^{(1)}(x)$ is a function of x. Inserting Eq. (5.52) into the homogenous form of Eq. (5.49), it follows that the expression given by Eq. (5.52) can be considered as an approximate solution, provided

$$\mu k^2 e^{-3kz}\left[\frac{1}{k^2}\frac{d^2 P_g^{(1)}}{dx^2}\sin 3(kx - \omega t) + \frac{6}{k}\frac{dP_g^{(1)}}{dx}\cos 3(kx - \omega t)\right] \approx 0 \tag{5.53}$$

Hence $P_g^{(1)}(x)$ must be assumed to be a function which varies slowly with x, which means that

$$1 \gg \frac{1}{k^2}\frac{d^2 P_g^{(1)}}{dx^2} \approx 0, \quad 1 \gg \frac{6}{k}\frac{dP_g^{(1)}}{dx} \approx 0 \tag{5.54}$$

The physical meaning of Eq. (5.54) is that the variation of the amplitude is very small within a wavelength. Using Eqs. (5.51) and (5.52), Eq. (5.50) can be written as

$$p^{(1)} = \mu P_g^{(1)}e^{-3kz}\sin 3\left(kx - \omega t\right) + \frac{2}{\zeta}\left(\eta_2 + \frac{b}{k}\eta_3\right)G\bar{A}^3 e^{-3bz}\cos 3\left(kx - \omega t\right) \tag{5.55}$$

In view of Eqs. (5.46), (5.47) and (5.55), Eqs. (5.24) and (5.25) can now be rewritten as

$$\nabla u^{(1)} - \frac{\rho}{\mu} \frac{\partial^2 u^{(1)}}{\partial t^2}$$
$$= 3k P_g^{(1)} e^{-3kz} \cos 3(kx - \omega t) - 6b \frac{1}{\zeta} \left(\frac{b}{k} \eta_2 + \eta_3 \right) \frac{G}{\mu} \bar{A}^3 e^{-3bz} \sin 3(kx - \omega t) \quad (5.56)$$

$$\nabla w^{(1)} - \frac{\rho}{\mu} \frac{\partial^2 w^{(1)}}{\partial t^2}$$
$$= -3k P_g^{(1)} e^{-3kz} \sin 3(kx - \omega t) - 6k \frac{1}{\zeta} \left(\frac{b}{k} \eta_2 + \eta_3 \right) \frac{G}{\mu} \bar{A}^3 e^{-3bz} \cos 3(kx - \omega t) \quad (5.57)$$

The right-hand sides of Eqs. (5.56) and (5.57) give rise to a resonant surface harmonic wave due to the combination of the decay term e^{-3bz} and the harmonic terms $\sin 3(kx - \omega t)$ and $\cos 3(kx - \omega t)$. The amplitudes of the resonant surface harmonics increase with the propagation distance x. So the solutions to Eqs. (5.56) and (5.57) are considered to be in the form

$$u^{(1)} = \left(\bar{U}^{(1)}(x) e^{-3kz} + U^{(1)} x e^{-3bz} \right) \cos 3(kx - \omega t) \quad (5.58)$$

$$w^{(1)} = \left(\bar{W}^{(1)}(x) e^{-3kz} + W^{(1)} x e^{-3bz} \right) \sin 3(kx - \omega t) \quad (5.59)$$

where $\bar{U}^{(1)}(x)$ and $\bar{W}^{(1)}(x)$ are functions of x, and $U^{(1)}$ and $W^{(1)}$ are constants. Inserting Eq. (5.58) and (5.59) into Eqs. (5.56) and (5.57) and equating the terms on both sides results in

$$\bar{U}^{(1)} = \frac{1}{3k\zeta} P_g^{(1)}(x), \qquad U^{(1)} = \frac{b}{k} \frac{1}{\zeta} \left(\frac{b}{k} \eta_2 + \eta_3 \right) \frac{G}{\mu} \bar{A}^3,$$
$$\bar{W}^{(1)} = -\frac{1}{3k\zeta} P_g^{(1)}(x), \qquad W^{(1)} = -\frac{1}{\zeta} \left(\frac{b}{k} \eta_2 + \eta_3 \right) \frac{G}{\mu} \bar{A}^3 \quad (5.60)$$

Here the assumption defined by Eq. (5.54) has been used. In terms of Eq. (5.60), Eqs. (5.58) and (5.59) can be rewritten as

$$u^{(1)} = \frac{b}{k} \frac{1}{\zeta} \left(\frac{b}{k} \eta_2 + \eta_3 \right) \frac{G}{\mu} \bar{A}^3 x e^{-3bz} \cos 3(kx - \omega t)$$
$$+ \frac{1}{3k\zeta} P_g^{(1)}(x) e^{-3kz} \cos 3(kx - \omega t) \quad (5.61)$$

$$w^{(1)} = -\frac{1}{\zeta}\left(\frac{b}{k}\eta_2 + \eta_3\right)\frac{G}{\mu}\bar{A}^3 x e^{-3bz}\sin 3(kx - \omega t)$$
$$-\frac{1}{3k\zeta}P_g^{(1)}(x)e^{-3kz}\sin 3(kx - \omega t)$$

(5.62)

The unknown quantity $P_g^{(1)}$ can be determined from the first-order boundary conditions, Eqs. (5.26) and (5.27).

Substitution of the pressure, Eq. (5.55), and the displacement expressions, Eqs. (5.61) and (5.62), into the expressions for the stresses defined by Eqs. (5.26) and (5.27), and leaving out the terms whose amplitudes are independent of x, yields

$$\tau_{zz}^{(1)} = \left[\mu\left(\frac{2}{\zeta} - 1\right)P_g^{(1)}e^{-3kz} + 6b\frac{1}{\zeta}\left(\frac{b}{k}\eta_2 + \eta_3\right)G\bar{A}^3 x e^{-3bz}\right]\sin 3(kx - \omega t) \quad (5.63)$$

$$\tau_{xz}^{(1)} = \left[-\mu\frac{2}{\zeta}P_g^{(1)}e^{-3kz} - 3\frac{1}{\zeta}(2 - \zeta)(b\eta_2 + k\eta_3)G\bar{A}^3 x e^{-3bz}\right]\cos 3(kx - \omega t) \quad (5.64)$$

Equations (5.63) and (5.64) are valid approximately when the surface waves have propagated a sufficiently large distance. The stress free conditions on the surface $z = 0$ imply that

$$\left(\frac{2}{\zeta} - 1\right)P_g^{(1)} = -6b\frac{1}{\zeta}\left(\frac{b}{k}\eta_2 + \eta_3\right)\frac{G}{\mu}\bar{A}^3 x \tag{5.65}$$

$$-\frac{2}{\zeta}P_g^{(1)} = 3k\frac{2 - \zeta}{\zeta}\left(\frac{b}{k}\eta_2 + \eta_3\right)\frac{G}{\mu}\bar{A}^3 x \tag{5.66}$$

Equations (5.65) and (5.66) both give solutions for the unknown quantity $P_g^{(1)}$. The solution to Eq. (5.65) is

$$P_g^{(1)} = -\frac{6b}{2 - \zeta}\left(\frac{b}{k}\eta_2 + \eta_3\right)\frac{G}{\mu}\bar{A}^3 x \tag{5.67}$$

while the solution to Eq. (5.66) is

$$P_g^{(1)} = -\frac{3}{2}k(2 - \zeta)\left(\frac{b}{k}\eta_2 + \eta_3\right)\frac{G}{\mu}\bar{A}^3 x \tag{5.68}$$

Since these two solutions should be the same, we have

$$-\frac{6b}{2-\zeta}\left(\frac{b}{k}\eta_2+\eta_3\right)\frac{G}{\mu}\overline{A}^3 x = -\frac{3}{2}k\left(2-\zeta\right)\left(\frac{b}{k}\eta_2+\eta_3\right)\frac{G}{\mu}\overline{A}^3 x \qquad (5.69)$$

After some simple manipulation, Eq. (5.69) can be rewritten as

$$\left(2-\zeta\right)^2 - 4\sqrt{1-\zeta} = 0 \qquad (5.70)$$

Equation (5.70) is the same as the secular equation (5.38), which implies that the resonant third harmonic propagates with the classic Rayleigh wave velocity, which can be obtained from Eq. (5.38) or (5.70) as

$$\zeta = 0.9126 \qquad (5.71)$$

Based on Eqs. (5.67) and (5.71), we check that the assumption defined by Eq. (5.54) is reasonable for the far-field solution. The first equation is obviously satisfied in that

$$\frac{\partial^2 P_g^{(1)}}{\partial x^2} = 0 \qquad (5.72)$$

The second equation can be rewritten as

$$0 \approx \frac{6}{k}\frac{dP_g^{(1)}}{dx} = 12.7794\frac{G}{\mu}\overline{A}^3 << 1 \qquad (5.73)$$

It may be assumed that the amplitude of the primary surface wave $\overline{A}$ is a small quantity. Thus, $\overline{A}^3$ is expected to be very small. It is known that the ratio of the nonlinear material constant to the linear material constant (i.e. G/μ) will not be too large. So the assumption given by Eq. (5.54) is reasonable.

Since we only consider terms that increase with x, the second term in Eq. (5.55) can be omitted, and using Eq. (5.67) in the first term, Eq. (5.55) can be rewritten as

$$p^{(1)} = \mu A_N(x)e^{-3kz}\sin[3\omega(t-\frac{x}{c})] \qquad (5.74)$$

where

$$A_N(x) = 3b \frac{1}{\eta_1} \frac{1}{\varsigma} \left(\frac{b}{k} \eta_2 + \eta_3 \right) \frac{G}{\mu} \bar{A}^3 x \tag{5.75}$$

By combining the two terms in Eqs. (5.61) and (5.62) where $P_g^{(1)}$ is given by Eq. (5.67) or (5.68), we obtain

$$u^{(1)} = \frac{1}{3k} \left(\eta_1 e^{-3bz} - \frac{1}{\varsigma} e^{-3kz} \right) A_N(x) \cos[3\omega(t - \frac{x}{c})] \tag{5.76}$$

$$w^{(1)} = \frac{1}{3k} \left(\frac{k}{b} \eta_1 e^{-3bz} - \frac{1}{\varsigma} e^{-3kz} \right) A_N(x) \sin[3\omega(t - \frac{x}{c})] \tag{5.77}$$

Equation (5.75) is the important term in the amplitude of the resonant third surface harmonic, since it increases with the propagation distance x, due to the effect of material nonlinearity. Such a harmonic surface wave may become measurable when the propagation distance is sufficiently large.

5.5 Transmission through an interface with linear material
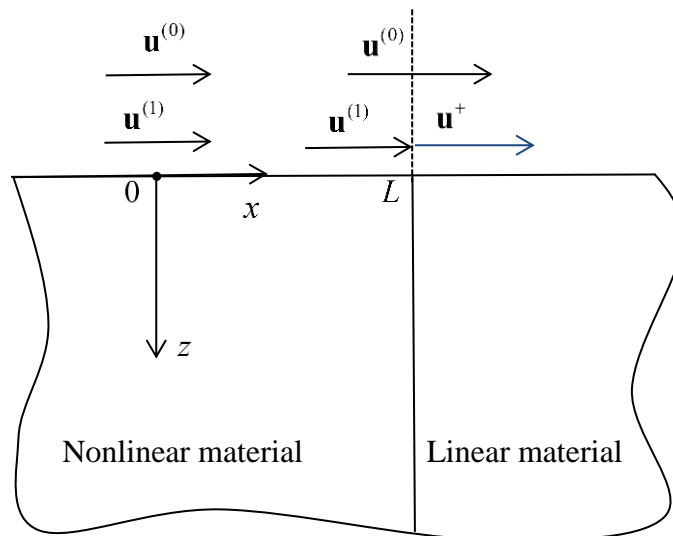
Fig. 5.2 Half-space with interface at $x = L$

As an application, we investigate the transmission of the harmonic, which is

defined by Eqs. (5.74), (5.76) and (5.77), through an interface with linear material, where the interface is located in the far-field at $x = L$. Because of its location in the far-field the quantities which do not contain a multiplicative L are neglected at the interface. The geometry is shown in Fig. 5.2. The incident wave, $\mathbf{u}^{(0)}$, is not affected by the interface, since it propagates in both the linear and the nonlinear material.

In general, the incidence of a wave on an interface will generate both a reflected and a transmitted wave. For the present case, however, only a transmitted wave is generated. The transmitted wave is a linear wave of the form

$$p^+ = \mu H^+ e^{-3kz} \sin[3\omega(t - \frac{L}{c} - \frac{x-L}{c})] \tag{5.78}$$

$$u^+ = \frac{1}{3k}\left(\eta_1 e^{-3bz} - \frac{1}{\zeta} e^{-3kz}\right) H^+ \cos[3\omega(t - \frac{L}{c} - \frac{x-L}{c})] \tag{5.79}$$

$$w^+ = \frac{1}{3k}\left(\frac{k}{b}\eta_1 e^{-3bz} - \frac{1}{\zeta} e^{-3kz}\right) H^+ \sin[3\omega(t - \frac{L}{c} - \frac{x-L}{c})] \tag{5.80}$$

The above expressions for the transmitted wave should satisfy the linear equations of motion and the boundary conditions at the free surface. By comparing Eqs. (5.78)-(5.80) with Eqs. (5.74), (5.76) and (5.77), it is evident that continuity of pressure and displacements at $x = L$ is satisfied by

$$H^+ = A_N(L) = 3b\frac{1}{\eta_1}\frac{1}{\zeta}\left(\frac{b}{k}\eta_2 + \eta_3\right)\frac{G}{\mu}\bar{A}^3 L \tag{5.81}$$

The stresses τ_{xx} and τ_{xz} corresponding to Eqs. (5.74), (5.76) and (5.77) at $x = L^-$ are represented by

$$\tau_{xx} = \mu\left[-e^{-3kz} + 2\left(\eta_1 e^{-3bz} - \frac{1}{\zeta} e^{-3kz}\right)\right] A_N(L)\sin[3\omega(t - \frac{L}{c})] \tag{5.82}$$

$$\tau_{xz} = \mu\left[\frac{1}{3k}\left(-3b\eta_1 e^{-3bz} + 3k\frac{1}{\zeta} e^{-3kz}\right) - \left(\frac{k}{b}\eta_1 e^{-3bz} - \frac{1}{\zeta} e^{-3kz}\right)\right] A_N(L)\cos[3\omega(t - \frac{L}{c})] \tag{5.83}$$

It should be noted that the terms that are independent of L and have much smaller

values, have been ignored in Eqs. (5.82) and (5.83). The stresses τ_{xx} and τ_{xz} corresponding to Eqs. (5.78)-(5.80) at $x > L$ are

$$\tau_{xx} = \mu\left[-e^{-3kz} + 2\left(\eta_1 e^{-3bz} - \frac{1}{\zeta}e^{-3kz}\right)\right]A_N(L)\sin[3\omega(t - \frac{L}{c} - \frac{x-L}{c})] \quad (5.84)$$

$$\tau_{xz} = \mu\left[\begin{array}{c} \frac{1}{3k}\left(-3b\eta_1 e^{-3bz} + 3k\frac{1}{\zeta}e^{-3kz}\right) \\[2mm] -\left(\frac{k}{b}\eta_1 e^{-3bz} - \frac{1}{\zeta}e^{-3kz}\right) \end{array}\right]A_N(L)\cos[3\omega(t - \frac{L}{c} - \frac{x-L}{c})] \quad (5.85)$$

Clearly, at $x = L^+$, Eqs. (5.84) and (5.85) are the same as Eqs. (5.82) and (5.83), respectively. So the continuity of stresses is also satisfied.

The system of the transmitted waves can then be written as

$$p^+ = \mu A_N(L)e^{-3kz}\sin[3\omega(t - \frac{L}{c} - \frac{x-L}{c})] \quad (5.86)$$

$$u^+ = \frac{1}{3k}\left(\eta_1 e^{-3bz} - \frac{1}{\zeta}e^{-3kz}\right)A_N(L)\cos[3\omega(t - \frac{L}{c} - \frac{x-L}{c})] \quad (5.87)$$

$$w^+ = \frac{1}{3k}\left(\frac{k}{b}\eta_1 e^{-3bz} - \frac{1}{\zeta}e^{-3kz}\right)A_N(L)\sin[3\omega(t - \frac{L}{c} - \frac{x-L}{c})] \quad (5.88)$$

The exact analysis of the continuity of pressure, stresses and displacements located at an interface at arbitrary value of x is quite complicated. However, for large x, the incident harmonic near the interface in the far field is simple, which simplifies the transmission problem significantly. The transmitted wave has the same form as the incident harmonic for $t \geq L/c$, $x \geq L$ and the constant $A_N(L)$ is defined by Eq. (5.81).

5.6 Concluding comments

For a half-space of isotropic incompressible material of cubic material nonlinearity, a perturbation method has been used to determine the resonant third harmonic surface wave, which is generated by the propagation of a linear surface

wave. For a trigonometric primary surface wave of amplitude $\overline{A}$ and frequency ω, the frequency of the resonant third harmonic shows a frequency 3ω, and an amplitude A_N which depends on $\overline{A}^3$ and the nonlinear material constant G, and which increases linearly with the distance of propagation, x. It has been shown that the resonant surface wave harmonic propagates with the velocity of classic Rayleigh waves of the corresponding linear material. Measurement of the third harmonic can provide information on G.

As an application, we have investigated the transmission of an incident resonant third harmonic surface wave by an interface located at $x = L$ between regions of nonlinear and linear behavior. The required continuity of pressure, stresses and displacements shows that no reflected surface wave is generated, only a transmitted surface wave. The transmitted surface wave, which is of the same general form as the incident harmonic surface wave propagates with a constant amplitude defined by $A_N(x)$ at $x = L$, and a phase which for $t > L/c$ is centered at $x = L$. The linear dependence of the amplitude on both L and G suggest that measurement of the transmitted surface wave can be used to determine these quantities.

Chapter 6 Analysis of Harmonics Propagating in Pipes of Quadratic Material Nonlinearity using Shell Theory

6.1 Introduction

Higher harmonics in non-dispersive media have attracted wide attention, including experimental, numerical and analytical investigations (Gol'dberg, 1961; Bender et al., 2013; Matlack et al. 2015; Chen et al.; 2014), which have also been investigated in Chapters 4 and 5. However, there are few investigations of higher guided harmonics in dispersive structures like pipes and rods. Due to the dispersion of guided waves, which will lead to frequency dependent phase velocities and multi-modes, the analysis of harmonics in wave guides becomes quite complex. Recent investigations about the generation of higher guided harmonics have been made by Deng (1998, 1999), Pau and Scalea (2015) and de Lima and Hamilton (2003) by using the method of normal mode expansion. De Lima and Hamilton (2005) adopted perturbation and modal analysis together with numerical simulation to calculate the second harmonics propagating in cylindrical rods and shells. Liu et al. (2014a, 2014b) proposed a generalized method and used a numerical approach to analyze the cumulative nature and the physical interpretation of the generation of higher harmonics in hollow circular cylinders.

Since rods and pipes are widely used in structures such as pipelines, it is highly desirable to increase our understanding of nonlinear waves propagating in cylindrical wave guides on the basis of a theory that allows relevant analytical solutions (Morsbøl and Sorokin, 2015). In this chapter, we present an analytical investigation of higher harmonics in pipes based on shell theory with quadratic nonlinear material behavior. An analytical approach based on shell theory provides physical insight in the deformation modes. Whereas exact three dimensional theory has to be dealt with numerically, shell theory yields analytical solutions.

The work presented in this chapter consists of three parts: the derivation of nonlinear equations of axisymmetric material behavior of a shell, the mixing of axisymmetric longitudinal and torsional waves, and the self-interaction of axisymmetric longitudinal waves. To verify the accuracy of the present linear version of the shell theory, the dispersion curves of longitudinal waves have been compared with the corresponding curves obtained from thick shell theory and three dimensional theory. For axisymmetric longitudinal wave propagation in pipes, the dispersion curves agree very well with the curves for the exact theory. For axisymmetric torsional waves, we only take the lowest torsional wave mode, derived directly from the three dimensional theory, into consideration. It is shown that for mixing of longitudinal and torsional waves, no resonant longitudinal waves with sum or difference frequency exist. Using the perturbation method, analytical expressions for the resonant torsional waves have next been obtained. The resonant torsional waves with difference frequencies propagate in the opposite direction of the primary waves, which may have potential application to the inspection of pipes.

For the self-interaction of longitudinal waves in pipes, we have employed a more simplified shell theory for thin-walled pipes. A nonlinear displacement equation of motion with uncoupled linear part was obtained, which is used to obtain analytical expressions of cumulative second longitudinal harmonics. Since longitudinal waves according to this theory are dispersive, the phase velocities are frequency dependent. The phase-match conditions have been obtained, which, together with the dispersion relations, have been used to determine the phase-match points. At the phase-match points, the phase velocity of the second harmonic is the same as the corresponding phase velocity of the primary wave.

6.2 Basic equations of axisymmetric motion in a pipe derived from nonlinear shell theory

Consider a pipe of thickness h and radius of the middle surface R, see Fig. 6.1, where r is the distance from the middle surface, thus $\bar{r} = R + r$ is the radial position of any particle in the pipe. In this paper, axisymmetric wave propagation in the pipe will be investigated. The displacements for the shell theory are taken in the form:

$$\overline{u} = u(x,t), \quad \overline{v} = \frac{1}{2}v(x,t)\overline{r}, \quad \overline{w} = w(x,t) + r\phi(x,t), \tag{6.1}$$

where u and w are the displacement components in the middle surface, in the radial and axial direction, respectively, and ϕ is the slope of the axial displacement in the $x-r$ plane. The forms of $\overline{u}$ and $\overline{w}$ in Eq. (6.1) can also be found in Herrmann and Mirsky (1956). The expression of the circumferential displacement $\overline{v}$ in Eq. (6.1) is chosen to represent the lowest torsional mode, see Wang and Achenbach (2016).
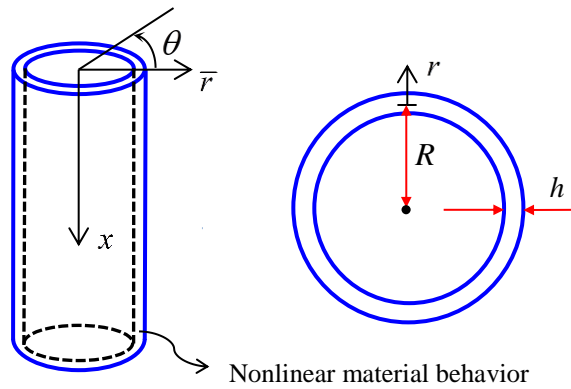
Fig. 6.1 An elastic pipe

The simple form of the radial displacement given by Eq. (6.1₁) has advantages, but it also poses a problem in that it yields a zero radial strain, $\varepsilon_{rr} = \partial\overline{u}/\partial r = 0$. As proposed by Herrmann and Mirsky (1956), a much better assumption is that the linear radial stress is zero through the thickness of the shell, i.e.

$$\tau_{rr}^L = 0 \tag{6.2}$$

This equation yields

$$\frac{\partial\overline{u}}{\partial r} = -\frac{v}{1-v}\left(\frac{\overline{u}}{r} + \frac{\partial\overline{w}}{\partial x}\right) \tag{6.3}$$

where v is Poison's ratio. Here the linear stress-displacement relation (Achenbach, 1999, page 74) has been used. In this paper, we use Eq. (6.3), except when the thickness behavior of the shell is irrelevant, when we use Eq. (6.1₁). Substituting Eq. (6.3) into the general linear axisymmetric stress-displacement relations, the resulting linear parts of stresses are

$$\tau_{rx}^{L} = \mu\left(\frac{\partial \overline{u}}{\partial x} + \frac{\partial \overline{w}}{\partial r}\right), \quad \tau_{\theta\theta}^{L} = 2\mu\frac{\overline{u}}{r} + \overline{\lambda}\left(\frac{\overline{u}}{r} + \frac{\partial \overline{w}}{\partial x}\right),$$

$$\tau_{xx}^{L} = \overline{\lambda}\left(\frac{\overline{u}}{r} + \frac{\partial \overline{w}}{\partial x}\right) + 2\mu\frac{\partial \overline{w}}{\partial x}, \quad \tau_{r\theta}^{L} = 0, \quad \tau_{\theta x}^{L} = \mu\frac{\partial \overline{v}}{\partial x} \tag{6.4}$$

where $\overline{\lambda} = [(1-2\nu)/(1-\nu)]\lambda$, and λ and μ are Lamé's elastic constants. The superscripts "L" and "NL" denote the linear and nonlinear parts of the stresses, respectively. The nonlinear parts of stresses are caused by the nonlinear material behavior, which is given by Eqs. (A1)-(A6) in Appendix 6A. Employing Eq. (6.3) into the nonlinear stress-displacement relations, the nonlinear parts of the stresses can be written as

$$\tau_{rx}^{NL} = \left[\left(B - \frac{2\nu}{1-\nu}\lambda_4\right)\frac{\overline{u}}{r} + 2\frac{1-2\nu}{1-\nu}\lambda_4\frac{\partial \overline{w}}{\partial x}\right]\left(\frac{\partial \overline{w}}{\partial r} + \frac{\partial \overline{u}}{\partial x}\right) \tag{6.5}$$

$$\tau_{\theta\theta}^{NL} = \lambda_1\frac{\overline{u}^2}{r^2} + 2\lambda_2\frac{\overline{u}}{r}\frac{\partial \overline{w}}{\partial x} + \lambda_3\left(\frac{\partial \overline{w}}{\partial x}\right)^2 + \frac{1}{2}B\left(\frac{\partial \overline{u}}{\partial x} + \frac{\partial \overline{w}}{\partial r}\right)^2 + \lambda_4\left(\frac{\partial \overline{v}}{\partial x}\right)^2 \tag{6.6}$$

$$\tau_{xx}^{NL} = \lambda_1\left(\frac{\partial \overline{w}}{\partial x}\right)^2 + 2\lambda_2\frac{\overline{u}}{r}\frac{\partial \overline{w}}{\partial x} + \lambda_3\frac{\overline{u}^2}{r^2} + \lambda_4\left[\left(\frac{\partial \overline{u}}{\partial x} + \frac{\partial \overline{w}}{\partial r}\right)^2 + \left(\frac{\partial \overline{v}}{\partial x}\right)^2\right] \tag{6.7}$$

$$\tau_{r\theta}^{NL} = \frac{1}{4}A\left(\frac{\partial \overline{u}}{\partial x} + \frac{\partial \overline{w}}{\partial r}\right)\frac{\partial \overline{v}}{\partial x} \tag{6.8}$$

$$\tau_{\theta x}^{NL} = \left(\frac{A}{2} + \frac{1-2\nu}{1-\nu}B\right)\left(\frac{\overline{u}}{r} + \frac{\partial \overline{w}}{\partial x}\right)\frac{\partial \overline{v}}{\partial x} \tag{6.9}$$

where

$$\lambda_1 = A + 3B + C + \frac{(3\nu-2)\nu}{(1-\nu)^2}(B+C), \quad \lambda_2 = \frac{1-3\nu+3\nu^2}{(1-\nu)^2}(B+C) - \frac{\nu}{1-\nu}C,$$

$$\lambda_3 = \frac{1-2\nu+2\nu^2}{(1-\nu)^2}(B+C) - \frac{2\nu}{1-\nu}C, \quad \lambda_4 = \frac{A}{4} + \frac{1}{2}B \tag{6.10}$$

Here, A, B and C are the third-order elastic coefficients, and the relation $\overline{v}/r - \overline{v}_{,r} = 0$, which follows from Eq. (6.1$_2$), has been used.

Since we only take axisymmetric motion into consideration, the differential equations of motion are given by

$$\frac{\partial \tau_{rr}}{\partial r} + \frac{\partial \tau_{rx}}{\partial x} + \frac{\tau_{rr} - \tau_{\theta\theta}}{\bar{r}} = \rho \frac{\partial^2 \bar{u}}{\partial t^2}$$

$$\frac{\partial \tau_{r\theta}}{\partial r} + \frac{\partial \tau_{\theta x}}{\partial x} + \frac{2\tau_{r\theta}}{\bar{r}} = \rho \frac{\partial^2 \bar{v}}{\partial t^2} \qquad (6.11)$$

$$\frac{\partial \tau_{rx}}{\partial r} + \frac{\partial \tau_{xx}}{\partial x} + \frac{\tau_{rx}}{\bar{r}} = \rho \frac{\partial^2 \bar{w}}{\partial t^2}$$

where ρ is the material density. To obtain the equations of motion for the shell, we multiply the three equations in Eq. (6.11) by $\bar{r}$ on each side, and then integrate the equations at both sides through the thickness of the shell. We obtain

$$\frac{\partial N_{rx}}{\partial x} - \frac{N_{\theta\theta}}{R} = \rho h \frac{\partial^2 u}{\partial t^2} \qquad (6.12)$$

$$\frac{\partial N_{xx}}{\partial x} = \rho h \frac{\partial^2 w}{\partial t^2} + \frac{\rho h^3}{12R} \frac{\partial^2 \phi}{\partial t^2} \qquad (6.13)$$

$$\frac{\partial N_{\theta x}}{\partial x} + \frac{N_{r\theta}}{R} = \frac{1}{2} \rho R h \left(1 + \frac{h^2}{12R^2}\right) \frac{\partial^2 v}{\partial t^2} \qquad (6.14)$$

We also multiply the third equation in Eq. (6.11) by $r\bar{r}$, and integrate over the thickness of the shell to obtain

$$\frac{\partial M_x}{\partial x} - N_{rx} = \frac{\rho h^3}{12} \frac{\partial^2 \phi}{\partial t^2} + \frac{\rho h^3}{12R} \frac{\partial^2 w}{\partial t^2} \qquad (6.15)$$

where

$$N_{\theta\theta} = \int_{-h/2}^{h/2} \left(\tau_{\theta\theta}^L + \tau_{\theta\theta}^{NL}\right) dr, \quad N_{xx} = \int_{-h/2}^{h/2} \left(\tau_{xx}^L + \tau_{xx}^{NL}\right)\left(1 + \frac{r}{R}\right) dr,$$

$$N_{rx} = \int_{-h/2}^{h/2} \left(\tau_{rx}^L + \tau_{rx}^{NL}\right)\left(1 + \frac{r}{R}\right) dr, \quad M_x = \int_{-h/2}^{h/2} \left(\tau_{xx}^L + \tau_{xx}^{NL}\right) r\left(1 + \frac{r}{R}\right) dr, \qquad (6.16)$$

$$N_{r\theta} = \int_{-h/2}^{h/2} \left(\tau_{r\theta}^L + \tau_{r\theta}^{NL}\right) dr, \quad N_{\theta x} = \int_{-h/2}^{h/2} \left(\tau_{\theta x}^L + \tau_{\theta x}^{NL}\right)\left(1 + \frac{r}{R}\right) dr$$

Equations (6.12)-(6.15) are the equations governing axisymmetric motion of the shell. The justification for these multiplications to obtain these equations stems from energy considerations (Herrmann and Mirsky, 1956). By the use of Eqs. (6.4)-(6.9), Eq. (6.16) can be written as

$$N_{\theta\theta} = \left(\bar{\lambda} + 2\mu\right)\beta u + \bar{\lambda} h \frac{\partial w}{\partial x} + N_{\theta\theta}^{NL} \qquad (6.17)$$

$$N_{xx} = (\bar{\lambda} + 2\mu)\left(h \frac{\partial w}{\partial x} + \frac{h^3}{12R} \frac{\partial \phi}{\partial x}\right) + \bar{\lambda} h \frac{u}{R} + N_{xx}^{NL} \qquad (6.18)$$

$$M_x = (\bar{\lambda} + 2\mu)\frac{h^3}{12R}\left(\frac{\partial w}{\partial x} + R\frac{\partial \phi}{\partial x}\right) + M_x^{NL} \tag{6.19}$$

$$N_{rx} = \kappa\mu h(\frac{\partial u}{\partial x} + \phi) + N_{rx}^{NL} \tag{6.20}$$

$$N_{\theta x} = \frac{1}{2}\mu\frac{\partial v}{\partial x}Rh\left(1 + \frac{h^2}{12R^2}\right) + N_{\theta x}^{NL} \tag{6.21}$$

$$N_{r\theta} = N_{r\theta}^{NL} \tag{6.22}$$

where

$$\beta = \ln\frac{1 + \bar{h}/2}{1 - \bar{h}/2}, \quad \bar{h} = \frac{h}{R} \tag{6.23}$$

Here κ is the shear coefficient, which is introduced to modify the shear stress of the shell or plate theory. The motivation is to make the velocity of very short waves in the lowest mode coincide with the corresponding velocity of the three dimensional theory. Here κ is taken as 0.86 when the Poisson's ratio v is 0.3 (Herrmann and Mirsky, 1956). The nonlinear parts of the resultant forces can be expressed as

$$N_{\theta\theta}^{NL} = \int_{-h/2}^{h/2}\tau_{\theta\theta}^{NL}dr, \quad N_{xx}^{NL} = \int_{-h/2}^{h/2}\tau_{xx}^{NL}\left(1 + \frac{r}{R}\right)dr, \quad N_{rx}^{NL} = \int_{-h/2}^{h/2}\tau_{rx}^{NL}\left(1 + \frac{r}{R}\right)dr,$$

$$M_x^{NL} = \int_{-h/2}^{h/2}\tau_{xx}^{NL}r\left(1 + \frac{r}{R}\right)dr, \quad N_{r\theta} = \int_{-h/2}^{h/2}\tau_{r\theta}^{NL}dr, \quad N_{\theta x} = \int_{-h/2}^{h/2}\tau_{\theta x}^{NL}\left(1 + \frac{r}{R}\right)dr \tag{6.24}$$

where the nonlinear stresses are given by Eqs. (6.5)-(6.9).

Substitution of Eqs. (6.17)-(6.22) into Eqs. (6.12)-(6.15) yields the following displacement equations of motion.

$$\kappa\mu h(\frac{\partial^2 u}{\partial x^2} + \frac{\partial \phi}{\partial x}) - (\bar{\lambda} + 2\mu)\beta\frac{u}{R} - \bar{\lambda}\bar{h}\frac{\partial w}{\partial x} - \rho h\frac{\partial^2 u}{\partial t^2} = F_1[u, \bar{v}, \bar{w}]$$

$$\bar{\lambda}\bar{h}\frac{\partial u}{\partial x} + (\bar{\lambda} + 2\mu)h\frac{\partial^2 w}{\partial x^2} - \rho h\frac{\partial^2 w}{\partial t^2} + (\bar{\lambda} + 2\mu)\frac{h^3}{12R}\frac{\partial^2 \phi}{\partial x^2} - \frac{\rho h^3}{12R}\frac{\partial^2 \phi}{\partial t^2} = F_2[u, \bar{v}, \bar{w}]$$

$$(\bar{\lambda} + 2\mu)\frac{h^3}{12R}\frac{\partial^2 w}{\partial x^2} - \kappa\mu h(\frac{\partial u}{\partial x} + \phi) - \frac{\rho h^3}{12R}\frac{\partial^2 w}{\partial t^2} + (\bar{\lambda} + 2\mu)\frac{h^3}{12}\frac{\partial^2 \phi}{\partial x^2} - \frac{\rho h^3}{12}\frac{\partial^2 \phi}{\partial t^2} = F_3[u, \bar{v}, \bar{w}]$$

$$\frac{1}{2}\mu Rh\left(1 + \frac{h^2}{12R^2}\right)\frac{\partial^2 v}{\partial x^2} - \frac{1}{2}\rho Rh\left(1 + \frac{h^2}{12R^2}\right)\frac{\partial^2 v}{\partial t^2} = F_4[u, \bar{v}, \bar{w}]$$

$$\tag{6.25}$$

where

$$F_1[u, \bar{v}, \bar{w}] = \int_{-h/2}^{h/2}\left[\frac{\tau_{\theta\theta}^{NL}}{R} - \frac{\partial \tau_{rx}^{NL}}{\partial x}\left(1 + \frac{r}{R}\right)\right]dr \tag{6.26}$$

$$F_2[u,\overline{v},\overline{w}] = -\int_{-h/2}^{h/2} \frac{\partial \tau_{xx}^{NL}}{\partial x}\left(1+\frac{r}{R}\right)dr \tag{6.27}$$

$$F_3[u,\overline{v},\overline{w}] = \int_{-h/2}^{h/2}\left(\tau_{rx}^{NL}-\frac{\partial \tau_{xx}^{NL}}{\partial x}r\right)\left(1+\frac{r}{R}\right)dr \tag{6.28}$$

$$F_4[u,\overline{v},\overline{w}] = -\int_{-h/2}^{h/2}\left[\frac{\partial \tau_{\theta x}^{NL}}{\partial x}\left(1+\frac{r}{R}\right)+\frac{\tau_{r\theta}^{NL}}{R}\right]dr \tag{6.29}$$

Equations (6.26)-(6.29) define the nonlinear parts of Eqs. (6.25). If they are omitted, Eqs. (6.25) reduce to the linear equations governing the propagation of axisymmetric waves in a pipe.

Since Eqs. (6.25) are a set of nonlinear equations, the perturbation method is used to determine the effects of nonlinearity. Thus, we consider

$$u = u^{(0)}+u^{(1)}, \ \overline{w}=\overline{w}^{(0)}+\overline{w}^{(1)}, \ \overline{v}=\overline{v}^{(0)}+\overline{v}^{(1)} \tag{6.30}$$

where it is assumed that $\left\|\bullet\right\|^{(0)} \gg \left\|\bullet\right\|^{(1)}$ and $\left\|\bullet\right\|^{(0)^2} \propto \left\|\bullet\right\|^{(1)}$ are satisfied, where "$\bullet$" denotes u, $\overline{v}$ and $\overline{w}$. Based on these order of magnitude considerations, we can obtain zero-order and first-order linear governing equations. The zero-order equations are the ones presented in Eqs. (6.25) if the right-side terms are omitted. The first-order equations are given by

$$\kappa\mu h(\frac{\partial^2 u^{(1)}}{\partial x^2}+\frac{\partial \phi^{(1)}}{\partial x})-\left(\overline{\lambda}+2\mu\right)\beta\frac{u^{(1)}}{R}-\overline{\lambda}\overline{h}\frac{\partial w^{(1)}}{\partial x}-\rho h\frac{\partial^2 u^{(1)}}{\partial t^2} = F_1[u^{(0)},\overline{v}^{(0)},\overline{w}^{(0)}]$$

$$\overline{\lambda}\overline{h}\frac{\partial u^{(1)}}{\partial x}+(\overline{\lambda}+2\mu)h\frac{\partial^2 w^{(1)}}{\partial x^2}-\rho h\frac{\partial^2 w^{(1)}}{\partial t^2}$$
$$+(\overline{\lambda}+2\mu)\frac{h^3}{12R}\frac{\partial^2 \phi^{(1)}}{\partial x^2}-\frac{\rho h^3}{12R}\frac{\partial^2 \phi^{(1)}}{\partial t^2} = F_2[u^{(0)},\overline{v}^{(0)},\overline{w}^{(0)}]$$

$$(\overline{\lambda}+2\mu)\frac{h^3}{12R}\frac{\partial^2 w^{(1)}}{\partial x^2}-\kappa\mu h(\frac{\partial u^{(1)}}{\partial x}+\phi^{(1)})-\frac{\rho h^3}{12R}\frac{\partial^2 w^{(1)}}{\partial t^2}$$
$$+(\overline{\lambda}+2\mu)\frac{h^3}{12}\frac{\partial^2 \phi^{(1)}}{\partial x^2}-\frac{\rho h^3}{12}\frac{\partial^2 \phi^{(1)}}{\partial t^2} = F_3[u^{(0)},\overline{v}^{(0)},\overline{w}^{(0)}]$$

$$\frac{1}{2}\mu R h\frac{\partial^2 v^{(1)}}{\partial x^2}-\frac{1}{2}\rho R h\frac{\partial^2 v^{(1)}}{\partial t^2} = F_4[u^{(0)},\overline{v}^{(0)},\overline{w}^{(0)}]$$

$$\tag{6.31}$$

Here, it has been assumed that terms of orders $h^2/R^2 \ll 1$ can be omitted.

The solutions to the zero-order equations are taken in the forms:

$$u^{(0)} = Ue^{i(\omega t - kx)}, \ w^{(0)} = We^{i(\omega t - kx)}, \phi^{(0)} = \frac{\Phi}{R}e^{i(\omega t - kx)}, v^{(0)} = De^{i\omega(t - \frac{x}{c_T})} \quad (6.32)$$

where $c_T = \sqrt{\mu/\rho}$ is the shear wave velocity, ω is the circular frequency and k is the wave number. Equations (6.25) show that, for the axisymmetric case, linear longitudinal waves are uncoupled from linear torsional waves, as is evident from the left-side of Eq. (6.25₄), which is uncoupled from the linear parts of the other three equations. Substituting Eq. (6.32₄) into Eq. (6.31₄) and omitting the right side-term, the resulting equation governing torsional wave motion is satisfied by

$$\overline{v}^{(0)} = \frac{1}{2}(R + r)D\cos\omega(t - \frac{x}{c_T}) \quad (6.33)$$

where D is a constant. Equation (6.33) is the well-known representation of the lowest torsional mode in a pipe.

The following relations are introduced.

$$\omega = \frac{2\pi c}{\lambda}, \ k = \frac{2\pi}{\lambda} \quad (6.34)$$

where $c = \omega/k$ is the phase velocity and λ is the wavelength. After substituting the first three expressions of Eq. (6.32) into the first three zero-order equations, the equations governing the relation between U, W and Φ become

$$\left(n^2\frac{1-\nu}{2} - \kappa\frac{1-\nu}{2} - \frac{1}{4\pi^2\delta^2}\beta\overline{h}\right)U + \nu\overline{h}i\frac{1}{2\pi\delta}W - i\kappa\frac{1-\nu}{2}\frac{1}{2\pi\delta}\overline{h}\Phi = 0$$

$$-\nu\overline{h}i\frac{1}{2\pi\delta}U + \left(\frac{1-\nu}{2}n^2 - 1\right)W = 0 \quad (6.35)$$

$$\frac{1-\nu}{2}i\frac{1}{2\pi\delta}\kappa U + \overline{h}\left(\frac{1-\nu}{2}\frac{n^2}{12} - \frac{1-\nu}{2}\kappa\frac{1}{4\pi^2\delta^2} - \frac{1}{12}\right)\Phi = 0$$

where $n = c/c_T$ and $\delta = h/\lambda$ are the dimensionless phase velocity and the reciprocal of dimensionless wavelength. For simplicity, the approximation has been made in the calculation that the terms containing h^3/R in the zero-order equations are negligible. The validation will be shown by comparison with the exact solution, see Fig. 6.2. As a consequence, part of the rotary inertia and flexural stiffness are neglected. For non-dispersive structures, the value of n equates to c_L/c_T, where $c_L = \sqrt{(\lambda + 2\mu)/\rho}$ is the longitudinal wave velocity.

The determinant of the coefficient matrix of Eq. (6.35) must vanish, which yields the dispersion relation (also called the characteristic equation), which relates the dimensionless phase velocity and the reciprocal of the dimensionless wavelength. The dispersion curves are shown in Figs. 6.2a and 6.2b for two values of h/R.
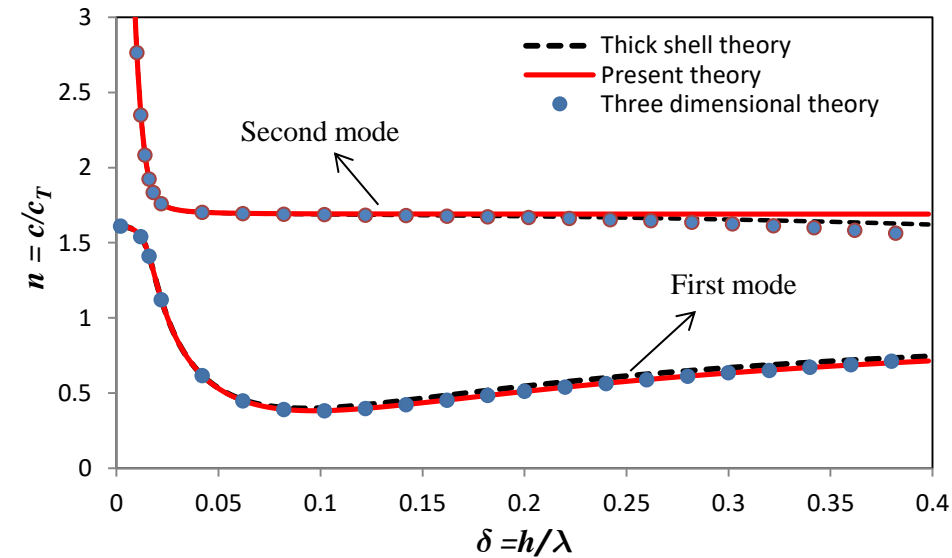
(a) $h/R = 1/10$
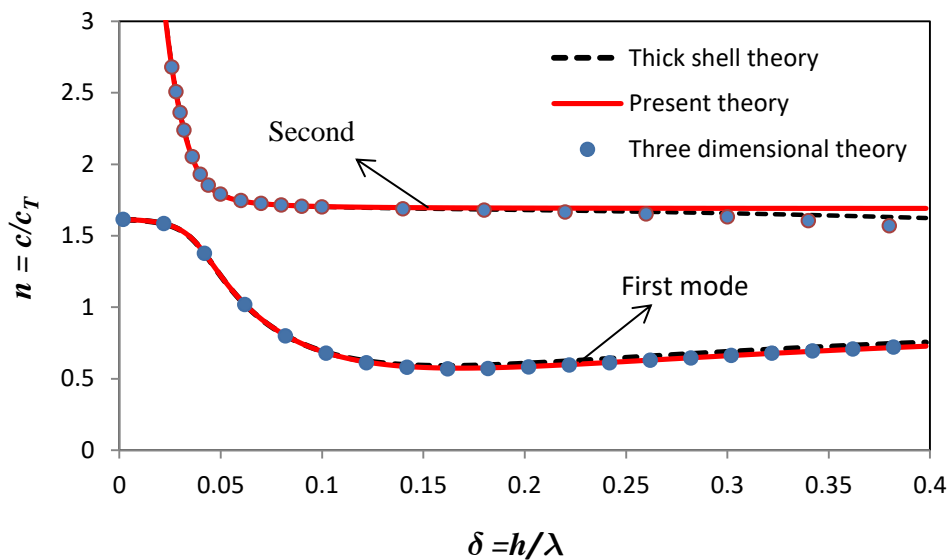
(b) $h/R = 1/4$

Fig. 6.2 Comparison of phase velocity versus the reciprocal of wavelength with the corresponding results obtained from thick shell theory (Mirsky and G. Herrmann, 1958) and three dimensional theory (Herrmann and Mirsky, 1956) for $\kappa = 0.86$ and $\nu = 0.3$

Figures 6.2a and 6.2b show the comparison of the dispersion curves obtained from Eq. (6.35) with the ones obtained from three dimensional theory (Herrmann and Mirsky, 1956) and thick shell theory (Mirsky and G. Herrmann, 1958). When the ratio of shell thickness to wavelength is small, $h/\lambda \le 0.4$ in this case, which can be called a lower frequency region, the dispersion curves for the first and second mode agree very well with the curves obtained from the other two theories. As the wavelength becomes smaller, the difference becomes larger for the second mode, while the first mode still remains sufficiently accurate. The results confirm that shell theory is more suitable in the lower frequency region, where the wall thickness of a pipe is sufficiently smaller than the wavelength. As shown in Li and Rose (2006), at higher frequencies (i.e. shorter wavelengths), guided waves in pipes can be treated as Lamb waves. The separation line between higher and lower frequencies depends on the ratio of the wall thickness to the diameter. Pipes of the same wall thickness with larger diameter will have a lower frequency value as the separation line. As shown in Fig. 6.2b, the present shell theory is still valid for fairly thick pipes. The dispersion curves show that the curve obtained from the present theory is more accurate for the first mode than the curve from the thick shell theory. One possible explanation is that the assumption used in Eq. (6.2) releases the restriction due to the assumed form of the displacement given by Eq. (6.1_1), which increases the stiffness. However, the discrepancy between three theories is very small for a small ratio of the thickness to wavelength.

We can express the radial displacement and the angle of rotation of the normal to the middle surface in terms of the axial displacement of the middle surface. The relations between the amplitudes can be obtained from Eqs. (6.35_2) and (6.35_3) as follows:

$$U = i\eta_1 W, \ \Phi = \eta_2 W \tag{6.36}$$

where

$$\eta_1 = -\frac{2\pi}{\nu \bar{h}} \delta \left(\frac{1-\nu}{2} n^2 - 1 \right)$$

$$\eta_2 = \frac{12\pi}{\bar{h}} \frac{(1-\nu)\kappa\delta}{2\pi^2\delta^2(1-\nu)n^2 - 6(1-\nu)\kappa - 4\pi^2\delta^2} \eta_1$$

It follows that the expressions of $u^{(0)}$ and $\phi^{(0)}$ can be written as

$$\bar{u}^{(0)} = u^{(0)} = i\eta_1 w^{(0)}, \ \phi^{(0)} = \frac{\eta_2}{R} w^{(0)} \tag{6.37}$$

We then obtain

$$\bar{w}^{(0)} = w^{(0)} + r\phi^{(0)} = (1 + \frac{r}{R}\eta_2)w^{(0)} \tag{6.38}$$

6.3 The mixing of longitudinal and torsional waves

Let us consider the case that a longitudinal wave and a torsional wave are excited at the same time. As mentioned in the previous section, these two waves will not interact with each other within the linear theory. However, when nonlinear material behavior is taken into consideration, resonant waves and higher harmonics will be generated. In this section, we are interested in investigating mixing primary longitudinal and torsional waves, to obtain a resonant wave with difference or sum frequency.

We consider the axial displacement in the middle surface in the form

$$w^{(0)} = W\cos(\omega_1 t - k_1 x) \tag{6.39}$$

The primary longitudinal wave with frequency ω_1 and wave number k_1 can then be determined through Eqs. (6.37$_1$) and (6.38) as

$$u^{(0)} = \mathrm{Re}\left[i\eta_1 We^{i(\omega_1 t - k_1 x)} \right] = -\eta_1 W \sin(\omega_1 t - k_1 x),$$
$$\bar{w}^{(0)} = \mathrm{Re}\left[(1 + \frac{r}{R}\eta_2)e^{i(\omega_1 t - k_1 x)} \right] = (1 + \frac{r}{R}\eta_2)W \cos(\omega_1 t - k_1 x) \tag{6.40}$$

where η_1 and η_2 are defined by:

$$\eta_1 = -\frac{2\pi}{v\bar{h}}\delta_1\left(\frac{1-v}{2}n_1^2 - 1 \right) \tag{6.41}$$

$$\eta_2 = \frac{12\pi}{\bar{h}}\frac{(1-v)\kappa\delta_1}{2\pi^2\delta_1^2(1-v)n_1^2 - 6(1-v)\kappa - 4\pi^2\delta_1^2}\eta_1 \tag{6.42}$$

Here $\delta_1 = h/\lambda_1$, with $\lambda_1 = 2\pi/k_1$ being the wavelength of the longitudinal wave, and $n_1 = \omega_1/(k_1 c_T)$. The primary torsional wave with frequency ω_2 and wave number k_2 is given by

$$\bar{v}^{(0)} = \frac{1}{2}D(R+r)\cos(\omega_2 t - k_2 x) \tag{6.43}$$

where $\omega_2/k_2 = c_T$ for the lowest torsional wave mode.

It is noted that there are no terms in the expressions (6.26)-(6.28) of F_1, F_2 and F_3 containing the coupling of $\bar{v}$ with u or $\bar{w}$, which is evident by the absence of products of $\bar{v}$ with u or $\bar{w}$ in the nonlinear stress-strain relation (6.5)-(6.7). Thus, we can conclude that the mixing of primary longitudinal waves and torsional waves will not give rise to nonlinear terms with sum or difference frequency for the first three equations in Eq. (6.31), which govern the generation of resonant longitudinal waves. Thus, resonant longitudinal waves with sum or difference frequencies cannot occur through the mixing of primary longitudinal waves and torsional waves in a pipe. A similar conclusion that the mixing of primary transverse waves and longitudinal waves in an unbounded nonlinear media cannot give rise to a resonant longitudinal wave with difference or sum frequency, was stated in Korneev and Demčenko (2014). However, a different condition exists for the expression of F_4. Substituting Eqs, (6.40) and (6.43) into Eqs. (6.8), (6.9) and (6.29), we have

$$F_4 = \frac{1}{2}\mu\Psi_1 WDk^+ \sin(\omega^+ t - k^+ x) - \frac{1}{2}\mu\Psi_2 WDk^- \sin(\omega^- t - k^- x) \qquad (6.44)$$

where $\omega^+ = \omega_1 + \omega_2$ and $\omega^- = \omega_1 - \omega_2$, also $k^+ = k_1 + k_2$ and $k^- = k_1 - k_2$, and

$$
\begin{aligned}
\Psi_1 &= \left(\frac{A}{2\mu} + \frac{1-2v}{1-v}\frac{B}{\mu} \right)\Psi_0 - \frac{1}{8}\frac{A}{\mu}\frac{\bar{h}\delta_2}{(\delta_1+\delta_2)}\left(\frac{2\pi\delta_1}{\bar{h}}\eta_1 + \eta_2 \right), \\
\Psi_2 &= \left(\frac{A}{2\mu} + \frac{1-2v}{1-v}\frac{B}{\mu} \right)\Psi_0 - \frac{1}{8}\frac{A}{\mu}\frac{\bar{h}\delta_2}{(\delta_1-\delta_2)}\left(\frac{2\pi\delta_1}{\bar{h}}\eta_1 + \eta_2 \right)
\end{aligned} \qquad (6.45)
$$

where

$$\Psi_0 = -\pi\delta_2\eta_1 + 2\pi^2\frac{\delta_1\delta_2}{\bar{h}} + \frac{\pi^2\bar{h}\delta_1\delta_2}{6}\left(1 + 2\eta_2 \right) \qquad (6.46)$$

and $\delta_2 = h/\lambda_2$, and $\lambda_2 = 2\pi/k_2$ is the wavelength of the torsional wave. It should be noted that the special condition $\delta_1 - \delta_2 = 0$, for which the resonant wave with difference frequency does not exist, is not considered here. The quantities $\Psi_i (i = 0, 1, 2)$, as defined by Eqs. (6.45) and (6.46), defines three coefficients for the specified primary waves. In view of Eqs. (6.31$_4$) and (6.44), we have

$$\frac{\partial^2 v^{(1)}}{\partial x^2} - \frac{1}{c_T^2}\frac{\partial^2 v^{(1)}}{\partial t^2} = \Psi_1 \frac{WDk^+}{Rh}\sin(\omega^+ t - k^+ x) - \Psi_2 \frac{WDk^-}{Rh}\sin(\omega^- t - k^- x) \qquad (6.47)$$

The resonant waves have to meet the phase-match conditions, which are given by

$$\left|\frac{\omega^-}{c_T}\right| = \left|k^-\right| \text{ or } \left|\frac{\omega^+}{c_T}\right| = \left|k^+\right| \tag{6.48}$$

For case one: $\left|\omega^-/c_T\right| = \left|k^-\right|$, the longitudinal phase velocity can be expressed by

$$c_1 = \frac{\omega_1}{k_1} = n_1 c_T \tag{6.49}$$

Then, the first resonant condition in Eq. (6.48) becomes

$$\frac{\omega_2}{\omega_1} = \frac{n_1+1}{2n_1} \tag{6.50}$$

For this case, we assume $n_1 \neq 1$. Thus, the wave solution to Eq. (6.47) will have the following form

$$v^{(1)} = a^+ \sin(\omega^+ t - k^+ x) + a^- x \cos(\omega^- t - k^- x) \tag{6.51}$$

Substituting Eq. (6.51) into Eq. (6.47), we can get the following equality

$$a^+\left(\frac{\omega^{+2}}{c_T^2} - k^{+2}\right)\sin(\omega^+ t - k^+ x) + 2k^- a^- \sin(\omega^- t - k^- x)$$

$$= \Psi_1 \frac{WDk^+}{Rh}\sin(\omega^+ t - k^+ x) - \Psi_2 \frac{WDk^-}{Rh}\sin(\omega^- t - k^- x) \tag{6.52}$$

The values of amplitudes in Eq. (6.52) can then be calculated as

$$a^+ = \frac{\Psi_1 Dk^+}{R\left(\omega^{+2}/c_T^2 - k^{+2}\right)}\frac{W}{h}, \quad a^- = -\frac{\Psi_2 D}{2R}\frac{W}{h} \tag{6.53}$$

In view of Eq. (6.50), the phase velocities of the generated waves are given by

$$c^+ = \frac{\omega^+}{k^+} = \frac{3n_1+1}{3+n_1}c_T, \quad c^- = \frac{\omega^-}{k^-} = -c_T \tag{6.54}$$

The minus phase velocity in Eq. (6.54$_2$) means that the corresponding wave travels in the opposite direction of the primary waves. Finally, by virtue of Eqs. (6.51)-(6.54), the generated torsional wave can be expressed by

$$\bar{v}^{(1)} = \frac{1}{2}(R+r)\left[\frac{\Psi_1 WDk^+}{Rh\left(\omega^{+2}/c_T^2 - k^{+2}\right)}\sin\omega^+(t - \frac{3+n_1}{3n_1+1}\frac{x}{c_T}) - \frac{\Psi_2 D}{2R}\frac{W}{h}x\cos\omega^-(t + \frac{x}{c_T})\right]$$

$$\tag{6.55}$$

which shows that there is no cumulative behavior for the wave with sum frequency. For the wave with difference frequency the amplitude increases, however, linearly with the propagation distance. It should be noted that the waves with difference frequency propagates in the opposite direction of the primary waves. This back-propagating resonant wave may be useful for nondestructive testing purposes.

Table 6.1 Values of Ψ_1 and Ψ_2 calculated from Eq. (6.45) for several combinations of primary torsional wave modes with the first and second modes of longitudinal waves

Group	$\delta_1 = h/\lambda_1$	$n_1 = \omega_1/(k_1 c_T)$	$\delta_2 = h/\lambda_2$	Ψ_1	Ψ_2
With the first mode of longitudinal waves					
1	0.025	1.000	0.05	1.191	1.188
2	0.1	0.383	0.05	9.717	10.101
3	0.2	0.511	0.10	44.355	48.808
4	0.3	0.633	0.15	109.220	124.499
With the second mode of longitudinal waves					
5	0.1	1.692	0.05	-4.086	-4.086
6	0.2	1.691	0.10	-16.283	-16.283
7	0.3	1.691	0.15	-36.669	-36.669

For case two: $\left|\omega^+/c_T\right| = \left|k^+\right|$, the value of n_1 must be equal to 1, which is possible for longitudinal waves propagating in pipes, see Fig. 6.2. The wave solution has the following form

$$v^{(1)} = a^+ x\cos(\omega^+ t - k^+ x) + a^- x\cos(\omega^- t - k^- x) \tag{6.56}$$

Substituting Eq. (6.56) into Eq. (6.47) and following the analysis procedure (i.e. Eqs. (6.52)-(6.54)) used in case one, the expression of the generated torsional wave for case two is obtained as

$$\bar{v}^{(1)} = \frac{1}{2}(R+r)\left[\frac{\Psi_1 D}{2R}\frac{W}{h}x\cos\omega^+(t-\frac{x}{c_T}) - \frac{\Psi_2 D}{2R}\frac{W}{h}x\cos\omega^-(t+\frac{x}{c_T})\right] \tag{6.57}$$

To obtain this kind of resonant waves, the phase velocity of the primary longitudinal wave c_1 has to be equal to c_T, which implies that the primary longitudinal wave has to propagate at a frequency where its velocity equals to the shear wave velocity.

The analytical expressions of resonant waves with sum and difference frequencies are shown in Eqs. (6.55) and (6.57). The coefficients Ψ_1 and Ψ_2 can be calculated through Eq. (6.45) for the specific primary longitudinal and torsional waves.

As examples, we determine the numerical values of Ψ_1 and Ψ_2 for several combinations of primary longitudinal and torsional waves, see Table I. The ratio of thickness to mean radius h/R is taken as $1/10$. The material constants are the same as used in Liu *et al.* (2013b), i.e.

$$\lambda = 116.2 \text{ GPa}, \mu = 82.7 \text{ GPa}, A = -325 \text{ GPa}, B = -310 \text{ GPa}, C = -800 \text{ GPa} \qquad (6.58)$$

The Poison's ratio ν is 0.3 and the shear coefficient κ is 0.86.

It is noted that the combination of primary waves in group 1 applies to case two (i.e. $n_1 = 1$). The analytical expressions presented in this section are not limited to the combinations in Table 6.1. They are applicable to any combination of primary longitudinal and torsional waves, except the case that $\delta_1 = \delta_2$. It can be noted from Fig. 6.2 and Table 6.1 that the change of phase velocity is very small for points lying on the dispersion curve of the second longitudinal mode. This means that the dispersion effect of the longitudinal wave is weak in these regions. So the group velocity is very close to the phase velocity and the longitudinal wave is undistorted in these regions.

6.4 The self-interaction of longitudinal waves in a pipe

In this section, we analyze the self-interaction of axisymmetric longitudinal waves propagating in a thin-walled pipe. Compared with the equations of motion of plates in rectangular coordinates, the equations of motion of pipes in cylindrical coordinates become quite complex and require a numerical approach. Here, we will, however, investigate the second longitudinal harmonics propagating in thin-walled pipes using shell theory with nonlinear material behavior. For thin-walled pipes, we

further simplify the nonlinear governing equations (6.12)-(6.14) by neglecting rotatory inertia (the terms containing $\rho h^3 / 12$). We then have

$$\frac{\partial N_{rx}}{\partial x} - \frac{N_{\theta\theta}}{R} = \rho h \frac{\partial^2 u}{\partial t^2} \tag{6.59}$$

$$\frac{\partial N_{xx}}{\partial x} = \rho h \frac{\partial^2 w}{\partial t^2} \tag{6.60}$$

$$\frac{\partial M_x}{\partial x} - N_{rx} = 0 \tag{6.61}$$

Substituting Eq. (6.61) into Eq. (6.59), we obtain

$$\frac{\partial^2 M_x}{\partial x^2} - \frac{N_{\theta\theta}}{R} = \rho h \frac{\partial^2 u}{\partial t^2} \tag{6.62}$$

For thin-walled pipes, we also assume that the shear deformation is very small and may be neglected, which implies

$$\varepsilon_{rx} = \frac{\partial u}{\partial x} + \frac{\partial \overline{w}}{\partial r} = 0 \ \ \text{or} \ \ \phi = -\frac{\partial u}{\partial x} \tag{6.63}$$

Using Eq. (6.63), the nonlinear stresses for longitudinal waves given by Eqs. (6.5)-(6.7) are further simplified to

$$\tau_{rx}^{NL} = 0, \ \ \tau_{\theta\theta}^{NL} = \lambda_1 \frac{u^2}{r^2} + 2\lambda_2 \frac{u}{r} \frac{\partial \overline{w}}{\partial x} + \lambda_3 \left(\frac{\partial \overline{w}}{\partial x} \right)^2,$$
$$\tau_{xx}^{NL} = \lambda_1 \left(\frac{\partial \overline{w}}{\partial x} \right)^2 + 2\lambda_2 \frac{u}{r} \frac{\partial \overline{w}}{\partial x} + \lambda_3 \frac{u^2}{r^2} \tag{6.64}$$

In this section, the definitions of $N_{\theta\theta}^{NL}$, N_{xx}^{NL} and M_x^{NL} are the same as stated by Eq. (6.24), while the expressions of the nonlinear stresses (6.5)-(6.7) should be replaced by the corresponding stresses in Eq. (6.64). Substituting Eqs. (6.17)-(6.19) into Eqs. (6.60) and (6.62), with consideration of zero shear deformation (i.e. Eq. (6.63)), we obtain the displacement equations of motion as

$$(\overline{\lambda} + 2\mu) \frac{h^3}{12} \frac{\partial^4 u}{\partial x^4} + (\overline{\lambda} + 2\mu) \beta \frac{u}{R} + \overline{\lambda} \frac{h}{R} \frac{\partial w}{\partial x} + \rho h \frac{\partial^2 u}{\partial t^2} = \frac{\partial^2 M_x^{NL}}{\partial x^2} - \frac{N_{\theta\theta}^{NL}}{R} \tag{6.65}$$

$$(\overline{\lambda} + 2\mu) h \frac{\partial^2 w}{\partial x^2} + \overline{\lambda} \frac{h}{R} \frac{\partial u}{\partial x} - \rho h \frac{\partial^2 w}{\partial t^2} = -\frac{\partial N_{xx}^{NL}}{\partial x} \tag{6.66}$$

Here, the terms containing h^2 / R^2 have been neglected. The corresponding linear homogenous equations of Eqs. (6.65) and (6.66) are the Donnell's equation for axially symmetric motion of a thin shell given by Junger and Feit (1986, page 217).

After some simple manipulations, Eqs. (6.65) and (6.66) can be written as two equations with uncoupled linear parts.

$$\frac{\partial w}{\partial x} = \frac{1}{\bar{\lambda}\bar{h}}\left(-\rho h \frac{\partial^2 u}{\partial t^2} - (\bar{\lambda}+2\mu)\frac{h^3}{12}\frac{\partial^4 u}{\partial x^4} - (\bar{\lambda}+2\mu)\beta\frac{u}{R} + \frac{\partial^2 M_x^{NL}}{\partial x^2} - \frac{N_{\theta\theta}^{NL}}{R}\right) \quad (6.67)$$

and

$$-\rho h \frac{\partial^4 u}{\partial x^2 \partial t^2} - (\bar{\lambda}+2\mu)\frac{h^3}{12}\frac{\partial^6 u}{\partial x^6} + \frac{\rho^2}{\bar{\lambda}+2\mu}h\frac{\partial^4 u}{\partial t^4} + \rho\frac{h^3}{12}\frac{\partial^6 u}{\partial t^2 \partial x^4}$$
$$+ \left(\frac{\bar{\lambda}^2}{\bar{\lambda}+2\mu}\frac{\bar{h}^2}{h} - (\bar{\lambda}+2\mu)\frac{\bar{h}}{R}\right)\frac{\partial^2 u}{\partial x^2} + \rho\frac{\bar{h}}{R}\frac{\partial^2 u}{\partial t^2} = F[u,\bar{w}] \quad (6.68)$$

where

$$F[u,\bar{w}] = -\frac{\bar{\lambda}}{\bar{\lambda}+2\mu}\frac{\bar{h}}{h}\frac{\partial^2 N_{xx}^{NL}}{\partial x^2} + \frac{\rho}{\bar{\lambda}+2\mu}\left(\frac{\partial^4 M_x^{NL}}{\partial t^2 \partial x^2} - \frac{1}{R}\frac{\partial^2 N_{\theta\theta}^{NL}}{\partial t^2}\right)$$
$$- \left(\frac{\partial^4 M_x^{NL}}{\partial x^4} - \frac{1}{R}\frac{\partial^2 N_{\theta\theta}^{NL}}{\partial x^2}\right) \quad (6.69)$$

Note that for a thin shell (i.e. $\bar{h} \ll 1$), we have

$$\beta \approx \bar{h} \quad (6.70)$$

To solve Eq. (6.68), we consider in the usual manner.

$$u = u^{(0)} + u^{(1)}, \quad \bar{w} = \bar{w}^{(0)} + \bar{w}^{(1)} \quad (6.71)$$

Substituting Eq. (6.71) into Eq. (6.68), we get a zero-order and a first-order equation. The zero-order equation is the same as Eq. (6.68) when the right-hand side term F is omitted.

The first-order equation is obtained as

$$-\rho h \frac{\partial^4 u^{(1)}}{\partial x^2 \partial t^2} - (\bar{\lambda}+2\mu)\frac{h^3}{12}\frac{\partial^6 u^{(1)}}{\partial x^6} + \frac{\rho^2}{\bar{\lambda}+2\mu}h\frac{\partial^4 u^{(1)}}{\partial t^4} + \rho\frac{h^3}{12}\frac{\partial^6 u^{(1)}}{\partial t^2 \partial x^4}$$
$$+ \left(\frac{\bar{\lambda}^2}{\bar{\lambda}+2\mu}\frac{\bar{h}^2}{h} - (\bar{\lambda}+2\mu)\frac{\bar{h}}{R}\right)\frac{\partial^2 u^{(1)}}{\partial x^2} + \rho\frac{\bar{h}}{R}\frac{\partial^2 u^{(1)}}{\partial t^2} = F[u^{(0)},\bar{w}^{(0)}] \quad (6.72)$$

The solution to the zero-order equation is taken in the following form.

$$u^{(0)} = U\cos(\omega t - kx) = \text{Re}\left[Ue^{i(\omega t - kx)}\right] \quad (6.73)$$

where "Re" denotes the real part of the quantity in the bracket. Substituting Eq. (6.73) into the zero-order equation, we obtain the following dispersion relation for a thin pipe.

$$-2\pi^2\left(1-v\right)\delta^2 n^2 + \pi^2\left(1-v\right)^2\delta^2 n^4 + \frac{4}{3}\pi^4\delta^4$$

$$-\frac{2}{3}\pi^4\left(1-v\right)n^2\delta^4 - \left(v^2-1\right)\bar{h}^2 - \frac{1-v}{2}\bar{h}^2 n^2 = 0 \tag{6.74}$$

where n and δ are defined in Eq. (6.35).
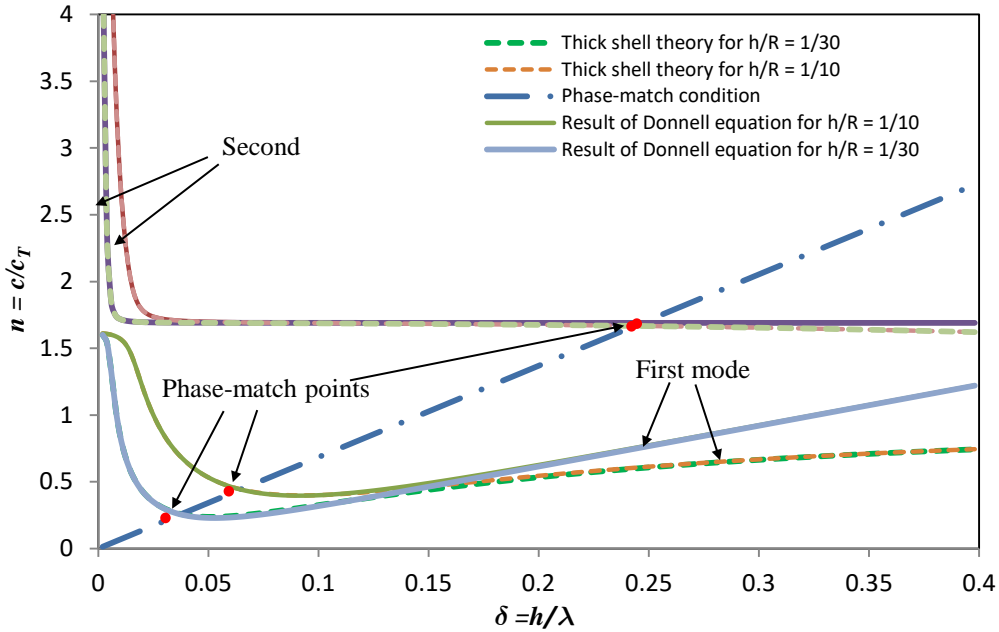
Fig. 6.3 Dispersion curves and phase-match points for $v = 0.3$

Figure 6.3 shows the comparison between the dispersion curves obtained from the Donnell equation and thick shell theory (Mirsky and Herrmann, 1958). When the ratio of wall thickness to wavelength is small, these two results agree very well with each other. The thick shell theory fits well with the exact theory for small values of δ, as shown in Fig. 6.2. Therefore, on the basis of dispersive behavior, the governing equation (6.68) is acceptable for waves with long wavelengths in a thin-walled pipe.

By the use of Eqs. (6.1$_3$) and (6.63), the following relations can be obtained.

$$\frac{\partial \bar{w}^{(0)}}{\partial r} = \phi^{(0)} = \text{Re}\left[kiu^{(0)} \right] \tag{6.75}$$

In view of Eqs. (6.67) and (6.73), the relation between $w^{(0)}$ and $u^{(0)}$ can be written as

$$w^{(0)} = \text{Re}\left[iC_1 u^{(0)} \right] \tag{6.76}$$

where

$$C_1 = \pi \frac{1-v}{v} \frac{1}{\bar{h}} n^2 \delta - \frac{2}{3} \pi^3 \frac{1}{v} \frac{1}{\bar{h}} \delta^3 - \frac{1}{2\pi} \frac{1}{v} \bar{h} \frac{1}{\delta} \tag{6.77}$$

We can then express the axial displacement by

$$\overline{w}^{(0)} = iC_1 u^{(0)} + ikr u^{(0)} = \mathrm{Re}\left[i\left(C_1 + kr\right) u^{(0)} \right] \tag{6.78}$$

Using Eqs. (6.73) and (6.78), together with Eqs. (6.24) and (6.64), the nonlinear resultant forces become

$$N_{xx}^{NL} = \Gamma_1 \lambda_2 \frac{U^2}{h} \cos^2(\omega t - kx) \tag{6.79}$$

$$M_x^{NL} = \Gamma_2 \lambda_2 U^2 \cos^2(\omega t - kx) \tag{6.80}$$

$$N_{\theta\theta}^{NL} = \Gamma_3 \lambda_2 \frac{U^2}{h} \cos^2(\omega t - kx) \tag{6.81}$$

where

$$\Gamma_1 = 4\pi^2 \frac{\lambda_1}{\lambda_2} \delta^2 \left(C_1^2 + \frac{1}{3}\pi^2 \delta^2 + \frac{1}{3}\pi \bar{h} C_1 \delta \right) + 4\pi C_1 \bar{h} \delta + \frac{\lambda_3}{\lambda_2} \bar{h}^2,$$

$$\Gamma_2 = 4\pi^2 \frac{\lambda_1}{\lambda_2} \left(C_1^2 \frac{\bar{h}}{12} + \frac{1}{3}\pi C_1 \delta + \frac{1}{20}\pi^2 \bar{h}\delta^2 \right) \delta^2 + \frac{2}{3}\pi^2 \bar{h}\delta^2, \tag{6.82}$$

$$\Gamma_3 = \frac{\lambda_1}{\lambda_2} \bar{h}^2 + 4\pi \bar{h} C_1 \delta + \frac{\lambda_3}{\lambda_2}\left(4\pi^2 C_1^2 \delta^2 + \frac{4}{3}\pi^4 \delta^4 \right)$$

These expressions define three coefficients for the longitudinal primary wave. Substituting Eqs. (6.79)-(6.81) into Eq. (6.69), we obtain

$$F = 4\pi^2 \delta^2 \lambda_2 \left[\frac{2\bar{\lambda}}{\bar{\lambda}+2\mu} \bar{h} \Gamma_1 + \left(\frac{\mu}{\bar{\lambda}+2\mu} n^2 - 1 \right)\left(32\Gamma_2 \pi^2 \delta^2 + 2\bar{h}\Gamma_3 \right) \right] \frac{U^2}{h^4} \cos 2(\omega t - kx) \tag{6.83}$$

Let us consider a solution to Eq. (6.72) in the form

$$u^{(1)} = \bar{U} x \sin 2(\omega t - kx) \tag{6.84}$$

Substituting Eqs. (6.83) and (6.84) into Eq. (6.72), we get the following equation:

$$\frac{32\pi^2 \delta^2 \mu}{h^3(1-v)} \Lambda \bar{U} x \sin 2(\omega t - kx)$$

$$-\frac{16\pi\delta\mu}{h^2}\left[8\pi^2 \delta^2 n^2 - \frac{64}{1-v}\pi^4 \delta^4 + \frac{64}{3}\pi^4 \delta^4 n^2 - \bar{h}^2(v+1) \right]\bar{U} \cos 2(\omega t - kx) \tag{6.85}$$

$$= 8\pi^2 \delta^2 \lambda_2 \left[v\bar{h}\Gamma_1 + \left(\frac{1-v}{2}n^2 - 1 \right)\left(16\Gamma_2 \pi^2 \delta^2 + \bar{h}\Gamma_3 \right) \right] \frac{U^2}{h^4} \cos 2(\omega t - kx)$$

where

$$\Lambda = -8(1-\nu)\pi^2\delta^2 n^2 + \frac{64}{3}\pi^4\delta^4 + 4\pi^2(1-\nu)^2\delta^2 n^4$$
$$-\frac{32}{3}(1-\nu)\pi^4\delta^4 n^2 - (\nu^2-1)\bar{h}^2 - \frac{1-\nu}{2}\bar{h}^2 n^2 \tag{6.86}$$

Equation (6.85) has a solution which does not depend on time when $\Lambda = 0$, which implies

$$-8(1-\nu)\pi^2\delta^2 n^2 + \frac{64}{3}\pi^4\delta^4 + 4\pi^2(1-\nu)^2\delta^2 n^4$$
$$-\frac{32}{3}(1-\nu)\pi^4\delta^4 n^2 - (\nu^2-1)\bar{h}^2 - \frac{1-\nu}{2}\bar{h}^2 n^2 = 0 \tag{6.87}$$

Since $\Lambda = 0$, we can obtain the amplitude of the second longitudinal harmonic, Eq. (6.84), from Eq. (6.85) as

$$\bar{U} = \Psi_3 \frac{U^2}{h^2} \tag{6.88}$$

where

$$\Psi_3 = \frac{\pi\lambda_2\delta\left[\nu\bar{h}\Gamma_1 + \left(\frac{1-\nu}{2}n^2-1\right)\left(4\Gamma_2 4\pi^2\delta^2 + \bar{h}\Gamma_3\right)\right]}{2\mu\left[-8\pi^2\delta^2 n^2 - \frac{64}{3}\pi^4\delta^4 n^2 + \frac{64}{1-\nu}\pi^4\delta^4 + (1+\nu)\bar{h}^2\right]} \tag{6.89}$$

Basically, Eq. (6.87), which gives the relation between 2ω and $2k$, is the dispersion relation for second harmonics. For a non-dispersive structure like an unbounded medium, the dispersion relation for the primary wave is the same as the corresponding relation for the second harmonics, and the phase velocities keep unchanged when the frequencies vary. For waves in dispersive structures, there exist only limited phase-match points where the phase velocities of primary waves are the same as the corresponding phase velocities of second harmonics. If we plot the two dispersion relations (6.74) and (6.87) in the same figure, the intersections of the two curves are phase-match points. In this paper, we obtain a relation between δ and n by subtracting Eq. (6.74) from Eq. (6.87). The resulting equation can be reduced to

$$\left[5\pi^2\delta^2 - 3\left(\frac{1-\nu}{2}\right)n^2\right]\left(1 - \frac{1-\nu}{2}n^2\right) = 0 \tag{6.90}$$

which gives rise to the following relations

$$n = \pi \sqrt{\frac{10}{3(1-v)}} \delta \tag{6.91}$$

and

$$n = \sqrt{\frac{2}{1-v}} \tag{6.92}$$

Equations (6.91) and (6.92) are phase-match conditions, which are independent of the ratio of the thickness to radius of a pipe. Equation (6.91) defines a straight line in the $\delta - n$ plane, shown in Fig. 6.3. The intersections of the line with the dispersion curves yield the phase-match points. The numerical values of the phase-match points have been verified by substitution in Eqs. (6.74) and (6.87). Another two phase-match points can be obtained by substitution of Eq. (6.92) into Eq. (6.74) or Eq. (6.87) for the two different ratios of wall thickness to mean radius considered here. For the pipes with the ratio of thickness to mean radius of 1/10 and 1/30, the phase-match point lying on the dispersion curve of the first mode is in the region of accuracy of the Donnell theory, see Fig. 6.3. The dispersion curves of the second harmonics are neglected in Fig. 6.3. Since the ratio of thickness to wavelength of the second harmonic is 2δ, the region of accuracy of the second harmonic is smaller. The phase-match points lying on the dispersion curve of the second mode are out of the accuracy region shown in Fig. 6.3. Considering the second longitudinal harmonics in the pipe with ratio of thickness to mean radius of 1/10 and 1/30, we can determine the phase-match points by using the present theory, which lie on the dispersion curves of the first mode in Fig. 6.3. Once the phase-match points have been calculated, the amplitudes of the second harmonics can be obtained through Eqs. (6.89) and (6.94). The phase-match points and the corresponding amplitude coefficients of the second harmonics in Eqs. (6.89) and (6.94) are given in Table 6.2. The material constants used here are given by Eq. (6.58).

Substitution of Eqs. (6.80), (6.81), (6.84) and (6.88) into Eq. (6.67) yields the expression for the axial strain as

$$\frac{\partial w^{(1)}}{\partial x} = \Psi_4 \frac{U^2}{h^2} \frac{x}{h} \sin 2(\omega t - kx) - \Psi_5 \frac{U^2}{h^2} \cos 2(\omega t - kx) - \Psi_6 \frac{U^2}{h^2} \qquad (6.93)$$

where the amplitude coefficients in Eq. (6.93) are given by

$$\Psi_4 = \left(8\pi^2 \frac{1-\nu}{\nu \bar{h}} \delta^2 n^2 - \frac{64}{3} \pi^4 \frac{\delta^4}{\nu \bar{h}} - \frac{\bar{h}}{\nu} \right) \Psi_3$$

$$\Psi_5 = \frac{64}{3} \pi^3 \frac{\delta^3}{\nu \bar{h}} \Psi_3 + 4\pi^2 \frac{\lambda_2}{\mu \bar{h}} \frac{1-\nu}{\nu} \delta^2 \Gamma_2 + \frac{1-\nu}{4\nu} \frac{\lambda_2}{\mu} \Gamma_3 \qquad (6.94)$$

$$\Psi_6 = \frac{1-\nu}{4\nu} \frac{\lambda_2}{\mu} \Gamma_3$$

As the propagation distance increases, the cumulative second harmonic with the amplitude coefficient Ψ_4 will be dominant in Eq. (6.93).

Table 6.2 The phase-match points and the corresponding coefficients of the amplitudes of second harmonics

h/R	$\delta = h/\lambda$	$n = c/c_T$	Ψ_3	Ψ_4	Ψ_5	Ψ_6
1/10	0.065	0.445	1.80×10^{-2}	-5.11×10^{-4}	-2.80×10^{-3}	-8.77×10^{-2}
1/30	0.037	0.252	2.45×10^{-3}	-3.67×10^{-5}	-1.53×10^{-4}	-9.34×10^{-3}

From Table 6.2, we observe that the amplitudes of second harmonics in the thinner-walled pipe are smaller than the amplitudes of second harmonics in the thicker-walled pipe. That means a lower power flux from the primary wave to the second harmonic occurs in the thinner pipe.

To validate the analysis in this section, the phase-match point lying on the dispersion curve of first mode is compared with the corresponding point given by Liu *et al.* (2013b). The ratio of thickness to mean radius is 150/975. Our result is $(\delta = 0.080, \, n = 0.546)$ compared with the result of Liu *et al.* $(\delta = 0.086, \, n = 0.536)$. The discrepancy between the two results is small.

6.5 Conclusions

In this chapter, guided waves propagating in pipes with quadratic material nonlinearity have been investigated. This chapter is composed of three main parts: the derivation of the shell equations, the mixing of longitudinal and torsional waves, and the self-interaction of longitudinal waves. Analytical expressions of cumulative second harmonics have been obtained based on shell theory.

The derivation of governing equations of axisymmetric motion of a pipe with nonlinear material behavior has been given in the first part. By use of the perturbation method, the zero and first order equations have been derived. The dispersion curves obtained from the linear version of the present theory, the linear thick shell theory and the linear three dimensional theory show excellent agreement. It was shown that no resonant longitudinal harmonic with sum or difference frequency exists. Analytical expressions of the resonant torsional harmonics with difference and sum frequencies were obtained. The resonant torsional harmonics generated by the mixing of longitudinal and torsional waves propagate in the opposite direction of the primary wave.

For thin-walled shells, the shell theory has been further simplified to yield uncoupled linear and nonlinear parts of the governing equations. The simplified shell theory has been used to analytically investigate the self-interaction of longitudinal waves in thin-walled pipes. To validate the thin shell theory, the dispersion curves for longitudinal waves were compared with the corresponding curves obtained from thick shell theory. It was shown that the dispersion curves agree very well with each other when the ratio of thickness to wavelength is small. For second longitudinal harmonics in pipes, analytical expressions for the phase-match conditions are presented, which together with the corresponding dispersion relation, have been used to determine the phase-match points. The analytical solutions presented in this paper may provide a benchmark to numerical and experimental investigations.

Appendix 6A: The nonlinear parts of the Cauchy stress

In cylindrical coordinates, the nonlinear parts of the Cauchy stress components only including quadratic material nonlinearity for axisymmetric wave fields are given by

$$\tau_{rr}^{NL} = \left(B+C\right)\left(\frac{\overline{u}^2}{\overline{r}^2}+\overline{w}_{,x}^2\right)+2C\frac{\overline{uw}_{,x}}{\overline{r}}+\left(2B+2C\right)\left(\frac{\overline{uu}_{,r}}{\overline{r}}+\overline{u}_{,r}\overline{w}_{,x}\right)$$
$$+\left(A+3B+C\right)\overline{u}_{,r}^2+\frac{1}{2}B\overline{v}_{,x}^2+\left(\frac{1}{4}A+\frac{1}{2}B\right)\left(\overline{u}_{,x}^2+\frac{\overline{v}^2}{\overline{r}^2}+\overline{w}_{,r}^2+\overline{v}_{,r}^2\right) \qquad (6A.1)$$
$$+\left(\frac{1}{2}A+B\right)\left(\overline{u}_{,x}\overline{w}_{,r}-\frac{\overline{vv}_{,r}}{\overline{r}}\right)$$

$$\tau_{r\theta}^{NL} = \left(\frac{1}{2}A+B\right)\left(\overline{u}_{,r}\overline{v}_{,r}-\frac{\overline{uv}}{\overline{r}^2}+\frac{\overline{uv}_{,r}}{\overline{r}}-\frac{\overline{vu}_{,r}}{\overline{r}}\right)+\frac{1}{4}A\left(\overline{u}_{,x}\overline{v}_{,x}+\overline{v}_{,x}\overline{w}_{,r}\right)$$
$$+B\left(\overline{v}_{,r}\overline{w}_{,x}-\frac{\overline{vw}_{,x}}{\overline{r}}\right) \qquad (6A.2)$$

$$\tau_{rx}^{NL} = \left(\frac{1}{2}A+B\right)\left(\overline{u}_{,r}\overline{u}_{,x}+\overline{w}_{,r}\overline{w}_{,x}+\overline{u}_{,r}\overline{w}_{,r}+\overline{u}_{,x}\overline{w}_{,x}\right)$$
$$+\frac{A}{4}\left(\overline{v}_{,r}\overline{v}_{,x}-\frac{\overline{vv}_{,x}}{\overline{r}}\right)+B\left(\frac{\overline{uu}_{,x}}{\overline{r}}+\frac{\overline{uw}_{,r}}{\overline{r}}\right) \qquad (6A.3)$$

$$\tau_{\theta\theta}^{NL} = \left(A+3B+C\right)\frac{\overline{u}^2}{\overline{r}^2}+B\overline{u}_{,x}\overline{w}_{,r}+2C\overline{u}_{,r}\overline{w}_{,x}+\left(2B+2C\right)\left(\frac{\overline{uu}_{,r}}{\overline{r}}+\frac{\overline{uw}_{,x}}{\overline{r}}\right)$$
$$+\left(B+C\right)\left(\overline{u}_{,r}^2+\overline{w}_{,x}^2\right)+\frac{1}{2}B\left(\overline{u}_{,x}^2+\overline{w}_{,r}^2\right)-\left(\frac{A}{2}+B\right)\frac{\overline{vv}_{,r}}{\overline{r}} \qquad (6A.4)$$
$$+\left(\frac{A}{4}+\frac{1}{2}B\right)\left(\frac{\overline{v}^2}{\overline{r}^2}+\overline{v}_{,r}^2+\overline{v}_{,x}^2\right)$$

$$\tau_{\theta x}^{NL} = \frac{1}{4}A\left(\overline{u}_{,x}\overline{v}_{,r}-\frac{\overline{vw}_{,r}}{\overline{r}}+\overline{v}_{,r}\overline{w}_{,r}-\frac{\overline{vu}_{,x}}{\overline{r}}\right)$$
$$+\left(\frac{A}{2}+B\right)\left(\frac{\overline{uv}_{,x}}{\overline{r}}+\overline{v}_{,x}\overline{w}_{,x}\right)+B\overline{u}_{,r}\overline{v}_{,x} \qquad (6A.5)$$

$$\tau_{xx}^{NL} = \left(A+3B+C\right)\overline{w}_{,x}^2+\left(B+C\right)\left(\frac{\overline{u}^2}{\overline{r}^2}+\overline{u}_{,r}^2\right)+2C\frac{\overline{uu}_{,r}}{\overline{r}}$$
$$-B\frac{\overline{vv}_{,r}}{\overline{r}}+\frac{B}{2}\left(\frac{\overline{v}^2}{\overline{r}^2}+\overline{v}_{,r}^2\right)+\left(\frac{1}{4}A+\frac{1}{2}B\right)\left(\overline{u}_{,x}^2+\overline{v}_{,x}^2+\overline{w}_{,r}^2+2\overline{u}_{,x}\overline{w}_{,r}\right) \qquad (6A.6)$$
$$+\left(2B+2C\right)\left(\frac{\overline{uw}_{,x}}{\overline{r}}+\overline{u}_{,r}\overline{w}_{,x}\right)$$

Equations. (A1)-(A6) can also be reduced from the corresponding equations in Liu et al. (2013a) if we only consider axisymmetric motion with small deformations (but considering material nonlinearities). The subscript letter following the comma denotes the corresponding differential derivative.

Chapter 7 Reflection of ultrasound from a region of cubic material nonlinearity due to harmonic generation

7.1 Introduction

In recent years, the researches about elastic waves propagating in solids of nonlinear material behavior occupying unbounded bodies have attracted intensive attentions. From the practical point of view, the reflection, transmission and scattering of incident waves from an inclusion of nonlinear material is of obvious interest. The reflection of second harmonics from a stress-free boundary was studied by Bender et al. (2013). An experimental investigation was presented by Donskoy et al. (2001) to observe the modulation effect of highly nonlinear material behavior caused by weakly or incompletely bounded interfaces. Achenbach et al. (1989) represented the failure of an adhesive bond by a cubically nonlinear elastic model. For that case the strength of the adhesive bond can be directly measured from the reflected waves. For simplicity, the interfaces or adhesive bonds studied above were frequently modeled by nonlinear springs. Using a Green's function, the analytical solution to the scattering of elastic waves from an inclusion of quadratic nonlinearity was obtained by Tang et al. (2012).

The main purpose of this work is to investigate the reflection and backscattering of plane elastic waves by a region of cubically nonlinear material behavior. The constitutive relation is obtained from the expansion of the elastic energy function by only retaining the second and fourth order elastic constants, for which the condition of symmetric tension and compression material response is satisfied. The analytical solutions to cumulative first and third harmonic generation have been derived by using the perturbation method. Two simple models of practical interest are proposed to obtain the nonlinear elastic constants (i.e. the fourth order elastic constants) of the region by making use of reflection and back-scattered waves. In the case where the region is large, incidence of ultrasound on the interface

between the regions of linear and nonlinear material behaviors, which are perfectly joined, yields very useful information. Making use of the continuity condition of stress and displacement at the interface, expressions for the compensatory waves have been obtained, whose amplitudes contain the nonlinear material constants near the interface. When the nonlinear region is an inclusion, the nonlinear body force induced by the material nonlinearity generates a backscattered wave. The reciprocity theorem is employed to obtain an analytical solution for the backscattered wave. The nonlinear material constants and the size of the inclusion can be obtained from the amplitude of the backscattered wave. For a small nonlinear region, the superposition of back-propagated compensatory waves generated from the two interfaces gives an expression for the backscattered wave, which is of the same form as the one obtained by the reciprocity theorem.

7.2 Governing Equations

In this section, the equations governing the propagation of plane elastic waves in an unbounded elastic solid are presented. The material displays material nonlinearity which has a strong correlation with material degradation. For small-amplitude waves propagating in solids with high material nonlinearity, the geometrical nonlinearity is negligible. For most materials, their tension-compression material response is symmetric (Rauch and Leslie, 1972). However, the even order material nonlinearities, due to quadratic nonlinearity appearing in the stress-strain relation, lead to asymmetry of tension and compression. In this paper, we consider cubic material nonlinearity of the stress-strain relation, which leads to a symmetric stress-stain relation.

For plane elastic waves propagating in the x-direction, the displacement fields can be represented by

$$u = u(x,t), \ v = v(x,t) \tag{7.1}$$

for longitudinal and transverse waves, respectively. Considering only cubic material nonlinearity, the one-dimensional stress-strain relation can be derived from Eq. (2) in (Liu et al., 2013)

$$\tau_{xx} = (\lambda + 2\mu)\frac{\partial u}{\partial x} + 4(F + H + E + G)\left(\frac{\partial u}{\partial x}\right)^3 + \left(\frac{3}{2}E + F + 2G\right)\frac{\partial u}{\partial x}\left(\frac{\partial v}{\partial x}\right)^2 \quad (7.2)$$

and

$$\tau_{xy} = \mu\frac{\partial v}{\partial x} + \left(\frac{3}{2}E + F + 2G\right)\left(\frac{\partial u}{\partial x}\right)^2\frac{\partial v}{\partial x} + G\left(\frac{\partial v}{\partial x}\right)^3 \quad (7.3)$$

where E, F, G and H are fourth order elastic constants. Equations (7.2) and (7.3) indicate that the third order elastic constants in the stress-strain relation which are related to quadratic nonlinearity have all been set equal to zero. The constitutive relations given by Eqs. (7.2) and (7.3) agree with the Taylor expansion of stress presented in (Chillara and Lissenden, 2016) when the deformation is small.

7.2.1 Primary longitudinal wave
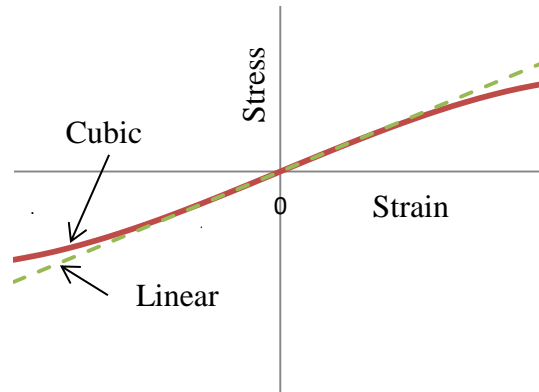
Fig. 7.1 Linear stress-strain relation and stress-strain curve for cubic nonlinearity under tension and compression

The stress-strain relation for pure longitudinal deformation follows from Eq. (7.2) as

$$\tau_{xx} = (\lambda + 2\mu)\frac{\partial u}{\partial x} + 4(F + H + E + G)\left(\frac{\partial u}{\partial x}\right)^3 \quad (7.4)$$

where the fourth order elastic constants E, F, G and H are defined as negative quantities, which indicates a softening effect. A symmetric stress-strain relation has

been obtained by neglecting the quadratic material nonlinearity, see Fig. 7.1. The second harmonics caused by the quadratic material nonlinearity have disappeared.

For the problem at hand, the equation of motion is

$$\frac{\partial \tau_{xx}}{\partial x} = \rho \frac{\partial^2 u}{\partial t^2} \tag{7.5}$$

Substituting Eq. (7.4) into Eq. (7.5), we obtain

$$\rho \frac{\partial^2 u}{\partial t^2} - (\lambda + 2\mu) \frac{\partial^2 u}{\partial x^2} = F_L \tag{7.6}$$

where the nonlinear term F_L is given by

$$F_L = 12(F + H + E + G) \left(\frac{\partial u}{\partial x} \right)^2 \frac{\partial^2 u}{\partial x^2} \tag{7.7}$$

Making use of the perturbation method, the displacement can be expanded as

$$u = u^{(0)} + u^{(1)} + \cdots \tag{7.8}$$

where we assume $\left| u^{(0)} \right| \gg \left| u^{(0)} \right|^3$. Substitution of Eqs. (7.8) into Eqs. (7.6) gives rise to the following equations

$$\rho \frac{\partial^2 u^{(0)}}{\partial t^2} - (\lambda + 2\mu) \frac{\partial^2 u^{(0)}}{\partial x^2} = 0 \tag{7.9}$$

$$\rho \frac{\partial^2 u^{(1)}}{\partial t^2} - (\lambda + 2\mu) \frac{\partial^2 u^{(1)}}{\partial x^2} = F_L^{(1)} \tag{7.10}$$

where

$$F_L^{(1)} = 12(F + H + E + G) \left(\frac{\partial u^{(0)}}{\partial x} \right)^2 \frac{\partial^2 u^{(0)}}{\partial x^2} \tag{7.11}$$

For the homogeneous equation (7.9), we have the longitudinal wave solution, which is given in the following form:

$$u^{(0)} = U \cos[\omega(t - \frac{x}{c_L})] \tag{7.12}$$

where U is a constant and $c_L = \sqrt{(\lambda + 2\mu)/\rho}$ is the longitudinal wave velocity. Substituting Eq. (7.12) into Eqs. (7.11), we obtain

$$F_L^{(1)} = 3(F + H + E + G)\frac{\omega^4}{c_L^4}U^3\left\{\cos[3\omega(t - \frac{x}{c_L})] - \cos[\omega(t - \frac{x}{c_L})]\right\} \tag{7.13}$$

In view of Eq. (7.13), evaluation of Eq. (7.10) yields the resonant harmonic

$$u^{(1)} = \frac{1}{2}\kappa_L\frac{\omega^3}{c_L^3}U^3 x\left\{\sin[3\omega(t - \frac{x}{c_L})] - 3\sin[\omega(t - \frac{x}{c_L})]\right\} \tag{7.14}$$

where the nonlinear tensile coefficient is defined by

$$\kappa_L = \frac{F + H + E + G}{\lambda + 2\mu} \tag{7.15}$$

7.2.2   Primary transverse wave

The stress-strain relation for transverse deformation can be obtained from Eq. (7.3) as

$$\tau_{xy} = \mu\frac{\partial v}{\partial x} + G\left(\frac{\partial v}{\partial x}\right)^3 \tag{7.16}$$

Equation (7.16) indicates that the nonlinear shear stress is symmetric with respect to the origin. The equation of motion for the transverse wave is given by

$$\frac{\partial \tau_{xy}}{\partial x} = \rho\frac{\partial^2 v}{\partial t^2} \tag{7.17}$$

Substitution of Eq. (7.16) into Eq. (7.17) yields

$$\rho\frac{\partial^2 v}{\partial t^2} - \mu\frac{\partial^2 v}{\partial x^2} = F_T \tag{7.18}$$

where

$$F_T = 3G\left(\frac{\partial v}{\partial x}\right)^2 \frac{\partial^2 v}{\partial x^2} \tag{7.19}$$

By taking the perturbation method, the displacement is expanded as

$$v = v^{(0)} + v^{(1)} + \cdots \tag{7.20}$$

where $\left|v^{(0)}\right| >> \left|v^{(0)}\right|^3$ is satisfied. Substituting Eq. (7.20) into Eq. (7.18), we get

$$\rho \frac{\partial^2 v^{(0)}}{\partial t^2} - \mu \frac{\partial^2 v^{(0)}}{\partial x^2} = 0 \tag{7.21}$$

$$\rho \frac{\partial^2 v^{(1)}}{\partial t^2} - \mu \frac{\partial^2 v^{(1)}}{\partial x^2} = F_T^{(1)} \tag{7.22}$$

where

$$F_T^{(1)} = 3G\left(\frac{\partial v^{(0)}}{\partial x}\right)^2 \frac{\partial^2 v^{(0)}}{\partial x^2} \tag{7.23}$$

The primary transverse wave solution to Eq. (7.21) can be taken as

$$v^{(0)} = V \cos[\omega(t - \frac{x}{c_T})] \tag{7.24}$$

where V is a constant and $c_T = \sqrt{\mu/\rho}$ is the shear wave velocity. Substitution of Eq. (7.24) into Eq. (7.23) gives rise to

$$F_T^{(1)} = \frac{3}{2}G\frac{\omega^4}{c_T^4}V^3\left\{\cos[3\omega(t - \frac{x}{c_T})] - \cos[\omega(t - \frac{x}{c_T})]\right\} \tag{7.25}$$

By virtue of Eq. (7.25), evaluation of Eq. (7.22) yields the resonant harmonic

$$v^{(1)} = \frac{1}{4}\kappa_T \frac{\omega^3}{c_T^3}V^3 x \sin[3\omega(t - \frac{x}{c_T})] - \frac{3}{2}\kappa_T \frac{\omega^3}{c_T^3}V^3 x \sin[\omega(t - \frac{x}{c_T})] \tag{7.26}$$

where the nonlinear shear coefficient is defined by

$$\kappa_T = \frac{G}{\mu} \qquad (7.27)$$

Equations (7.14) and (7.26) show that the first and third longitudinal and transverse harmonics depend on the nonlinear tensile coefficient κ_L and the nonlinear shear coefficient κ_T, respectively. The nonlinear tensile coefficient is the sum of all four fourth order elastic constants, while the nonlinear shear coefficient only depends on one fourth order elastic constant, G. The amplitudes of the higher harmonics, Eqs. (7.14) and (7.26), increase linearly with the propagation distance.

7.3 Generation of compensatory waves at the interface
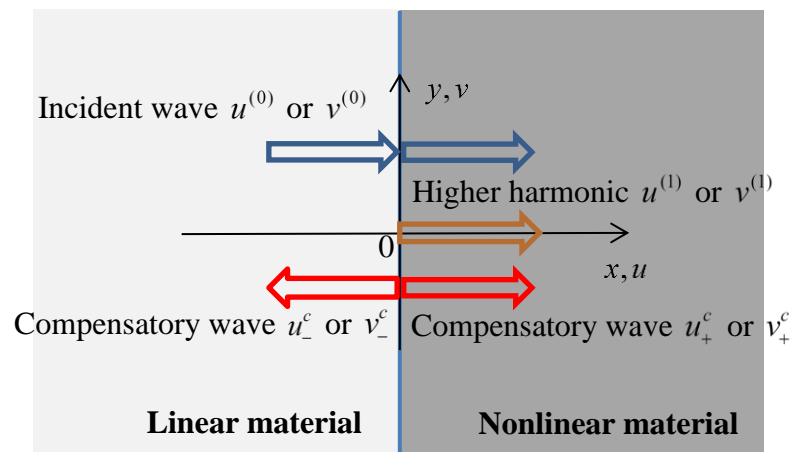
Fig. 7.2 Compensatory wave generation at an interface between a linear and a nonlinear material

Due to the strong correlation of microstructural damage with material nonlinearity, the generation of a higher harmonic has a potential applicability to the nondestructive evaluation of structures and materials. It is, however, desirable to develop a simple model, which can be easily used for practical purposes. If the region of nonlinear material is large, the model presented in Fig. 7.2 can be used to obtain the nonlinear material properties from a wave reflected by the interface. This model is suitable for the structures where the nonlinear region is not accessible. In this section, it is shown that the back-propagated wave is a compensatory wave which is introduced to meet the conditions of continuity of stress and strain at the

interface. The linear material properties (i.e. λ and μ) are assumed to be same across the whole body. The nonlinear material behavior only exists in the region for $x \geq 0$ where the micro damage has developed.

7.3.1 Incidence of a longitudinal wave

It can be checked that due to the generation of a higher harmonic for $x \geq 0$ the displacement and the stress are not automatically continuous when the incident wave reaches the interface connecting the regions of linear and nonlinear material. To obtain the required continuity, compensatory waves are proposed to compensate the continuity conditions at the interface.

For the incident longitudinal waves, the displacement fields on both sides of the interface at $x = 0$ are

$$u_- = u^{(0)} + u_-^c \qquad (7.28)$$

$$u_+ = u^{(0)} + u^{(1)} + u_+^c \qquad (7.29)$$

where the incident and harmonic waves were defined by Eqs. (7.12) and (7.14), respectively. The compensatory waves propagating in opposite directions are assumed to have the following forms

$$u_-^c = U_-^{c1} \cos[\omega(t + \frac{x}{c_L})] + U_-^{c3} \cos[3\omega(t + \frac{x}{c_L})] \qquad (7.30)$$

$$u_+^c = U_+^{c1} \cos[\omega(t - \frac{x}{c_L})] + U_+^{c3} \cos[3\omega(t - \frac{x}{c_L})] \qquad (7.31)$$

Since the linear waves can pass the interface without interference. The displacement field at $x = 0$ should meet the following continuity condition

$$u_-^c = u^{(1)} + u_+^c \qquad (7.32)$$

In view of Eqs. (7.14), (7.30) and (7.31), we obtain

$$U_-^{c1} = U_+^{c1}, \quad U_-^{c3} = U_+^{c3} \qquad (7.33)$$

For the continuity of stress at $x = 0$, we have

$$\frac{\partial u^{(1)}}{\partial x} + \frac{\partial u_+^c}{\partial x} + 4\kappa_L \left(\frac{\partial u^{(0)}}{\partial x} \right)^3 = \frac{\partial u_-^c}{\partial x} \tag{7.34}$$

Substitution of Eqs. (7.12), (7.14), (7.30) and (7.31) into Eq. (7.34) yields

$$-\frac{1}{2}\kappa_L \frac{\omega^3}{c_L^3} U^3 [\sin(3\omega t) - 3\sin(\omega t)] + \frac{\omega}{c_L} U_+^{c1} \sin(\omega t) + \frac{3\omega}{c_L} U_+^{c3} \sin(3\omega t)$$
$$= -\frac{\omega}{c_L} U_-^{c1} \sin(\omega t) - \frac{3\omega}{c_L} U_-^{c3} \sin(3\omega t) \tag{7.35}$$

The stresses with smaller amplitudes in Eq. (7.35) are omitted. The following decomposition relation has been used for the calculation in Eq. (7.35).

$$\sin^3(\omega t) = \frac{1}{4}[3\sin(\omega t) - \sin(3\omega t)] \tag{7.36}$$

In view of Eqs. (7.33) and (7.35), we obtain

$$U_-^{c3} = \frac{1}{12}\kappa_L \frac{\omega^2}{c_L^2} U^3, \quad U_-^{c1} = -\frac{3}{4}\kappa_L \frac{\omega^2}{c_L^2} U^3 \tag{7.37}$$

Using Eq. (7.37), the expressions of the compensatory waves can be given by

$$u_-^c = -\frac{3}{4}\kappa_L \frac{\omega^2}{c_L^2} U^3 \cos[\omega(t + \frac{x}{c_L})] + \frac{1}{12}\kappa_L \frac{\omega^2}{c_L^2} U^3 \cos[3\omega(t + \frac{x}{c_L})] \tag{7.38}$$

$$u_+^c = -\frac{3}{4}\kappa_L \frac{\omega^2}{c_L^2} U^3 \cos[\omega(t - \frac{x}{c_L})] + \frac{1}{12}\kappa_L \frac{\omega^2}{c_L^2} U^3 \cos[3\omega(t - \frac{x}{c_L})] \tag{7.39}$$

7.3.2   Incidence of a transverse wave

For an incident transverse wave, the total displacement fields in the negative and positive regions can be separately given by

$$v_- = v^{(0)} + v_-^c \tag{7.40}$$

$$v_+ = v^{(0)} + v^{(1)} + v_+^c \tag{7.41}$$

where the incident transverse wave and the generated harmonic wave were defined by Eqs. (7.24) and (7.26), respectively. The displacements of the compensatory waves are taken to have the following forms

$$v_-^c = V_-^{c1} \cos[\omega(t + \frac{x}{c_T})] + V_-^{c3} \cos[3\omega(t + \frac{x}{c_T})] \tag{7.42}$$

$$v_+^c = V_+^{c1} \cos[\omega(t - \frac{x}{c_T})] + V_+^{c3} \cos[3\omega(t - \frac{x}{c_T})] \tag{7.43}$$

In view of Eqs. (7.26), (7.40) and (7.41), the continuity of the displacement at $x = 0$ yields

$$v_-^c = v_+^c \tag{7.44}$$

Substituting Eqs. (7.42) and (7.43) into Eq. (7.44), we obtain

$$V_-^{c1} = V_+^{c1}, \quad V_-^{c3} = V_+^{c3} \tag{7.45}$$

The continuity of stress at the interface $x = 0$ gives rise to

$$\frac{\partial v^{(1)}}{\partial x} + \frac{\partial v_+^c}{\partial x} + \kappa_T \left(\frac{\partial v^{(0)}}{\partial x} \right)^3 = \frac{\partial v_-^c}{\partial x} \tag{7.46}$$

Substitution of Eqs. (7.24), (7.26), (7.42) and (7.43) into Eq. (7.46) yields

$$-\frac{1}{4}\kappa_T \frac{\omega^3}{c_T^3} V^3 \sin(3\omega t) + \frac{3}{4}\kappa_T \frac{\omega^3}{c_T^3} V^3 \sin(\omega t) + \frac{\omega}{c_T} V_+^{c1} \sin(\omega t) + \frac{3\omega}{c_T} V_+^{c3} \sin(3\omega t)$$
$$= -\frac{\omega}{c_T} V_-^{c1} \sin(\omega t) - \frac{3\omega}{c_T} V_-^{c3} \sin(3\omega t) \tag{7.47}$$

In view of Eqs. (7.45) and (7.47), we obtain

$$V_-^{c1} = -\frac{3}{8}\kappa_T \frac{\omega^2}{c_T^2} V^3, \quad V_-^{c3} = \frac{1}{24}\kappa_T \frac{\omega^2}{c_T^2} V^3 \tag{7.48}$$

In view of Eqs. (7.48), (7.42) and (7.43), the expressions of the compensatory waves can be expressed by

$$v_-^c = -\frac{3}{8}\kappa_T\frac{\omega^2}{c_T^2}V^3\cos[\omega(t+\frac{x}{c_T})] + \frac{1}{24}\kappa_T\frac{\omega^2}{c_T^2}V^3\cos[3\omega(t+\frac{x}{c_T})] \qquad (7.49)$$

$$v_+^c = -\frac{3}{8}\kappa_T\frac{\omega^2}{c_T^2}V^3\cos[\omega(t-\frac{x}{c_T})] + \frac{1}{24}\kappa_T\frac{\omega^2}{c_T^2}V^3\cos[3\omega(t-\frac{x}{c_T})] \qquad (7.50)$$

It is of interest to note that the amplitudes of the back-propagated compensatory waves given by Eqs. (7.38) and (7.49) contain the nonlinear material constants, κ_L and κ_T, respectively.

7.4 Backscattering from a small zone of cubic material nonlinearity
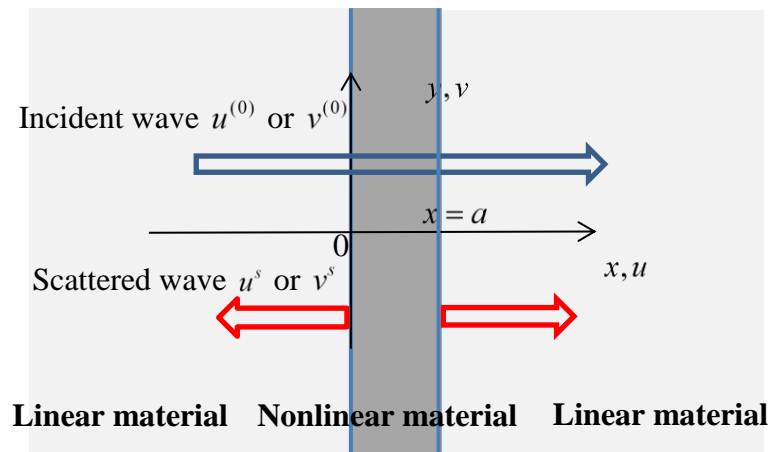
Fig. 7.3 Scattering of an incident wave from a small zone of cubic material nonlinearity

In this section, we assume the region of nonlinear material is small enough compared with the wavelength, which is defined by $0 \le x \le a$, see Fig. 7.3. For this case, the problem can be converted into a scattering problem, whereby the nonlinear term in the equations of motion is regarded as a body force. In the following, we will investigate the backscattering from a small zone of cubic material nonlinearity using the reciprocity theorem of elastodynamics.

7.4.1 Incidence of a longitudinal wave

A longitudinal wave, defined by Eq. (7.12), is incident on the region of nonlinear material behavior depicted in Fig. 7.3, and gives rise to a backscattered wave. The total displacement is represented by the superposition of the incident wave $u^{(0)}$ and the scattered wave u^s

$$u = u^{(0)} + u^s \tag{7.51}$$

where it is assumed that $|u^s| << |u^{(0)}|$. Using the perturbation method, we can obtain the equations governing scattering problem as

$$\rho \frac{\partial^2 u^s}{\partial t^2} - (\lambda + 2\mu) \frac{\partial^2 u^s}{\partial x^2} = 0, \quad x > a \text{ or } x < 0 \tag{7.52}$$

$$\rho \frac{\partial^2 u^s}{\partial t^2} - (\lambda + 2\mu) \frac{\partial^2 u^s}{\partial x^2} = F_L^{(1)}, \quad 0 \le x \le a \tag{7.53}$$

where the nonlinear term $F_L^{(1)}$ on the right-hand of Eq. (7.53) is defined by Eq. (7.11), which is in terms of the known incident wave. The inhomogeneous equation (7.53) remains a linear equation governing the scattered wave. The problem described by Eqs. (7.52) and (7.53) is suitable to be solved by the reciprocity theorem (Achenbach, 2003), where the nonlinear term in Eq. (7.53) is regarded as a body force. For the use of the reciprocity theorem, we rewrite the body force as a sum of exponential terms

$$F_L^{(1)} = f_1 + f_2 + f_3 + f_4 \tag{7.54}$$

where

$$f_1 = -\frac{3}{2}(\lambda + 2\mu)\kappa_L \frac{\omega^4}{c_L^4} U^3 e^{i\frac{\omega}{c_L}x} \cdot e^{-i\omega t} \tag{7.55}$$

$$f_2 = -\frac{3}{2}(\lambda + 2\mu)\kappa_L \frac{\omega^4}{c_L^4} U^3 e^{-i\frac{\omega}{c_L}x} \cdot e^{i\omega t} \tag{7.56}$$

$$f_3 = \frac{3}{2}(\lambda + 2\mu)\kappa_L \frac{\omega^4}{c_L^4} U^3 e^{i\frac{3\omega}{c_L}x} \cdot e^{-3i\omega t} \tag{7.57}$$

$$f_4 = \frac{3}{2}(\lambda + 2\mu)\kappa_L \frac{\omega^4}{c_L^4} U^3 e^{-i\frac{3\omega}{c_L}x} \cdot e^{3\omega t} \tag{7.58}$$

The body forces listed in Eq. (7.54) should be separated into two groups, namely, f_1, f_3 and f_2, f_4 in conjunction with the harmonic time terms $e^{-i\omega t}$ and $e^{i\omega t}$. The harmonic-time terms are omitted in the following calculation.
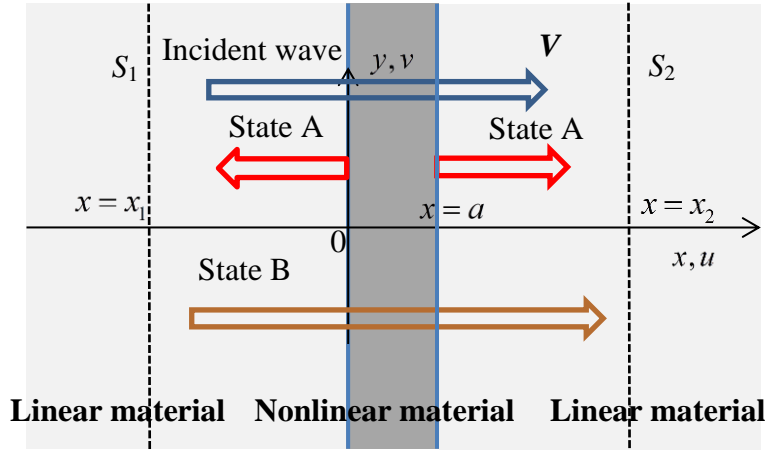
Fig. 7.4 Scattered and virtual waves for State A and State B

The reciprocity theorem is given by

$$\int_V (f_i^A u_i^B - f_i^B u_i^A)dV = \int_{S_1}(u_i^A \tau_{ij}^B - u_i^B \tau_{ij}^A)n_j dS + \int_{S_2}(u_i^A \tau_{ij}^B - u_i^B \tau_{ij}^A)n_j dS \tag{7.59}$$

where n_j is the component of the outward normal of the region. Equation (7.59) is an integration over a region V with boundary S which relates two waves labeled state A and state B, respectively. For the problem under consideration, we label the scattered wave as state A. For the configuration shown in Fig. 7.4, Eq. (7.59) can be simplified to

$$\int_l f^A u^B dl = -(u_s^A \tau_{xx}^B - u^B \tau_{xx}^A)_{x=x_1} + (u_s^A \tau_{xx}^B - u^B \tau_{xx}^A)_{x=x_2} \tag{7.60}$$

where the integral domain is defined by $x_1 \le x \le x_2$. Next we apply Eq. (7.60) to investigate backscattering from the body forces, defined by Eqs. (7.55)-(7.58).

For the body force f_1, state A can be defined as:

Body force:

$$f^A = -f_1 = \frac{3}{2}(\lambda + 2\mu)\kappa_L \frac{\omega^4}{c_L^4} U^3 e^{i\frac{\omega}{c_L}x}, \quad 0 \le x \le a \tag{7.61}$$

The forward scattered wave is defined by

$$x \gg a : \; u_s^A = A_s e^{i\frac{\omega}{c_L}x}, \; \tau_{xx}^A = (\lambda + 2\mu)\frac{\omega}{c_L} i A_s e^{i\frac{\omega}{c_L}x} \tag{7.62}$$

where A_s is the amplitude of the scattered wave.

Backscattered wave:

$$x \ll 0 : \; u_s^A = A_s e^{-i\frac{\omega}{c_L}x}, \; \tau_{xx}^A = -(\lambda + 2\mu)\frac{\omega}{c_L} i A_s e^{-i\frac{\omega}{c_L}x} \tag{7.63}$$

To use the reciprocity theorem, we have to select a virtual wave for state B, which is a longitudinal wave propagating along *x*-direction. This wave is a free wave which is independent of the problem under consideration. That is to say there's no body force for the virtual wave. State B can be defined as:

Body force:

$$f^B = 0 \tag{7.64}$$

Virtual wave:

$$u^B = A_v e^{i\frac{\omega_v}{c_L}x}, \; \tau_{xx}^B = (\lambda + 2\mu)\frac{\omega_v}{c_L} i A_v e^{i\frac{\omega_v}{c_L}x} \tag{7.65}$$

Substituting Eqs. (7.61)-(7.65) into Eq. (7.60) yields

$$\int_0^a \left(\frac{3}{2}(\lambda+2\mu)\kappa_L \frac{\omega^4}{c_L^4} U^3 e^{i\frac{\omega}{c_L}x} \right) A_v e^{i\frac{\omega_v}{c_L}x} dx =$$

$$-\left(A_s e^{-i\frac{\omega}{c_L}x_1} (\lambda+2\mu)\frac{\omega_v}{c_L} iA_v e^{i\frac{\omega_v}{c_L}x_1} + A_v e^{i\frac{\omega_v}{c_L}x_1} (\lambda+2\mu)\frac{\omega}{c_L} iA_s e^{-i\frac{\omega}{c_L}x_1} \right) \quad (7.66)$$

$$+\left(A_s e^{i\frac{\omega}{c_L}x_2} (\lambda+2\mu)\frac{\omega_v}{c_L} iA_v e^{i\frac{\omega_v}{c_L}x_2} - A_v e^{i\frac{\omega_v}{c_L}x_2} (\lambda+2\mu)\frac{\omega}{c_L} iA_s e^{i\frac{\omega}{c_L}x_2} \right)$$

The frequency of the virtual wave is selected as

$$\omega_v = \omega \qquad (7.67)$$

Then, Eq. (7.66) reduces to

$$\int_0^a A_v \frac{3}{2}(\lambda+2\mu)\kappa_L \frac{\omega^4}{c_L^4} U^3 e^{i\frac{2\omega}{c_L}x} dx = -2(\lambda+2\mu)\frac{\omega}{c_L} iA_v A_s \qquad (7.68)$$

It is evident from Eqs. (7.66) and (7.68) that the third set of terms vanishes and that the interaction of the virtual wave and the scattered wave only yield a contribution when they propagate in opposite directions, as shown by the second set of terms in Eq. (7.66). Evaluation of Eq. (7.68) then yields the amplitude of the backscattered wave as follows

$$A_s = \frac{3}{8}\kappa_L \frac{\omega^4}{c_L^4} U^3 \frac{c_L^2}{\omega^2} \left(e^{i\frac{2\omega}{c_L}a} - 1 \right) \qquad (7.69)$$

Substituting Eq. (7.69) into Eq. (7.63) and adding the time term $e^{-i\omega t}$, the full expression of the backscattered wave can be rewritten as

$$u_s^A = i\frac{3}{4}\kappa_L \frac{\omega^4}{c_L^4} U^3 \frac{c_L^2}{\omega^2} \sin(\frac{\omega}{c_L}a)e^{-i\omega(t+\frac{x-a}{c_L})} \qquad (7.70)$$

For the body force f_3, we have

$$f^A = -f_3 = -\frac{3}{2}(\lambda+2\mu)\kappa_L \frac{\omega^4}{c_L^4} U^3 e^{i\frac{3\omega}{c_L}x}, \quad 0 \le x \le a \qquad (7.71)$$

The same procedure is used to obtain the backscattered wave as

$$u_s^A = -i\frac{1}{12}\kappa_L \frac{\omega^2}{c_L^2} U^3 \sin(\frac{3\omega}{c_L}a)e^{-i3\omega(t+\frac{x-a}{c_L})} \tag{7.72}$$

For the body force f_2, state A can be defined as:

Body force:

$$f^A = -f_2 = \frac{3}{2}(\lambda+2\mu)\kappa_L \frac{\omega^4}{c_L^4} U^3 e^{-i\frac{\omega}{c_L}x}, \quad 0 \le x \le a \tag{7.73}$$

Forward scattered wave:

$$x \gg a: \ u_s^A = A_s e^{-i\frac{\omega}{c_L}x}, \ \tau_{xx}^A = -(\lambda+2\mu)\frac{\omega}{c_L}iA_s e^{-i\frac{\omega}{c_L}x} \tag{7.74}$$

Backscattered wave:

$$x \ll 0: \ u_s^A = A_s e^{i\frac{\omega}{c_L}x}, \ \tau_{xx}^A = (\lambda+2\mu)\frac{\omega}{c_L}iA_s e^{i\frac{\omega}{c_L}x} \tag{7.75}$$

State B can be defined as:

Body force:

$$f^B = 0 \tag{7.76}$$

Virtual wave:

$$u^B = A_v e^{-i\frac{\omega}{c_L}x}, \ \tau_{xx}^B = -(\lambda+2\mu)\frac{\omega}{c_L}iA_v e^{-i\frac{\omega}{c_L}x} \tag{7.77}$$

Substitution of Eqs. (7.73)-(7.77) into Eq. (7.60) yields

$$\int_0^a \frac{3}{2}(\lambda+2\mu)\kappa_L \frac{\omega^4}{c_L^4} U^3 A_v e^{-2i\frac{\omega}{c_L}x} dx = 2(\lambda+2\mu)\frac{\omega}{c_L}iA_v A_s \tag{7.78}$$

Evaluation of Eq. (7.78) yields

$$A_s = \frac{3}{8}\kappa_L \frac{\omega^4}{c_L^4} U^3 \frac{c_L^2}{\omega^2}\left(e^{-2i\frac{\omega}{c_L}a} - 1 \right) \tag{7.79}$$

Substituting Eq. (7.79) into Eq. (7.75) and adding the time term $e^{i\omega t}$, the full expression of the backscattered wave is given by

$$u_s^A = -i\frac{3}{4}\kappa_L \frac{\omega^4}{c_L^4} U^3 \frac{c_L^2}{\omega^2}\sin(\frac{\omega}{c_L}a)e^{i\omega(t+\frac{x-a}{c_L})} \tag{7.80}$$

For the body force f_4, we have

$$f^A = -f_4 = -\frac{3}{2}(\lambda+2\mu)\kappa_L \frac{\omega^4}{c_L^4}U^3 e^{-i\frac{3\omega}{c_L}x}, \quad 0 \le x \le a \tag{7.81}$$

Making use of Eq. (7.81), the backscattered wave is obtained as

$$u_s^A = i\frac{1}{12}\kappa_L \frac{\omega^2}{c_L^2}U^3 \sin(\frac{3\omega}{c_L}a)e^{i3\omega(t+\frac{x-a}{c_L})} \tag{7.82}$$

Summation of Eqs. (7.70), (7.72), (7.80) and (7.82) yields the total displacement of the backscattered wave as

$$u_s^A = -\frac{3}{4}\kappa_L \frac{\omega^2}{c_L^2}U^3 \sin(\frac{\omega}{c_L}a)\left[ie^{i\omega(\frac{x-a}{c_L}+t)} - ie^{-i\omega(\frac{x-a}{c_L}+t)}\right]$$
$$+\frac{1}{12}\kappa_L \frac{\omega^2}{c_L^2}U^3 \sin(\frac{3\omega}{c_L}a)\left[ie^{i3\omega(\frac{x-a}{c_L}+t)} - ie^{-i3\omega(\frac{x-a}{c_L}+t)}\right] \tag{7.83}$$

Equation (7.83) can be further simplified to

$$u_s = \frac{3}{2}\kappa_L \frac{\omega^2}{c_L^2}U^3 \sin(\frac{\omega}{c_L}a)\sin[\omega(\frac{x-a}{c_L}+t)]$$
$$-\frac{1}{6}\kappa_L \frac{\omega^2}{c_L^2}U^3 \sin(\frac{3\omega}{c_L}a)\sin[3\omega(\frac{x-a}{c_L}+t)] \tag{7.84}$$

7.4.2   Incidence of a transverse wave

In this section, the scattering of a transverse wave by the inclusion of nonlinear material is investigated. In the usual manner, the total displacement field is

$$v = v^{(0)} + v^s \tag{7.85}$$

where $v^{(0)}$ represents the incident wave, which was defined by Eq. (7.24), and v^s represents the scattered transverse wave. Here it is assumed that $\left|v^s\right| << \left|v^{(0)}\right|$. Substituting Eq. (7.85) into the displacement equation of motion Eq. (7.18), the equations governing the scattering problem are obtained as

$$\rho \frac{\partial^2 v^s}{\partial t^2} - \mu \frac{\partial^2 v^s}{\partial x^2} = 0, \quad x > a \text{ or } x < 0 \tag{7.86}$$

$$\rho \frac{\partial^2 v^s}{\partial t^2} - \mu \frac{\partial^2 v^s}{\partial x^2} = F_T^{(1)}, \quad 0 \le x \le a \tag{7.87}$$

where the nonlinear term $F_T^{(1)}$ in Eq. (7.87) is defined by Eq. (7.25), which can be rewritten as

$$F_T^{(1)} = f_1 + f_2 + f_3 + f_4 \tag{7.88}$$

where

$$f_1 = -\frac{3}{4}\mu\kappa_T \frac{\omega^4}{c_T^4} V^3 e^{i\frac{\omega}{c_T}x} \cdot e^{-i\omega t} \tag{7.89}$$

$$f_2 = -\frac{3}{4}\mu\kappa_T \frac{\omega^4}{c_T^4} V^3 e^{-i\frac{\omega}{c_T}x} \cdot e^{i\omega t} \tag{7.90}$$

$$f_3 = \frac{3}{4}\mu\kappa_T \frac{\omega^4}{c_T^4} V^3 e^{i\frac{3\omega}{c_T}x} \cdot e^{-i3\omega t} \tag{7.91}$$

$$f_4 = \frac{3}{4}\mu\kappa_T \frac{\omega^4}{c_T^4} V^3 e^{-i\frac{3\omega}{c_T}x} \cdot e^{i3\omega t} \tag{7.92}$$

The reciprocity theorem can be used to calculate the backscattered wave. The procedure is analogous to the one used in Section 7.4.1. The detailed derivation is not given here. The total scattered displacement is obtained as:

$$v_s = \frac{3}{4} \kappa_T \frac{\omega^2}{c_T^2} V^3 \sin(\frac{\omega}{c_T} a) \sin[\omega(t + \frac{x-a}{c_T})]$$

$$-\frac{1}{12} \kappa_T \frac{\omega^2}{c_T^2} V^3 \sin(\frac{3\omega}{c_T} a) \sin[3\omega(t + \frac{x-a}{c_T})] \qquad (7.93)$$

The advantage of the scattering model of this section is that the amplitudes of the backscattered waves not only depend on the nonlinear material constants but also on the length of the nonlinear region.

7.5 Determination of the backscattered wave based on the compensatory wave model
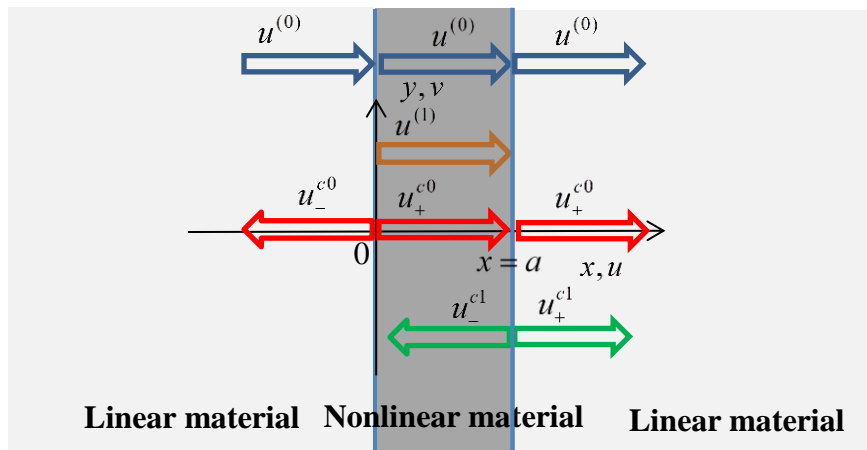
Fig. 7.5 Compensatory waves generated by the two interfaces of a strip of nonlinear material between regions of linear material

In an alternative approach, the compensatory waves generated by a first and second interface are determined. In this approach, the back-propagated wave is the superposition of two compensatory waves generated by the interfaces at $x = 0$ and $x = a$ shown in Fig. 7.5. The solution to the compensatory waves generation at the first interface ($x = 0$) has been given in Section 7.3.

When the incident longitudinal wave and the higher harmonic reach the second interface ($x = a$), see Fig. 7.5, the total displacements for $x < a$ and $x > a$ of the interface are

$$u_- = u^{(0)} + u^{(1)} + u_+^{c0} + u_-^{c1} \tag{7.94}$$

$$u_+ = u^{(0)} + u_+^{c0} + u_+^{c1} \tag{7.95}$$

where the incident wave and the higher harmonic are defined by Eqs. (7.12) and (7.14), respectively. The compensatory waves propagating in opposite directions are taken to have the following form

$$u_-^{c1} = U_-^{c1} \cos[\omega(t - \frac{a}{c_L} + \frac{x-a}{c_L})] + U_-^{c3} \cos[3\omega(t - \frac{a}{c_L} + \frac{x-a}{c_L})] \tag{7.96}$$

$$\begin{aligned} u_+^{c1} = &U_+^{c1} \cos[\omega(t - \frac{a}{c_L} - \frac{x-a}{c_L})] + U_+^{c3} \cos[3\omega(t - \frac{a}{c_L} - \frac{x-a}{c_L})] \\ &+ \bar{U}_+^{c1} \sin[\omega(t - \frac{a}{c_L} - \frac{x-a}{c_L})] + \bar{U}_+^{c3} \sin[3\omega(t - \frac{a}{c_L} - \frac{x-a}{c_L})] \end{aligned} \tag{7.97}$$

The last two terms in Eq. (7.97) are introduced to cancel the displacements of the harmonic waves, which is a different condition from the first interface at $x=0$ where the displacements of the harmonic waves is zero, see the expression of Eq. (7.14). In view of Eqs. (7.94) and (7.95), the displacement field on both sides of the interface at $x=a$ should meet the following continuity condition

$$u^{(1)}(a) + u_-^{c1}(a) = u_+^{c1}(a) \tag{7.98}$$

Substitution of Eqs. (7.14), (7.96) and (7.97) into Eq. (7.98) gives

$$\begin{aligned} &\frac{a}{2} \kappa_L \frac{\omega^3}{c_L^3} U^3 \sin[3\omega(t - \frac{a}{c_L})] - \frac{a}{2} \kappa_L \frac{\omega^3}{c_L^3} U^3 3\sin[\omega(t - \frac{a}{c_L})] \\ &\quad + U_-^{c1} \cos[\omega(t - \frac{a}{c_L})] + U_-^{c3} \cos[3\omega(t - \frac{a}{c_L})] \\ &= U_+^{c1} \cos[\omega(t - \frac{a}{c_L})] + U_+^{c3} \cos[3\omega(t - \frac{a}{c_L})] \\ &\quad + \bar{U}_+^{c1} \sin[\omega(t - \frac{a}{c_L})] + \bar{U}_+^{c3} \sin[3\omega(t - \frac{a}{c_L})] \end{aligned} \tag{7.99}$$

Equation (7.99) is satisfied by

$$U_-^{c1} = U_+^{c1}, \quad U_-^{c3} = U_+^{c3}$$

$$\bar{U}_+^{c3} = \frac{a}{2}\kappa_L \frac{\omega^3}{c_L^3}U^3, \quad \bar{U}_+^{c1} = -\frac{3a}{2}\kappa_L \frac{\omega^3}{c_L^3}U^3 \qquad (7.100)$$

For the equality of stress at $x = a$, we obtain

$$\frac{\partial u^{(1)}}{\partial x} + \frac{\partial u_-^{c1}}{\partial x} + 4\kappa_L\left(\frac{\partial u^{(0)}}{\partial x}\right)^3 = \frac{\partial u_+^{c1}}{\partial x} \qquad (7.101)$$

In view of Eqs. (7.12), (7.14), (7.96) and (7.97), Eq. (7.101) can be rewritten as

$$\frac{1}{2}\kappa_L\frac{\omega^3}{c_L^3}U^3\sin[3\omega(t-\frac{a}{c_L})] - \frac{3}{2}\kappa_L\frac{\omega^3}{c_L^3}U^3\sin[\omega(t-\frac{a}{c_L})]$$

$$-\frac{3a}{2}\kappa_L\frac{\omega^4}{c_L^4}U^3\cos[3\omega(t-\frac{a}{c_L})] + \frac{3a}{2}\kappa_L\frac{\omega^4}{c_L^4}U^3\cos[\omega(t-\frac{a}{c_L})]$$

$$+4\kappa_L\left(\frac{3}{4}\frac{\omega^3}{c_L^3}U^3\sin[\omega(t-\frac{a}{c_L})] - \frac{1}{4}\frac{\omega^3}{c_L^3}U^3\sin[3\omega(t-\frac{a}{c_L})]\right) \qquad (7.102)$$

$$= \frac{6\omega}{c_L}U_-^{c3}\sin[3\omega(t-\frac{a}{c_L})] + 2\frac{\omega}{c_L}U_-^{c1}\sin[\omega(t-\frac{a}{c_L})]$$

$$-\frac{3a}{2}\kappa_L\frac{\omega^4}{c_L^4}U^3\cos[3\omega(t-\frac{a}{c_L})] + \frac{3a}{2}\kappa_L\frac{\omega^4}{c_L^4}U^3\cos[\omega(t-\frac{a}{c_L})]$$

where Eq. (7.36) has been used. Using Eq. (7.100), evaluation of Eq. (7.102) yields

$$U_-^{c3} = -\frac{1}{12}\kappa_L\frac{\omega^2}{c_L^2}U^3, \quad U_-^{c1} = \frac{3}{4}\kappa_L\frac{\omega^2}{c_L^2}U^3 \qquad (7.103)$$

Substituting Eq. (7.103) into Eq. (7.96), the expression of the back-propagated longitudinal compensatory wave is obtained as

$$u_-^{c1} = \frac{3}{4}\kappa_L\frac{\omega^2}{c_L^2}U^3\cos[\omega(t-\frac{a}{c_L}+\frac{x-a}{c_L})] - \frac{1}{12}\kappa_L\frac{\omega^2}{c_L^2}U^3\cos[3\omega(t-\frac{a}{c_L}+\frac{x-a}{c_L})]$$

$$(7.104)$$

The summation of Eqs. (7.38) and (7.104) gives the full expression of the displacement of the back-propagated longitudinal waves as follows

$$u_-^c = u_-^{c0} + u_-^{c1}$$

$$= -\frac{3}{4}\kappa_L \frac{\omega^2}{c_L^2} U^3 \cos[\omega(t+\frac{x}{c_L})] + \frac{1}{12}\kappa_L \frac{\omega^2}{c_L^2} U^3 \cos[3\omega(t+\frac{x}{c_L})]$$

$$+ \frac{3}{4}\kappa_L \frac{\omega^2}{c_L^2} U^3 \cos[\omega(t-\frac{a}{c_L}+\frac{x-a}{c_L})] - \frac{1}{12}\kappa_L \frac{\omega^2}{c_L^2} U^3 \cos[3\omega(t-\frac{a}{c_L}+\frac{x-a}{c_L})] \quad (7.105)$$

$$= \frac{3}{2}\kappa_L \frac{\omega^2}{c_L^2} U^3 \sin(\frac{a\omega}{c_L}) \sin[\omega(t+\frac{x-a}{c_L})] - \frac{1}{6}\kappa_L \frac{\omega^2}{c_L^2} U^3 \sin(\frac{3a\omega}{c_L}) \sin[3\omega(t+\frac{x-a}{c_L})]$$

The expressions for the back-propagated waves given by Eqs. (7.84) and (7.105) are of the same form, which shows the validity of obtaining the back-propagated wave using the two approaches. In comparing the two methods presented in Sections 7.4 and 7.5, the reciprocity theorem has an advantage over the method used in Section 7.5. When the geometry of the inclusion of nonlinear material becomes more complicated, the reciprocity theorem has greater utility.

7.6 Conclusions

Based on the generation of higher harmonics by cubically nonlinear material behavior, the results of this paper may have utility for the detection of micro damage in materials, which is often caused by fatigue and plasticity. The constitutive model of cubic nonlinearity is symmetric with respect to the tension and compression, which is an advantage over the quadratic model. In an unbounded solid, the analytical solutions to the cumulative first and third harmonics generated by plane elastic waves have been obtained in this paper. Two simple models have been proposed to determine the nonlinear elastic constants (i.e. the fourth order elastic constants). When the region of nonlinear material behavior is large, the interface between the perfectly joined regions of linear and nonlinear material behavior yields very useful information. Compensatory waves are introduced to meet the continuity of stress and displacement at the interface in conjunction with higher harmonics. The amplitudes of back-propagated compensatory waves depend on the fourth order elastic constants. For a nonlinear inclusion, the nonlinear body force induced by the material nonlinearity generates a backscattered wave. The reciprocity theorem of elastodynamics was used to obtain the analytical solution to the backscattered wave. The amplitude of the backscattered wave depends on the nonlinear material

constants and the size of the inclusion. In addition, compensatory waves which are generated when the incident waves and higher harmonics have multiple interactions with the two interfaces have been investigated. The total back-propagated waves can be represented by the superposition of all back-propagated compensatory waves. Agreement of the expression of backscattered waves with the back-propagated compensatory waves shows that both methods are of equal utility. It should, however, be noted that the use of the reciprocity theorem has greater utility for more complicated configurations of the inclusion.

Chapter 8 The effect of cubic material nonlinearity on the propagation of torsional wave modes in a pipe

8.1 Introduction

Due to their efficiency and sensitivity, ultrasonic guided waves are widely used in nondestructive testing to detect defects in pipes. They can be used to inspect the whole cross sectional area for long distances, including inaccessible zones. There are three kinds of wave mode in pipes, torsional modes, longitudinal modes and flexural modes. The lowest axially symmetric torsional mode is most frequently selected as an incident wave for many tests due to its simple wave structure and low interference with the surroundings. Ratassepp et al. (2010) investigated the scattering of the lowest axially symmetric torsional wave mode by an axial crack in a pipe using a finite element simulation and experimental results. A study of the reflection of the lowest torsional wave from two or three small holes in pipes was presented by Løvstad and Cawley (2011). For a practical application, Rose et al. (1994) explored the use of guided waves to increase the efficiency and sensitivity of nuclear steam generator tubing evaluation. They also introduced a guided ultrasonic nondestructive system to rapidly detect and quantify the reduction of wall thickness caused by corrosion (Rose et al., 1996).

The references mentioned above are concerned with the interaction of guided waves with macroscopic defects, such as holes, cracks and thickness reduction. It is, however, also desirable to develop a technique to detect the deterioration of material properties, which can provide an early warning of possible structural failure. In this context, the use of higher harmonics was proven to be efficient for sensing microstructural changes of material properties (Hikata et al., 1965; Hikata et al., 1966).

This work provides new results for the propagation of guided waves in a pipe of cubic material nonlinearity, which may be caused by material deterioration. This chapter is split into two parts. The first part deals with the propagation of the lowest

axially symmetric torsional wave mode in a pipe, where the material of the whole pipe is of cubic nonlinearity. It is shown that such a material generates a third harmonic, but also a first harmonic. Using a perturbation method, analytical expressions of the first and third cumulative harmonics have been obtained. It is perhaps surprising that cubic nonlinearity gives rise to a harmonic whose frequency is the same as for the primary wave but whose amplitude increases linearly with propagation distance.

The different condition for the second part is that only a small region of the pipe is nonlinear, which leads to a scattering problem. The nonlinear term in the governing equation of motion is regarded as a distribution of body forces. We employ the elastodynamic reciprocity theorem to obtain an analytical expression for the backscattered wave. The amplitude of the scattered wave is determined by the nonlinearity coefficient, the size of the nonlinear domain and the geometry of the pipe. Due to the weakness of the scattered waves, we use another wave of higher frequency in combination with the primary wave to increase the overall amplitude. An example whereby the originally scattered wave is amplified by a factor of 50 is presented.

8.2   Governing equations
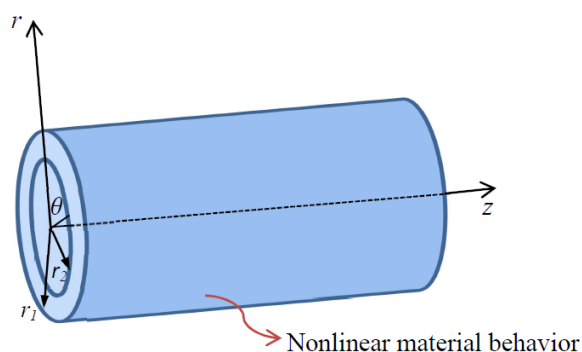
Fig. 8.1 The geometry of a pipe and corresponding coordinate system

In this paper, we consider the propagation of torsional waves in a pipe. The geometry and corresponding coordinate system $\{r, \theta, z\}$ are shown in Fig. 8.1, where r_1 and r_2 are the outer and inner radii of the pipe, respectively.

For time harmonic axially symmetric purely torsional waves propagating in the z-direction, the single displacement component is

$$v(r,z,t) = \overline{v}(r)e^{ik(z-ct)} \tag{8.1}$$

where c is the phase velocity and $\omega = kc$. The corresponding stress components are

$$\tau_{r\theta} = \overline{\tau}_{r\theta}e^{ik(z-ct)} \tag{8.2}$$

where

$$\overline{\tau}_{r\theta} = \mu\left(\frac{d\overline{v}}{dr} - \frac{\overline{v}}{r}\right) \tag{8.3}$$

and

$$\tau_{z\theta} = \overline{\tau}_{z\theta}e^{ik(z-ct)} \tag{8.4}$$

where

$$\overline{\tau}_{z\theta} = ik\mu\overline{v} \tag{8.5}$$

The stress equation of motion is

$$\frac{\partial \tau_{r\theta}}{\partial r} + \frac{\partial \tau_{z\theta}}{\partial z} + \frac{2}{r}\tau_{r\theta} = \rho\frac{\partial^2 v}{\partial t^2} \tag{8.6}$$

Substitution of Eqs. (8.1), (8.2) and (8.4) into Eq. (8.6) yields the displacement equation of motion

$$\frac{d^2\overline{v}}{dr^2} + \frac{1}{r}\frac{d\overline{v}}{dr} - \frac{\overline{v}}{r^2} - k^2\overline{v} = -k^2c^2\frac{\rho}{\mu}\overline{v} \tag{8.7}$$

The general solution of this equation is

$$\overline{v} = \frac{1}{q}\left[C_J J_1(qr) + C_Y Y_1(qr)\right] \tag{8.8}$$

where J_1 and Y_1 are Bessel functions of the first and second kind, respectively, C_J and C_Y are constants, and

$$q^2 = \frac{\omega^2}{c_T^2} - k^2, \quad c_T^2 = \frac{\mu}{\rho} \tag{8.9}$$

By a careful limiting process, it can be shown that for $q = 0$, Eq. (8.8) reduces to

$$\bar{v} = \frac{1}{2}Ar, \quad \bar{\tau}_{r\theta} = 0 \quad \text{and} \quad \bar{\tau}_{z\theta} = ik\mu\frac{1}{2}Ar \tag{8.10}$$

where A is a constant. Equation (8.10$_1$) defines the lowest axially symmetric torsional mode. It can be checked that Eq. (8.10$_1$) satisfies the displacement equation of motion (8.7), provided that

$$k^2\bar{v} = \frac{k^2c^2}{c_T^2}\bar{v}, \quad \text{i.e.,} \quad c = c_T \tag{8.11}$$

The set of governing equations can now be extended to the case of nonlinearity in the constitutive relation. In this paper, we select the displacement as $\mathbf{U} = \{0,\ v,\ 0\}$ for pure shear deformation of a pipe. For the case of axial symmetry, small deformations and nonlinear material behavior and omitting quadratic terms, the expressions for $\tau_{r\theta}$ and $\tau_{\theta z}$ follow from the relations presented in the Appendix 4A in Chapter 4 as

$$\tau_{r\theta} = \mu\left(\frac{\partial v}{\partial r} - \frac{v}{r}\right) + G\left(\frac{\partial v}{\partial r} - \frac{v}{r}\right)\left[\left(\frac{\partial v}{\partial r} - \frac{v}{r}\right)^2 + \left(\frac{\partial v}{\partial z}\right)^2\right] \tag{8.12}$$

$$\tau_{\theta z} = \mu\frac{\partial v}{\partial z} + G\left[\frac{\partial v}{\partial z}\left(\frac{\partial v}{\partial r} - \frac{v}{r}\right)^2 + \left(\frac{\partial v}{\partial z}\right)^3\right] \tag{8.13}$$

where G is the fourth order elastic coefficient. In view of Eqs. (8.1) and (8.10$_1$), we have $\partial v/\partial r - v/r = 0$ for the lowest axially symmetric torsional mode. Thus, Eqs. (8.12) and (8.13) can be further simplified to

$$\tau_{r\theta} = 0 \tag{8.14}$$

$$\tau_{\theta z} = \mu \frac{\partial v}{\partial z} + G\left(\frac{\partial v}{\partial z}\right)^3, \quad G < 0 \tag{8.15}$$

A stress-strain relation of the type Eq. (8.15) is shown in Fig. 1.7, together with a stress-strain relation of the quadratic type. This figure shows that, for both quadratic and cubic nonlinear behavior, a positive strain requires a smaller stress than for the linear stress-strain relation. On the other hand, for quadratic behavior, a negative strain requires a negative stress whose absolute value is larger than for the linear stress-strain relation. This behavior which happens for some materials is referred to as the strength differential effect, see Hirth and Cohen (1970), Gil et al. (1999) and Rauch and Leslie (1972) for the corresponding curves for tensile and compressive strain.

8.3 Higher harmonics

In this section, we study the lowest torsional wave mode propagating in a pipe considering cubic material nonlinearity, see Fig. 1. Substituting Eqs. (8.14) and (8.15) into the equation of motion (8.6), we obtain

$$\mu \frac{\partial^2 v}{\partial z^2} - \rho \frac{\partial^2 v}{\partial t^2} = f \tag{8.16}$$

where

$$f = -3G\left(\frac{\partial v}{\partial z}\right)^2 \frac{\partial^2 v}{\partial z^2} \tag{8.17}$$

Equation (8.16) is the displacement equation governing axially symmetric torsional waves propagating in a pipe. A solution of Eq. (8.16) can be obtained in the form

$$v = v^{(0)} + v^{(1)} \tag{8.18}$$

Substitution of Eq. (8.18) into Eq. (8.16) yields in the usual manner by assuming $\left|v^{(0)}\right| \gg \left|v^{(1)}\right|$ and $\left|v^{(0)}\right|^2 \propto \left|v^{(1)}\right|$

$$\mu \frac{\partial^2 v^{(0)}}{\partial z^2} - \rho \frac{\partial^2 v^{(0)}}{\partial t^2} = 0 \tag{8.19}$$

and

$$\mu \frac{\partial^2 v^{(1)}}{\partial z^2} - \rho \frac{\partial^2 v^{(1)}}{\partial t^2} = f[v^{(0)}] \tag{8.20}$$

where the right-hand side of Eq. (8.20) is

$$f[v^{(0)}] = -3G \left(\frac{\partial v^{(0)}}{\partial z} \right)^2 \frac{\partial^2 v^{(0)}}{\partial z^2} \tag{8.21}$$

The primary solution of Eq. (8.19) is now taken in the form

$$v^{(0)} = \frac{1}{2} A_0 r \cos(kz - \omega t) \tag{8.22}$$

Substitution of Eq. (8.22) into Eq. (8.21) yields

$$f[v^{(0)}] = 3G k^4 A_0^3 \left(\frac{1}{2} r \right)^3 \cos(kz - \omega t) \sin^2(kz - \omega t) \tag{8.23}$$

After some simple manipulations, the above expression can be rewritten as

$$f[v^{(0)}] = \frac{3}{32} G \frac{\omega^4}{c_T^4} A_0^3 r^3 \left\{ \cos[\omega(t - \frac{z}{c_T})] - \cos[3\omega(t - \frac{z}{c_T})] \right\} \tag{8.24}$$

A solution of Eq. (8.20) in the form of propagating waves can be taken in the form

$$\begin{aligned} v^{(1)} = V_1^{(1)} z \sin[\omega(t - \frac{z}{c_T})] + V_2^{(1)} z \cos[\omega(t - \frac{z}{c_T})] \\ + V_3^{(1)} z \sin[3\omega(t - \frac{z}{c_T})] + V_4^{(1)} z \cos[3\omega(t - \frac{z}{c_T})] \end{aligned} \tag{8.25}$$

Substituting Eq. (8.25) into Eq. (8.20) yields

$$V_1^{(1)} = -\frac{3}{64} \frac{G}{\mu} \frac{\omega^3}{c_T^3} A_0^3 r^3, \quad V_2^{(1)} = 0, \quad V_3^{(1)} = \frac{1}{64} \frac{G}{\mu} \frac{\omega^3}{c_T^3} A_0^3 r^3, \quad V_4^{(1)} = 0 \tag{8.26}$$

It follows that the cubic nonlinearity of the material gives rise to the harmonics of the forms

$$v^{(1)} = -\frac{3}{64}\frac{G}{\mu}\frac{\omega^3}{c_T^3}A_0^3 r^3 z \sin[\omega(t-\frac{z}{c_T})] + \frac{1}{64}\frac{G}{\mu}\frac{\omega^3}{c_T^3}A_0^3 r^3 z \sin[3\omega(t-\frac{z}{c_T})] \qquad (8.27)$$

It was to be expected that the cubic nonlinearity would give rise to a higher harmonic of frequency 3ω, but it is perhaps surprising that it also gives rise to a harmonic of frequency ω.

Attenuation may have a large influence on the amplitude of a wave as the frequency increases. However, the governing equations considering attenuation become quite complicated. For illustrative purposes, we give a simple analysis here to discuss the effects of attenuation on harmonics. The primary wave is supposed to have the following form

$$v^{(0)} = \frac{1}{2}A_0 r e^{-\alpha_1 z}\cos\left(kz - \omega t\right) \qquad (8.28)$$

where α_1 is the attenuation coefficient corresponding to frequency ω.

Adopting the method used in (Ju et al., 2017), we can get the expressions for the harmonics which include the effect of attenuation.

$$\begin{aligned} v^{(1)} = &-\frac{3}{64}\frac{G}{\mu}\frac{\omega^3}{c_T^3}A_0^3 r^3 \frac{e^{-\alpha_1 z}-e^{-3\alpha_1 z}}{2\alpha_1}\sin[\omega(t-\frac{z}{c_T})] \\ &+\frac{1}{64}\frac{G}{\mu}\frac{\omega^3}{c_T^3}A_0^3 r^3 \frac{e^{-\alpha_3 z}-e^{-3\alpha_1 z}}{3\alpha_1-\alpha_3}\sin[3\omega(t-\frac{z}{c_T})] \end{aligned} \qquad (8.29)$$

where α_3 is the attenuation coefficient corresponding to frequency 3ω. Actually, the attenuation term in the expression for the third harmonic in Eq. (8.29) agrees with the corresponding one in (Hikata and Elbaum, 1966), which has been proven to satisfy the equation of motion in an attenuative medium. The analysis of attenuation presented here can be considered a reasonable approximation. Even though the harmonics grow initially with propagation distance, they may subsequently attenuate faster due to the exponential attenuation terms, see Eq. (8.29). These harmonics may therefore be difficult to measure. Each of the two harmonics in Eq. (8.29) has a maximum amplitude at a distance $z_{\max}$, which is given by

$$z_{\max} = \frac{\ln 3}{2\alpha_1} \text{ for first harmonic with frequency } \omega \qquad (8.30)$$

$$z_{\max} = \frac{\ln(3\alpha_1/\alpha_3)}{3\alpha_1 - \alpha_3} \text{ for third harmonic with frequency } 3\omega \qquad (8.31)$$

8.4 Backscattering from a zone of nonlinearity
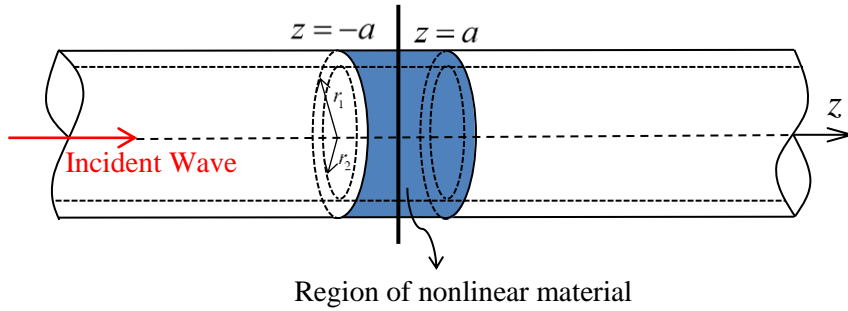
Fig. 8.2 A pipe with a small zone of material nonlinearity

In this section, we consider the case that the pipe is perfectly elastic, except for a small zone defined by $z \le |a|$, see Fig. 8.2, where the behavior in shear is defined by Eq. (8.15). This nonlinear behavior might be due to dislocations (Hikata et al., 1966; Liu et al., 2013), or some other effects of material deterioration. An axially symmetric torsional wave, defined by Eq. (8.22), is launched into the pipe, and when it reaches the zone of nonlinearity, this wave is backscattered. Scattering of an incident wave by an inclusion of nonlinear material in an unbounded linearly elastic solid has been investigated by Tang et al. (2012).

For the problem at hand, the incident and scattered torsional waves are defined by $v^{(0)}$ and v_s, respectively. In the usual manner, we write the total displacement as

$$v_t = v^{(0)} + v_s \qquad (8.32)$$

where $v^{(0)}$ is given by Eq. (8.22). Since $\left|v_s\right| << \left|v^{(0)}\right|$, substitution of Eq. (8.32) into Eq. (8.16) yields by the usual perturbation procedure, which was discussed in Section 8.3,

$$\mu \frac{\partial^2 v_s}{\partial z^2} - \rho \frac{\partial^2 v_s}{\partial t^2} = 0, \quad |z| > a \qquad (8.33)$$

$$\mu \frac{\partial^2 v_s}{\partial z^2} - \rho \frac{\partial^2 v_s}{\partial t^2} = f[v^{(0)}], \quad |z| \leq a \qquad (8.34)$$

Equation (8.34) shows that the incident wave generates an inhomogeneous term equivalent to a body force. Since the region of nonlinearity and the adjoining region have the same linearly elastic properties, the incident wave will not be reflected by the region of nonlinearity.

It follows from Eq. (8.24) that the body force can be written as

$$f = f_1 + f_2 \qquad (8.35)$$

where

$$f_1 = \frac{3}{32} A_0^3 r^3 G k^4 \operatorname{Re}[e^{ikz} \cdot e^{-i\omega t}] \qquad (8.36)$$

$$f_2 = -\frac{3}{32} A_0^3 r^3 G k^4 \operatorname{Re}[e^{3ikz} \cdot e^{-3i\omega t}] \qquad (8.37)$$

Even though f is a nonlinear term in the known quantity $v^{(0)}$, the backscattering problem for v_s is clearly linear. Thus, the reciprocity theorem is still valid. Hence we will consider the backscattering from f_1 and f_2 separately. For f_1, we will consider the backscattering in some detail. Leaving out the term $\exp(-i\omega t)$, and for future reference labeling the backscattering problem as state A, see Fig. 8.3, we define:

Body force:

$$z \leq |a|: \ f^A = -f_1 = -\frac{3}{32} A_0^3 r^3 G k^4 e^{ikz} \qquad (8.38)$$

Incident wave:

$$v^A = \frac{1}{2} A_0 r e^{ikz}, \quad \tau_{\theta z}^A = \frac{1}{2} \mu A_0 r i k e^{ikz} \qquad (8.39)$$

Forward scattered wave:

$$z \gg a: \quad v_s^A = \frac{1}{2} A_s r e^{ikz}, \quad \tau_{\theta z}^A = \frac{1}{2} \mu A_s r i k e^{ikz} \qquad (8.40)$$

Backscattered wave:

$$z \ll -a: \quad v_s^A = \frac{1}{2} A_s r e^{-ikz}, \quad \tau_{\theta z}^A = -\frac{1}{2} \mu A_s r i k e^{-ikz} \qquad (8.41)$$

The problem at hand is the determination of the amplitude A_s. This will be done by the use of the elastodynamic reciprocity theorem.
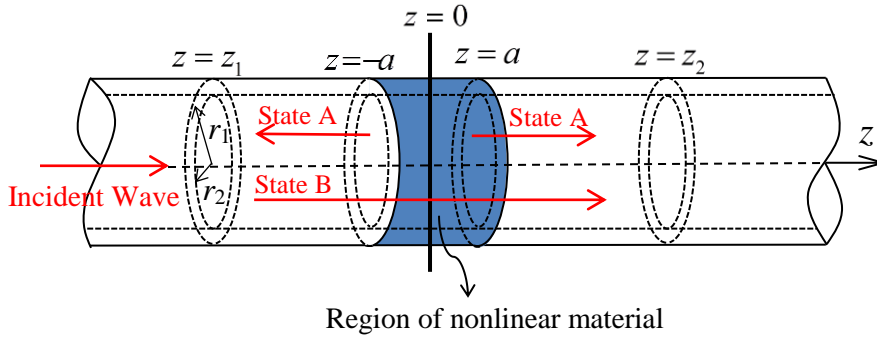
Fig. 8.3 Scattered and virtual waves for state A and state B

8.5   Use of the elastodynamic reciprocity theorem

For a linearly elastic isotropic body, the reciprocity theorem has been derived elsewhere (Achenbach, 2003). The reciprocity theorem is an integral relation over the interior of a region *V* and its boundary *S*, of the displacements, the surface tractions, and the body forces of two elastodynamic states, State A and State B. We will use the elastodynamic reciprocity theorem for time-harmonic fields, but the time factor $\exp(-i\omega t)$ will be omitted.

The elastodynamic reciprocity theorem for a region *V* with boundary *S* may then be written as (Achenbach, 2003)

$$\int_V (f_i^A u_i^B - f_i^B u_i^A) dV = \int_S (u_i^A \tau_{ij}^B - u_i^B \tau_{ij}^A) n_j dS = \int_S (u_i^A t_i^B - u_i^B t_i^A) dS \qquad (8.42)$$

where t_i^A and t_i^B are surface tractions.

For the present problem, we select for state B a torsional wave propagating in the positive z-direction. We call this wave a virtual wave since it is not directly related to the backscattering problem that is being considered. State B is defined by

Body force:

$$f^B = 0 \tag{8.43}$$

Virtual wave:

$$v^B = \frac{1}{2}\bar{A}re^{ikz}, \quad \tau_{\theta z}^B = \mu\frac{1}{2}\bar{A}rike^{ikz} \tag{8.44}$$

The geometry for state A and B is shown in Fig. 8.4.

The elastodynamic reciprocity theorem now reduces to

$$\int_V (f^A v^B)dV = \int_{S'} (\tau_{\theta z}^B v_s^A - \tau_{\theta z}^A v^B)n_z dS' \tag{8.45}$$

The volume V is the region defined by $r_2 \le r \le r_1$, $z \le |a|$. The cylindrical surfaces defined by $r = r_1$ and $r = r_2$ are free of tractions. The remaining surfaces S' are the end-surfaces $r_2 \le r \le r_1$ for $z = z_1$ and $z = z_2$, respectively. We have

$$\int_{-a}^{a}\int_{r_2}^{r_1} f^A v^B rdrdz = -\left(\int_{r_2}^{r_1}(\tau_{\theta z}^B v_s^A - \tau_{\theta z}^A v^B)rdr\right)_{z=z_1} + \left(\int_{r_2}^{r_1}(\tau_{\theta z}^B v_s^A - \tau_{\theta z}^A v^B)rdr\right)_{z=z_2} \tag{8.46}$$

Because of the axisymmetry of the problem, we have omitted the integrations of θ over the range $0 \le \theta \le 2\pi$. Equation (8.46) can be written in detail as

$$\int_{-a}^{a}\int_{r_2}^{r_1}(-\frac{3}{32}A_0^3 r^3 Gk^4 e^{ikz})\frac{1}{2}\bar{A}re^{ikz}rdrdz$$

$$= -\left(\int_{r_2}^{r_1}(\mu\frac{1}{2}\bar{A}rike^{ikz}\frac{1}{2}A_s re^{-ikz} + \frac{1}{2}\mu A_s rike^{-ikz}\frac{1}{2}\bar{A}re^{ikz})rdr\right)_{z=z_1} \tag{8.47}$$

$$+ \left(\int_{r_2}^{r_1}(\mu\frac{1}{2}\bar{A}rike^{ikz}\frac{1}{2}A_s re^{ikz} - \frac{1}{2}\mu A_s rike^{ikz}\frac{1}{2}\bar{A}re^{ikz})rdr\right)_{z=z_2}$$

Equation (8.47) shows that the integration that is to be determined at $z = z_2$ vanishes, which implies that the waves of state A and state B do not yield a contribution to the reciprocity relation when they propagate in the same direction. Equation (8.47) then simplifies to

$$\int_{-a}^{a}\int_{r_2}^{r_1}(\frac{3}{64}A_0^3\bar{A}r^5Gk^4e^{2ikz})drdz = \left(\int_{r_2}^{r_1}(\frac{1}{2}\mu\bar{A}A_s ikr^3)dr\right)_{z=z_1} \tag{8.48}$$

Evaluation of both sides of Eq. (8.48) yields the amplitude of the backscattered wave as

$$A_s = -\frac{1}{16}\frac{iGk^2(r_1^6 - r_2^6)A_0^3}{\mu(r_1^4 - r_2^4)}\sin(2ka) \tag{8.49}$$

The corresponding displacement is

$$v_s^A = -\frac{1}{32}r\frac{Gk^2(r_1^6 - r_2^6)A_0^3}{\mu(r_1^4 - r_2^4)}\sin(2ka)\sin(kz + \omega t) \tag{8.50}$$

The wave backscattered due to f_2 can be obtained in the same manner. The backscattering problem is defined as

Body force:

$$f^A = -f_2 = \frac{3}{32}A_0^3 r^3 Gk^4 e^{3ikz} \tag{8.51}$$

Forward scattered wave:

$$z \gg a: \quad v_s^A = \frac{1}{2}A_s re^{3ikz}, \quad \tau_{\theta z}^A = \frac{3}{2}\mu A_s rike^{3ikz} \tag{8.52}$$

Backscattered wave:

$$z \ll -a: \quad v_s^A = \frac{1}{2}A_s re^{-3ikz}, \quad \tau_{\theta z}^A = -\frac{3}{2}\mu A_s rike^{-3ikz} \tag{8.53}$$

The virtual wave is again defined by Eqs. (8.43) and (8.44) with k being replaced by $3k$.

Application of the reciprocity theorem yields

$$A_s = \frac{1}{144} \frac{iGk^2(r_1^6 - r_2^6)A_0^3}{\mu(r_1^4 - r_2^4)} \sin(6ka) \qquad (8.54)$$

It follows that the total backscattered wave is given by

$$
\begin{aligned}
v_s &= v_{s1} + v_{s2} \\
&= -\frac{1}{32} r \frac{G\omega^2 (r_1^6 - r_2^6)A_0^3}{\mu c_T^2 (r_1^4 - r_2^4)} \left\{ \sin(2ka)\sin(kz + \omega t) - \frac{1}{9}\sin(6ka)\sin 3(kz + \omega t) \right\}
\end{aligned} \qquad (8.55)
$$

It is noted that the backscattered wave is $O\left|A_0^3\right|$. Hence it is very small as compared to the incident wave. In the next section we propose a way to increase the magnitude of the backscattered wave.

8.6 Increase of the amplitude of the backscattered wave

The most suitable term to detect the region of material nonlinearity is the first term of Eq. (8.55), because it has a lower frequency and it is therefore less susceptible to attenuation, and it is also larger in magnitude than the second term due to the factor 1/9. The significant quantities in the first term are the frequency ω_1 and the amplitude in A_0^3. Neither quantity can be increased without increasing the attenuation of the wave term $\sin k(z - c_T t)$. In this section, we will, however, show that it is possible to increase the amplitude of the scattered displacement by combining the incident wave of frequency ω_1 given by Eq. (8.39) with a second incident wave of frequency ω_2, where

$$\omega_2 > \omega_1 \qquad (8.56)$$

in such a way that we still have a scattered wave of the type $\sin k_1 (z + c_T t)$. Combining two waves to obtain better results is similar to the mixing of waves, which is, however, generally achieved with two waves of different polarization (Chen et al., 2014; Liu et al., 2013).

The total incident wave field which consists of two torsional waves has the following form.

$$v = V_1 \cos[\omega_1(t - \frac{z}{c_T})] + V_2 \cos[\omega_2(t - \frac{z}{c_T})] \tag{8.57}$$

where $V_1 = 1/2 \, A_1 r$ and $V_2 = 1/2 \, A_2 r$. The body force can then be calculated from Eq. (21) as

$$f = 3G \left\{ \begin{array}{l} \left(\dfrac{1}{2} \dfrac{\omega_1^2 \omega_2^2}{c_T^4} V_1 V_2^2 + \dfrac{1}{4} \dfrac{\omega_1^4}{c_T^4} V_1^3 \right) \cos[\omega_1(t - \dfrac{z}{c_T})] \\[4mm] + \left(\dfrac{1}{2} \dfrac{\omega_1^2 \omega_2^2}{c_T^4} V_1^2 V_2 + \dfrac{1}{4} \dfrac{\omega_2^4}{c_T^4} V_2^3 \right) \cos[\omega_2(t - \dfrac{z}{c_T})] \\[4mm] + \left(\dfrac{1}{2} \dfrac{\omega_1 \omega_2^3}{c_T^4} - \dfrac{1}{4} \dfrac{\omega_1^2 \omega_2^2}{c_T^4} \right) V_1 V_2^2 \cos[(\omega_1 - 2\omega_2)(t - \dfrac{z}{c_T})] \\[4mm] + \left(\dfrac{1}{2} \dfrac{\omega_1^3 \omega_2}{c_T^4} - \dfrac{1}{4} \dfrac{\omega_1^2 \omega_2^2}{c_T^4} \right) V_1^2 V_2 \cos[(2\omega_1 - \omega_2)(t - \dfrac{z}{c_T})] \\[4mm] - \left(\dfrac{1}{4} \dfrac{\omega_1^2 \omega_2^2}{c_T^4} + \dfrac{1}{2} \dfrac{\omega_1 \omega_2^3}{c_T^4} \right) V_1 V_2^2 \cos[(\omega_1 + 2\omega_2)(t - \dfrac{z}{c_T})] \\[4mm] - \left(\dfrac{1}{4} \dfrac{\omega_1^2 \omega_2^2}{c_T^4} + \dfrac{1}{2} \dfrac{\omega_1^3 \omega_2}{c_T^4} \right) V_1^2 V_2 \cos[(2\omega_1 + \omega_2)(t - \dfrac{z}{c_T})] \\[4mm] - \dfrac{1}{4} \dfrac{\omega_1^4}{c_T^4} V_1^3 \cos 3[\omega_1(t - \dfrac{z}{c_T})] - \dfrac{1}{4} \dfrac{\omega_2^4}{c_T^4} V_2^3 \cos 3[\omega_2(t - \dfrac{z}{c_T})] \end{array} \right\} \tag{8.58}$$

The cosine which appears in the first term has the right argument. All the other terms have the cosine terms with higher frequency. Thus, we select

$$f = \frac{3}{16} \frac{\omega_1^2 \omega_2^2}{c_T^4} G A_1 A_2^2 r^3 \cos[\omega_1(t - \frac{z}{c_T})] \tag{8.59}$$

Using this expression for f as the body force term, we obtain

$$v_s = -\frac{1}{16} r \frac{G\omega_2^2 (r_1^6 - r_2^6) A_1 A_2^2}{\mu c_T^2 (r_1^4 - r_2^4)} \sin(2k_1 a) \sin(k_1 z + \omega_1 t) \tag{8.60}$$

In comparison with the first term in Eq. (8.55) $\omega = \omega_1$, we note that the ratio of amplitudes of Eq. (8.60) and Eq. (8.55) is

$$\frac{(v_s)_2}{(v_s)_1} = \frac{A_{s2}}{A_{s_1}} = 2\frac{\omega_2^2}{\omega_1^2}\frac{A_1 A_2^2}{A_0^3} \tag{8.61}$$

where it follows from Eqs. (8.50) and (8.60) that

$$A_{s1} = -\frac{1}{32}\frac{G\omega_1^2(r_1^6 - r_2^6)A_0^3}{\mu c_T^2(r_1^4 - r_2^4)}\sin(2k_1 a) \tag{8.62}$$

$$A_{s2} = -\frac{1}{16}\frac{G\omega_2^2(r_1^6 - r_2^6)A_1 A_2^2}{\mu c_T^2(r_1^4 - r_2^4)}\sin(2k_1 a) \tag{8.63}$$

Equation (8.62) can be rewritten in the form

$$\frac{A_{s1}}{A_0^3} = -\frac{1}{32}\pi^2\frac{G}{\mu}\left(\frac{2a}{\lambda_1}\right)^2\left(\frac{r_1}{a}\right)^2\frac{(1 - r_2^6/r_1^6)}{(1 - r_2^4/r_1^4)}\sin\left(2\pi\frac{2a}{\lambda_1}\right) \tag{8.64}$$

where $\lambda_1 = 2\pi/k_1 = 2\pi c_T/\omega_1$ is the wavelength for frequency ω_1. Since it may be assumed that the amplitudes are such that

$$\frac{A_1 A_2^2}{A_0^3} \simeq 1, \tag{8.65}$$

and using

$$\omega_2^2 = \frac{\omega_2^2}{\omega_1^2}\frac{4\pi^2 c_T^2}{\lambda_1^2}, \tag{8.66}$$

Eq. (8.63) can also be expressed as

$$\frac{A_{s2}}{A_0^3} \simeq -\frac{1}{16}\pi^2\frac{\omega_2^2}{\omega_1^2}\frac{G}{\mu}\left(\frac{2a}{\lambda_1}\right)^2\left(\frac{r_1}{a}\right)^2\frac{(1 - r_2^6/r_1^6)}{(1 - r_2^4/r_1^4)}\sin(2\pi\frac{2a}{\lambda_1}) \tag{8.67}$$

Thus, in view of Eqs. (8.64) and (8.67), we have

$$\frac{A_{s2}}{A_{s_1}} \simeq 2\frac{\omega_2^2}{\omega_1^2} \tag{8.68}$$
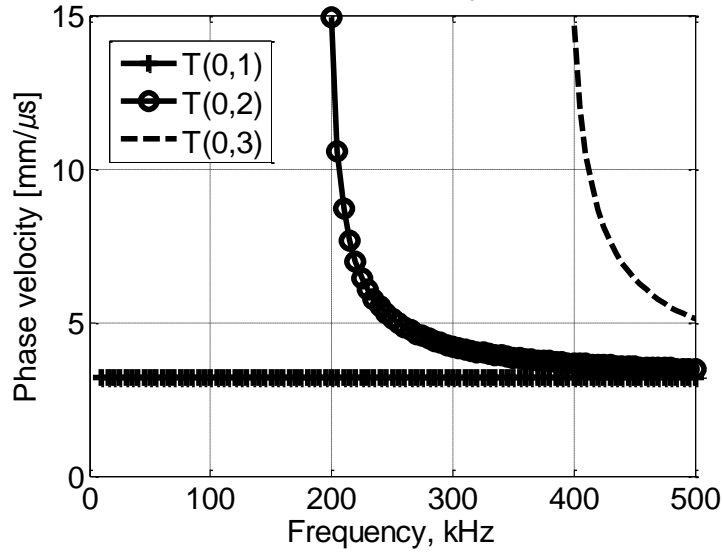
Fig. 8.4 Phase velocity c versus frequency $\omega/2\pi$ for three lowest modes, for

$$c_T = 3200 \; m/s$$

To prevent interference with higher order torsional modes, the frequency ω_2 cannot be too large. Figure 8.4 shows the dispersion curves for the three lowest axisymmetric torsional wave modes. If we select $\omega_1/2\pi = 40$ kHz and $\omega_2/2\pi = 200$ kHz, we may assume that higher modes are not generated.

Figure 8.5 shows the amplification of the normalized amplitude of the scattered wave with frequency $\omega = \omega_1 = 80\pi$ kHz as it is combined with an incident wave of frequency $\omega_2 = 400\pi$ kHz versus the dimensionless length of the nonlinear domain, $2a/\lambda_1$. Since $\omega_2/\omega_1 = 5$, the amplitude after amplification of the scattered wave (i.e. Eq. (8.67)) becomes

$$\frac{A_{s2}}{A_0^3} = -\frac{25}{16}\pi^2 \frac{G}{\mu}\left(\frac{2a}{\lambda_1}\right)^2 \left(\frac{r_1}{a}\right)^2 \frac{(1-r_2^6/r_1^6)}{(1-r_2^4/r_1^4)} \sin\left(2\pi \frac{2a}{\lambda_1}\right) \qquad (8.69)$$

For the specific example of Fig. 8.5, the fourth order elastic constant G is set as -2.4μ, and the ratio of the inside and outside radius, r_2/r_1, is taken as 0.9. For the combination of the two waves, the amplitude of the scattered wave is amplified by almost 50 times. It is noted that, in principle, we can obtain the length of the

nonlinear domain by measuring the amplitude of the scattered wave.
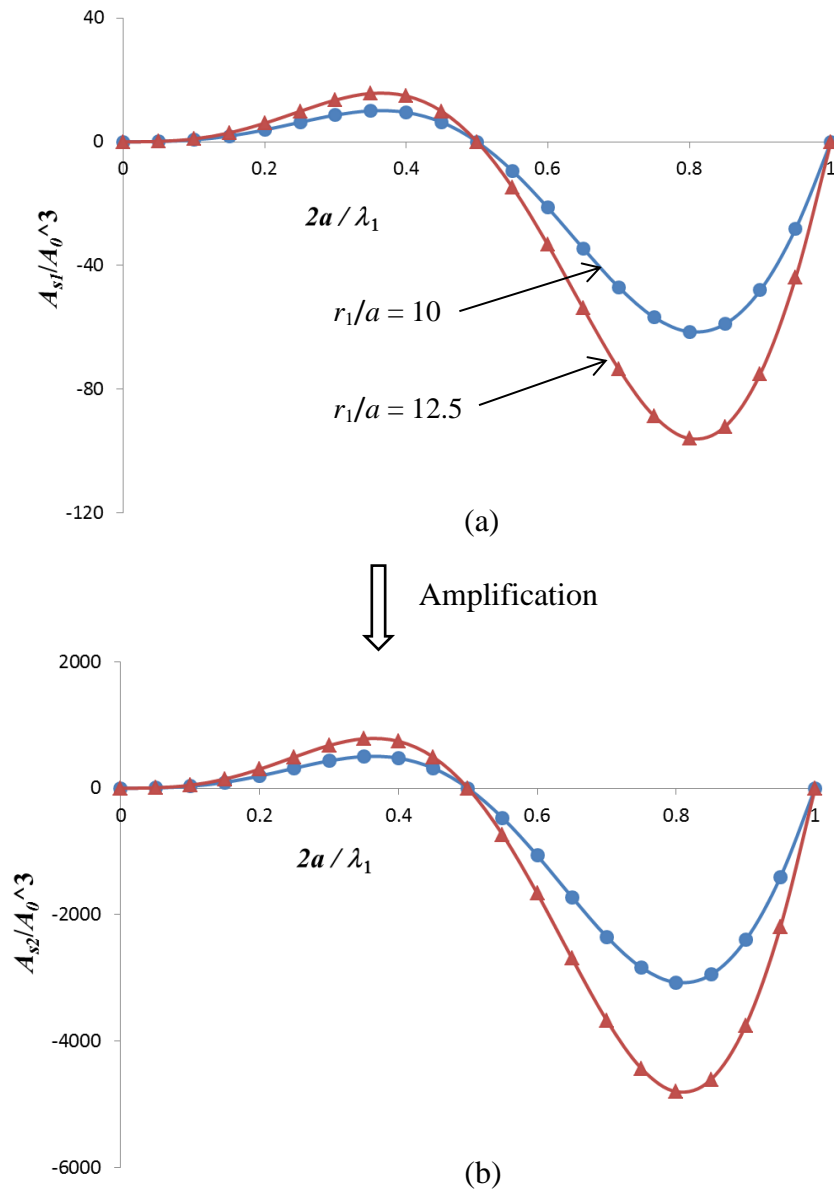
Fig. 8.5. Amplification of the normalized amplitude of the scattered wave with frequency $\omega = \omega_1$ by a combination of incident waves of frequency ω_1 and ω_2 versus the dimensionless length of the nonlinear domain, $2a/\lambda_1$, (a) Eq. (8.64), (b) Eq. (8.69)
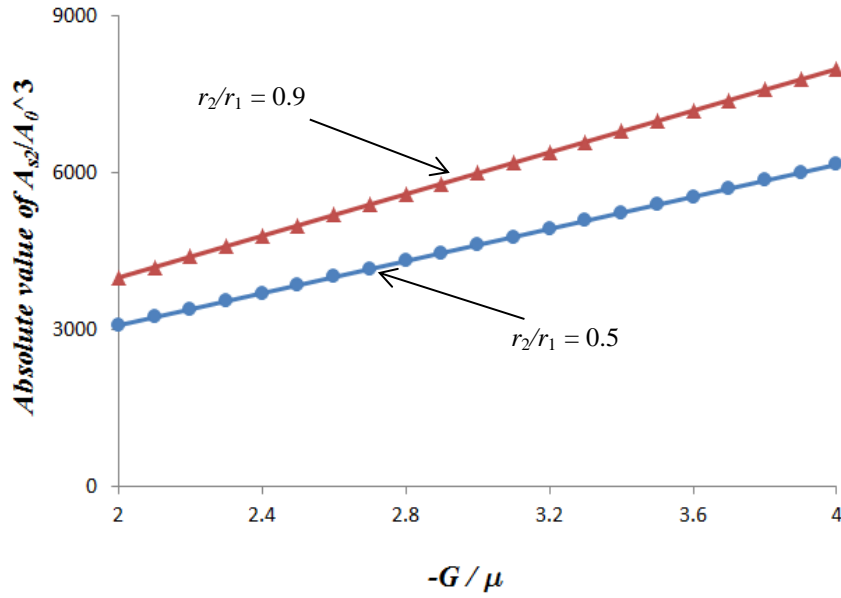
Fig. 8.6. Variation of the normalized amplitude, $A_{s2}\big/A_0^3$, Eq. (8.69), of the scattered wave versus the fourth order elastic constant

Figure 8.6 shows the variation of the normalized amplitude, $A_{s2}\big/A_0^3$, versus the change of the fourth order elastic constant after amplification. The parameter r_1/a is 12.5 and $2a/\lambda_1$ is 0.8, which corresponds to $a = 3.2\ \text{cm}$. The fourth order elastic constant may be changed by material loss, which can be sensed by the detection of the amplitude of the scatted wave.

8.7　Conclusions

Torsional wave propagating in a pipe was investigated for cubic material nonlinearity. The generation of cumulative harmonics and the backscattering of a torsional wave from a small zone of material nonlinearity were considered. For the first problem, we not only obtained an analytical expression for the third harmonic, but also one for a harmonic whose frequency is the same as the frequency of the incident wave. The amplitudes of the two harmonics grow linearly with propagation distance. For the scattering problem, the analytical expression of the backscattered wave was obtained by using the elastodynamic reciprocity theorem. The amplitude is determined by the nonlinearity coefficient, G, the size of the nonlinear region, $2a$, and the geometry of the pipe, r_1, r_2. Combining the primary wave with a higher

frequency wave was proposed to increase the magnitude of the backscattered wave. An example that the original scattered wave is amplified by a factor 50 was presented.

Chapter 9 Intersection of two elastic waves at the region of material nonlinearity in an elastic layer

9.1 Introduction

Several methods have been proposed by using elastic waves to measure material nonlinearity. The harmonic generation technique is the most widely reported method. The drawback of the harmonic generation technique is that it is hard to separate the underlying system nonlinearity from the material nonlinearity. To avoid such interferences, the mixing wave technique has been proposed, which includes collinear and non-collinear mixing wave technique. The outstanding character of this technique is that the frequency of the mixing wave is selectable, which can be the sum or difference frequencies of the incident waves. Another important advantage of the mixing wave technique over the harmonic generation technique is the spatial selectivity that the nonlinear interaction is only limited to the region where the incident beams intersect (Croxford et al., 2009). For the collinear mixing wave, the position of the intersection region is figured out by making use of the wave velocity and the propagation time. While the intersection region can be determined directly through a geometrical means for the non-collinear mixing wave technique in an easier way. The investigations on collinear mixing wave have been conducted in Chapters 7 and 8. In this chapter, we consider the intersection of two non-collinear waves at a region of material nonlinearity.

On the other hand, from the practical point of view, the reflection, transmission and scattering of incident waves from an inclusion of nonlinear material behavior are of obvious interest. Recently, the interactions of elastic waves with a local region of nonlinear material behavior have some interesting studies. Tang et al. (2012) investigated the scattering of an incident longitudinal wave from a region of spatially-dependent quadratic nonlinearity. The scattering of elastic waves from a heterogeneous inclusion of nonlinearity contained in a linear host material was investigated by Kube (2017).

However, little attention has been paid to the investigation on scattering of

incident waves from a local region of material nonlinearity in structures like plates, which motivates the present work. In this chapter, the scattering of two orthogonal SH waves of lowest mode from a cylindrical region of nonlinear material behavior in an elastic layer is investigated. For this end, the perturbation method is taken to reduce the nonlinear governing equations and the boundary conditions to a set of linear equations at different orders. The two incident SH waves are viewed as the solutions of the zero-order equations. Taking a substitution of the expressions of the two SH waves into the nonlinear terms in the first-order equations, the inhomogeneous equations can be obtained, which have the same form as the equations used to describe the forced wave motion induced by the local body forces and the local surface tractions in an elastic layer. The inhomogeneous terms which collect the contribution from the material nonlinearity can be equivalent to the corresponding body forces and the surface tractions. Then, the scattering problem is transferred to the problem of forced wave motion in a three-dimensional elastic layer. In general, such problems can be solved through wave mode expansions (Achenbach and Xu, 1999; Diligent et al., 2002) or integral transforms (Weaver and Pao, 1982; Santosa and Pao, 1989). In the present chapter, the reciprocity relation in elastodynamics (Achenbach, 2003) is adopted to obtain the expressions of wave amplitudes based on the superposition of wave modes. It is of interest to note that only the coefficient of the lowest wave mode is found nonzero for the scattered SH wave. The amplitudes of the scattered waves are affected by the size of the nonlinear region, the nonlinear material constants, the detection angle, the wavelength, and the ratio between the two frequencies of the incident waves. These effects are shown graphically by numerical examples for the scattered Lamb wave of zero-order mode and SH wave.

9.2   Basic equations

9.2.1   Wave motion in an elastic layer with quadratic material nonlinearity

The displacements in the x_i (i=1, 2, 3) directions in Cartesian coordinates are represented by u_i. The displacement equations of motion of an isotropic solid are given by (Tang et al., 2012)

$$\rho\frac{\partial^2 u_i}{\partial t^2} - (\lambda + \mu)\frac{\partial^2 u_j}{\partial x_j \partial x_i} - \mu\frac{\partial^2 u_i}{\partial x_j \partial x_j} = f_i[u_1, u_2, u_3] \tag{9.1}$$

where λ and μ are the Lamé's constants, ρ is the mass density, and

$$
\begin{aligned}
f_i = & \frac{A}{4}\left(\frac{\partial^2 u_k}{\partial x_l \partial x_l}\frac{\partial u_k}{\partial x_i} + \frac{\partial^2 u_k}{\partial x_i \partial x_l}\frac{\partial u_i}{\partial x_k} + 2\frac{\partial^2 u_i}{\partial x_l \partial x_k}\frac{\partial u_l}{\partial x_k}\right) \\
& + B\frac{\partial^2 u_i}{\partial x_l \partial x_l}\frac{\partial u_k}{\partial x_k} + (B + 2C)\frac{\partial^2 u_k}{\partial x_i \partial x_k}\frac{\partial u_l}{\partial x_l} \\
& + \left(\frac{A}{4} + B\right)\left(\frac{\partial^2 u_l}{\partial x_i \partial x_k}\frac{\partial u_l}{\partial x_k} + \frac{\partial^2 u_k}{\partial x_i \partial x_k}\frac{\partial u_i}{\partial x_l} + \frac{\partial^2 u_k}{\partial x_i \partial x_k}\frac{\partial u_l}{\partial x_i} + \frac{\partial^2 u_l}{\partial x_i \partial x_k}\frac{\partial u_k}{\partial x_l}\right)
\end{aligned}
\tag{9.2}
$$

where A, B and C are the third-order elastic constants and f_i collects all the contribution from the material nonlinearity. Repeated subscripts denote summation. It should be pointed out that only the material nonlinearity is considered in this paper. Thus, the coefficients of the nonlinear terms in Eq. (9.2) only depend on the third-order elastic constants.

(a) An elastic layer   (b) The side view
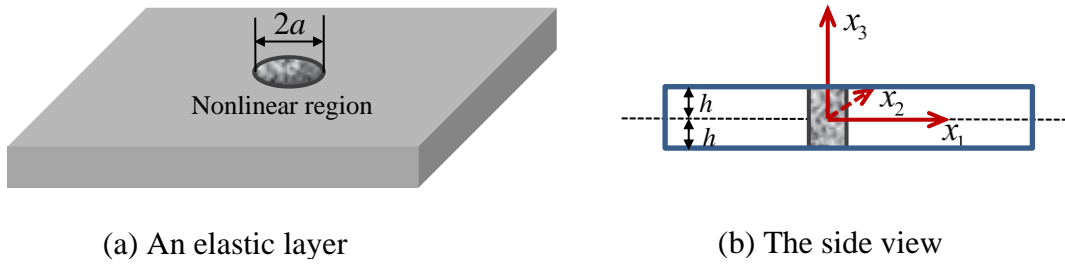
Fig. 9.1. An elastic layer with a cylindrical region of quadratic material nonlinearity across the thickness and the corresponding rectangular coordinates

The upper and bottom surfaces are free of tractions, which can be described by

$$\tau_{13} = \tau_{23} = \tau_{33} = 0, \text{ at } x_3 = h \text{ or } x_3 = -h \tag{9.3}$$

where the expressions of stresses are represented by

$$\tau_{i3} = \lambda\frac{\partial u_l}{\partial x_l}\delta_{i3} + \mu\left(\frac{\partial u_i}{\partial x_3} + \frac{\partial u_3}{\partial x_i}\right) + \tau_{i3}^{NL}, \quad (i = 1, 2, 3) \tag{9.4}$$

with the nonlinear parts being

$$
\tau_{i3}^{NL} = \frac{A}{4}\left(\frac{\partial u_l}{\partial x_i}\frac{\partial u_l}{\partial x_3} + \frac{\partial u_i}{\partial x_l}\frac{\partial u_3}{\partial x_l} + \frac{\partial u_l}{\partial x_3}\frac{\partial u_i}{\partial x_l} + \frac{\partial u_3}{\partial x_l}\frac{\partial u_l}{\partial x_i} \right)
$$
$$
+ \frac{B}{2}\left(\frac{\partial u_l}{\partial x_k}\frac{\partial u_l}{\partial x_k}\delta_{i3} + \frac{\partial u_l}{\partial x_k}\frac{\partial u_k}{\partial x_l}\delta_{i3} + 2\frac{\partial u_i}{\partial x_3}\frac{\partial u_l}{\partial x_l} + 2\frac{\partial u_3}{\partial x_i}\frac{\partial u_l}{\partial x_l} \right) \quad (9.5)
$$
$$
+ C \frac{\partial u_l}{\partial x_l}\frac{\partial u_m}{\partial x_m}\delta_{i3}
$$

9.2.2 Scattering of two lowest SH waves from a local zone of material nonlinearity
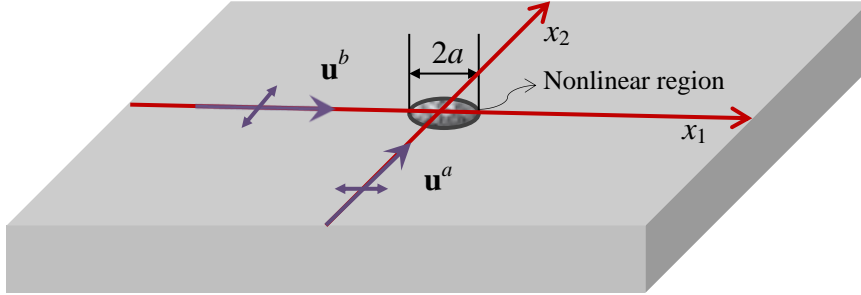
Fig. 9.2. Incidence of two SH waves intersecting vertically at the cylindrical region of nonlinear material

In this section, two SH waves of lowest modes are considered as the incident waves. The propagation directions of these two waves are perpendicular to each other, which intersect at the nonlinear cylindrical region, see Fig. 9.2. Thus, the total wave field can be represented by the summation of the incident waves and the scattered waves as follows:

$$
u_1 = u_1^0(x_2,t) + u_1^1(x_1,x_2,x_3,t),
$$
$$
u_2 = u_2^0(x_1,t) + u_2^1(x_1,x_2,x_3,t), \quad (9.6)
$$
$$
u_3 = u_3^1(x_1,x_2,x_3,t)
$$

where $u_1^0(x_2,t)$ and $u_2^0(x_1,t)$ are the displacement components of wave a ($\mathbf{u}^a$) and wave b ($\mathbf{u}^b$), respectively. The SH wave of lowest mode only has a single

displacement component, which is independent of the coordinate variable in the thickness direction.

Since the scattered waves are generated by the interaction of SH waves with the region of weak material nonlinearity, we assume

$$\left|u_i^0\right| \propto O(\varepsilon^0), \ \left|u_i^0\right| \cdot \left|u_j^0\right| \propto O(\varepsilon^1), \ \left|u_i^1\right| \propto O(\varepsilon^1) \tag{9.7}$$

where ε is a small quantity. Substituting Eq. (9.6) into Eq. (9.1), the governing equations can be separated into two sets of equations at two different orders. At ε^0, the displacement equations of motion are obtained as

$$\rho \frac{\partial^2 u_1^0}{\partial t^2} - \mu \frac{\partial^2 u_1^0}{\partial x_2^2} = 0 \tag{9.8}$$

for wave a, and

$$\rho \frac{\partial^2 u_2^0}{\partial t^2} - \mu \frac{\partial^2 u_2^0}{\partial x_1^2} = 0 \tag{9.9}$$

for wave b. By virtue of Eqs. (9.8) and (9.9), the expressions of the SH waves of lowest modes can be represented by

$$u_1^0 = -A_a \cos \omega_a \left(\frac{x_2}{c_T} - t \right), \tag{9.10}$$

for wave a, and

$$u_2^0 = A_b \cos \omega_b \left(\frac{x_1}{c_T} - t \right) \tag{9.11}$$

for wave b, where A_a and A_b are the amplitudes of wave a and wave b, respectively, and ω_a and ω_b are the corresponding frequencies.

The boundary conditions, Eq. (9.3), at ε^0, then become

$$\tau_{13}^0 = \tau_{23}^0 = \tau_{33}^0 = 0 \tag{9.12}$$

The free boundary conditions on the bottom and top surfaces are satisfied automatically.

At ε^1, the displacement equations of motion can be represented by

$$\rho \frac{\partial^2 u_i^1}{\partial t^2} - (\lambda + \mu) \frac{\partial^2 u_j^1}{\partial x_j \partial x_i} - \mu \frac{\partial^2 u_i^1}{\partial x_j \partial x_j} = f_i, \quad x_1^2 + x_2^2 \leq a \tag{9.13}$$

$$\rho \frac{\partial^2 u_i^1}{\partial t^2} - (\lambda + \mu) \frac{\partial^2 u_j^1}{\partial x_j \partial x_i} - \mu \frac{\partial^2 u_i^1}{\partial x_j \partial x_j} = 0, \quad x_1^2 + x_2^2 \geq a \tag{9.14}$$

where f_i ($i = 1, 2, 3$) can be obtained through Eq. (9.2) by replacing u_i ($i = 1, 2$) with u_i^0, and ignoring the terms containing u_3 and x_3, and are represented by

$$f_1 = \left(\frac{A}{2} + B\right) \frac{\partial^2 u_2^0}{\partial x_1^2} \left(\frac{\partial u_2^0}{\partial x_1} + \frac{\partial u_1^0}{\partial x_2}\right) \tag{9.15}$$

$$f_2 = \left(\frac{A}{2} + B\right) \frac{\partial^2 u_1^0}{\partial x_2^2} \left(\frac{\partial u_1^0}{\partial x_2} + \frac{\partial u_2^0}{\partial x_1}\right) \tag{9.16}$$

$$f_3 = 0 \tag{9.17}$$

In this chapter, only the scattered waves of sum frequency, i.e. $\omega = \omega_a + \omega_b$, is taken into account. The scattered waves of difference frequency can be obtained in a similar way. Substituting Eqs. (9.10) and (9.11) into Eqs. (9.15) and (9.16) and only retaining the cross terms with sum frequency, we obtain

$$f_1 = F \omega_b \sin\left[\frac{\omega_b x_1 + \omega_a x_2}{c_T} - (\omega_b + \omega_a) t\right] \tag{9.18}$$

$$f_2 = F \omega_a \sin\left[\frac{\omega_b x_1 + \omega_a x_2}{c_T} - (\omega_b + \omega_a) t\right] \tag{9.19}$$

where

$$F = -\frac{1}{2}\left(\frac{A}{2} + B\right) \frac{\omega_a \omega_b}{c_T^3} A_a A_b \tag{9.20}$$

By considering Eqs. (9.10) and (9.11), the boundary conditions of free tractions on bottom and top surfaces (i.e. $x_3=h$ and $x_3=-h$) at ε^1 can be satisfied when

$$\lambda \frac{\partial u_l^1}{\partial x_l} \delta_{i3} + \mu \left(\frac{\partial u_i^1}{\partial x_3} + \frac{\partial u_3^1}{\partial x_i} \right) = -t_i, \quad x_1^2 + x_2^2 \leq a \tag{9.21}$$

$$\lambda \frac{\partial u_l^1}{\partial x_l} \delta_{i3} + \mu \left(\frac{\partial u_i^1}{\partial x_3} + \frac{\partial u_3^1}{\partial x_i} \right) = 0_i, \quad x_1^2 + x_2^2 \geq a \tag{9.22}$$

where

$$t_1 = t_2 = 0, \tag{9.23}$$

$$t_3 = \frac{B}{2} A_a A_b \frac{\omega_a \omega_b}{c_T^2} \cos \left\{ (\omega_b + \omega_a) \left[\frac{\omega_b x_1 + \omega_a x_2}{(\omega_b + \omega_a) c_T} - t \right] \right\} \tag{9.24}$$
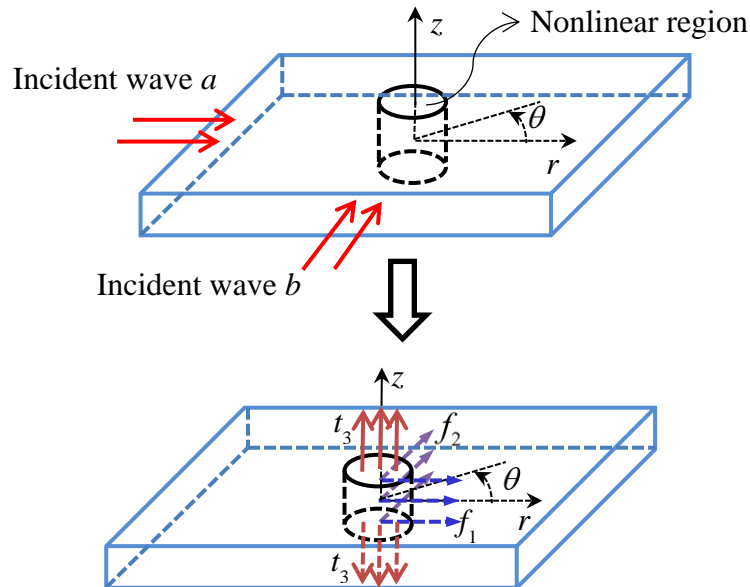
Fig. 9.3. The transformation of the nonlinear scattering problem into an equivalent linear problem of forced wave motion excited by the body forces and the surface tractions

In Eq. (9.13), the inhomogeneous terms specified in Eqs (9.18) and (9.19) can be viewed as local body forces distributed within the nonlinear region. Similarly, t_i in Eq. (9.21) can be viewed as local surface tractions in the thickness direction on the bottom and top surfaces. Mathematically, the displacement equations of motion at the first-order (i.e. Eqs. (9.13) and (9.14)) together with the equations of boundary conditions (i.e. Eqs. (9.21) and (9.22)) can be used to describe the waves propagating in a linearly elastic layer excited by the distributed body force and the distributed surface tractions. Thus, the nonlinear scattering problem has been transformed into an equivalent linear problem of forced wave motion in an elastic layer. The above analysis can be understood via the flow diagram in Fig. 9.3.

9.3 Use of elastodynamic reciprocity relation

9.3.1 Wave motion excited by a point force in x_1-direction

The waves excited by the distributed body forces and the surface tractions can be equivalent to the superposition of the waves excited by the point forces. Thus, the solutions of these two problems should be in the same form. Since the waves generated by a point force will propagate in the radial direction, it is convenient to use cylindrical coordinates instead of rectangular coordinates. The following transform relation between the two coordinate systems will be used:

$$x_1 = r\cos\theta, \ x_2 = r\sin\theta, \ x_3 = z \tag{9.25}$$

The displacement solution in the cylindrical coordinates can be obtained from Eqs. (9A.1)-(9A.3) in Appendix 9A by using the above transformation, which can be given by

$$u_r^n = \frac{1}{k_n} V^n(z) \frac{\partial \varphi(r,\theta)}{\partial r} \tag{9.26}$$

$$u_\theta^n = \frac{1}{k_n} V^n(z) \frac{1}{r} \frac{\partial \varphi(r,\theta)}{\partial \theta} \tag{9.27}$$

$$u_z^n = W^n(z)\varphi(r,\theta) \tag{9.28}$$

$$\frac{\partial^2 \varphi(r,\theta)}{\partial r^2} + \frac{1}{r}\frac{\partial \varphi(r,\theta)}{\partial r} + \frac{1}{r^2}\frac{\partial^2 \varphi(r,\theta)}{\partial \theta^2} + k_n^2 \varphi(r,\theta) = 0 \qquad (9.29)$$

for the Lamb waves. Equations (9A.4), (9A.5) and (9A.7) can be rewritten as

$$u_r^n = \frac{1}{l_n}U^n(z)\frac{1}{r}\frac{\partial \psi(r,\theta)}{\partial \theta} \qquad (9.30)$$

$$u_\theta^n = -\frac{1}{l_n}U^n(z)\frac{\partial \psi(r,\theta)}{\partial r} \qquad (9.31)$$

$$\frac{\partial^2 \psi(r,\theta)}{\partial r^2} + \frac{1}{r}\frac{\partial \psi(r,\theta)}{\partial r} + \frac{1}{r^2}\frac{\partial^2 \psi(r,\theta)}{\partial \theta^2} + l_n^2 \psi(r,\theta) = 0 \qquad (9.32)$$

for the SH waves.

From the reference Achenbach and Xu (1999), we know that the solution to Eq. (9.29) for the point load applied in the x_1-direction should take the following form for the Lamb wave:

$$\varphi(r,\theta) = \Phi(r)\cos\theta \qquad (9.33)$$

The solutions for an outgoing wave and an incoming wave are, separately, given by

$$\Phi(k_n r) = H_1^{(2)}(k_n r) \qquad (9.34)$$

and

$$\bar{\Phi}(k_n r) = H_1^{(1)}(k_n r) \qquad (9.35)$$

where Φ is, separately, written as Φ and $\bar{\Phi}$ for clarity, and $H_1^{(1)}$ and $H_1^{(2)}$ are Hankel functions. Hereafter, the notation of $\Phi'(\xi)$ denotes $d\Phi(\xi)/d\xi$. According to the property of Hankel function, the approximate representations of Eqs. (9.34) and (9.35) for large values of $k_n r$ can be given by

$$H_\chi^{(1)}(k_n r) \approx \sqrt{\frac{2}{\pi k_n r}}e^{i(k_n r - \frac{\chi\pi}{2} - \frac{\pi}{4})}, \quad H_\chi^{(2)}(k_n r) \approx \sqrt{\frac{2}{\pi k_n r}}e^{-i(k_n r - \frac{\chi\pi}{2} - \frac{\pi}{4})} \qquad (9.36)$$

It is noted that Φ represents an outgoing wave compatible with the time factor $e^{i\omega t}$ or an incoming wave compatible with the time factor $e^{-i\omega t}$. The opposite rule is applicable to $\bar{\Phi}$. The solution to Eq. (9.32) for SH waves takes the following form

$$\psi(r,\theta) = \Psi(r)\sin\theta \tag{9.37}$$

where $\Psi(r)$ has the same definition as $\Phi(k_n r)$ in Eqs. (9.34) and (9.35), which is denoted as $\Psi(l_n r)$ and $\bar{\Psi}(l_n r)$, respectively, instead of $\Phi(k_n r)$ and $\bar{\Phi}(k_n r)$. Equations (9.33) and (9.37) are the solutions of carrier waves for Lamb waves and SH waves, respectively. The displacement fields of Lamb wave and SH wave can be determined through the superposition of the carrier wave and the thickness vibration. For the symmetric problem, the total wave field can be written as the summation of the symmetric Lamb wave and the symmetric SH wave.

9.3.2   The body force in x_1-direction

In this section, the wave generated by the body force in the x_1-direction is investigated. By virtue of Eq. (9.25), the body force defined by Eq. (9.18) can be written in the cylindrical coordinate system as

$$f_r = F\omega_b \sin\left\{(\omega_b+\omega_a)\left[\frac{\omega_b\cos\theta+\omega_a\sin\theta}{c_T(\omega_b+\omega_a)}r-t\right]\right\}\cos\theta \tag{9.38}$$

$$f_\theta = -F\omega_b \sin\left\{(\omega_b+\omega_a)\left[\frac{\omega_b\cos\theta+\omega_a\sin\theta}{c_T(\omega_b+\omega_a)}r-t\right]\right\}\sin\theta \tag{9.39}$$

The body forces only exist within the region $r \le a$. To use the reciprocity relation in the following part, we rewrite Eqs. (9.38) and (9.39) in the form of exponential function instead of trigonometric function. The following transformation between exponential function and trigonometric function is used.

$$\sin\zeta = \frac{e^{i\zeta}-e^{-i\zeta}}{2i} \tag{9.40}$$

Then, Eqs. (9.38) and (9.39) can be rewritten as

$$f_r = -\frac{1}{2}iF\omega_b\left[e^{i\left(\frac{\omega_b\cos\theta+\omega_a\sin\theta}{c_T}r-(\omega_b+\omega_a)t\right)} - e^{-i\left(\frac{\omega_b\cos\theta+\omega_a\sin\theta}{c_T}r-(\omega_b+\omega_a)t\right)}\right]\cos\theta \qquad (9.41)$$

$$f_\theta = \frac{1}{2}iF\omega_b\left[e^{i\left(\frac{\omega_b\cos\theta+\omega_a\sin\theta}{c_T}r-(\omega_b+\omega_a)t\right)} - e^{-i\left(\frac{\omega_b\cos\theta+\omega_a\sin\theta}{c_T}r-(\omega_b+\omega_a)t\right)}\right]\sin\theta \qquad (9.42)$$

It is noted from Eqs. (9.41) and (9.42) that the body forces induced by the interaction of the lowest SH wave with the region of quadratic material nonlinearity are independent of z, which means that the body forces are symmetric with respect to the middle plane of the elastic layer (i.e. $z = 0$). It is expected that the scattered wave field is also symmetric with respect to the middle plane.

9.3.3   The generation of Lamb wave
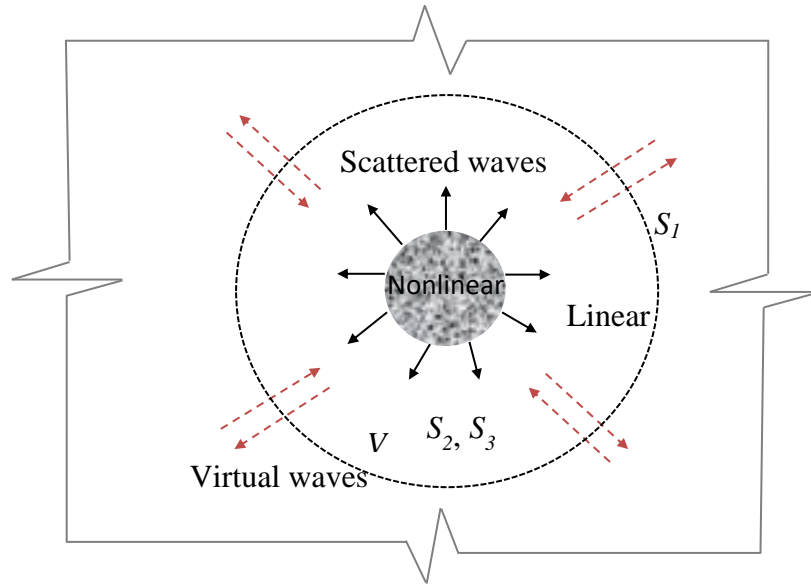
Fig. 9.4. Scattered waves and virtual waves in the annular domain (top view)

The reciprocity relation is utilized to obtain the amplitudes of the generated waves. For two different time-harmonic states, denoted by state A and state B, the reciprocity relation can be represented by (Achenbach, 2003)

$$\int_V\left(f_i^A u_i^B - f_i^B u_i^A\right)dV = \int_S\left(u_i^A\tau_{ij}^B - u_i^B\tau_{ij}^A\right)n_j dS \qquad (9.43)$$

where V is the selected annular domain ($-h \leq z \leq h$, $r \leq b$) with the boundary surfaces S_1 (lateral surface), S_2 and S_3 (top and bottom surfaces), and n_j is the outward normal of the lateral surface S_j (see Fig. 4), b is the radius of the domain. For the problem at hand, Eq. (9.43) can be specified as

$$\int_V \left(f_r^A u_r^B + f_\theta^A u_\theta^B \right) dV$$
$$= \left[\int_{S_1} \left(u_r^A \tau_{rr}^B - u_r^B \tau_{rr}^A \right) + \left(u_\theta^A \tau_{\theta r}^B - u_r^B \tau_{\theta r}^A \right) + \left(u_z^A \tau_{zr}^B - u_z^B \tau_{zr}^A \right) dS \right]_{r=b} \tag{9.44}$$

where the boundary conditions of free tractions on the top and bottom surfaces have been used.

We firstly consider the following body forces with the time factor $e^{i(\omega_a + \omega_b)t}$, which is a part of the body forces defined by Eqs. (9.41) and (9.42):

$$f_r = \begin{cases} \dfrac{1}{2} iF\omega_b e^{-i\frac{\omega_b\cos\theta + \omega_a\sin\theta}{c_T}r} \cos\theta, & r \leq a \\ 0, & r > a \end{cases} \tag{9.45}$$

$$f_\theta = \begin{cases} -\dfrac{1}{2} iF\omega_b e^{-i\frac{\omega_b\cos\theta + \omega_a\sin\theta}{c_T}r} \sin\theta, & r \leq a \\ 0, & r > a \end{cases} \tag{9.46}$$

Hereafter the time factor $e^{i(\omega_a + \omega_b)t}$ is omitted for simplicity. For an elastic layer, the outgoing symmetric scattered waves are represented by the summation of the outgoing symmetric Lamb wave and SH wave, which is labeled by state A:

$$u_r^s = \sum_{e=0}^{\infty} A_e^s V_S^e \Phi'(k_e r)\cos\theta + \sum_{e=0}^{\infty} H_e^s \cos\left(\frac{e\pi z}{h}\right)\frac{1}{l_e r}\Psi(l_e r)\cos\theta \tag{9.47}$$

$$u_\theta^s = \sum_{e=0}^{\infty} A_e^s V_S^e \left(\frac{-1}{k_e r}\right)\Phi(k_e r)\sin\theta - \sum_{e=0}^{\infty} H_e^s \cos\left(\frac{e\pi z}{h}\right)\Psi'(l_e r)\sin\theta \tag{9.48}$$

$$u_z^s = \sum_{e=0}^{\infty} A_e^s W_S^e \Phi(k_e r)\cos\theta \tag{9.49}$$

Equations (9.47)-(9.49) can be directly obtained through mode expansion and V_S^e and W_S^e have the same definitions as the corresponding ones in Eqs. (9A.8) and (9A.9) in Appendix 9A with the replacement of n by e. k_e and l_e are the solutions of the dispersion relations for a specific frequency $\omega = \omega_a + \omega_b$ for Lamb wave and SH wave, respectively. The superscript "1" of u_i representing the first-order is neglected for simplicity here and after.

For state B, we choose a summation of single outgoing and incoming symmetric Lamb waves as a virtual wave in this section, which is represented by

$$u_r^m = \frac{1}{2} V_S^m(z) \left[\Phi'(k_m r) + \bar{\Phi}'(k_m r) \right] \cos\theta \tag{9.50}$$

$$u_\theta^m = \frac{1}{2} V_S^m(z) \left(\frac{-1}{k_m r} \right) \left[\Phi(k_m r) + \bar{\Phi}(k_m r) \right] \sin\theta \tag{9.51}$$

$$u_z^m = \frac{1}{2} W_S^m(z) \left[\Phi(k_m r) + \bar{\Phi}(k_m r) \right] \cos\theta \tag{9.52}$$

where V_S^m and W_S^m have been defined by Eqs. (9A.8) and (9A.9) in Appendix 9A with the replacement of n with m, respectively. k_m is the wave number of the m-th order Lamb wave mode for a specific frequency $\omega = \omega_a + \omega_b$. In addition, it is also assumed that there is no body force for state B (i.e., $f_i^B = 0$).

Next, the terms on the left- and right-hand sides of Eq. (9.44) will be manipulated separately. The left-hand terms of Eq. (9.44), which represents the contribution from the body force, then results in

$$\int_V \left(f_r^A u_r^B + f_\theta^A u_\theta^B \right) dV = \frac{i}{2} F \omega_b B_L^{m+} \bar{V}_s^m \tag{9.53}$$

where

$$\bar{V}_s^m = \int_{-h}^h V_S^m dz = 2 \left(\frac{s_1}{p} \sin(ph) + \frac{s_2}{q} \sin(qh) \right),$$

$$B_L^{m+} = \int_0^a \int_0^{2\pi} \mathfrak{R}_L^m e^{-i\frac{\omega_b \cos\theta + \omega_a \sin\theta}{c_T}r} d\theta dr \qquad (9.54)$$

where

$$\mathfrak{R}_L^m = \frac{1}{2}J_0(k_m r)r + \cos 2\theta \left(\frac{1}{2}J_0(k_m r)r - \frac{1}{k_m}J_1(k_m r) \right) \qquad (9.55)$$

The following identities have been used:

$$J_1'(k_m r) = J_0(k_m r) - \frac{1}{k_m r}J_1(k_m r),$$

$$H_1^{(1)}(k_m r) + H_1^{(2)}(k_m r) = 2J_1(k_m r)$$

To simplify the evaluation of the terms on the right-hand side of Eq. (9.44), we only consider the far-field wave that the terms containing $1/r$ can be neglected. It is reasonable when the propagation distance or the radius of the selected domain (i.e. b) in Fig. 9.4 is large enough. Substitution of Eqs. (9.47)-(9.52) into the integral on the right-hand side of Eq. (9.44) gives rise to

$$Q_{mm} = -A_m^s I_{mm} \frac{2i}{k_m} \qquad (9.56)$$

It should be pointed out that the nonzero result is only available for $e = m$ due to the orthogonality of wave modes (Achenbach, 2003). The detailed derivation of Eq. (9.56) and the definition of I_{mm} are both given in Appendix 9B.

Substituting Eqs. (9.53) and (9.56) into Eq. (9.44) yields

$$\frac{i}{2}F\omega_b B_L^{m+}\bar{V}_s^m = -A_m^s I_{mm} \frac{2i}{k_m} \qquad (9.57)$$

Evaluation of Eq. (9.57) yields the amplitude of the scattered Lamb waves as follows

$$A_m^s = -\frac{1}{4}F\omega_b k_m \frac{B_L^{m+}\bar{V}_s^m}{I_{mm}} \qquad (9.58)$$

The body forces with the time factor $e^{-i(\omega_a+\omega_b)t}$ can be obtained from Eqs. (9.41) and (9.42) as

$$f_r = \begin{cases} -\dfrac{1}{2}iF\omega_b e^{i\frac{\omega_b\cos\theta+\omega_a\sin\theta}{c_T}r}\cos\theta, & r \le a \\ 0 & , r > a \end{cases} \tag{9.59}$$

$$f_\theta = \begin{cases} \dfrac{1}{2}iF\omega_b e^{i\frac{\omega_b\cos\theta+\omega_a\sin\theta}{c_T}r}\sin\theta, & r \le a \\ 0 & , r > a \end{cases} \tag{9.60}$$

For this case, the outgoing symmetric scattered waves can be represented by Eqs. (9.47)-(9.49) by replacing Φ with $\overline{\Phi}$. Proceeding in the same way, we can rewrite Eq. (9.44) as

$$-\frac{i}{2}F\omega_b B_L^{m-}\overline{V}_s^m = A_m^s I_{mm}\frac{2i}{k_m} \tag{9.61}$$

where

$$B_L^{m-} = \int_0^a \int_0^{2\pi} \mathfrak{R}_L^m e^{i\frac{\omega_b\cos\theta+\omega_a\sin\theta}{c_T}r} d\theta dr \tag{9.62}$$

Evaluation of Eq. (9.61) yields

$$A_m^s = -\frac{1}{4}F\omega_b k_m \frac{B_L^{m-}\overline{V}_s^m}{I_{mm}} \tag{9.63}$$

In view of Eqs. (9.36), (9.47)-(9.49), (9.58) and (9.63), the displacement components of the far-field Lamb wave can be represented by the superposition of above the two results as

$$u_r^s = -\frac{1}{2}F\omega_b \sum_{e=0}^{\infty}\frac{\overline{V}_s^e}{I_{ee}}\sqrt{\frac{2k_e}{\pi r}}\cos\theta V_S^e\left(C_{Le}\cos\beta_e^r - S_{Le}\sin\beta_e^r\right) \tag{9.64}$$

$$u_z^s = -\frac{1}{2}F\omega_b \sum_{e=0}^{\infty}\frac{\overline{V}_s^e}{I_{ee}}\sqrt{\frac{2k_e}{\pi r}}\cos\theta W_S^e\left(C_{Le}\cos\beta_e^z - S_{Le}\sin\beta_e^z\right) \tag{9.65}$$

where

$$\beta_e^r = k_e r - (\omega_a + \omega_b)t - \frac{\pi}{4}, \quad \beta_e^z = \beta_e^r - \frac{\pi}{2}$$

and

$$C_{Le} = \int_0^a \int_0^{2\pi} \Re_L^e \left[\cos \left(\frac{\omega_b \cos\theta + \omega_a \sin\theta}{c_T} r \right) \right] d\theta dr,$$

$$S_{Le} = \int_0^a \int_0^{2\pi} \Re_L^e \left[\sin \left(\frac{\omega_b \cos\theta + \omega_a \sin\theta}{c_T} r \right) \right] d\theta dr$$

From Eq. (9.48), it is known that the displacement component in the circumferential direction is very small for the far field Lamb wave due to the factor $1/r$. So it is omitted here. The selected virtual wave defined in Eqs. (9.50)-(9.52) only has a contribution to the solution of generated Lamb waves.

9.3.4 The generation of SH wave

To obtain the solution of the generated SH wave, the symmetric SH wave is then selected as a virtual wave for state B, which contains both outgoing and incoming symmetric SH waves as follows

$$u_r^m = \frac{1}{2} \cos \left(\frac{m\pi z}{h} \right) \frac{1}{l_m r} [\Psi(l_m r) + \bar{\Psi}(l_m r)] \cos\theta,$$

$$u_\theta^m = -\frac{1}{2} \cos \left(\frac{m\pi z}{h} \right) [\Psi'(l_m r) + \bar{\Psi}'(l_m r)] \sin\theta \tag{9.66}$$

The form of the scattered wave keeps unchanged (i.e. Eqs. (9.47)-(9.52)) for state A. The reciprocity relation, Eq. (9.44), is again used. Making use of the body forces defined by Eqs. (9.45) and (9.46) and the virtual wave defined by Eqs. (9.66), the evaluation of the integral on the left-hand side of Eq. (9.44) can be given by

$$\int_V \left(f_r^A u_r^B + f_\theta^A u_\theta^B \right) dV = \frac{1}{2} iF \omega_b S^m B_T^{m+} \tag{9.67}$$

where

$$S^m = \int_{-h}^{h} \cos\left(\frac{m\pi z}{h}\right) dz = \begin{cases} 0, & m \neq 0 \\ 2h, & m = 0 \end{cases} \tag{9.68}$$

and

$$B_T^{m+} = \int_0^a \int_0^{2\pi} \mathfrak{R}_T^m e^{-i\frac{\omega_b \cos\theta + \omega_a \sin\theta}{c_T} r} \, d\theta dr$$

$$\mathfrak{R}_T^m = \frac{1}{2} J_0(l_m r) r - \cos 2\theta \left(\frac{1}{2} J_0(l_m r) r - \frac{1}{l_m} J_1(l_m r)\right) \tag{9.69}$$

Making use of Eqs. (9.47)-(9.49) and (9.66), the evaluation of the surface integral on the right-hand side of Eq. (9.44) yields

$$Q_{mm} = 2\mu H_m^s J_{mm} i \tag{9.70}$$

where $J_{mm} = h$ for $m \neq 0$ or $J_{mm} = 2h$ for $m = 0$. It should be pointed out that Eq. (9.70) only has nonzero values for $e = m$ due to the orthogonality of wave modes. The detailed derivation of Eq. (9.70) is presented in Appendix 9C. By virtue of Eqs. (9.67) and (9.70), Eq. (9.44) can be rewritten as

$$\frac{1}{2} i F \omega_b S^m B_T^{m+} = 2\mu H_m^s J_{mm} i \tag{9.71}$$

From the expression of S^m in Eq. (9.68), we find that only the amplitude of the SH wave of lowest mode (i.e. $m = 0$) is nonzero, which can be represented by

$$H_0^s = \frac{1}{4} \frac{F}{\mu} \omega_b B_T^{0+} \tag{9.72}$$

The virtual wave defined by Eqs. (9.66) only contributes to the scattered SH wave.

For the body forces defined by Eqs. (9.59) and (9.60), together with the virtual wave defined by Eqs. (9.66), Eq. (9.44) can be specified through the same procedure as

$$-\frac{1}{2} i F \omega_b S^m B_T^{m-} = -2\mu H_m^s J_{mm} i \tag{9.73}$$

where

$$B_T^{m-} = \int_0^a \int_0^{2\pi} \Re_T^m e^{i\frac{\omega_b \cos\theta + \omega_a \sin\theta}{c_T}r} d\theta dr \tag{9.74}$$

Equation (9.73) gives rise to

$$H_0^s = \frac{1}{4}\frac{F}{\mu}\omega_b B_T^{0-} \tag{9.75}$$

By virtue of Eqs. (9.36), (9.48), (9.72) and (9.75), the summation of the above two results yields the far-field symmetric SH wave, as follows

$$u_\theta^s = -\sqrt{\frac{1}{r}}\frac{F}{\mu}\omega_b \sqrt{\frac{1}{2\pi}}\sqrt{\frac{c_T}{\omega_a + \omega_b}} B_T^0 \sin\theta \cos\left(\beta_e^\theta + \vartheta_0^T\right) \tag{9.76}$$

where

$$B_T^0 = \sqrt{C_{T0}^2 + S_{T0}^2}, \quad \vartheta_0^T = \arccos\frac{C_{T0}}{B_T^0}, \quad \beta_e^\theta = l_0 r - (\omega_a + \omega_b)t - \frac{\pi}{4} \tag{9.77}$$

with

$$C_{T0} = \int_0^a \int_0^{2\pi} \Re_T^0 \cos\left(\frac{\omega_b \cos\theta + \omega_a \sin\theta}{c_T}r\right) d\theta dr,$$

$$S_{T0} = \int_0^a \int_0^{2\pi} \Re_T^0 \sin\left(\frac{\omega_b \cos\theta + \omega_a \sin\theta}{c_T}r\right) d\theta dr$$

where R_T^0 is defined in Eq. (9.69) by setting $m = 0$.

Here $l_{m=0} = (\omega_a + \omega_b)/c_T$ has been used for the SH wave of lowest mode. It can be noted from Eq. (9.47) that the displacement component in the radial direction is small in the far field due to the factor of $1/r$. It is of interest to note that only the lowest SH wave has been excited for the incidence of two lowest SH waves.

9.4 Total displacement field of scattered wave

9.4.1 Wave generation by the force in x_2-direction

The waves excited by the body force in the x_2-direction can be obtained directly from the solution to the waves excited by the body force in the x_1-direction.

Intuitively, whether the external force is applied in the x_1- or x_2-direction, both generated waves should have the same expression when the elastic layer is rotated by an angle $\pi/2$. In this case, the solution to the waves excited by the body force defined in Eq. (9.19) can be obtained based on the solution to the waves excited by the body force defined by Eq. (9.18) by making use of the ratio of f_2 and f_1 as well as the rotation of the coordinate system. By virtue of Eq. (9.18) and (9.19), the ratio of f_2 and f_1 is given by

$$\frac{f_2}{f_1} = \frac{\omega_a}{\omega_b} \tag{9.78}$$

When the coordinate system is rotated by $\pi/2$ clockwise, the transformation between these two coordinate systems can be given by

$$r' = r, \quad \theta' = \theta - \pi/2, \quad z' = z \tag{9.79}$$

For the coordinate system (r', θ', z'), we can obtain the solution in the same form as the ones given in Eqs. (9.64), (9.65) and (9.76) by replacing θ with θ'. And making use of Eq. (9.78), the solution to the wave excited by the force f_2 can be obtained in the new coordinate system. When we use the transformation between θ and θ' given in Eq. (9.79), the expression of the outgoing Lamb wave excited by the body force in the x_2-direction can be obtained, which is represented in the old coordinates (r, θ, z) as

$$u_r^s = -\frac{1}{2} F \omega_a \sum_{e=0}^{\infty} \frac{\bar{V}_s^e}{I_{ee}} \sqrt{\frac{2k_e}{\pi r}} \sin \theta V_S^e \left(C_{Le} \cos \beta_e^r - S_{Le} \sin \beta_e^r \right) \tag{9.80}$$

$$u_z^s = -\frac{1}{2} F \omega_a \sum_{e=0}^{\infty} \frac{\bar{V}_s^e}{I_{ee}} \sqrt{\frac{2k_e}{\pi r}} \sin \theta W_S^e \left(C_{Le} \cos \beta_e^z - S_{Le} \sin \beta_e^z \right) \tag{9.81}$$

Proceeding with the same procedure, the expression of the outgoing SH wave can be represented by

$$u_\theta^s = \sqrt{\frac{1}{r}} \frac{F}{\mu} \omega_a \sqrt{\frac{1}{2\pi}} \sqrt{\frac{c_T}{\omega_a + \omega_b}} B_T^0 \cos \theta \cos \left(\beta_e^\theta + \vartheta_0^T \right) \tag{9.82}$$

9.4.2   Wave generation by the surface traction t_3

In this section, we consider the waves induced by the normal tractions t_3 on the bottom and top surfaces shown in Fig. 9.3. In view of Eq. (9.25), the traction t_3 defined in Eq. (9.24) can be rewritten in the cylindrical coordinate system as

$$t_3 = \frac{B}{4} A_a A_b \frac{\omega_a \omega_b}{c_T^2} \left[e^{i\frac{\omega_b \cos\theta + \omega_a \sin\theta}{c_T}r} \cdot e^{-i(\omega_b + \omega_a)t} + e^{-i\frac{\omega_b \cos\theta + \omega_a \sin\theta}{c_T}r} \cdot e^{i(\omega_b + \omega_a)t} \right] \quad (9.83)$$

The reciprocity relation is also utilized to obtain the solutions for the wave excited by the surface tractions. The integrals on the upper and bottom surfaces are nonzero, while the body force is considered to be zero for this case. Thus, Eq. (9.44) can be specified to

$$0 = \left[\int_{S_1} \left(u_r^A \tau_{rr}^B - u_r^B \tau_{rr}^A \right) + \left(u_\theta^A \tau_{\theta r}^B - u_r^B \tau_{\theta r}^A \right) + \left(u_z^A \tau_{zr}^B - u_z^B \tau_{zr}^A \right) dS \right]_{r=b}$$
$$+ \left[\int_{S_2} \left(u_z^B t_3 \right) dS \right]_{z=h} + \left[\int_{S_3} \left(u_z^B t_3 \right)(-1) dS \right]_{z=-h} \quad (9.84)$$

where t_3 is the surface traction, which is defined by Eq. (9.83). When the free Lamb wave is selected as the virtual wave, which is represented by Eqs. (9.50)-(9.52), the expression of the Lamb wave excited by the surface tractions can be obtained. The first integral in Eq. (9.84) has been given in Eqs. (9.56) and in Eq. (9.61) (the right-hand side), respectively, for different time factors. For the tractions with the time factor $e^{i(\omega_b + \omega_a)t}$ or $e^{-i(\omega_b + \omega_a)t}$, the evaluations of Eq. (9.84) for different time factors can be rewritten separately by

$$-A_m^S I_{mm} \frac{2i}{k_m} + \frac{B}{2} A_a A_b \frac{\omega_a \omega_b}{c_T^2} W_s^m(h) T_m^+ = 0;$$
$$A_m^S I_{mm} \frac{2i}{k_m} + \frac{B}{2} A_a A_b \frac{\omega_a \omega_b}{c_T^2} W_s^m(h) T_m^- = 0 \quad (9.85)$$

which successively result in

$$A_m^S = -i \frac{B}{4} \frac{k_m}{I_{mm}} A_a A_b \frac{\omega_a \omega_b}{c_T^2} W_s^m(h) T_m^+ \quad (9.86)$$

and

$$A_m^S = i \frac{B}{4} \frac{k_m}{I_{mm}} A_a A_b \frac{\omega_a \omega_b}{c_T^2} W_s^m(h) T_m^- \tag{9.87}$$

where

$$
\begin{aligned}
T_m^+ &= \int_0^{2\pi} \int_0^a J_1(k_m r) \cos\theta\, e^{-i \frac{\omega_b \cos\theta + \omega_a \sin\theta}{c_T} r} r\, d\theta dr, \\
T_m^- &= \int_0^{2\pi} \int_0^a J_1(k_m r) \cos\theta\, e^{i \frac{\omega_b \cos\theta + \omega_a \sin\theta}{c_T} r} r\, dr d\theta
\end{aligned}
\tag{9.88}
$$

Substitution of the expressions of the amplitudes into Eqs.(9.47)-(9.49) gives rise to the expression of Lamb wave. It should be noted that Φ should be replaced by $\bar{\Phi}$ for the waves induced by the tractions of the time factor $e^{-i(\omega_b + \omega_a)t}$. In view of Eq. (9.36), the expressions of the displacement components for the far-field Lamb wave can be represented by

$$u_r^s = \sum_{e=0}^{\infty} A_e^{LT} V_S^e \left(S_{Le}^T \cos\beta_e^r + C_{Le}^T \sin\beta_e^r \right) \tag{9.89}$$

$$u_z^s = \sum_{e=0}^{\infty} A_e^{LT} W_S^e \left(S_{Le}^T \cos\beta_e^z + C_{Le}^T \sin\beta_e^z \right) \tag{9.90}$$

where

$$A_e^{LT} = -\frac{B}{2} \frac{A_a A_b}{I_{ee}} \frac{\omega_a \omega_b}{c_T^2} W_s^e(h) \sqrt{\frac{2k_e}{\pi r}} \cos\theta$$

and

$$S_{Le}^T = \int_0^{2\pi} \int_0^a J_1(k_e r) r \cos\theta \sin\left(\frac{\omega_b \cos\theta + \omega_a \sin\theta}{c_T} r \right) d\theta dr$$

$$C_{Le}^T = \int_0^{2\pi} \int_0^a J_1(k_e r) r \cos\theta \cos\left(\frac{\omega_b \cos\theta + \omega_a \sin\theta}{c_T} r \right) d\theta dr$$

Intuitively, the normal tractions have no contribution to the generation of SH wave. It can be easily proved by changing the virtual wave from Lamb wave to SH

wave.

9.4.3 The total expressions of the scattered waves

The superposition of the wave fields excited separately by the body forces and the surface tractions is equivalent to the waves scattered by the nonlinear region. The displacement components of the far-filed Lamb wave can be given by

$$u_r^s = \sum_{e=0}^{\infty} A_e^L V_S^e \cos\left(\beta_e^r + \vartheta_e^L\right) \tag{9.91}$$

$$u_z^s = \sum_{e=0}^{\infty} A_e^L W_S^e \cos\left(\beta_e^z + \vartheta_e^L\right) \tag{9.92}$$

where the amplitude of the eth-order Lamb wave mode is

$$A_e^L = \sqrt{\left(A_e^{LB} C_{Le} + A_e^{LT} S_{Le}^T\right)^2 + \left(A_e^{LB} S_{Le} - A_e^{LT} C_{Le}^T\right)^2} \tag{9.93}$$

with

$$A_e^{LB} = \left(-\frac{1}{2} F \frac{\bar{V}_s^e}{I_{ee}} \sqrt{\frac{2k_e}{\pi r}}\right)\left(\omega_b \cos\theta + \omega_a \sin\theta\right),$$

$$\vartheta_e^L = \arccos \frac{A_e^{LB} C_{Le} + A_e^{LT} S_{Le}^T}{A_e^L}$$

where F is defined by Eq. (9.20), B_L^e, $\bar{V}_s^e$ and I_{ee} are defined in Eqs. (9.54) and (9B.10) in Appendix B, respectively, by the replacement of m with e; the expressions of V_S^e and W_S^e are given in Eqs. (9A.8) and (9A.9) in Appendix 9A, respectively, with the replacement of n with e; and k_e is the eth-order wave number corresponding to the wave frequency $\omega = \omega_a + \omega_b$. The displacement component in the circumferential direction is neglected due to its' small magnitude in the far field.

The total expression of the SH wave can be given by

$$u_\theta^s = A^{SH} \cos\left(\beta_e^\theta + \vartheta_0^T\right) \tag{9.94}$$

where

$$A^{SH} = \sqrt{\frac{1}{r}}\frac{F}{\mu}\sqrt{\frac{1}{2\pi}}\sqrt{\frac{c_T}{\omega_a + \omega_b}}B_T^0\left(\omega_a\cos\theta - \omega_b\sin\theta\right) \tag{9.95}$$

where B_T^0 has been defined in Eq. (9.77). The displacement component in the radial direction is omitted due to its' small magnitude in the far field. The scattered SH wave is remarkably advantageous over the Lamb wave due to its' simple mathematical structure. Using the measurement of the amplitude of SH wave or Lamb wave, the values of the nonlinear material constants, A and B, can be figured out. The method utilized this chapter can't give rise to the evaluation of the nonlinear material constant C.

9.5 Numerical results and discussions

The analytical solutions for the scattering of two lowest SH waves from a cylindrical region of nonlinear material have been obtained. In this section, the results will be shown graphically based on the expressions given by Eqs. (9.91)-(9.95). The effects of the radius of the nonlinear region, the magnitudes of the nonlinear material constants, the detection angles and the wavelengths of the incident waves on the amplitudes of the scattered waves will be investigated.

For the incident waves, we assume

$$A_a = A_b = H, \quad \omega_a = \eta\omega_b \tag{9.96}$$

where H and η are the wave amplitude and the ratio of the frequencies of the two incident waves, respectively. For the sake of illustration, the following dimensionless quantities are introduced:

$$\bar{r} = \frac{r}{h}, \ C_N = \frac{1}{\mu}\left(\frac{A}{2} + B\right), \ \alpha = \frac{A}{2B}, \ \bar{\lambda} = \frac{\lambda^w}{h}, \ \bar{\lambda}_b = \frac{\lambda_b}{h},$$
$$\bar{H} = \frac{H}{h}, \ \bar{a} = \frac{a}{h}, \ \bar{A}^{SH} = \frac{A^{SH}}{h}, \ \bar{A}^L = \frac{A_0^L}{h} \tag{9.97}$$

where $\lambda^w = 2\pi c_T/(\omega_a + \omega_b)$ and $\bar{\lambda} = \bar{\lambda}_b/(\eta + 1)$ should be noticed; λ_b is the wavelength of the incident wave of frequency ω_b, and $2h$ is the thickness of the elastic layer.

For the scattered Lamb wave, we take the zero-order mode as an example and the amplitude, i.e. A_0^L in Eq. (9.93), is considered. The assumption of long wavelength of the incident wave or thin thickness of the elastic layer, i.e. $1/\bar{\lambda}_b \to 0$ or $\bar{a}/\bar{\lambda}_b \ll 1$ is made in this section. Thus, the wavenumber of the Lamb wave of zero-order mode can be obtained approximately by a limiting process (Achenbach, 2012) as

$$k_0 = \sqrt{\frac{1-\upsilon}{2}} \frac{\omega_a + \omega_b}{c_T} \tag{9.98}$$
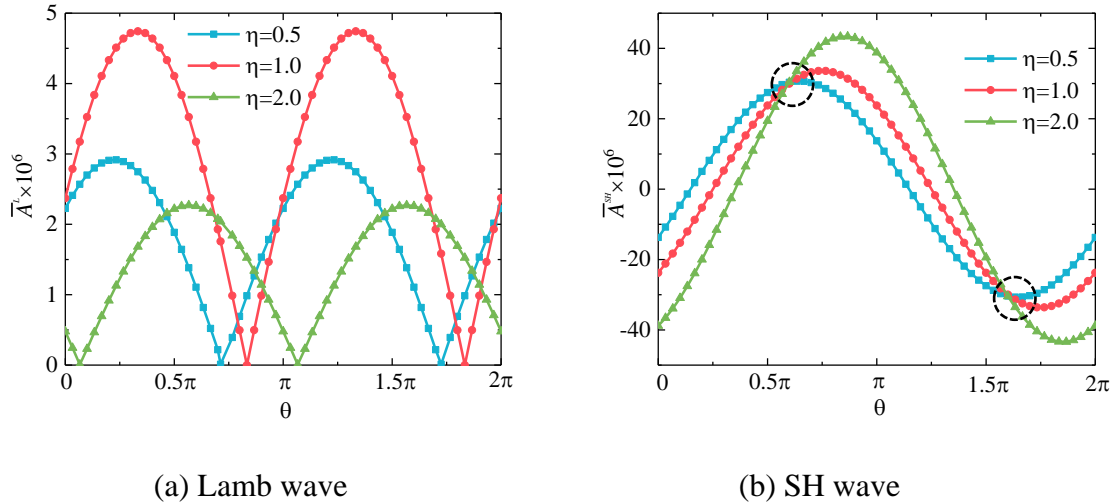
(a) Lamb wave   (b) SH wave

Fig. 9.5 Distribution of the amplitudes of the scattered waves along the circumferential direction

Figures 9.5a and 9.5b show the distributions of the amplitudes of the scattered Lamb waves and SH waves along the circumferential direction. The wavelength of the incident wave b is fixed as $\bar{\lambda}_b = 100$, while the ratio of the frequencies of the two incident waves (wave a and wave b) is in three different cases, i.e. $\eta=0.5$, $\eta=1$ and

$\eta=2$. Other parameters are fixed as $C_N = 100$, $\alpha = 1/2$, $\bar{r} = 1000$, $\bar{H} = 0.01$, $\upsilon = 0.3$ and $\bar{a} = 50$. These two figures can be used to determine the best detection angles, where the amplitudes of the scattered waves are the largest, which correspond to the strongest signals. At the meantime, the dead angles where the amplitudes are zero can be avoided. From both figures, we can find that the ratio of frequencies of the incident waves has significant influence on the wave amplitudes of the scattered waves. However, for two special points, which are marked by circles in Fig. 9.5b, they almost keep unchanged even if the ratio of the frequencies varies. The selection of the ratio of the frequencies can be regarded as an effective manner to adjust the position of the best detection angle and the dead angle, see Figs. 9.5a and 9.5b. The largest amplitude also varies with the ratio of frequencies. For example, the amplitude for $\eta=1$ is the largest for the scattered Lamb waves, see Fig. 9.5a, while the amplitude for $\eta=2$ is the largest for the scattered SH waves, see Fig. 9.5b.

(a) Lamb wave   (b) SH wave
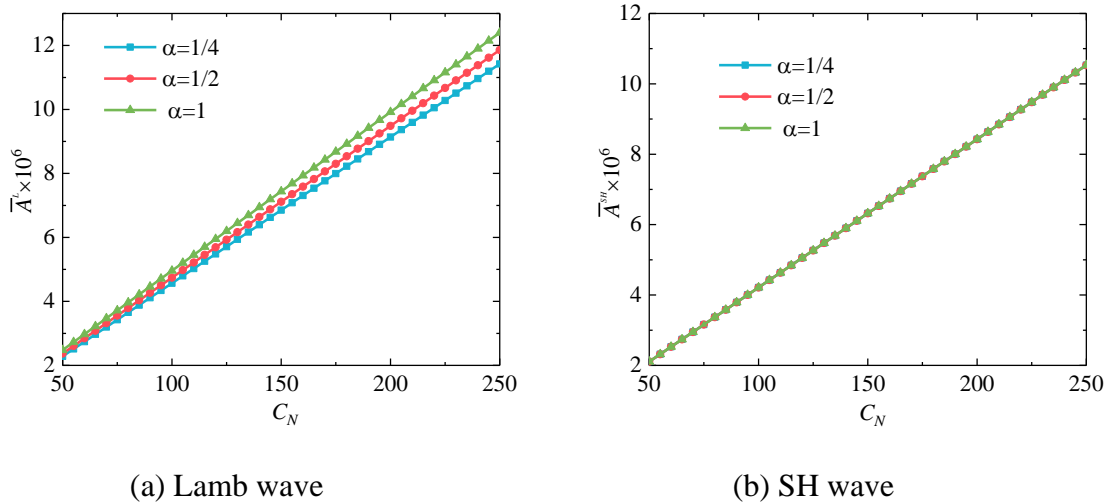
Fig. 9.6 Variations of the amplitudes of the scattered waves with the dimensionless nonlinear material constant C_N at the angle $\theta = \pi/3$

Figure 9.6a and 9.6b show the variations of the amplitudes of the scattered waves with the dimensionless nonlinear material constant C_N at the angle $\theta = \pi/3$. Another dimensionless nonlinear constant α is considered for three different cases

when it equals 1/4, 1/2 and 1, respectively. Other parameters are fixed as $\bar{r} = 1000$, $\eta = 1$, $\bar{\lambda}_b = 100$, $\bar{H} = 0.01$, $\upsilon = 0.3$ and $\bar{a} = 50$. The nonlinear material constants have a strong correlation with material micro-damages. Thus, through Figs. 9.6a and 9.6b, we can establish a direct relation of the level of material damage with the amplitudes of the scattered waves. The amplitudes of the scattered Lamb waves and SH waves both increase linearly with the increase of C_N, see Figs. 9.6a and 9.6b. Comparing Fig. 9.6a with Fig. 9.6b, it is observed that the dimensionless material constant α only has an influence on the amplitudes of the Lamb waves, which comes from the contribution of the equivalent surface tractions, see Eq. (9.93). Since the normal surface tractions have no contribution to the generation of SH waves, the amplitudes of SH waves only depend on the nonlinear material constant C_N. In this way, the scattered SH waves may be easier to be used to evaluate material damages. For the scattered Lamb waves, the material constant α has a small influence on the wave amplitudes when the material constant C_N is small, see the curves located around $C_N = 50$ in Fig. 9.6a. Thus, we may not have to consider the effects of α in this zone. With the increase of C_N, the influence of α becomes more significant on the amplitudes of the Lamb waves.

The relations between the amplitudes of the scattered waves and the radius of the nonlinear region are presented graphically in Figs. 9.7a and 9.7b for the incident waves of different ratios of frequencies, i.e., $\eta = 0.5$, 1, 2. Other parameters are fixed as $\bar{r} = 1000$, $C_N = 100$, $\alpha = 1/2$, $\bar{\lambda}_b = 100$, $\bar{H} = 0.01$, and $\upsilon = 0.3$. Ultrasound is often viewed as a powerful tool to measure the size of the damage zone. However, for the curves in Figs. 9.7a and 9.7b, there exist many congestion areas where the amplitudes vary up and down quickly with the increase of the radius, see the zones marked by circles in Figs. 9.7a and 9.7b. In these zones, the radius of the nonlinear region is difficult to be determined by using the inverse computation. It's better to measure the radius of the nonlinear region in the zones where the amplitudes of the scattered waves increase monotonously with the radius of the nonlinear region.

(a) Lamb wave   (b) SH wave
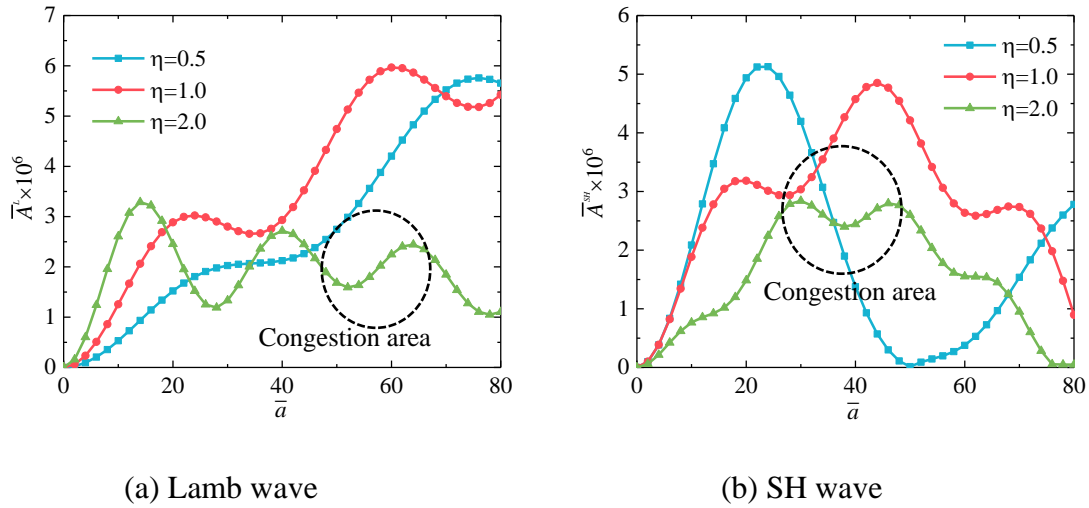
Fig. 9.7 Variations of the amplitudes of the scattered waves versus the dimensionless radius of the nonlinear region at the angle $\theta = \pi/3$

From Fig. 9.7a, it is observed that the range of the monotone zones depends largely on the ratio of the frequencies of the two incident waves. For example, the curve corresponding to $\eta = 0.5$ in Fig. 9.7a is nearly monotonous, while the other two curves are not. Moreover, the ratio of the frequencies can also be used to adjust the positions of the monotone zones. For example, the zones around $\bar{a} = 60$ in Fig. 9.7a and $\bar{a} = 40$ in Fig. 9.7b are choppy for $\eta = 2$, while these zones become monotonous for $\eta = 0.5$. For the mixing of two incident waves, the adjustment of the ratio of the frequencies is an important manner to optimize the measurement.

In Figs. 9.8a and 9.8b, the relations between the amplitudes of the scattered waves and the wavelengths of the incident waves are presented for different ratios of frequencies at the angle $\theta = \pi/3$. The other parameters are fixed as $\bar{r} = 1000$, $C_N = 100$, $\alpha = 1/2$, $\bar{H} = 0.01$, $\upsilon = 0.3$ and $\bar{a} = 50$. For the wavelengths under consideration, the amplitudes of the Lamb waves corresponding to $\eta = 0.5$ and 1.0 decrease as the wavelength increases, while the amplitudes corresponding to $\eta = 2$ is not monotonous, see Fig. 9.8a. For the scattered SH waves, the variations of the amplitudes are not monotonous with the increase of the wavelength for all the three ratios of the frequencies, see Fig. 9.8b.

(a) Lamb wave

(b) SH wave
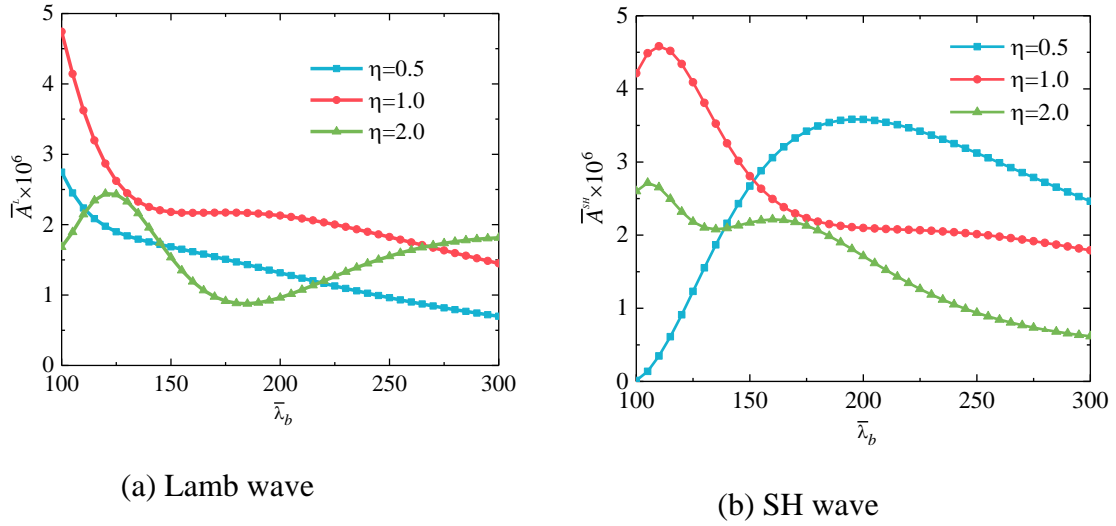
Fig. 9.8 Variations of the amplitudes of the scattered waves versus the wavelengths of the incident waves at the angle $\theta = \pi/3$

Overall, the ratios of the frequencies have obvious influences on the relation between the amplitude and the wavelength. Thus, an appropriate wavelength of the incident waves can be determined by using the curves shown in Figs. 9.8a and 9.8b combining with the consideration of the ratios of the frequencies.

9.6　Concluding remarks

The materials with microstructural defects behave in a nonlinear manner, which are described by a quadratic constitutive relation in this paper. An elastic layer with a cylindrical region of quadratic material nonlinearity across the thickness is considered. Two SH waves of lowest modes are launched from two orthogonal directions, which intersect at the nonlinear region. A three-dimensional nonlinear scattering problem is thus studied.

Using the perturbation method, the nonlinear governing equations and the boundary conditions are reduced to two sets of linear equations at different orders. The zero-order equations can be specified to the governing equations for the SH waves of lowest modes with free boundary conditions. Substitution of the expressions of the SH waves into the nonlinear terms in the first-order equations gives rise to a series of inhomogeneous equations. Mathematically, these equations are same as those that are used to describe the problem of forced wave motion

caused by the local body forces and the local surface tractions. By referring to the solutions for waves induced by the point force, the reciprocity relation in elastodynamics is used to obtain the amplitudes of the waves induced by the equivalent body forces and the equivalent surface tractions. The analytical solutions for the far-field Lamb wave and SH wave scattered from the nonlinear region are then readily obtained. It is of interest to find out that only the coefficient of the lowest mode is non-zero for the scattered SH wave.

Numerical examples are presented for the scattered Lamb wave of zero-order mode and SH wave propagating in a thin elastic layer. The influences of the detection angle, the nonlinear material constants, the size of nonlinear region, the ratio of frequencies of two incident waves and the wavelengths of incident waves on the amplitudes of the scattered waves are investigated. The direct relations between the amplitudes of the scattered waves and the size of the nonlinear region and the nonlinear material constants, which have a strong correlation with the damage level, are presented graphically. Based on the theoretical analysis, some possible methods are proposed to optimize the measurements or detections for the nonlinear nondestructive evaluation and test. These methods include the adjustments of the detection angle and the change of the ratio of the frequencies and/or the wavelengths of the incident waves.

Appendix 9A: Free wave propagation in a linearly elastic layer

The free wave propagation in an elastic layer is studied. The analytical solution to this problem has been shown in Achenbach and Xu (1999). The waves propagating in an elastic layer were decomposed into a superposition of thickness vibration and a membrane carrier wave. Since the thickness motion keeps unchanged, we only need to solve the membrane equations for different problems. For the Lamb wave mode, the displacement components can be written in the following forms:

$$u_i^n = \frac{1}{k_n} V^n(x_3) \frac{\partial \varphi(x_1, x_2)}{\partial x_i}, \; i = 1, \; 2 \tag{9A.1}$$

$$u_3^n = W^n(x_3)\varphi(x_1, x_2) \tag{9A.2}$$

where the time harmonic factor $e^{-i\omega t}$ (or $e^{i\omega t}$) is neglected for simplicity, k_n is a wave number of nth-order Lamb wave mode, and $\varphi(x_1, x_2)$ is a solution of the reduced membrane wave equation in the x_1-x_2 plane, which is given by

$$\frac{\partial^2 \varphi(x_1, x_2)}{\partial x_1^2} + \frac{\partial^2 \varphi(x_1, x_2)}{\partial x_2^2} + k_n^2 \varphi(x_1, x_2) = 0 \tag{9A.3}$$

In addition to Lamb waves, SH waves should also be considered for an elastic layer. SH waves are equivoluminal waves, whose vibration plane is parallel to the x_1-x_2 plane. Their wave modes can be represented by

$$u_1^n = \frac{1}{l_n} U^n(x_3) \frac{\partial \psi(x_1, x_2)}{\partial x_2} \tag{9A.4}$$

$$u_2^n = -\frac{1}{l_n} U^n(x_3) \frac{\partial \psi(x_1, x_2)}{\partial x_1} \tag{9A.5}$$

$$u_3^n \equiv 0 \tag{9A.6}$$

where l_n is a wave number of nth-order SH wave mode and ψ has to satisfy the following membrane equation as

$$\frac{\partial^2 \psi(x_1, x_2)}{\partial x_1^2} + \frac{\partial^2 \psi(x_1, x_2)}{\partial x_2^2} + l_n^2 \psi(x_1, x_2) = 0 \qquad (9A.7)$$

The wave modes, U^n, V^n and W^n, of the thickness vibration are given in the following:

a. Lamb wave

V^n and W^n are the nth-order wave modes along the thickness direction for Lamb waves, which can be separated into symmetric and antisymmetric modes relative to the middle plane of an elastic layer. Considering the free boundary conditions, the symmetric mode can be represented by

$$V_S^n = s_1 \cos(p_n x_3) + s_2 \cos(q_n x_3) \qquad (9A.8)$$

$$W_S^n = s_3 \sin(p_n x_3) + s_4 \sin(q_n x_3) \qquad (9A.9)$$

where

$$\begin{aligned} & s_1 = 2\cos(q_n h), \ s_2 = -[(k_n^2 - q_n^2)/k_n^2]\cos(p_n h), \\ & s_3 = -2(p_n/k_n)\cos(q_n h), \ s_4 = -[(k_n^2 - q_n^2)/(q_n k_n)]\cos(p_n h) \end{aligned} \qquad (9A.10)$$

Here we define

$$\begin{aligned} & p_n^2 = \frac{\omega^2}{c_L^2} - k_n^2, \ q_n^2 = \frac{\omega^2}{c_T^2} - k_n^2 \\ & c_L = \sqrt{(\lambda + 2\mu)/\rho_0}, \ c_T = \sqrt{\mu/\rho_0} \end{aligned} \qquad (9A.11)$$

For the antisymmetric modes, we have

$$V_A^n = a_1 \sin(p_n x_3) + a_2 \sin(q_n x_3) \qquad (9A.12)$$

$$W_A^n = a_3 \cos(p_n x_3) + a_4 \cos(q_n x_3) \qquad (9A.13)$$

where

$$\begin{aligned} & a_1 = 2\sin(q_n h), \ a_2 = -[(k_n^2 - q_n^2)/k_n^2]\sin(p_n h), \\ & a_3 = 2(p_n/k_n)\sin(q_n h), \ a_4 = [(k_n^2 - q_n^2)/(q_n k_n)]\sin(p_n h) \end{aligned} \qquad (9A.14)$$

b. SH wave

U^n is the SH wave mode distributed along the thickness direction, which is represented by

$$U^n(x_3) = \cos(q_n x_3) \quad \text{for symmetric modes.} \tag{9A.15}$$

$$U^n(x_3) = \sin(q_n x_3) \quad \text{for antisymmetric modes.} \tag{9A.16}$$

and $q_n^2 = \omega^2/c_T^2 - l_n^2$. Using the free boundary condition, we have

$$q_n = \frac{n\pi}{2h} \tag{9A.17}$$

where n =0, 2, 4, … for symmetric modes, and n =1, 3, 5, … for antisymmetric modes.

Appendix 9B: The derivation of Eq. (9.56)

Substitution of Eqs. (9.47)-(9.52) into the integral on the right-hand side of Eq. (9.44) gives rise to

$$
\begin{aligned}
Q_{em} &= \left[\int_{S_1} \left[\left(u_r^A \tau_{rr}^B - u_r^B \tau_{rr}^A \right) + \left(u_\theta^A \tau_{\theta r}^B - u_r^B \tau_{\theta r}^A \right) + \left(u_z^A \tau_{zr}^B - u_z^B \tau_{zr}^A \right) \right] dS \right]_{r=b} \\
&= \left[\int_0^{2\pi} \int_{-h}^h \left[\left(u_r^A \tau_{rr}^B - u_r^B \tau_{rr}^A \right) + \left(u_\theta^A \tau_{\theta r}^B - u_r^B \tau_{\theta r}^A \right) + \left(u_z^A \tau_{zr}^B - u_z^B \tau_{zr}^A \right) \right] r d\theta dz \right]_{r=b} \\
&= b \int_0^{2\pi} \int_{-h}^h \left[\left(u_r^A \tau_{rr}^B - u_r^B \tau_{rr}^A \right) + \left(u_\theta^A \tau_{\theta r}^B - u_r^B \tau_{\theta r}^A \right) + \left(u_z^A \tau_{zr}^B - u_z^B \tau_{zr}^A \right) \right] d\theta dz \\
&= \frac{1}{2} \pi b \sum_{e=0}^\infty A_e^s \int_{-h}^h
\left\{
\begin{array}{l}
\left[V_S^e(z) \Sigma_{rr}^{Sm}(z) + W_S^m(z) \Sigma_{rz}^{Se}(z) \right] \Phi(k_m r) \Phi'(k_e r) \\
- \left[V_S^m(z) \Sigma_{rr}^{Se}(z) + W_S^e(z) \Sigma_{rz}^{Sm}(z) \right] \Phi(k_e r) \Phi'(k_m r) \\
+ \left[V_S^e(z) \Sigma_{rr}^{Sm}(z) + W_S^m(z) \Sigma_{rz}^{Se}(z) \right] \bar{\Phi}(k_m r) \Phi'(k_e r) \\
- \left[V_S^m(z) \Sigma_{rr}^{Se}(z) + W_S^e(z) \Sigma_{rz}^{Sm}(z) \right] \Phi(k_e r) \bar{\Phi}'(k_m r)
\end{array}
\right\} dz \\
&= \frac{1}{2} \pi b \sum_{e=0}^\infty A_e^s
\left\{
\begin{array}{l}
I_{me} \Phi(k_m r) \Phi'(k_e r) - I_{em} \Phi(k_e r) \Phi'(k_m r) \\
+ I_{me} \bar{\Phi}(k_m r) \Phi'(k_e r) - I_{em} \Phi(k_e r) \bar{\Phi}'(k_m r)
\end{array}
\right\}
\end{aligned} \tag{9B.1}
$$

where

$$I_{em} = \int_{-h}^{h} \left[V_S^m(z) \Sigma_{rr}^{Se}(z) + W_S^e(z) \Sigma_{rz}^{Sm}(z) \right] dz \tag{9B.2}$$

and $\Sigma_{rr}^{Se}(z)$ and $\Sigma_{rz}^{Sm}(z)$ are defined by

$$\Sigma_{rr}^{Se}(z) = \mu \left[c_1 \cos(p_e z) + c_2 \cos(q_e z) \right] \tag{9B.3}$$

where

$$c_1 = \left[2 \left(2p_e^2 - k_e^2 - q_e^2 \right) / k_e \right] \cos(q_e h),$$
$$c_2 = \left[2 \left(k_e^2 - q_e^2 \right) / k_e \right] \cos(p_e h) \tag{9B.4}$$

and

$$\Sigma_{rz}^{Sm}(z) = \mu \left[c_3 \sin(p_m z) + c_4 \sin(q_m z) \right] \tag{9B.5}$$

with

$$c_3 = 4 p_m \cos(q_m h),$$
$$c_4 = \left[\left(k_m^2 - q_m^2 \right)^2 / (q_m k_m^2) \right] \cos(p_m h) \tag{9B.6}$$

The orthogonality relation, which was derived in Section III in (Achenbach and Xu, 1999), has been used, which reads

$$I_{em} \equiv I_{me} \equiv 0, \quad \text{for} \ e \neq m \tag{9B.7}$$

The following equality should also be noted:

$$I_{me} \Phi(k_m r) \Phi'(k_e r) - I_{em} \Phi(k_e r) \Phi'(k_m r) \equiv 0, \quad \text{for} \ e = m \tag{9B.8}$$

By setting $e = m$, Eq. (9.55) can be simplified to

$$Q_{mm} = \frac{1}{2} \pi b A_m^s I_{mm} \left\{ \bar{\Phi}(k_m b) \Phi'(k_m b) - \Phi(k_m b) \bar{\Phi}'(k_m b) \right\}$$
$$= -A_m^s I_{mm} \frac{2i}{k_m} \tag{9B.9}$$

where

$$I_{mm} = \mu[c_1^s \cos^2(ph) + c_2^s \cos^2(qh)] \tag{9B.10}$$

and the constants are defined by

$$
\begin{aligned}
c_1^s &= \frac{(k_m^2 - q^2)(k_m^2 + q^2)}{2q^3 k_m^3}[2qh(k_m^2 - q^2) - (k_m^2 + 7q^2)\sin(2qh)], \\
c_2^s &= \frac{k_m^2 + q^2}{pk_m^3}[4k_m^2 ph + 2(k_m^2 - 2p^2)\sin(2ph)]
\end{aligned}
\tag{9B.11}
$$

This result is the same as the corresponding one in (Achenbach and Xu, 1999) and the following identity for Hankel function has been used

$$\frac{d}{d\xi}H_\upsilon^{(1)}(\xi)H_\upsilon^{(2)}(\xi) - H_\upsilon^{(1)}(\xi)\frac{d}{d\xi}H_\upsilon^{(2)}(\xi) = \frac{4i}{\pi\xi} \tag{9B.12}$$

Appendix 9C: The derivation of Eq. (9.70)

The detailed derivation of Eq. (9.70) are presented below

$$
\begin{aligned}
Q_{em} &= \int_{S_1}\left(u_i^A \sigma_{ij}^B - u_i^B \sigma_{ij}^A\right)n_j dS \\
&= b\sum_{e=0}^{\infty}\int_0^{2\pi}\int_{-h}^{h}H_e^s \mu \frac{1}{2}\cos\left(\frac{e\pi z}{h}\right)\cos\left(\frac{m\pi z}{h}\right)\begin{bmatrix} l_e\Psi\left(l_e b\right)\Psi'(l_m b) - l_m\Psi(l_m b)\Psi'(l_e b) \\ + l_e\Psi\left(l_e b\right)\bar{\Psi}'(l_m b) - l_m\bar{\Psi}(l_m b)\Psi'(l_e b) \end{bmatrix}\sin^2\theta d\theta dz \\
&= b\sum_{e=0}^{\infty}\int_0^{2\pi}\int_{-h}^{h}H_e^s \mu \frac{1}{2}\cos\left(\frac{e\pi z}{h}\right)\cos\left(\frac{m\pi z}{h}\right)\left[l_e\Psi\left(l_e b\right)\bar{\Psi}'(l_m b) - l_m\bar{\Psi}(l_m b)\Psi'(l_e b)\right]\sin^2\theta d\theta dz \\
&= \frac{1}{2}\mu b\sum_{e=0}^{\infty}H_e^s\left[l_e\Psi\left(l_e b\right)\bar{\Psi}'(l_m b) - l_m\bar{\Psi}(l_m b)\Psi'(l_e b)\right]\int_{-h}^{h}\cos\left(\frac{e\pi z}{h}\right)\cos\left(\frac{m\pi z}{h}\right)dz
\end{aligned}
\tag{9C.1}
$$

where the following relation has been used, which is given in section III in (Achenbach and Xu, 1999).

$$l_e\Psi\left(l_e b\right)\Psi'(l_m b) - l_m\Psi(l_m b)\Psi'\left(l_e b\right) = 0 \tag{9C.2}$$

The following orthogonality relation of trigonometric functions can be used.

$$\int_{-h}^{h}\cos\left(\frac{e\pi z}{h}\right)\cos\left(\frac{m\pi z}{h}\right)dz = 0 \quad \text{for} \quad e \neq m \tag{9C.3}$$

Thus, Eq. (9C.1) evolves to

$$
\begin{aligned}
Q_{mm} &= \mu H_m^s \frac{1}{2} bl_m \int_{-h}^{h} \cos^2\left(\frac{m\pi z}{h}\right) dz \left[\Psi\left(l_m b\right) \bar{\Psi}'(l_m b) - \bar{\Psi}(l_m b) \Psi'\left(l_m b\right) \right] \\
&= 2\mu H_m^s J_{mm} i
\end{aligned}
\tag{9C.4}
$$

where

$$
J_{mm} = \int_{-h}^{h} \cos^2\left(\frac{m\pi z}{h}\right) dz = \begin{cases} h, & \text{for } m \neq 0 \\ 2h, & \text{for } m = 0 \end{cases}
\tag{9C.5}
$$

and the identity of Hankel function, Eq. (9B.12), has also been used.

Chapter 10   Concluding remarks and future works

10.1 Concluding remarks

In this dissertation, several theoretical modellings of nonlinear wave propagation in materials and structures were investigated, which have the potential application to the design of novel acoustic devices and the development of nonlinear ultrasound techniques used for nondestructive evaluation. The whole dissertation contains two parts. In the first part, we mainly focused on the investigation of the tunability of solitary waves in soft bars by using the asymptotic expansions and the reductive perturbation method. In Chapter 2, the electric biasing field was used to modulate the solitary waves in soft electroactive bars. In Chapter 3, the pre-stretch is proven to be an effective means to adjust the kink and kink-like waves propagating in viscoelastic soft bars. In the second part, we developed several simplified theories and simple theoretical models to work out analytical solutions to higher harmonic generations by material nonlinearity, which can promote the application of nonlinear ultrasound technique for nondestructive evaluation. The reciprocity theorem in elastodynamics and the shell theory have been used to solve the related problems. In Chapter 4, we presented a general analysis on the higher harmonic generation by plane waves based on quadratic and cubic material nonlinearities. Then, the harmonics of surface waves on a half-space of cubic material nonlinearity were investigated in Chapter 5. In Chapter 6, we conducted an investigation of higher harmonics in pipes, and the shell theory was used to obtain the analytical solution. From the point of view of practical interest, we studied the reflection and scattering from the local region of material nonlinearity induced by local micro-damages in Chapter 7. As an extension, in Chapter 8, we studied the scattering of the incident torsional waves of the lowest mode from a small segment of material nonlinearity in a pipe. In Chapter 9, we investigated the scattering of two SH waves of the lowest mode from a nonlinear cylindrical region in a plate. Detailed contributions of this dissertation are summarized as follows.

In Chapter 2, an asymptotic analysis of solitary waves propagating in an

incompressible isotropic electroactive circular rod subjected to a biasing longitudinal electric displacement was presented. Several asymptotic expansions were introduced to simplify the rod governing equations. The boundary conditions on the lateral surface of the rod were satisfied from the asymptotic point of view. In the limit of finite-small amplitude and long wavelength, a set of ten simplified one-dimensional nonlinear governing equations was established. To validate our approach and the derivation, we compared the linear dispersion relation with the one directly derived from the three-dimensional linear theory in the limit of long wavelength. Then, by the reductive perturbation method, we deduced the far-field equation (i.e. the KdV equation). Finally, the leading order of the electroelastic solitary wave solution was presented. Numerical examples were provided to show the influences of the biasing electric displacement and material constants on the solitary waves. It was found that the biasing electric displacement can modulate the velocity of solitary waves with a prescribed amplitude in the electroactive rod, a very interesting result which may promote the particular application of solitary waves in solids with multi-field coupling.

In Chapter 3, we theoretically investigated kink and kink-like waves propagating in pre-stretched Mooney-Rivlin viscoelastic rods. In the constitutive modeling, the Cauchy stress tensor was assumed to consist of an elastic part and a dissipative part. The asymptotic method was adopted to simplify the nonlinear dynamic equations in the limit of finite-small amplitude and long wavelength. Using the reductive perturbation method, we further derived the well-known far-field equation (i.e. the KdV-Burgers equation), to which two kinds of explicit traveling wave solutions were presented. Examples were given to show the influences of pre-stretch and viscosity on the wave shape and wave velocity. It was shown that pre-stretch could be an effective method for modulating the two types of waves. In addition, such waves may be utilized to measure the viscosity coefficient of the material. The competition between the effects of pre-stretch and viscosity on the kink and kink-like waves was also revealed.

In Chapter 4, harmonics of plane longitudinal and transverse waves in nonlinear elastic solids with up to cubic nonlinearity were investigated in a one-dimensional setting. It was shown that due to the quadratic nonlinearity a transverse

wave generates a second longitudinal harmonic, which, however, propagates with the velocity of transverse waves, as well as resonant transverse first and third harmonics due to the cubic and quadratic nonlinearities. A longitudinal wave generates a resonant longitudinal second harmonic as well as first and third harmonics whose amplitudes increase linearly and quadratically, respectively, with the distance propagated. In a second investigation incidence from the linear side of a primary wave on an interface between a linear and a nonlinear elastic solid was considered. The incident wave crosses the interface and generates a harmonic whose interface conditions are equilibrated by compensatory waves propagating away in both directions from the interface. The back-propagated compensatory wave provides information on the nonlinear elastic constants of the material behind the interface. It was shown that the amplitudes of the compensatory waves can be amplified by mixing two incident longitudinal waves with appropriate frequencies.

In Chapter 5, the analytical far-field solution for the cumulative third harmonic surface wave propagating on a half-space of isotropic incompressible cubically nonlinear material was obtained in a relatively simple and systematic manner. Using the perturbation method for a weakly nonlinear material, the governing equations and the boundary conditions were separated into two sets of uncoupled equations at the zero-order and the first-order, respectively. For a primary linear wave of frequency ω and amplitude $\overline{A}$, the resonant third harmonic has frequency 3ω and amplitude A_N which depends on $\overline{A}^3$ and the propagation distance. It was shown that, in the far field, the resonant third harmonic propagates with the classic Rayleigh wave velocity. We also considered the transmission of the resonant third harmonic across an interface at $x = L$ into a linear material. The transmitted wave has the same general form as the incident third harmonic except that the multiplying factor x now is constant at L, $t > L/c$, $x > L$, and the amplitude also depends on the nonlinear constant. Potential measurement of the transmitted wave can provide information on the location of the interface and the material nonlinearity.

In Chapter 6, higher harmonics in pipes of quadratic nonlinear material behavior were analyzed. Using the shell theory, the mixing of axisymmetric longitudinal waves and torsional waves, and the self-interaction of axisymmetric

longitudinal waves, have been investigated. The dispersion curves of longitudinal waves derived from the linear version of the governing equations show excellent agreement with the corresponding curves obtained from the thick shell theory and three dimensional theory, presented elsewhere. For torsional waves, only the lowest mode was taken into consideration. Using the perturbation method, analytical expressions for the resonant torsional waves generated by the mixing of longitudinal and torsional waves were obtained. The resonant waves with difference frequencies propagate in the opposite direction of the corresponding primary wave. The back-propagation effect has potential application for nondestructive evaluation. The nonlinear shell theory was further simplified for applicability to thin pipes, to obtain expressions for the cumulative second longitudinal harmonics generated by self-interaction of longitudinal waves. For this case, the phase-match conditions, which were used to determine phase-match points, were also presented in an analytical form.

In Chapter 7, two models were proposed to obtain information on the material nonlinearity of an inclusion in a solid body. Material nonlinearity is usually generated by the development of material micro-scale damage. When the region of nonlinear material is large, incidence of ultrasound on the interface between the perfectly joined regions of linear and nonlinear material behavior produces very useful information. Using the continuity condition of stress and displacement at the interface, the harmonics in the nonlinear region, together with the compensatory waves yield a reflected wave whose amplitude contains the defining constant of the material nonlinearity near the interface. The compensatory waves were introduced to ensure the continuity conditions at the interface. When the nonlinear region is an inclusion, the equivalent body force induced by the material nonlinearity generates a backscattered wave. The backscattered wave is determined in a simple manner by the use of the reciprocity theorem of elastodynamics. The backscattered wave obtained in this manner yields information on the nonlinear material properties and the size of the inclusion. In addition, a model based on the superposition of back-propagated compensatory waves from the two interfaces of the nonlinear region reveals the physical mechanism of wave scattering from the nonlinear inclusion.

In Chapter 8, the effect of cubic material nonlinearity on the propagation in a

pipe of the lowest axially symmetric torsional wave mode was investigated. Two cases, one that the material of the whole pipe is nonlinear, and the second that a small segment of the pipe is nonlinear, were considered. In the first case, a first and a third harmonic were obtained by the perturbation method. Analytical expressions for the two cumulative harmonics were derived. The second case leads to a scattering problem. The segment produces nonlinear terms in the equation of motion, which can be regarded as a distribution of body forces. The problem was then reduced to a linear scattering problem. An analytical expression for the backscattered wave was easily obtained by using the elastodynamic reciprocity theorem. Due to the low amplitude of the backscattered wave, we proposed to add another higher frequency wave to the primary wave, to increase the total magnitude of the scattered wave. An example that the originally scattered wave was amplified 50 times by selecting proper frequencies was presented. Both cases considered here have potential application to determine the material properties in a region of nonlinear material behavior.

In Chapter 9, the interaction of two SH waves of lowest modes with a local cylindrical region of quadratic material nonlinearity in an elastic layer was investigated. The nonlinear governing equations and the nonlinear boundary conditions were reduced to a set of linear equations at different orders by making use of the perturbation method. The incident waves were regarded as the solutions to the zero-order governing equations. The first-order equations are a series of inhomogeneous equations by substitution of the expressions of the incident waves, which beer the same form as the equations used to describe the forced wave motion in an elastic layer. Mathematically, the first-order equations can be solved in a similar way when the inhomogeneous terms are viewed as the equivalent body forces or surface tractions. Based on the mode expansions, the amplitudes of the Lamb wave and the SH wave generated by the body forces and surface tractions were obtained by using the reciprocity relation in elastodynamics. It is of interest to note that only the coefficient of the lowest mode is nonzero for the generated SH wave. The amplitudes of the scattered waves were determined by the size of the nonlinear region, the nonlinear material constants, the detection angle, the wavelength and the ratio between the two frequencies of the incident waves, which

were also graphically shown as the numerical examples.

10.2 Future works

As an extension of the works presented in this dissertation, the following interesting research topics will be investigated in the future:

1. The investigation of nonlinear elastic waves propagating in metamaterial, such as periodic structures or phononics, can be conducted based on the methods and the theories used in this dissertation, such as the asymptotic expansions, the reductive perturbation methods, the shell and plate theory, the reciprocity theorem and so on. Due to the attractive characters of metamaterials, it is expected to find some fancy phenomena, which have not been uncovered within the linear theory. The first model is the solitary waves propagating in a soft bar composed of periodic structures. Using the thin rod assumption, the analytical solution is expected to be obtained. The second model is the higher harmonic generation of plane waves by the periodic material nonlinearity. The analytical or semi-analytical solution for the reflected and transmitted higher harmonics could be obtained in a simple and elegant manner by using the reciprocity relation.

2. Experimental researches on higher harmonic generation by material nonlinearity induced by material micro-damages will be conducted. Based on the models and theories proposed in this dissertation, some efficient and useful nonlinear ultrasound techniques are expected to be developed, which may be exploited to detect and monitor the safety conditions of different structures and materials.

3. It has been reported that the blood pulse behaves like a solitary wave. So it is meaningful to model the blood flow as a solitary wave propagating in a blood vessel. In addition, the coupling of electric field and elastic field in most tissues has been uncovered. Thus, it is reasonable to model the blood vessel wall as a pipe of soft electroactive material. Such a model has not yet been proposed in the reported literatures. For the non-ideal blood, the viscoelasticity effect should be taken into account. By using the mathematical and mechanical models, we hope to understand and explain some medical diagnostic measurements used in the traditional Chinese medicine in the sense of modern science.

4. Nonlinear waves propagating in composite materials, anisotropic materials and porous materials have attracted extensive academic interests due to their wide application in industries and engineering. Through the design of such materials and structures, we hope to develop some novel acoustical devices and some ultrasound techniques for nondestructive evaluation based on the application of nonlinear elastic waves.

5. It was much desired to extend the application of the reciprocity theorem in elastodynamics to other fields of solid mechanics. For example, the forced wave propagation in materials with coupling physical fields and anisotropic materials, the non-axisymmetric scattering problem in pipes, and the reciprocity relation for wave propagation in metamaterials.

References

Achenbach JD, Parikh O, Sotiropoulos D. 1989. Nonlinear effects in the reflection from adhesive bonds. In Review of Progress in Quantitative Nondestructive Evaluation, pp. 1401-07: Springer

Achenbach JD. 2003. Reciprocity in Elastodynamics. Cambridge University Press.

Akbarov SD. 2007. Recent investigations on dynamic problems for an elastic body with initial (residual) stresses (review). International Applied Mechanics 43: 1305

Akbarov SD, Kepceler T, Egilmez MM. 2011. Torsional wave dispersion in a finitely pre-strained hollow sandwich circular cylinder. Journal of Sound and Vibration 330: 4519-37

Ali A, Hosseini M, Sahari BB. 2010. A review and comparison on some rubber elasticity models. Journal of Scientific & Industrial Research 69: 495-500

Anderson IA, Gisby TA, McKay TG, O'Brien BM, Calius EP. 2012. Multi-functional dielectric elastomer artificial muscles for soft and smart machines. Journal of Applied Physics 112: 041101

Banerjee R. 1993. Exact solutions of some nonlinear equations. International Journal of Theoretical Physics 32: 879-84

Bar-Cohen Y. 2002. Electroactive polymers as artificial muscles: a review. Journal of Spacecraft and Rockets 39: 822-27

Belward JA, Wright SJ. 1987. Small-amplitude waves with complex wave. Numbers in A Prestressed Cylinder of Mooney Material. 40: 383-99

Bender FA, Kim J-Y, Jacobs LJ, Qu J. 2013. The generation of second harmonic waves in an isotropic solid with quadratic nonlinearity under the presence of a stress-free boundary. Wave Motion 50: 146-61

Bermes C, Kim J-Y, Qu J, Jacobs LJ. 2007. Experimental characterization of material nonlinearity using Lamb waves. Applied physics letters 90: 021901

Biot MA. 1940. The Influence of Initial Stress on Elastic Waves. Journal of Applied Physics 11: 522-30

Bischoff JE, Arruda EM, Grosh K. 2001. A new constitutive model for the compressibility of elastomers at finite deformations. Rubber Chemistry and Technology 74: 541-59

Biwa S, Nakajima S, Ohno N. 2004. On the acoustic nonlinearity of solid-solid contact with pressure-dependent interface stiffness. Transactions-American Society of Mechanical Engineers Journal of Applied Mechanics 71: 508-15

Blanloeuil P, Meziane A. Earli Sig 15 on Special Educational Needs: Challenges in Learning and Instruction 2015: 621-25.

Boyce MC, Arruda EM. 2000. Constitutive models of rubber elasticity: a review. Rubber Chemistry and Technology 73: 504-23

Breazeale M, Thompson D. 1963. Finite-amplitude ultrasonic waves in aluminum. Applied Physics Letters 3: 77-78

Brochu P, Pei Q. 2010. Advances in dielectric elastomers for actuators and artificial muscles. Macromolecular Rapid Communications 31: 10-36

Cantrell JH, Yost WT. 2001. Nonlinear ultrasonic characterization of fatigue microstructures. International Journal of Fatigue 23: 487-90

Catheline S, Gennisson J-L, Fink M. 2003. Measurement of elastic nonlinearity of soft solid with transient elastography. The Journal of the Acoustical Society of America 114: 3087-91

Zhang WL, Qian J, Chen WQ. 2012. Indentation of a compressible soft electroactive half-space: Some theoretical aspects. Acta Mechanica Sinica 28: 1133-42

Chadwick P, Jarvis DA. 1979. Surface Waves in a Pre-Stressed Elastic Body. Proceedings of The Royal Society A 366: 517-36

Chen W, Dai H. 2012. Waves in pre-stretched incompressible soft electroactive cylinders: exact solution. Acta Mechanica Solida Sinica 25: 530-41

Chen Y, Huang Y, Lü C, Chen W. 2017. A Two-way unidirectional narrow-band acoustic filter realized by a graded phononic crystal. Journal of Applied Mechanics (In press)

Chen Z, Tang G, Zhao Y, Jacobs LJ, Qu J. 2014. Mixing of collinear plane wave pulses in elastic solids with quadratic nonlinearity. The Journal of the Acoustical Society of America 136: 2389-404

Chillara VK, Lissenden CJ. 2013. Analysis of second harmonic guided waves in pipes using a large-radius asymptotic approximation for axis-symmetric longitudinal modes. Ultrasonics 53: 862-69

Chillara VK, Lissenden CJ. 2016. Constitutive model for third harmonic generation in elastic solids. International Journal of Non-Linear Mechanics 82: 69-74

Choy YY, Tay KG, Ong CT. 2013. Modulation of nonlinear waves in an inviscid fluid (blood) contained in a stenosed artery. Applied Mathematical Science 7: 5003-12

Coleman BD, Newman DC. 1990. On waves in slender elastic rods. Archive for Rational Mechanics and Analysis 109: 39-61

Courtney C, Neild S, Wilcox P, Drinkwater B. 2010. Application of the bispectrum for detection of small nonlinearities excited sinusoidally. Journal of Sound and Vibration 329: 4279-93

Croxford AJ, Wilcox PD, Drinkwater BW, Nagy PB. 2009. The use of non-collinear mixing for nonlinear ultrasonic detection of plasticity and fatigue. The Journal of the Acoustical Society of America 126: EL117-EL22

Dace G, Thompson RB, Brasche LJ, Rehbein DK, Buck O. 1991. Nonlinear acoustics, a technique to determine microstructural changes in materials. In Review of Progress in Quantitative Nondestructive Evaluation. pp. 1685-92: Plenum Press

Dai H-H, Dai S, Huo Y. 2000. Head-on collision between two solitary waves in a compressible Mooney–Rivlin elastic rod. Wave Motion 32: 93-111

Dai H-H, Huo Y. 2002. Asymptotically approximate model equations for nonlinear dispersive waves in incompressible elastic rods. Acta Mechanica 157: 97-112

Dai H-H, Peng X. 2011. Weakly nonlinear long waves in a prestretched Blatz–Ko cylinder: solitary, kink and periodic waves. Wave Motion 48: 761-72

de Lima W, Hamilton M. 2003. Finite-amplitude waves in isotropic elastic plates. Journal of sound and vibration 265: 819-39

de Lima WJ, Hamilton MF. 2005. Finite amplitude waves in isotropic elastic waveguides with arbitrary constant cross-sectional area. Wave Motion 41: 1-11

Demčenko A, Akkerman R, Nagy P, Loendersloot R. 2012. Non-collinear wave mixing for non-linear ultrasonic detection of physical ageing in PVC. NDT & E International 49: 34-39

Demčenko A, Koissin V, Korneev V. 2014. Noncollinear wave mixing for measurement of dynamic processes in polymers: Physical ageing in thermoplastics and epoxy cure. Ultrasonics 54: 684-93

Demiray H, Dost S. 1998. Solitary waves in a thick walled elastic tube. Applied Mathematical Modelling 22: 583-99

Deng M. 1998. Cumulative second-harmonic generation accompanying nonlinear shear horizontal mode propagation in a solid plate. Journal of Applied Physics 84: 3500-05

Deng M. 1999. Cumulative second-harmonic generation of Lamb-mode propagation in a solid plate. Journal of Applied Physics 85: 3051-58

Deng M, Wang P, Lv X. 2005. Experimental observation of cumulative second-harmonic generation of Lamb-wave propagation in an elastic plate. Journal of Physics D: Applied Physics 38: 344

Destrade M. 2001. Surface waves in orthotropic incompressible materials. The Journal of the Acoustical Society of America 110: 837-40

Destrade M, Gilchrist MD, Saccomandi G. 2010. Third- and fourth-order constants of incompressible soft solids and the acousto-elastic effect. Journal of the Acoustical Society of America 127: 2759-63

Destrade M, Jordan PM, Saccomandi G. 2009. Compact travelling waves in viscoelastic solids. EPL 87: 48001

Destrade M, Martin PA, Ting TC. 2002. The incompressible limit in linear anisotropic elasticity, with applications to surface waves and elastostatics. Journal of the Mechanics and

Physics of Solids 50: 1453-68

Destrade M, Ogden RW. 2010. On the third- and fourth-order constants of incompressible isotropic elasticity. Journal of the Acoustical Society of America 128: 3334-43

Destrade M, Saccomandi G. 2004. Finite-amplitude inhomogeneous waves in Mooney–Rivlin viscoelastic solids. Wave Motion 40: 251-62

Destrade M, Saccomandi G. 2005. Finite amplitude elastic waves propagating in compressible solids. Physical Review E Statistical Nonlinear and Soft Matter Physics 72: 016620

Destrade M, Saccomandi G, Vianello M. 2013. Proper formulation of viscous dissipation for nonlinear waves in solids. Journal of the Acoustical Society of America 133: 1255-9

Donskoy D, Sutin A, Ekimov A. 2001. Nonlinear acoustic interaction on contact interfaces and its use for nondestructive testing. Ndt & E International 34: 231-38

Dorfmann A, Ogden RW. 2005. Nonlinear electroelasticity. Acta Mechanica 174: 167-83

Dorfmann A, Ogden RW. 2006. Nonlinear Electroelastic Deformations. Journal of Elasticity 82: 99-127

Dorfmann A, Ogden RW. 2010a. Electroelastic waves in a finitely deformed electroactive material. IMA Journal of Applied Mathematics 75: 603-36

Dorfmann A, Ogden RW. 2010b. Nonlinear electroelastostatics: Incremental equations and stability. International Journal of Engineering Science 48: 1-14

Dorfmann L, Ogden RW. 2017. Nonlinear electroelasticity: material properties, continuum theory and applications. Proceedings of the Royal Society A Mathematical Physical and Engineering Sciences 473: 20170311

Ericksen JL. 2007. Theory of Elastic Dielectrics Revisited. Archive for Rational Mechanics and Analysis 183: 299-313

Eringen AC, Maugin GA. 2012. Electrodynamics of continua I: foundations and solid media. Springer Science and Business Media.

Frouin J, Matikas TE, Na JK, Sathish S. 1999. In-situ monitoring of acoustic linear and nonlinear behavior of titanium alloys during cycling loading. In: Nondestructive Evaluation of Aging Materials and Composites III, pp. 107-17: International Society for Optics and Photonics

Fu Y, Devenish B. 1996. Effects of pre-stresses on the propagation of nonlinear surface waves in an incompressible elastic half-space. The Quarterly Journal of Mechanics and Applied Mathematics 49: 65-80

Galich PI, Fang NX, Boyce MC, Rudykh S. 2016. Elastic wave propagation in finitely deformed layered materials. Journal of the Mechanics and Physics of Solids 98: 390-410

Galich PI, Rudykh S. 2016. Manipulating pressure and shear waves in dielectric elastomers via external electric stimuli. International Journal of Solids and Structures 91: 18-25

Gil CM, Lissenden CJ, Lerch BA. 1999. Unusual nonlinear response of some metallic materials. Mechanics of Materials 31: 565-77

Gol'dberg Z. 1961. Interaction of plane longitudinal and transverse elastic waves. Soviet Physics Acoustics 6: 306-10

Goriely A. 2017. The Mathematics and Mechanics of Biological Growth. Springer New York.

Guz′ AN. 2002. Elastic Waves in Bodies with Initial (Residual) Stresses. International Applied Mechanics 38: 23-59

Hamilton MF, Blackstock DT. 1998. Nonlinear acoustics. Academic press.

Hamilton MF, Ilinskii YA, Zabolotskaya EA. 2004. Separation of compressibility and shear deformation in the elastic energy density (L). Journal of the Acoustical Society of America 116: 41-44

Harvey A, Craine R, Syngellakis S. 1992. Propagation of nonlinear surface acoustic waves on elastic and piezoelectric solids. Journal of the Mechanics and Physics of Solids 40: 1529-42

Hayes M, Rivlin RS. 1961. Propagation of a plane wave in an isotropic elastic material subjected to pure homogeneous deformation. Archive for Rational Mechanics and Analysis 8: 15-22

Hayes MA, Saccomandi G. 2000. Finite amplitude transverse waves in special incompressible viscoelastic solids. In: Advances in Continuum Mechanics and Thermodynamics of Material Behavior, pp. 213-25: Springer

Hayes MA, Saccomandi G. 2004. Antiplane shear motions for viscoelastic Mooney–Rivlin materials. The Quarterly Journal of Mechanics and Applied Mathematics 57: 379-92

Henann DL, Chester SA, Bertoldi K. 2013. Modeling of dielectric elastomers: design of actuators and energy harvesting devices. Journal of the Mechanics and Physics of Solids 61: 2047-66

Herrmann G, Mirsky I. 1955. Three dimensional and shell theory analysis of axially-symmetric motions of cylinder. Annals of Japan Association for Middle East Studies 139: 147-73

Herrmann J, Kim J-Y, Jacobs LJ, Qu J, Littles JW, Savage MF. 2006. Assessment of material damage in a nickel-base superalloy using nonlinear Rayleigh surface waves. Journal of Applied Physics 99: 124913

Hikata A, Chick BB, Elbaum C. 1965. Dislocation contribution to the second harmonic generation of ultrasonic waves. Journal of Applied Physics 36: 229-36

Hikata A, Elbaum C. 1966. Generation of ultrasonic second and third harmonics due to dislocations. I. Physical Review 144: 469

Hikata A, Sewell Jr F, Elbaum C. 1966. Generation of ultrasonic second and third harmonics due to dislocations. II. Physical Review 151: 442

Hillis AJ, Neild SA, Drinkwater BW, Wilcox PD. Global crack detection using bispectral analysis. AIP Conference Proceedings 2006a, 820: 89-96. AIP.

Hillis AJ, Neild SA, Drinkwater BW, Wilcox PD. Bispectral analysis of ultrasonic inter‐modulation data for improved defect detection. Proceedings of the Royal Society of London A: Mathematical, Physical and Engineering Sciences 2006b, 462: 1515-30. The Royal Society.

Hirth J, Cohen M. 1970. On the strength-differential phenomenon in hardened steel. Metallurgical Transactions 1: 3-8

Holzapfel AG. 2000. Nonlinear Solid Mechanics: A Continuum Approach for Engineering, Wiley, Chichester.

Huang Y, Shen XD, Zhang CL, Chen WQ. 2014. Mechanically tunable band gaps in compressible soft phononic laminated composites with finite deformation. Physics Letters A 378: 2285-89

Jacob X, Barriere C, Royer D. 2003. Acoustic nonlinearity parameter measurements in solids using the collinear mixing of elastic waves. Applied Physics Letters 82: 886-88

Jeffrey A, Engelbrecht J. 1994. Nonlinear waves in solids. Springer.

Jeffrey A, Kawahara T. 1982. Asymptotic methods in nonlinear wave theory. Pitman Advanced Pub.

Jeffrey A, Xu S. 1989. Exact solutions to the Korteweg-de Vries-Burgers equation. Wave Motion 11: 559-64

Jhang K-Y. 2009. Nonlinear ultrasonic techniques for nondestructive assessment of micro damage in material: a review. International Journal of Precision Engineering and Manufacturing 10: 123-35

Jiao J, Sun J, Li N, Song G, Wu B, He C. 2014. Micro-crack detection using a collinear wave mixing technique. Ndt & E International 62: 122-29

Johnson R. 1970. A non-linear equation incorporating damping and dispersion. Journal of Fluid Mechanics 42: 49-60

Ju T, Achenbach JD, Jacobs LJ, Guimaraes M, Qu J. 2017. Ultrasonic nondestructive evaluation of alkali–silica reaction damage in concrete prism samples. Materials and Structures 50: 60

Junger MC, Feit D. 1986. Sound, structures, and their interaction. MIT press Cambridge.

Kalyanasundaram N. 1981. Nonlinear surface acoustic waves on an isotropic solid. International Journal of Engineering Science 19: 279-86

Kalyanasundaram N, Ravindran R, Prasad P. 1982. Coupled amplitude theory of nonlinear surface acoustic waves. The Journal of the Acoustical Society of America 72: 488-93

Kim J-Y, Jacobs LJ, Qu J, Littles JW. 2006. Experimental characterization of fatigue damage in a nickel-base superalloy using nonlinear ultrasonic waves. The Journal of the Acoustical Society of America 120: 1266-73

Kofod G. 2008. The static actuation of dielectric elastomer actuators: how does pre-stretch improve actuation. Journal of Physics D Applied Physics 41: 2801-09

Korneev V, Demčenko A. 2014. Possible second-order nonlinear interactions of plane waves in an elastic solid. The Journal of the Acoustical Society of America 135: 591-98

Kube CM. 2017. Scattering of harmonic waves from a nonlinear elastic inclusion. Acoustical Society of America Journal 141: 4756

Landau LD, Lifshitz EM. 1986. Theory of Elasticity. Pergammon.

Lardner R. 1983. Nonlinear surface waves on an elastic solid. International Journal of Engineering Science 21: 1331-42

Li GY, He Q, Mangan R, Xu G, Mo C, Luo J, Destrade M, Cao Y. 2017. Guided waves in pre-stressed hyperelastic plates and tubes: Application to the ultrasound elastography of thin-walled soft materials. Journal of the Mechanics and Physics of Solids 102: 67-79

Li J, Rose JL. 2006. Natural beam focusing of non-axisymmetric guided waves in large-diameter pipes. Ultrasonics 44: 35-45

Lissenden C, Liu Y, Choi G, Yao X. 2014. Effect of localized microstructure evolution on higher harmonic generation of guided waves. Journal of Nondestructive Evaluation 33: 178-86

Liu M, Tang G, Jacobs LJ, Qu J. 2012. Measuring acoustic nonlinearity parameter using collinear wave mixing. Journal of Applied Physics 112: 375-81

Liu Y, Chillara VK, Lissenden CJ, Rose JL. 2013a. Third harmonic shear horizontal and Rayleigh Lamb waves in weakly nonlinear plates. Journal of Applied Physics 114: 114908

Liu Y, Khajeh E, Lissenden CJ, Rose JL. 2013b. Interaction of torsional and longitudinal guided waves in weakly nonlinear circular cylinders. The Journal of the Acoustical Society of America 133: 2541-53

Liu Y, Khajeh E, Lissenden CJ, Rose JL. 2014a. Higher order interaction of elastic waves in weakly nonlinear hollow circular cylinders. II: Physical interpretation and numerical results. Journal of Applied Physics 115: 214902

Liu Y, Lissenden CJ, Rose JL. Cumulative second harmonics in weakly nonlinear plates and shells. Proc. SPIE 2013c, 8695: 86950S. SPIE

Liu Y, Lissenden CJ, Rose JL. 2014b. Higher order interaction of elastic waves in weakly nonlinear hollow circular cylinders. I: Analytical foundation. Journal of Applied Physics 115: 214901

Løvstad A, Cawley P. 2011. The reflection of the fundamental torsional guided wave from multiple circular holes in pipes. NDT & E International 44: 553-62

Matlack K, Kim J-Y, Jacobs L, Qu J. 2015. Review of second harmonic generation measurement techniques for material state determination in metals. Journal of Nondestructive Evaluation 34: 273

Matlack KH, Kim J-Y, Jacobs LJ, Qu J. 2011. Experimental characterization of efficient second harmonic generation of Lamb wave modes in a nonlinear elastic isotropic plate. Journal of Applied Physics 109: 014905

Maugin G. 2007. Nonlinear surface waves and solitons. The European Physical Journal-Special Topics 147: 209-30

Maugin GA. 2011. Solitons in elastic solids (1938–2010). Mechanics Research Communications 38: 341-49

Maugin GA. 2013. Continuum mechanics of electromagnetic solids. Elsevier.

McDonald DA. 1974. Blood flow in arteries. Edward Arnold.

Mingxi D. 1998. Cumulative second-harmonic generation accompanying nonlinear shear horizontal mode propagation in a solid plate. Journal of Applied Physics 84: 3500-05

Morsbøl J, Sorokin SV. 2015. Elastic wave propagation in curved flexible pipes. International Journal of Solids and Structures 75-76: 143-55

Nagy PB. 1998. Fatigue damage assessment by nonlinear ultrasonic materials characterization. Ultrasonics 36: 375-81

Nagy PB, McGowan P, Adler L. 1990. Acoustic nonlinearities in adhesive joints. In Review of progress in quantitative nondestructive evaluation, pp. 1685-92: Springer

Nariboli G. 1970. Nonlinear longitudinal dispersive waves in elastic rods (Isotropic homogeneous elastic cylindrical rods, investigating nonlinear longitudinal dispersive waves corresponding to water wave theory analogs). Journal of Mathematical and Physical Sciences 4: 64-73

Ogden R. Large deformation isotropic elasticity-on the correlation of theory and experiment for incompressible rubberlike solids. Proceedings of the Royal Society of London A: Mathematical, Physical and Engineering Sciences 1972, 326: 565-84. The Royal Society.

Ogden RW. 1997. Non-linear elastic deformations. Courier Corporation.

Ogden RW, Sotiropoulos DA. 1997. The effect of pre-stress on the propagation and reflection of plane waves in incompressible elastic solids. Ima Journal of Applied Mathematics 59: 95-121

Ogden RW, Vinh PC. 2004. On Rayleigh waves in incompressible orthotropic elastic solids. The Journal of the Acoustical Society of America 115: 530-33

Patrick L, Gabor K, Silvain M. 2007. Characterization of dielectric elastomer actuators based on a hyperelastic film model. Current Genetics 135: 748-57

Pau A, Lanza di Scalea F. 2015. Nonlinear guided wave propagation in prestressed plates. The Journal of the Acoustical Society of America 137: 1529-40

Pelrine R, Kornbluh R, Kofod G. 2000a. High-strain actuator materials based on dielectric elastomers. Advanced Materials 12: 1223-25

Pelrine R, Kornbluh R, Pei Q, Joseph J. 2000b. High-speed electrically actuated elastomers with strain greater than 100%. Science 287: 836-39

Porubov AV. 2003. Amplification of nonlinear strain waves in solids. World Scientific.

Pouget J. 1986. Transient motion of a solitary wave in elastic ferroelectrics. Lecture Notes in Physics 249: 156-63

Pruell C, Kim J-Y, Qu J, Jacobs LJ. 2007. Evaluation of plasticity driven material damage using Lamb waves. Applied Physics Letters 91: 231911

Rasolofosaon P, Zinszner B, Johnson P. 1997. Propagation des ondes elastiques dans le materiaux non linéaires. Revue de l'institut français du pétrole 52: 585-608

Ratassepp M, Fletcher S, Lowe M. 2010. Scattering of the fundamental torsional mode at an axial crack in a pipe. The Journal of the Acoustical Society of America 127: 730-40

Rauch GC, Leslie W. 1972. The extent and nature of the strength-differential effect in steels. Metallurgical Transactions 3: 377-89

Rénier M, Gennisson J-L, Barrière C, Royer D, Fink M. 2008. Fourth-order shear elastic constant assessment in quasi-incompressible soft solids. Applied Physics Letters 93: 101912

Richardson JM. 1979. Harmonic generation at an unbonded interface—I. Planar interface between semi-infinite elastic media. International Journal of Engineering Science 17: 73-85

Rogerson GA, Fu YB. 1995. An asymptotic analysis of the dispersion relation of a pre-stressed incompressible elastic plate. Acta Mechanica 111: 59-74

Rose J, Ditri JJ, Pilarski A, Rajana K, Carr F. 1994. A guided wave inspection technique for nuclear steam generator tubing. NDT & E International 27: 307-10

Rose JL, Jiao D, Spanner Jr J. 1996. Ultrasonic guided wave NDE for piping. Materials Evaluation 54

Rudenko OV. 2007. Nonlinear waves: some biomedical applications. Physics-Uspekhi 50: 359

Samsonov AM, Maugin GA. 2001. Strain Ssolitons in Solids and How to Construct Them. Chapman & Hall/CRC.

Shearer T, Abrahams ID, Parnell WJ, Daros CH. 2013. Torsional wave propagation in a pre-stressed hyperelastic annular circular cylinder. Quarterly Journal of Mechanics and Applied Mathematics 66: 465-87

Shmuel G. 2013. Electrostatically tunable band gaps in finitely extensible dielectric elastomer fiber composites. International Journal of Solids and Structures 50: 680-86

Shmuel G, Debotton G. 2012. Band-gaps in electrostatically controlled dielectric laminates subjected to incremental shear motions. Journal of the Mechanics and Physics of Solids 60: 1970-81

Shmuel G, Debotton G. 2013. Axisymmetric wave propagation in finitely deformed dielectric elastomer tubes. Proceedings of the Royal Society A Mathematical Physical and Engineering Sciences 469: 30071

Shmuel G, Gei M, Debotton G. 2012. The Rayleigh–Lamb wave propagation in dielectric elastomer layers subjected to large deformations. International Journal of Non-Linear Mechanics 47: 307-16

Simo JC, Pister KS. 1984. Remarks on rate constitutive equations for finite deformation problems: computational implications. Computer Methods in Applied Mechanics and Engineering 46: 201-15

Sinha BK, Winkler KW. 1999. Formation nonlinear constants from sonic measurements at two borehole pressures. Geophysics 64: 1890-900

Sørensen MP, Christiansen PL, Lomdahl P. 1984. Solitary waves on nonlinear elastic rods. I. The Journal of the Acoustical Society of America 76: 871-79

Su YP, Wang HM, Zhang CL, Chen WQ. 2016. Propagation of non-axisymmetric waves in an infinite soft electroactive hollow cylinder under uniform biasing fields. International Journal of Solids and Structures 81: 262-73

Sun M, Xiang Y, Deng M, Xu J, Xuan F-Z. 2018. Scanning non-collinear wave mixing for nonlinear ultrasonic detection and localization of plasticity. NDT & E International 93: 1-6

Suo Z, Zhao X, Greene WH. 2008. A nonlinear field theory of deformable dielectrics. Journal of the Mechanics and Physics of Solids 56: 467-86

Tang G, Jacobs LJ, Qu J. 2012. Wave scattering by an elastic inclusion with quadratic nonlinearity. Journal of the Acoustical Society of America 131: 2570

Tang G, Liu M, Jacobs LJ, Qu J. 2014. Detecting localized plastic strain by a scanning collinear wave mixing method. Journal of Nondestructive Evaluation 33: 196-204

Tiersten H, Baumhauer J. 1974. Second harmonic generation and parametric excitation of surface waves in elastic and piezoelectric solids. Journal of Applied Physics 45: 4272-87

Tiersten H, Baumhauer J. 1985. An analysis of second harmonic generation of surface waves in piezoelectric solids. Journal of Applied Physics 58: 1867-75

Toupin R. 1963. A dynamical theory of elastic dielectrics. International Journal of Engineering Science 1: 101-26

Toupin RA. 1956. The elastic dielectric. Journal of Rational Mechanics and Analysis 5: 849-915

Treloar LRG, Montgomery DJ. 1975. The Physics of Rubber Elasticity. Oxford University Press.

Vaughan H. 1979. Effect of stretch on wave speed in rubberlike. Quarterly Journal of Mechanics and Applied Mathematics 32: 215-31

Walker SV, Kim J-Y, Qu J, Jacobs LJ. 2012. Fatigue damage evaluation in A36 steel using nonlinear Rayleigh surface waves. Ndt & E International 48: 10-15

Wright T. 1985. Nonlinear waves in a rod: results for incompressible elastic materials. Studies in Applied Mathematics 72: 149-60

Wright TW. Nonlinear waves in rods. Proceedings of the IUTAM Symposium on Finite Elasticity 1981: 423-43. Springer.

Wu B, Su Y, Chen W, Zhang C. 2017. On guided circumferential waves in soft electroactive tubes under radially inhomogeneous biasing fields. Journal of the Mechanics and Physics of Solids 99: 116-45

Wu B, Zhou W, Bao R, Chen W. 2018. Tuning Elastic Waves in Soft Phononic Crystal Cylinders Via Large Deformation and Electromechanical Coupling. Journal of Applied Mechanics 85: 031004

Wu J, Wheatley J, Putterman S, Rudnick. 1987. Observation of envelope solitons in solids. Physical review letters 59: 2744

Xu Y, Nesterenko VF. 2015. Attenuation of short stress pulses in strongly nonlinear dissipative metamaterial. Journal of Applied Physics 117: 114303

Xue C, Pan E, Zhang S. 2011. Solitary waves in a magneto-electro-elastic circular rod. Smart Materials and Structures 20: 105010

Yomosa S. 1987. Solitary waves in large blood vessels. Journal of the Physical society of Japan 56: 506-20

Yong DH, LeVeque RJ. 2003. Solitary waves in layered nonlinear media. SIAM Journal on Applied Mathematics 63: 1539-60

Zabolotskaya EA, Hamilton MF, Ilinskii YA, Meegan GD. 2004. Modeling of nonlinear shear waves in soft solids. The Journal of the Acoustical Society of America 116: 2807-13

Zabolotskaya EA, Ilinskii YA, Hamilton MF. 2007. Nonlinear surface waves in soft, weakly compressible elastic media. The Journal of the Acoustical Society of America 121: 1873-78

Zeitvogel DT, Matlack KH, Kim J-Y, Jacobs LJ, Singh PM, Qu J. 2014. Characterization of stress corrosion cracking in carbon steel using nonlinear Rayleigh surface waves. Ndt & E International 62: 144-52

Zhang Z, Liu D, Deng M, Ta D, Wang W. 2014. Experimental observation of cumulative second-harmonic generation of lamb waves propagating in long bones. Ultrasound in Medicine and Biology 40: 1660-70

Zhang Z, Nagy PB, Hassan W. 2016. Analytical and numerical modeling of non-collinear shear wave mixing at an imperfect interface. Ultrasonics 65: 165-76

Zhao X, Suo Z. 2010. Theory of dielectric elastomers capable of giant deformation of actuation. Physical Review Letters 104: 178302

Zhou S, Shui Y. 1992. Nonlinear reflection of bulk acoustic waves at an interface. Journal of Applied Physics 72: 5070-80

Zhou W, Chen W, Shen X, Su Y, Pan E. 2017. On surface waves in a finitely deformed coated half-space. International Journal of Solids and Structures 128: 50-66

Ziser Y, Shmuel G. 2017. Experimental slowing of flexural waves in dielectric elastomer films by voltage. Mechanics Research Communications 85

刘式适, 刘式达. 2012. 物理学中的非线性方程. 北京大学出版社.

Biography

Education

___

2017-2018:   **PhD in Solid Mechanics (3st part)**
Department of Engineering Mechanics, Zhejiang University, China
<u>Dissertation</u>: *Theoretical Modelling of solitary waves in soft bars and higher harmonics in nonlinear media.*
Advisors: Weiqiu Chen & Jan D. Achenbach

2015-2017:   **Visiting Pre-doctoral Fellow in Solid Mechanics (2st part)**
Department of Mechanical Engineering, Northwestern University, USA
<u>Research topic</u>: *Theoretical modelling of higher harmonic generation*
Advisor: Jan D. Achenbach

2013-2015:   **PhD in Solid Mechanics (1st part)**
Department of Engineering Mechanics, Zhejiang University, China
<u>Research topic</u>: *Mechanical behaviors of materials and structures with coupling fields*
Advisor: Weiqiu Chen

2009-2013:   **BSc in Engineering Mechanics**
School of Mechanics & Engineering, Southwest Jiaotong University, China
<u>Dissertation</u>: *Free vibration analysis of the pre-stretched plate with electro-mechanical coupling*
Advisors: Weiqiu Chen & Xiangyu Li

Awards & Honors

___

- China National Scholarship 2017;
- Excellent Graduate Student Scholarship (twice) 2015, 2017;
- China Space Subject Scholarship (three times) 2014, 2015, 2017;
- Cenkefa Scholarship Band One 2015;
- 3nd Scholarship of China Aerospace Science & Industry 2014;
- Graduate of Merit/triple A Graduate 2015;
- Award of Honor for Graduate (three times) 2014, 2015, 2017;
- Excellent Students' Paper at the 2013 Symposium on Piezoelectricity, Acoustic waves and Device Applications.

Publications

___

1. **Yanzheng Wang**, Weiqiu Chen, Jan D. Achenbach,
Analysis of harmonics propagating in pipes of quadratic material nonlinearity using shell theory,
International Journal of Solids and Structures, 2017, 125: 206-215.

2. **Yanzheng Wang**, Jan D. Achenbach,
   The effect of cubic material nonlinearity on the propagation of torsional wave modes in a pipe,
   The Journal of the Acoustical Society of America, 2016, 140(5): 3874-3883.

3. Jan D. Achenbach, **Yanzheng Wang**,
   Far-field resonant third harmonic surface wave on a half-space of incompressible material of cubic nonlinearity,
   Journal of the Mechanics and Physics of Solids, 2017 (In Press)
   DOI: 10.1016/j.jmps.2017.09.010

4. **Yanzheng Wang**, Jan D. Achenbach,
   Reflection of ultrasound from a region of cubic material nonlinearity due to harmonic generation,
   Acta Mechanica, 2018, 229(2): 763-778.

5. **Yanzheng Wang**, Jan D. Achenbach,
   Interesting effects in harmonic generation by plane elastic waves,
   Acta Mechanica Sinica, 2017, 33(4): 754-762.

6. **Yanzheng Wang**, Chunli Zhang, Weiqiu Chen,
   An analytical model to predict material gradient and anisotropy in bamboo,
   Acta Mechanica, 2017, 228, 2819-2833.

7. **Yanzheng Wang**, Chunli Zhang, Hui-Hui Dai, Weiqiu Chen,
   Adjustable solitary waves in electroactive circular rods,
   Journal of Sound and Vibration, 2015, 355, 188-207.

8. **Yanzheng Wang**, Hui-Hui Dai, Weiqiu Chen,
   Kink and kink-like waves in pre-stretched Mooney-Rivlin viscoelastic rods,
   AIP Advances, 2015, 5, 087167.

9. **Yanzheng Wang**, Weiqiu Chen, Xiangyu Li,
   Statics of an FGM circular plate with magneto-electro-elastic coupling: Axisymmetric solutions and their relations with those for a corresponding rectangular beam,
   Applied Mathematics and Mechanics, 2015, 36(5), 581-598.

10. **Yanzheng Wang**, Xiangyu Li, Weiqiu Chen,
    Free vibration analysis of pre-stretched plates with electromechanical coupling,
    In: Proceedings of the 2013 Symposium on Piezoelectricity, Acoustic Waves and Device Applications, edited by Han, X., Dai, H. L. and Chen, W. Q., 2013, pp. 318-323.

11. Xiaoyu Zhao, Guannan Wang, **Yanzheng Wang**,
    Micromechanical modeling in determining the transverse elastic moduli and stress distributions of bamboo,
    Journal of Materials Science, 2017, 53, 2553–2565.

12. Weiqiu Chen, **Yanzheng Wang**, Chunli Zhang,
    Growth-induced material gradient and anisotropy of bamboo.
    In: Mechanics of Functional Materials and Structures (Proceedings of ACMFMS 2014), edited by Ueda, S. and Uetsuji, Y., 2014, pp. 213-216.